NONLINEAR ANALYSIS OF LAYERED T-BEAMS WITH INTERLAYER SLIP

G. A. Tremblay

J. R. Goodman

E. G. Thompson

M. E. Criswell

J. Bodig

Structural Research Report No. 14
Civil Engineering Department
Colorado State University
Fort Collins, Colorado 80523

September 1974

ABSTRACT

NONLINEAR ANALYSIS OF LAYERED T-BEAMS
WITH INTERLAYER SLIP

An experimental program and verification study of a mathematical model for layered T-beams including the effect of nonlinear interlayer slip are described. A study of the member stresses and connection forces calculated by the nonlinear model is also presented. This study is a part of an overall program to develop a verified analysis procedure for wood joist floor systems.

A brief discussion of the full-scale testing program consisting of the determination of the mechanical properties of the materials used and the load-testing of sixteen two- and three-layered T-beams is given. A description of the development of the finite element solution for the nonlinear mathematical model and its capabilities is presented. The verification of the nonlinear model is based on the good agreement obtained in the comparisons of the observed deflection in the full-scale loading tests and the computed deflection predicted by the model for the beams tested beyond the working load range and to failure. These favorable results show the validity of this general beam theory.

A study of the member stresses and connection forces in the T-beam specimens as calculated by the nonlinear model and compared to those currently used in design is presented.

Gary A. Tremblay
Civil Engineering Department
Colorado State University
Fort Collins, Colorado 80521
September, 1974

ACKNOWLEDGMENTS

The author wishes to recognize the members of his graduate committee, Drs. James R. Goodman, Marvin E. Criswell, Jozsef Bodig, and Erik G. Thompson for their assistance throughout the course of this study. Special thanks to Dr. Goodman are in order for his assistance and guidance in the development of this work.

The National Science Foundation is acknowledged for their support of the reported research and the author's assistantship. The author is also indebted to Arlene Nelson for her assistance in typing and organizing the final form of this work.

TABLE OF CONTENTS

LIST OF TABLES

LIST OF FIGURES

LIST OF FIGURES (continued)

CHAPTER I

INTRODUCTION

1.1 Objective

In recent years, the growing concern of our society for the conservation and more efficient use of our natural resources has affected many facets of today's life. The construction of economical residential housing has certainly been affected by these concerns. The suitability of wood housing in providing a sizable portion of the needed construction is attested to by its wide use. Approximately 75 percent of all residential housing in this country is currently constructed with (37). A small savings in the total amount of wood and wood-based products used in residential housing will result in a sizable reduction of the total construction cost of housing and a more efficient use of our wood resources.

The current design methods used for wood lag behind more advanced procedures developed for steel and concrete. The structural design procedure used for layered wood construction is generally based on one of two overly simplified assumptions: (1) rigid connections between layers (complete composite action), or (2) no structural interaction (no composite action). Current design methods for joist-plywood floors are based on the latter and inherently conservative assumption. Thus floors designed using this assumption usually have excessive strength and stiffness and may be less economical than can be. For the most commonly used systems such as nailed wood construction and some glued wood construction, the assumption of either rigid connections or no connections is unrealistic. Interlayer slip at the connectors results in a degree of interaction among the layers that exists somewhere between the assumptions of the rigid connection and no connections.

In the fall of 1971 at Colorado State University, a team of researchers under the sponsorship of the National Science Foundation was organized. They began working to develop a rational analysis procedure for wood joist floor systems. A mathematical model was developed to represent the behavior of layered wood systems, including effects of interlayer slip, and allowing variable connector, sheathing and joist material properties. Discontinuities (gaps) in the individual layers were also treated. This mathematical model forms an integral part of the long range goal of the research: to develop a sufficiently complete and rational analysis of layered beams which can lead to a unified design procedure for layered beam systems. The objective of this phase of the research is to develop and verify a mathematical model of wood T-beam systems which recognizes the T-beam as a multilayered structural system with interlayer slip. The unique aspect of this study differing from Kuo's work (14) is the manner in which the slip modulus is handled in the mathematical model. The mathematical model utilized in Kuo's verification study included the simplifying assumption of a constant slip modulus along the full length of the T-beam specimen. The current study includes recognition of the nonlinear characteristic of the slip curve in the finite element model on an elemental basis. Data used for the verification of the mathematical model was obtained from full-scale test results. The mathematical model utilizes an iterative type finite element solution technique to compute the layered beam deflections, fiber stresses and connector forces. These computed deflections are then compared with the experimentally observed deflections from full-scale T-beam specimen having widely varied properties in order to verify the mathematical model.

1.2 Scope of Work

A description of the construction and testing procedures and the verification of the developed nonlinear mathematical model for 16 T-beams are included in this report. The T-beams constructed and tested included a variety of material, connector, and configuration combinations for both two- and three-layered systems.

A brief literature review is presented in the next section to give a more comprehensive understanding of the development of the layered beam theory. Chapter II contains a description of the material selection, testing equipment, general construction and testing procedures used in this study. Discussion of the material properties including the modulus of elasticity (MOE) values determined both by the Wood Science Laboratory and during construction along with the connector properties including the nail and glue load-slip curves is presented in Chapter III.

A brief description of the development of the nonlinear mathematical model, load-slip curve equations, and the solution methods used and their capabilities is contained in Chapter IV. Chapter V presents the verification of the nonlinear mathematical model by comparing the experimental deflection results and the theoretical calculations. A study of the fiber stresses and connector forces in the T-beam specimens as calculated by the nonlinear mathematical model is presented in Chapter VI. A summary of the report and the resulting conclusions are included in Chapter VII.

Appendices present data on material properties, specimen configurations, experimental test results, comparisons of experimental and theoretical load-deflection curves for all specimens, and a listing of the computer program used to produce the theoretical results.

1.3 Literature Review

A brief review of previously developed research and literature published related to this study follows. This review deals specifically with research developments in the area of composite beams with interlayer slip. Additional comments concerning some of these works are treated in more detail in later sections when these research developments relate to specific sections of the report of this current study.

Several authors have studied the behavior of layered beam systems. Even though their studies were made independently, most of their work has been based on the same assumptions and have been shown to be generally equivalent.

One of the earliest theoretical developments on layered beam systems was presented by Clark (5). His work was based on the assumptions of small deflection theory, negligible separation of laminates, negligible friction between the contact surfaces, and rigid connectors. Experimental results from layered beams of steel laminates and spot welded connectors verified his theory. His equations give a solution for the deflection and slope of beams which are rigidly connected at discrete intervals along the beam.

Granholm (8) developed a theory for layered beam systems including interlayer slip. His theory is based on the assumptions of constant connector spacing, uniformly distributed effects of the connectors along the length of the beam, and linear variation between the force on a connector and its deformation. Another assumption is the constant slip modulus. Pleshkov (27) also analyzed multilayer beam systems with interlayer slip.

Newmark, Seiss, and Viest (22,30) studied the problem of incomplete interaction between the steel girder and concrete slab of a composite T-beam. Their work was based on the assumptions of continuous shear connection, constant slip modulus, linear distribution of strain, and equal deflection of each layer at the same point, thus no separation of layers. They developed and solved differential equations for the force transmitted through the shear connection for a concentrated load and expressions for slip, shear flow, strain, and deflection. Good agreement was shown between theoretical and test results.

A theory based on sandwich construction was developed by Norris, Erickson, and Kommers (23). A series of tests was performed with laminated beams of 3 plys consisting of a low density wood core with a layer of high density veneer on both sides to verify their theory. The results of these tests showed a reasonable agreement between test values and computed values of effective modulus of elasticity. This theory was extended by Kuenzi and Wilkinson (17) to include composite wood beams constructed with adhesives or fasteners having finite rigidity. Their work is based on the assumption of a linear slip curve. Although their work was developed using a different approach than that used by Goodman et al. (6,7), these two theories are generally equivalent.

Hoyle (11) reported experimental work with layered beams and compared his test specimen deflections with the deflections computed by the Kuenzi-Wilkinson Formula. Hoyle tested beam specimen consisting of two equal layers bonded by a range of adhesives and loaded with a concentrated load at midspan. The computed deflections exceeded those actual measured deflections by a range of 20 percent to 40 percent. He concluded that this error could have been reduced if the MOE of the individual laminations had been determined with the actual lamination orientation in the composite beam.

In another of his research reports, Hoyle (12) examined the influence of adhesive rigidity on the performance of multilayered beams. He chose his wooden beam specimen with a cross section composed of two nominal 1 x 3 flanges and a 1 x 12 web with a widely varying range of adhesive connectors. Three of the adhesives were elastomeric adhesives of varying shear modulus values (low, medium, and high) and one rigid bond adhesive. Hoyle concluded that for all of the adhesives, the bonded T-beam did show some degree of composite action.

An investigation of the effects of certain parameters on the ultimate-moment capacity of reinforced laminated timber beams was performed by Krueger and Sandberg (16). The steel and epoxy tension reinforcement was placed in the outermost tension lamination to insure that the tensile stresses would not become critical and the wood in compression would yield and control the ultimate capacity. The major parameters evaluated were the modulus of elasticity of the composite in the longitudinal direction and the ultimate longitudinal stress and strain in wood. An iterative type solution using the finite element method, as outlined by Zienkiewicz (35), was developed. The analytical results as computed by the finite element model compared quite well with the observed experimental results.

Amana and Booth (1,2) have presented their theoretical studies of stiffened orthotropic plates for single rib T-beams and double or multiple ribbed panels with single or double stressed-skins. This study was based on the same assumptions as that of Newmark, Seiss, and Viest (22). The concept of effective flange width was introduced to account for the nonuniform distribution of stresses in the flanges. Stressed-skin beam models were constructed and tested for verification of the theory. Good agreement existed between the experimental and theoretical deflections. Amana and Booth concluded that the presence of slip has a greater effect on deflections than on the maximum tensile stress on the T-beam. They also concluded that the assumption of a constant slip modulus was adequate for loading within the working range of the components of the beam. Above this range, the slip modulus decreases appreciably with increasing load.

The problem of multilayered beams with interlayer slip was treated by Goodman (6). He proved that the final governing equations for the theories presented by Granholm (8), Pleshkov (27), and Newmark, Seiss and Viest (22) were virtually the same. These theories had severe limitations, most notably, the requirement of a linear slip curve. Goodman's theoretical study was aimed, in part, at removing these restrictions and developing a general theory to properly explain the behavior of multilayer beam systems with interlayer slip. His assumptions were generally the same as those of Granholm except that a nonlinear slip modulus was utilized by using a stepwise linear procedure. Experimental results for layered wood beam and plate systems showed excellent agreement with the predicted values.

Goodman's work was extended by Henghold (9). In his study, he developed a general theory for the vibration analysis of layered beams including the effect of interlayer slip. His general theory was developed for an arbitrary number of layers with a single axis of symmetry. He derived the governing equations for the special cases of two- and three-layered systems. This study was based on the same assumptions made by Goodman (6) except the requirement of a linear slip curve was introduced. A finite difference technique was presented to give approximate answers which could include the effect of variation of beam properties along the beam length. Although no extensive experimental work was attempted, the few simple experiments conducted showed agreement with the proposed theory.

Ko (13) treated the case of layered beam systems with interlayer slip as a part of a research project at Colorado State University sponsored by the National Science Foundation. He presented a general theory developed by Henghold (9) for the analysis of multilayered beam systems with a single axis of symmetry and an arbitrary number of layers including the effect of interlayer slip. His study was based on the same assumptions as were made by Goodman. This theory was developed for the particular cases of two- and three-layered systems with linear slip modulus values. The closed form solution and the finite difference approach for the special cases of two- and three-layered beams with uniform or concentrated loading case were solved. Five T-beam sepcimens were constructed with nailed connectors and deflections along the beam caused by a concentrated load were determined. In general, good theoretical agreement with experimental results was achieved except at higher loads. At the higher loads, the presence of local defects in the joist and the nonlinearity of the connector slip curve markedly effected the beam behavior.

In another report resulting from this research project at Colorado State University, Thompson et al. (31) developed a finite element solution technique using the same mathematical model and basic assumptions developed by Goodman (6) and extended by Ko (13) and Henghold (9). The assumption of a constant slip modulus was utilized in his solution technique. An extensive series of full-scale beam tests were conducted by Kuo (14) to verify this finite element form of the mathematical model. Sixteen T-beam specimen were constructed using varying combinations of wood species and connector types and tested to obtain deflections in the elastic range. While each test was conducted to failure, the thrust of the verification work of Kuo (14) was to evaluate the use of the model within the "elastic" or working-load range. Thus a constant slip modulus based on a secant line to the expected average connector force along the length of the beam was used for evaluations. Very good agreement resulted in the comparison of theoretical to experimental deflections.

Rose (29) presented the results of a series of adhesive and structural tests on glued and nailed T-beam and floor systems. Test results showed that the increase in stiffness for the T-beams with respect to that of the joist alone was about 20 percent for unglued tongue and groove joint and about 50 percent for glued tongue and groove joint. Rose proposed a "construction factor" which lowers the stiffness of a fully-composite T-beam assembly to the value of a partially-composite T-beam.

A general theory for the analysis of layer columns which included the effects of interlayer slip was developed by Rassam (28). Columns with double and single axes of symmetry were studied. The theoretical study considered long columns loaded within the elastic range. Columns consisting of 1" x 4" x 54" long laminations of air-dry Englemann spruce were tested. The 70 columns tested represented a wide variety of arrangements of layered and spaced columns. Excellent agreement was obtained between the developed theory and the experimental results.

Zakic (34) presented a stress analysis for the bending of beams with a rectangular cross section using an inelastic theory. This theory represents the behavior of wood beams in the plastic range and defined a more rational design criteria. Tests were performed on glued laminated wood beams. He concluded that the ratio between the ultimate inelastic and elastic bending moments obtained by the appropriate theories is 1.76 for the poplar species used in his tests. He also concluded that the assumed mathematical model of a second-degree parabolic stress-strain line in the compression zone and the straight line stress-strain relationship in the tension zone was satisfactorily consistent with the test results.

While the thrust of Zakic's work dealt with the stress-strain relationship of wood and its effect on the behavior of wood beams in the plastic range, this writer's study deals with the effect of nonlinear interlayer slip on the behavior of layered beams. The assumption of a linear stress-strain relationship for the individual layers is retained. The occurrence of nonlinear interlayer slip in layered beams has an important effect on the beam's performance that must first be studied separately from the effect of the inelastic stress-strain relationships of the individual components.

CHAPTER II

TESTING EQUIPMENT AND PROCEDURE

2.1 Description of Testing Equipment

2.1.1 Introduction

Facilities used for the structural testing of the T-beam specimens are located in the Structural Engineering Laboratory at the Engineering Research Center on the Colorado State University Foothills Campus. The material testing of the components used in the construction of the T-beam specimens was performed using the facilities of the Wood Science Laboratory on the main CSU campus. An extensive description of these facilities has been presented by Penner (26).

A brief description of the loading system and its capabilities is presented in Section 2.1.2. Since this study is concerned with the prediction of the behavior of layered beam systems and not the prediction or determination of the wood material components' properties, this author will delete the complete descriptions of the testing equipment and procedures used in determining the material properties of the wood components. These have previously been presented by Penner (26) and McLain (19) and Kuo (14). A description of the procedure used for collecting data during the tests is discussed in Section 2.1.3.

2.1.2 Loading System

The loading system used for all of the structural testing of the T-beam specimens in this study was a MTS closed-loop structural testing system including a 55 kip-capacity MTS hydraulic actuator. The MTS closed-loop system basically consists of three main components: the power supply, the control console, and the actuator. This system maintains a continuous control on the actual load or strain of the test specimen or the position of the actuator piston. The closed-loop control automatically compensates for changing characteristics in the test specimen due to such factors as creep, fatigue, and sudden jumps in deflections caused by interlayer slip or joist cracking. The actuator is suspended from a movable steel beam by means of a trolley specifically designed to roll along the bottom flange of a wide-flange beam. This movable steel beam is mounted to a supporting frame by the same type of trolley system. This arrangement gives the actuator the mobility to be easily moved to any point over the test area (see Figure 2.1).

The test specimens were supported on an elevated concrete frame with a centerline span of 12 feet. Along the length of each support, a 2 x 6 inch Engelmann spruce sill plate was fastened to the concrete frame and leveled by a layer of grout. The joists of the T-beam specimens rested upon this sill plate.

Two load cells are used in this system to allow adequate resolution of loads over a wide range. These two load cells have rated capacities of 2.5 kips and 50 kips. The 2.5 kip capacity load cell was used for all loading

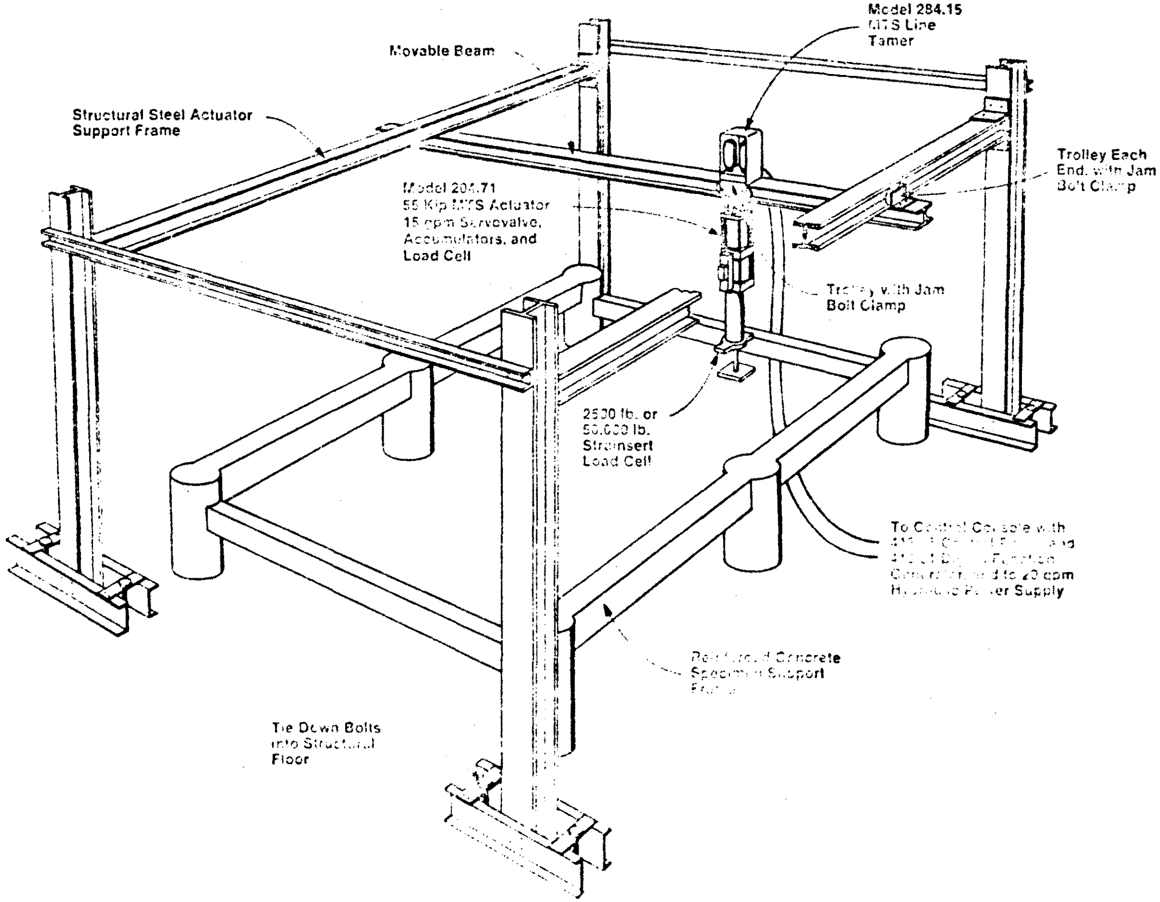

Figure 2.1 55-kip MTS loading actuator and support frame.

tests within the elastic range. When a T-beam specimen was loaded to failure, the 50 kip capacity load cell was used. The control console can operate the actuator in either the load control mode or the stroke control mode.

In order to produce a concentrated load, the force from the actuator ram was transmitted to the floor through the load cell atop a 4 by 4 inch steel pad. This pad and the load cell are joined by a ball bearing. The load cell positioned between the ram of the actuator and the steel loading pad measures the applied load and signals this quantity to the console which commands any necessary ram movement. This correction continues until the load called for by the control console and the load applied by the load cell match.

To provide the T-beam specimens with stability, a twin T-beam configuration was used (see Figure 2.2). Each individual T-beam was loaded equally by means of a loading bridge (see Figure 2.3). This loading bridge was a seven-inch deep channel beam loading each joist on a 4 x 4 inch aluminum pad. These pads and the loading bridge were separated by a steel roller. The actuator load pad was placed in the middle of the loading bridge.

2.1.3 Data Collection

Data collected in this study consisted of deflection values recorded at several load levels for various locations along the T-beam span. Deflections were recorded using three devices: dial gages, engineering scales, and

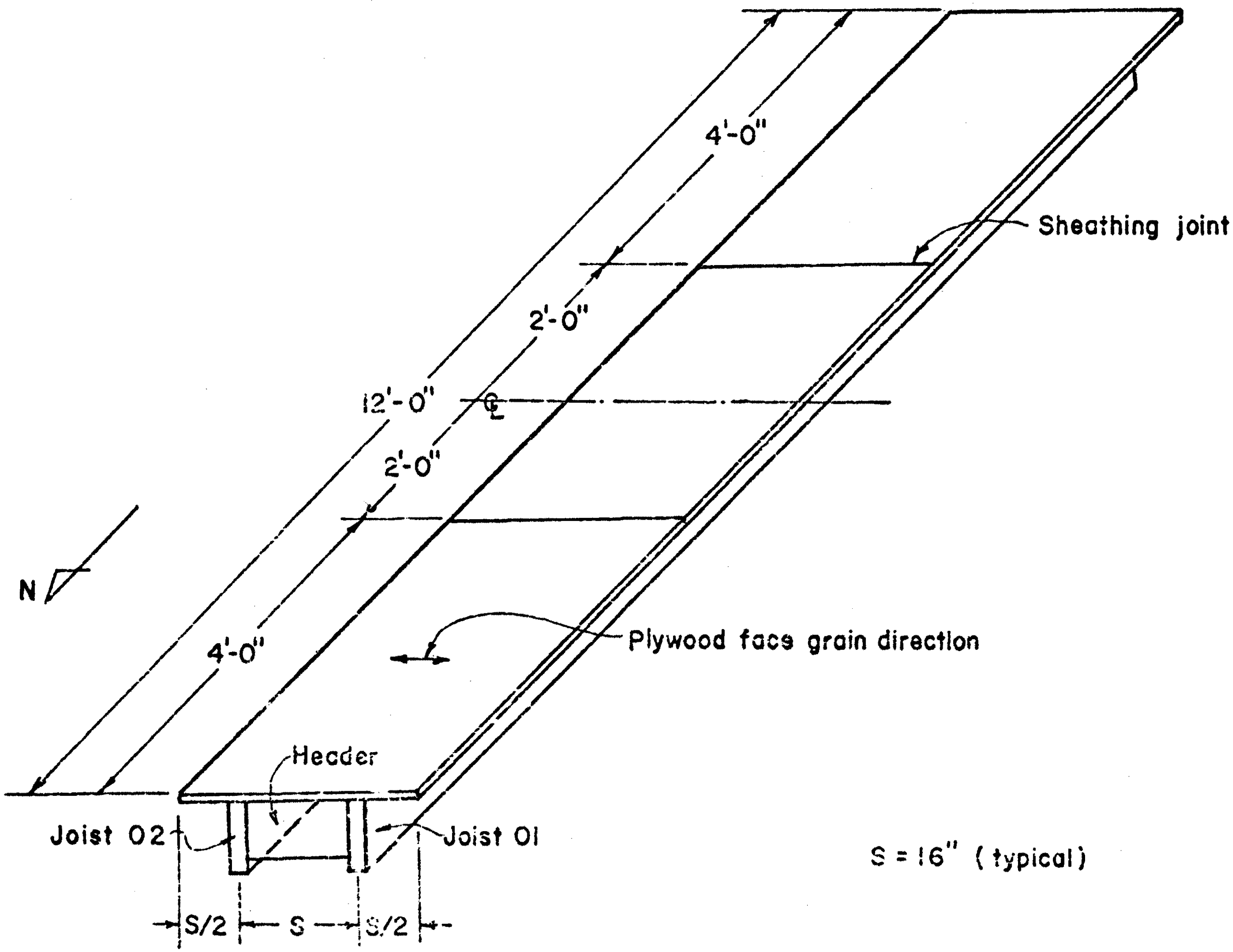

Figure 2.2 Typical two-layered T-beam system.

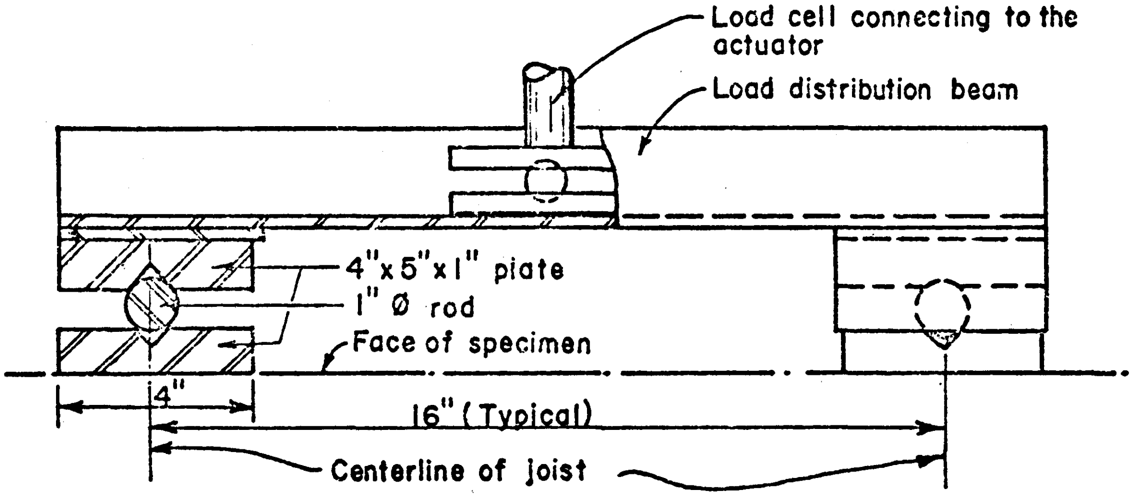

Figure 2.3 Load distribution apparatus.

LVDT's (linear variable differential transformers) connected to X-Y plotters.

During the testing sequences in the elastic range of the specimens, dial gages with ranges of one and two inches were used. These gages were located under the T-beam joists and were attached to a steel angle which was supported by a wood frame. This frame was oriented parallel to the specimen's span length and was supported one foot under the T-beam joist by the concrete frame. A detailed description of the support frame for the dial gages is presented by Penner (26) and various dial gage layouts are presented by Kuo (14).

After the elastic range tests were performed, the specimen was tested to failure. To prevent damage to the dial gages, engineering scales with 50 divisions to the inch were suspended from the specimen's joists at various locations. The deflections were recorded at each load level using a precise level.

The LVDT's were used to obtain continuous plots of the load versus deflection curve at the location of the load. The LVDT contained in the actuator was used to plot this load-deflection curve to failure for most tests; thus the plot was an average deflection of the two joists.

2.2 Test Specimens

2.2.1 Description of the Test Specimens

The material components of the various T-beams differed considerably. Each specimen was assigned an identification mark which identified several of the basic construction parameters. This identification mark was based on an alphanumeric system. An example of this system and its description is as follows:

T8-8D16-1

T = T-beam specimen — T

Sequential number of specimen — 8

Nominal joist depth, inches — 8

Joist species (D = Douglas-fir, E = Engelmann spruce) — D

Joist spacing, inches — 16

Number of sheathing layers — 1

Sixteen T-beams were built and tested. These full-scale specimens were constructed with both joist and sheathing components of Douglas-fir, Engelmann spruce, or a combination of the two species. A specimen consisting of joists and one layer of sheathing formed a two-layered T-beam system. Three of the sixteen specimens were selected to have one-half inch thick layer of particleboard added to the two-layered system to form a three-layered system. The nominal dimensions of the joist were 2 x 8 inches and 2 x 12 inches. Actual dimensions of each joist were measured and recorded by the Wood Science Laboratory and used in all the calculations. Each joist had a total length of 12 feet and 2 inches and a span length of 12 feet. The plywood had nominal thicknesses of 1/2 and 3/4 inches. Each joist was identified according to the alphanumeric identifying system below:

```
                           DW-S-08-18
                           ||  |  |  |
Lumber species ------------┘|  |  |  └---- Serial number within
(E = Engelmann spruce)      |  |  |         the category
(D = Douglas-fir)           |  |  |
Lumber supplier ------------┘  |  |
Lumber grade: -----------------┘  └------- Nominal depth of joist,
S = select structural, N = No. 3            inches
```

For the plywood and particleboard:

```
                           DP-12-07
                           ||  |  |
Sheathing species ---------┘|  |  └------- Serial number within
                            |  |            the category
                            |  |
Sheathing type -------------┘  └---------- Thickness of sheet,
(P = plywood)                              inches 12 = 1/2 in.
(B = particleboard)
```

The type of connectors used in the specimens were either 6d or 8d common nails placed at a constant spacing for each specimen or an elastomeric adhesive. The nail connector spacing varied from 2 inches to 8 inches. One of the T-beam specimens was constructed with a combination of glue and 8d nails at 8 inch spacings. Joist spacings were either 16, 19.2 or 24 inches.

To identify locations of loads and deflections along the length of the T-beam span, a general numbering system was developed. The location along a certain joist was described by first denoting the joist number and then the station number along that joist using the system shown in Figure 2.4.

2.2.2 Selection of Materials

Two methods were adopted for selecting the joist material for the specimens, In the first method, joists

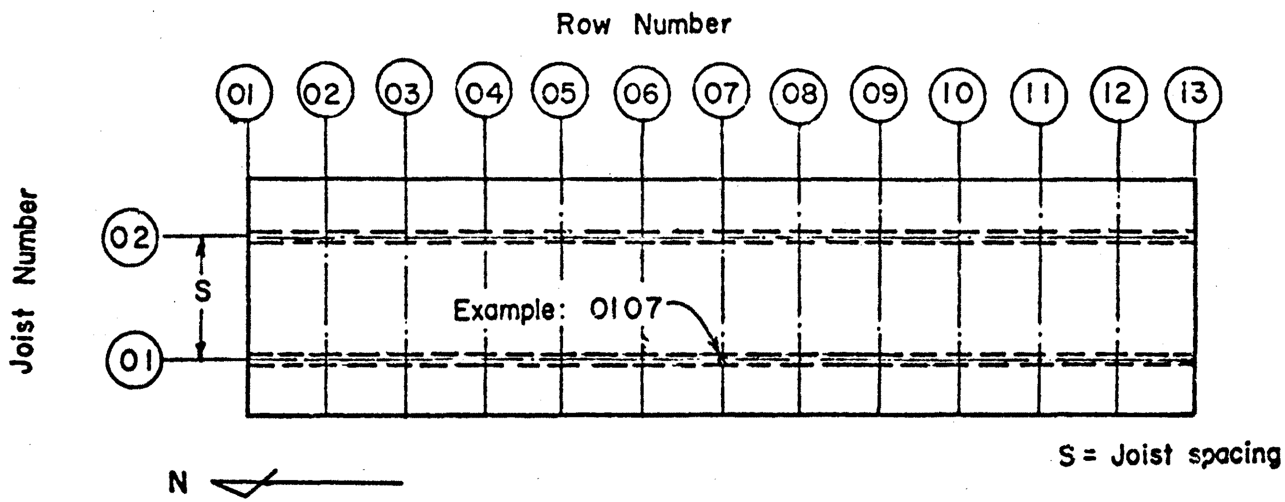

Figure 2.4 Numbering system to identify locations on specimen.

were selected within a specified range of average MOE value using data provided by the Wood Science Laboratory. From this selected group of joists, the ones with excessive crookedness or abnormal cracks or knots were discarded. Most of the joist selection was performed using this method. The second method was used only for a few T-beams. This was a random selection of joist without regard to their measured stiffnesses. Again, excessively crooked or abnormally cracked joists were discarded.

Plywood was selected from the top of the pile as it was needed without regard to measured stiffness.

All lumber was covered with plastic sheets during storage to maintain a stable moisture content. Joist moisture content measured during the MOE determinations at the Wood Science Laboratory ranged from 6.4 to 11.3 percent. These values were also measured after each T-beam was tested and ranged from 5.0 to 7.3 percent for the joists and from 5.6 to 6.9 for the plywood.

All of the T-beams were constructed using essentially the same procedure. The general construction procedure is presented in detail by Kuo (14). After each joist was selected as described in the previous section, a reference mark was placed at the midspan loaction to be used for the edgewise MOE tests. The joist was then placed on the elevated concrete frame, centered, leveled to prevent the joist from teetering, and nailed to the sill plate to prevent lateral and longitudinal displacements during testing.

The joists were oriented with big edge knots placed in the top area of the joist to prevent early failure in the loading tests.

For the MOE tests, the two joists of the double-T specimen were connected by a common header plate to provide stability. Tests to determine the MOE were performed by placing increasing incremental loads at the joist midspan in the elastic loading range and recording the deflections at the midspan. The number of nails used to connect the header plate to the joists affected the edgewise MOE values. The increasing number of nails resulted in an increasing stiffness of the joists since the degree of fixity at the joist ends caused an interaction between the joists when one joist was deflected and the other joist wasn't. Since the end conditions for the joists in the actual testing procedure was the header plate attached with 3 nails, this was the end condition used to determine the MOE values.

For most of the two-layered specimens, the face grain of the plywood sheathing was oriented perpendicular to the joist span. The plywood sheathing was connected to the joists using 8d nails at a constant nail spacing, an elastomeric glue (Franklin Construction Adhesive), or a combination of the two. Nail spacing ranged from 2 inches to 8 inches. One row of nails per joist was used always.

The details of the sheathing joints varied from specimen to specimen. Most of the sheathing joints were tightly butted tongue and groove. For some specimens, the sheathing joints were left with a 1/16 inch wide gap. The joints were glued and tightly butted in other specimens.

For three of the specimens, a layer of particleboard was added to form a three-layered system. After being selected as described in the previous section, it was oriented on the top flange of the double T-beam specimen to stagger the sheathing joints of the plywood and particleboard. Six penny nails were used as connectors and were driven into the plywood layer and the joist. The specimen configurations, gap locations, and nail spacings are presented in Appendix C. A brief description of the testing sequence for each specimen to indicate the load levels, load increments, load location, and failure load is also presented in Appendix C.

2.3 Testing Procedure

A complete description of the general testing procedures used during this study has been presented by Penner (26) and Kuo (14). Tests were first conducted in the working load range of the specimen. Since this load range is entirely dependent on the overall stiffness of each specimen, the load was limited to that which caused a maximum deflection of L/360 (0.40 inches for a 12 foot span). The tests were conducted with the load at the midspan location of the specimen and deflections being recorded at various locations along each joist span. Dial gages were used for the deflection recordings. The load was applied with incremental increases of 50, 100, 200, or 500 pounds.

Deflections were recorded at each increment. This procedure was repeated up to five times for each loading case.

For some of the specimens, the next step in the testing procedure was the sequential cutting of increasing number of gaps in the sheathing layer. The specimens were then tested as in the first step. This procedure is described in detail by Kuo (14). For the specimens that were formed into three-layered systems, this step was eliminated and replaced by the addition of the particleboard layer and the repetition of the first step.

Finally most of the specimens were tested to failure with the load applied to the midspan of the specimen. Load increments were 500 pounds. Deflection recordings were made at each increment of load. The LVDT from the actuator was connected to a X-Y plotter to develop a continuous load-deflection plot. After ultimate failure, the load was removed and the condition of the broken joists were examined. The specimen was then dismantled. Small samples of the joists and sheathing material of the specimen were cut to sizes conforming to the ASTM Standard D 2016-65 (3) and sent to the Wood Science Laboratory for moisture content determination.

The data collected using these facilities and testing procedures were utilized for the verification of the mathematical model. The material properties are discussed in Chapter III.

Chapter III

MATERIAL PROPERTIES

3.1 Introduction

The two most important material properties influencing the composite behavior of a layered beam system of given dimensions are the MOE (modulus of elasticity) values for the material in each layer and the slip modulus of the connectors. Difficulty in evaluating the material properties of wood arises from the fact that wood is not a homogeneous or isotropic material for which the MOE is theoretically constant throughout the material. The MOE values of wood vary from species to species, from one piece of lumber to another in the same species, and even from section to section along the length of a piece of lumber. Another factor affecting the MOE and other material properties values of wood is the direction in which it is loaded.

Several research institutions and agencies have studied and developed methods for evaluating lumber properties. These methods involve a visual grading technique or a combination of visual and machine grading systems (3,10,32). Plywood stiffness properties are evaluated by classifying plywood into 5 groups and assigning each group an allowable unit stress. Particleboard is assigned a minimum average MOE value ranging from 50,000 psi to 150,000 psi by the National Particleboard Association (4). These values are dependent on the geometry of the particles, the type of adhesive, and the manufacturing process used to produce the particleboard.

A short discussion of the method used in evaluating the MOE of joists and sheathing material for this study will be presented in the next section. A detailed discussion can be found in the reports of McLain (19), Wolfe (33), and Kuo (14).

Although nails are the most common connectors used in residential housing construction, very little work has been performed on the study of the forces on nails in a wood floor system. Elastomeric glue connectors have recently become more widely used also in the construction of wood floor systems. Although this fact has drawn more research attention to this area, neither a verified design criteria nor an economical benefit study for the elastomeric glued connection in a wood floor system has been made available to the designer. A short discussion of the slip modulus tests providing the load-slip relationship values used in this study is presented in Section 3.3. Patterson (25) and Kuo (14) have presented detailed discussions on this subject.

3.2 Joist and Sheathing Properties

3.2.1 Flexural MOE Determined by the Wood Science Laboratory

An adequate description of the material properties of the joist and sheathing materials was considered necessary for the verification of the mathematical model. Since the material properties of wood products can vary widely from piece to piece, the MOE values for each piece of lumber used in the T-beam specimens was determined individually. This could be done because the MOE values and other elastic material constants are easily determined using nondestructive testing procedures.

Preliminary nondestructive testing for the joist and sheathing material properties was conducted at the Wood Science Laboratory at the Colorado State University campus. A detailed description of the testing equipment and procedure for evaluating the MOE of the joist material is fully discussed by Wolfe (33) and Kuo (14). The equipment used in the nondestructive testing procedure consisted of a continuous deflection measurement device. The testing procedure entailed deflecting a piece of lumber as a plank over a three foot span with a concentrated load at the midspan. The deflections at midspan were recorded using a LVDT (Linear Variable Differential Transformer). The MOE values were then calculated from the recorded deflections using the average dimensions of the joist as measured at three locations along the joist length. The MOE was calculated for one foot intervals along the length of the joist and also averaged for the full length of the specimen. A correlation between the flatwise and edgewise MOE's has been evaluated through several studies. Regression analyses were used by O'Halloran (24) and Kuo (14) to substantiate a correlation between the plank and joist MOE. To insure accurate MOE values for the verification of the mathematical model, a second nondestructive test was performed with the joist in the edgewise orientation.

The in-plane elastic parameters were also determined for each piece of the five commonly used sheathing materials used in this study. These material were 1/2 and 3/4 inch thick Douglas-fir plywood, 1/2 and 3/4 inch thick Engelmann spruce plywood and 1/2 inch thick Douglas-fir particleboard. The static bending concept was used in the tests with the sheathing panel acting as a wide beam supported at one edge and near the middle with the remainder of the panel cantilevering out. Deflections were produced by a line load at the cantilever and recorded as the average of the three LVDT readings at the location of the load. The overall MOE values were determined since the effect of defects was considered not to be significant. The flexural MOE was determined along both major axes of the panel, i.e., parallel and perpendicular to the face grain. McLain (19) and Kuo (14) have described the testing equipment and procedure for these materials. Due to the orthotropic nature of wood and the cross layered construction of plywood, the transformed sectional properties were used in determining the MOE values in bending for axial loads a conversion factor, based on the gross section dimensions, was described by Liu (18).

Evaluation of the shear modulus was conducted using a test setup which permitted the application of loads at one set of diagonal corners of the panel and supports at the other two corners.

The MOE values for the lengthwise and crosswise directions and the shear modulus for each panel used in the T-beam specimens are listed in Appendix B.

3.2.2 Joist Properties Determined During Specimen Construction

The correlation between flatwise and edgewise MOE of structural lumber has been previously evaluated and reported (14,24) to be in the range of 0.70 to 0.92. An exact correlation is not possible. This is because the natural variations in wood such as grain angle, knots, and other defects have different effects on the specimen's MOE depending on the direction of bending. To obtain the most accurate value of MOE for the joist components of the T-beam specimens, each joist specimen was tested in its elastic range (bending stress less than 500 psi) for the edgewise MOE. The edgewise MOE was determined for each joist as a part of the specimen construction procedure because it was decided that these values of MOE were representative of the actual specimen's properties. It was also decided that these values might yield more consistent results when verifying the mathematical model.

Briefly, the testing procedure consisted of obtaining the corresponding deflection at the load location to each of three load increments applied at the center line of the joist placed in the edgewise orientation (14). By obtaining the slope of the load versus deflection plot in the linear region and substituting this value into a static deflection formula for this loading case, the edgewise MOE value was determined. The shear modulus term in the static deflection formula, $\Delta = PL^3/48EI + 0.3PL/AG$, is not considered; thus the effect of shear deformation is included in the total MOE value obtained. This lower MOE value is desirable since the effect of shear deformation is not considered in the mathematical model. This test was conducted for three joist support conditions: (1) no lateral support, (2) lateral support by a header plate attached with one 16d common nail at mid-depth of the joist, and (3) lateral support by a header plate attached with three symmetrically arranged 16d common nails.

Kuo (14) has reported on the relationship between the flatwise and edgewise MOE values determined by the material used in this study.

3.3 Properties of Nail and Glue Slip Moduli

One of the two important material properties affecting the composite behavior of a layered beam system is the slip modulus. It greatly influences the degree of interaction between layers. Interlayer slip is dependent on the load-slip characteristics of the connector-wood combination. This relationship is generally nonlinear. The slip modulus of a connector is defined as the slope of the load-slip curve of the connector-wood combination (see Figure 3.1). Patterson (25) has presented a detailed study of the nail slip modulus used in this study as a part of the overall

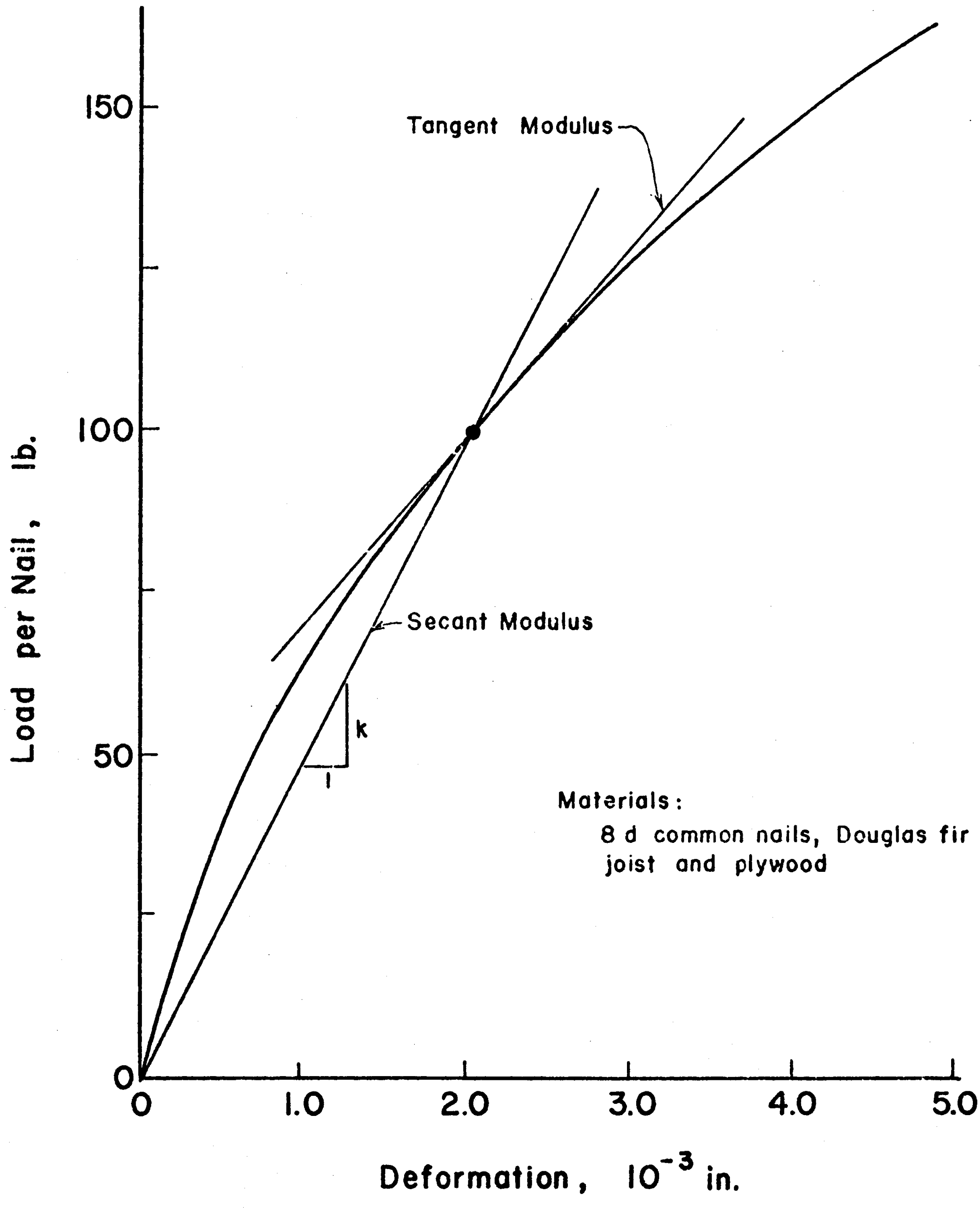

Figure 3.1 Typical load-slip curve.

wood joist floor project. He used the equation developed by Goodman (6) to fit a curve to the load-slip data.

In Patterson's work (25), the double shear test specimen, shown in Figure 3.2, was used. Different combinations of side member to center member materials were tested. The side members consisted of 3/4 inch thick Douglas-fir or Engelmann spruce plywood with the face grain oriented either parallel or perpendicular to the load. The center member was a 2 x 8 joist piece of either Douglas-fir or Engelmann spruce. The number of nails used to connect the side member to the center member was varied for the test specimens. The nails used were 8d common nails with 1,2, or 4 nails used for each side member.

Nail slip modulus tests were also conducted using 1/2 inch thick plywood as the two side members and 8d nails. The load-slip characteristics between particleboard and plywood were determined using a test specimen similar to the double shear specimen described before. The layer of particleboard was connected to the plywood member with two rows of 6d nails driven through the particleboard and plywood but not through the joist on each side of the joist center member.

The slip modulus properties of the elastomeric adhesive used in this study (Franklin Construction Adhesive) were determined using the test setup similar to the one used in the nail-slip tests by Patterson (25). The slip modulus for the glued connection is expressed in terms of pounds of

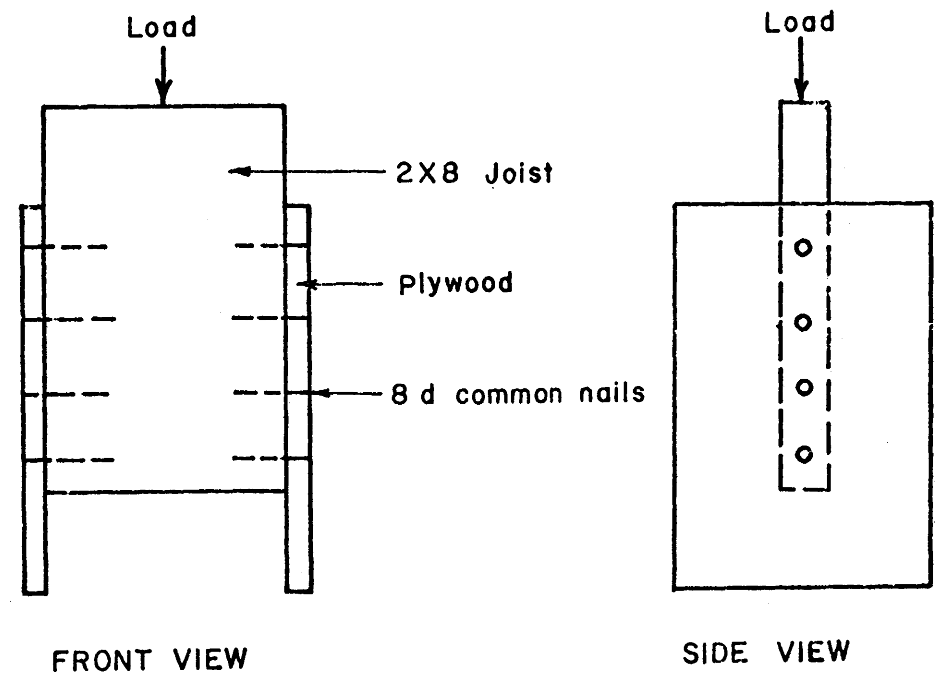

(a). PLYWOOD AND JOIST

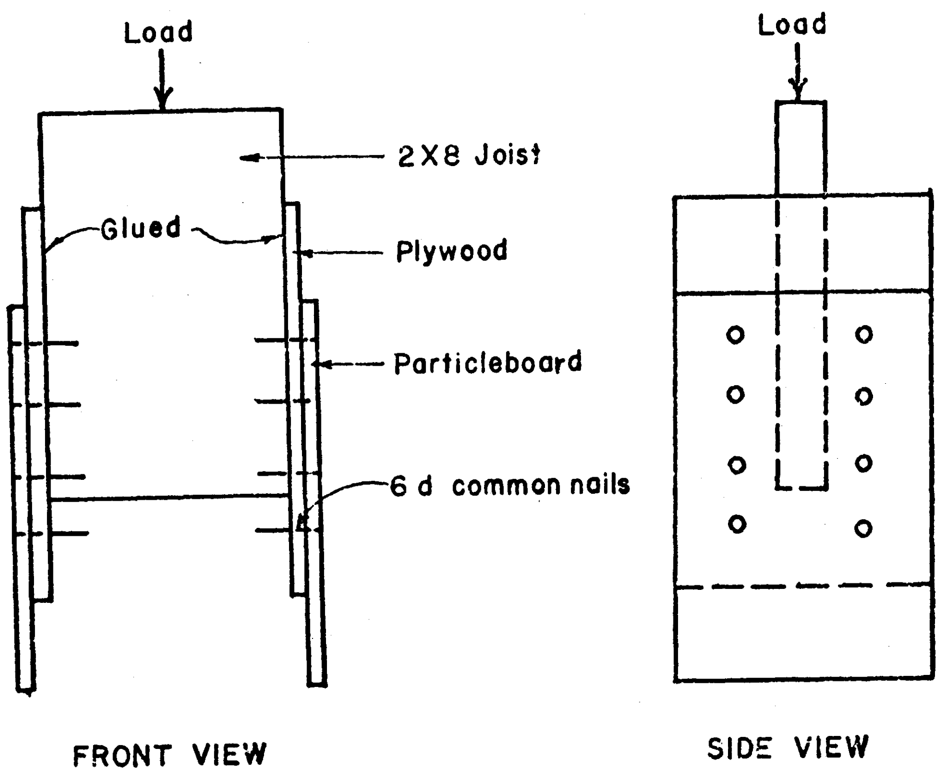

(b). PLYWOOD AND PARTICLEBOARD

Figure 3.2 Nail slip modulus test specimens.

lateral force resistance per square inch of glued surface per inch of horizontal motion.

A total of 168 nail slip tests were connected by Patterson (25). A less extensive series of tests were performed for the glued connection. The continuous connection eliminated the need to study the effect of the spacing of connectors and the distribution of the shear force among the connectors. A typical load-slip curve is shown in Figure 3.1. A composite load-slip curve was developed for each combination of material and connection type used in the slip tests. The nonlinear load-slip curve was composed for each type of test specimen by averaging the total slip observed in the individual test specimens at different load levels and plotting the resulting data. A power series equation was fit to the slip curves and defined the load-slip characteristics in the finite element solution technique of the mathematical model. Description of the power series equation is presented in Section 4.4.

The specimens tested in this study encompassed a wide range of T-beam configuration and material and connector property combinations. This author feels that the verification of the mathematical model using these specimens provides reasonable assurance that the mathematical model represents the behavior of any practical T-beam configuration.

CHAPTER IV

DEVELOPMENT OF A NONLINEAR MATHEMATICAL MODEL

4.1 Introduction

This chapter will present the governing equations used in the development of the nonlinear mathematical model. Two studies concerned with the development of mathematical solutions for computing T-beam deflections based on beam theory with consideration of interlayer slip have been conducted as a part of the overall research program at Colorado State University and form the basis for the nonlinear model development. A closed form solution for the mathematical model was developed by Goodman (6) and extended by Kuo (14).

In this study, these existing solutions have been further extended to include calculation of connection forces and fiber stresses in each layer along the span length. A stepwise process was used to take into account the effect of the nonlinearity of the slip curve. The formulation of the basic solution technique for the mathematical model is reviewed in Section 4.2. A finite element solution of this basic mathematical model was developed by Thompson et al. (31). This solution is based on the potential energy theorem and can include the effects of gaps within the individual layers. This solution technique has also been modified to calculate connection forces and fiber stresses along the beam span length and to take into account the nonlinearity of the slip curve by a stepwise method. The development of the basic solution technique is presented in Section 4.3.

The equations used to represent the nonlinear slip curves in the mathematical model are reviewed in Section 4.4. The capabilities and limitations of each solution technique are discussed and compared in Section 4.5.

4.2 Mathematical Model of T-Beam and Its Closed Form Solution

The solution for the mathematical model developed by Goodman (6) was extended by Kuo (14) to the special cases of two- and three-layered beam systems with a single axis of symmetry. The solution is developed using the basic assumptions of small deflections, linearly elastic materials, linear variation of strains over the depth of each layer, negligible shear deformations, equal curvature of each layer during bending, and linear slip modulus. Because the nonlinear analysis considers the slip curve nonlinearity by a stepwise linear procedure, this last assumption of the linear slip modulus could be retained and the governing equations for the system are not altered. A typical two-layered T-beam is shown in Figure 4.1. The two governing equations for this system developed by Goodman (6) and Kuo (14) are:

$$\frac{d^2y}{dx^2} = \frac{-M_T + C_{12} \cdot F}{E_1I_1 + E_2I_2} \qquad (4.1)$$

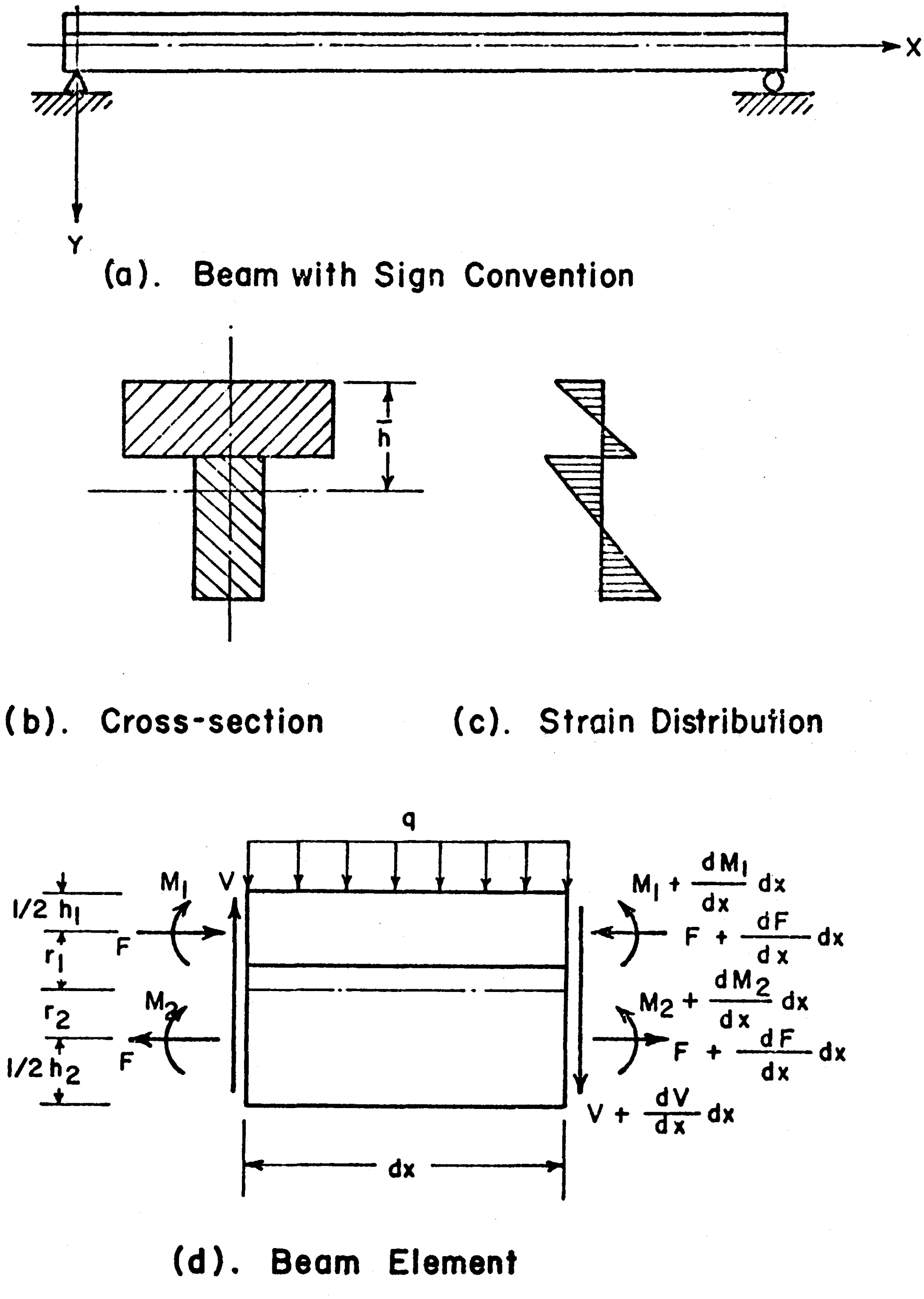

Figure 4.1 Two layered system.

and

$$\frac{s}{kn} \cdot \frac{d^2F}{dx^2} = \left[\frac{1}{E_1A_1} + \frac{1}{E_2A_2}\right] \cdot F + C_{12} \cdot \frac{d^2y}{dx^2} \qquad (4.2)$$

where E_i = the modulus of elasticity of the i^{th} layer, lb/in^2,

I_i = the moment of inertia of the i^{th} layer about its own neutral axis, in^4

A_i = cross section area of the i^{th} layer, in^2

s = the spacing between connector rows along the beam length, in.,

k = the conncetor modulus per connector, lb/in.,

n = the number of connectors per row,

M_T = total applied moment, in./lb,

$C_{12} = \frac{h_1 + h_2}{2}$

The solution of equations (4.1) and (4.2) for a concentrated load at midspan and boundary conditions for a simply supported beam result in the following closed form solution for the beam deflections.

$$Y_L(x) = Y_s(x)_L + \frac{C_{12}}{E_1I_1 + E_2I_2} \cdot \frac{1}{C_1} \cdot F_L(x) \qquad (4.3a)$$

and

$$Y_R(x) = Y_s(x)_R + \frac{C_{12}}{E_1I_1 + E_2I_2} \cdot \frac{1}{C_1} \cdot F_R(x) \qquad (4.3b)$$

where

$$F_L(x) = -\frac{C_2}{C_1}\cdot\frac{P}{\sqrt{C_i}}\cdot\frac{\sinh[\sqrt{C_1}(L-a)]}{\sinh(\sqrt{C_1}L)}\sinh(\sqrt{C_1}x) + \frac{C_2}{C_1}P(1-\frac{a}{L})x;$$

$$o \leq x \leq a \qquad (4.4a)$$

$$F_R(x) = -\frac{C_2}{C_1}\cdot\frac{P}{\sqrt{C_1}}\cdot\sinh(\sqrt{C_1}a)\cosh(\sqrt{C_1}x)$$

$$+\frac{C_2}{C_1}\cdot\frac{P}{\sqrt{C_1}}\frac{\sinh(\sqrt{C_1}a)}{\tanh(\sqrt{C_1}L)}\sinh(\sqrt{C_1}x) + \frac{C_2}{C_1}\cdot P\cdot a\,(1-\frac{x}{L});$$

$$a \leq x \leq L \qquad (4.4b)$$

$$C_1 = \frac{kn}{s}\left[\frac{1}{E_1A_1}+\frac{1}{E_2A_2}\right]\cdot\frac{I_s}{I_1+I_2}$$

$$C_2 = \frac{kn}{s}\left[\frac{C_{12}}{E_1I_1+E_2I_2}\right]$$

$F_{R\text{ or }L}(x)$	=	axial layer force, lbs.,
I_s	=	the moment of inertia of the rigidly connected section, in^4
$y_s(x)_{R\text{ or }L}$	=	deflection of the rigidly connected beam at location 'x' to the right or left of the concentrated load, in.,
$y_{R\text{ or }L}(x)$	=	deflection of the layered beam at location 'x' to the right or left of the concentrated load, in.

For these closed form solution of (4.3a) and (4.3b) equations, the section properties, connector spacing and slip modulus must be assumed constant along the length of the beam.

This mathematical model can be extended to allow calculation of nail forces and fiber stresses in each layer along the beam length. The equations for the shear values between the two layers are obtained by differentiating the axial force equations of (4.4a) and 4.4b) giving

$$q_L(x) = \frac{dF_L(x)}{dx} = -\frac{C_2}{C_1} P \frac{\sinh[\sqrt{C_1}(L-a)]}{\sinh(\sqrt{C_1}L)} \cosh(\sqrt{C_1}x)$$

$$+ \frac{C_2}{C_1} P(1 - \frac{a}{L}); \qquad o \leq x \leq a \qquad (4.5)$$

and

$$q_R(x) = \frac{dF_R(x)}{dx} = -\frac{C_2}{C_1} P \sinh(\sqrt{C_1}a)\sinh(\sqrt{C_1}x)$$

$$+ \frac{C_2}{C_1} P \frac{\sinh(\sqrt{C_1}a)}{\tanh(\sqrt{C_1}L)} \cosh(\sqrt{C_1}x) - \frac{C_2}{C_1} P \frac{a}{L};$$

$$a \leq x \leq L \qquad (4.6)$$

The nail forces are obtained by multiplying the shear flow values at the nail location by the spacing between the nails.

The fiber stresses can be calculated at the top and bottom of each beam layer from the basic stress equations. That is:

$$\sigma_i = \pm \frac{F_i}{A_i} \pm \frac{M_i c}{I_i} \qquad (4.7)$$

where, from basic flexural theory:

$$M_i = - EI_i \frac{d^2y}{dx^2} \qquad (4.8)$$

and, by double differentiation of Equations (4.3a) and (4.3b):

$$\frac{d^2y}{dx^2} = \frac{d^2y_s}{dx^2} + \frac{1}{C_1} \cdot \frac{C_{12}}{E_1I_1 + E_2I_2} \cdot \frac{d^2F}{dx^2} \tag{4.9}$$

Differentiation of Equations (4.5) and (4.6) gives the following relationships:

$$\frac{d^2F_L(x)}{dx^2} = -\frac{C_2}{C_1} P\sqrt{C_1} \frac{\sinh[\sqrt{C_1}(L-a)]}{\sinh(\sqrt{C_1}L)} \sinh(\sqrt{C_1}x);$$

$$o \leq x \leq a \tag{4.10}$$

$$\frac{d^2F_R(x)}{dx^2} = -\frac{C_2}{C_1} P\sqrt{C_1} \sinh(\sqrt{C_1}a)\cosh(\sqrt{C_1}x)$$

$$+ \frac{C_2}{C_1} P\sqrt{C_1} \frac{\sinh(\sqrt{C_1}a)}{\tanh(\sqrt{C_1}L)} \sinh(\sqrt{C_1}x);$$

$$a \leq x \leq L \tag{4.11}$$

and, from double differentiation of the expression for deflection of a point loaded simply supported beam:

$$\frac{d^2y_s(x)_L}{dx^2} = \frac{P \cdot b \cdot x}{L \cdot E_2 \cdot I_s} \qquad (o \leq x \leq a) \tag{4.12}$$

$$\frac{d^2y_s(x)_R}{dx^2} = \frac{P \cdot a \cdot (L-x)}{L \cdot E_2 \cdot I_s} \qquad (a \leq x \leq L) \qquad (4.13)$$

By substituting these values into equations (4.7),(4.8) and (4.9), the fiber stresses can be solved.

In Goodman's work (6) with layered beams having three equal layers, a stepwise linear numerical procedure was used to introduce the nonlinear effect of the connector slip curve into the mathematical model. This same procedure is used for the closed form solution of the T-beam mathematical model. A flow diagram is shown in Figure 4.2. As shown in the diagram, the slip modulus is re-evaluated by an equation within the model. This equation is an expression describing the nonlinear load-slip relationship for the type of connector used in the model. The solution of this equation is discussed in Section 4.4.

The slip modulus can be calculated as either a tangent or secant slope as shown in Figure 3.1. This stepwise linear solution is started by using the initial tangent to the connector load-slip curve for the first load increment. Upon completion of these calculations, the constant slip modulus along the beam length is recalculated as the tangent to the load-slip curve at an average force applied to each connector. This value of the force applied to each connector used in the re-evaluation of the slip modulus is calculated as the average of the nail forces over the exterior third of the beam from the preceding cycle. Thus, the

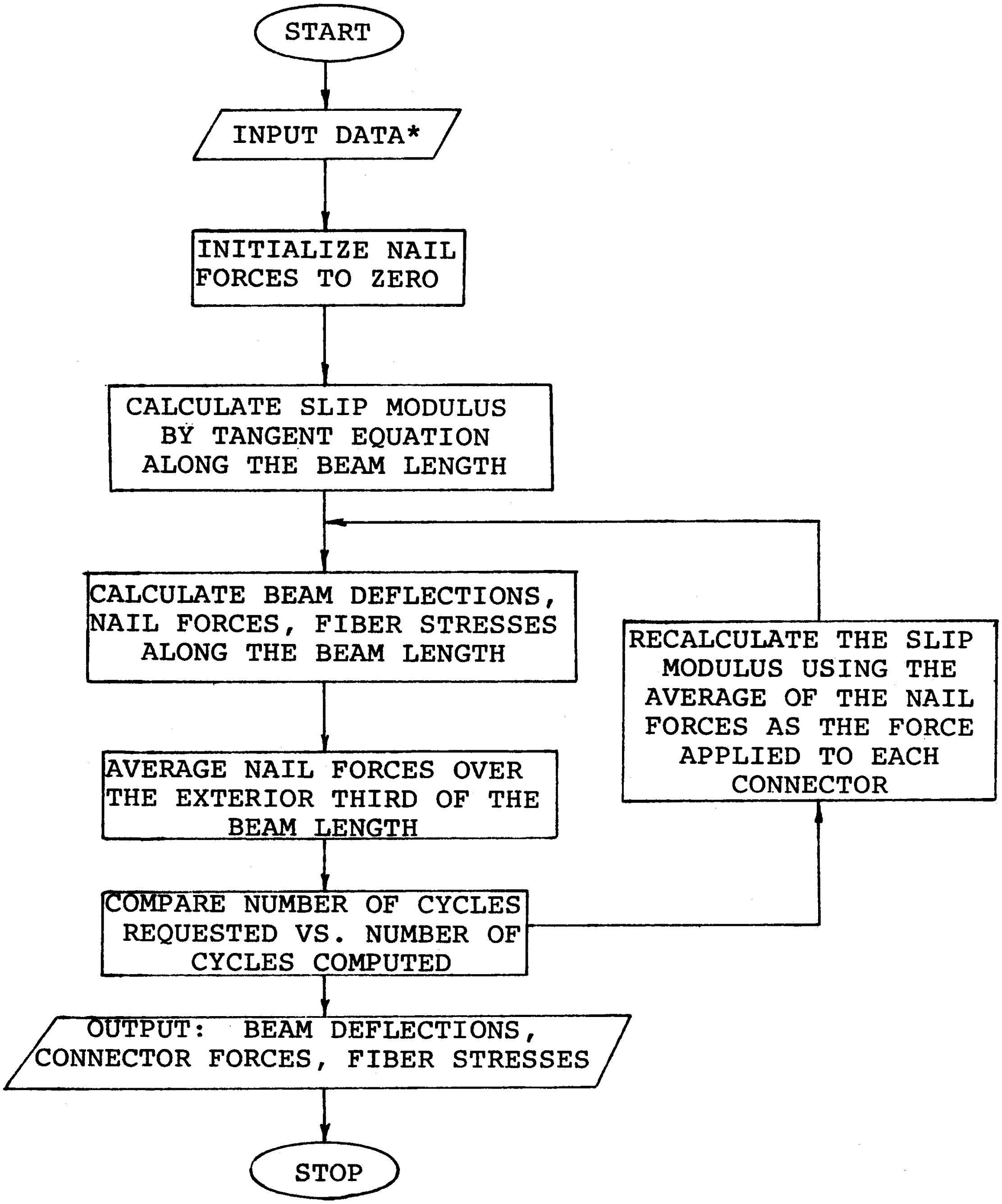

*Input data includes beam and layer dimensions and properties, connector slip modulus equation constants, connector spacing, and number of rows, load increment level and location.

Figure 4.2 Closed form solution computer program flow diagram.

solution proceeds using the tangent from the preceding calculations for the next load.

The closed form solution has some limiting restrictions that are discussed in Section 4.5. These restrictions reduce the capabilities of the closed-form solution to the degree that an approximate but more flexible solution technique is required. A finite element technique solution for the basic mathematical model is presented in the next section. This technique overcomes many of the restrictions of the closed-form method.

4.3 Mathematical Model of T-Beam and Its Finite Element Solution

Thompson et al. (31) developed a solution technique with the versatility to take into account the effects of gaps in the individual layers. This finite element solution method uses the same mathematical model and basic assumptions developed by Goodman (6) and is based on the concept of potential energy.

The energy expression of a layered beam is considered to be composed of the following four potential energy parts:

1. Pure bending of each layer,
2. Axial elongation of each layer,
3. Slip deformation of the connectors between each layer, and
4. The external loads on the beam.

By summing these four forms of potential energy, the total potential energy of an m-layered beam system is

$$J = \sum_{i=1}^{m} \int_{o}^{L} \{\frac{1}{2} E_i I_i (\frac{d^2 y}{dx^2})^2 + \frac{1}{2} E_i A_i (\frac{du_i}{dx})^2 \} dx$$

(bending) (axial)

$$+ \sum_{i=1}^{m-1} \int_{o}^{L} \frac{1}{2}(\frac{k_i n_i}{s_i}) [(U_{i+1} - U_i) - \frac{1}{2}(h_{i+1} + h_i) \frac{dy}{dx}]^2 dx$$

(slip deformation)

$$- \int_{o}^{L} wydx$$

(external loads) (4.14)

where y = beam deflection at load location, inches,

J = total energy, in./lbs.,

u_i = axial displacement in the i^{th} layer, in.,

w = loading on beam, lbs.,

k_i = slip modulus of connector between the i^{th} and $(i + 1)^{th}$ layers, lb/in.,

n_i = number of rows of connectors between the i^{th} and $(i + 1)^{th}$ layers, and

s_i = spacing of connectors between the i^{th} and $(i + 1)^{th}$ layers, in.

The principle of virtual work requires the potential energy to have a stationary value at the equilibrium position of the layered beam, i.e.

$$\delta J = 0 \tag{4.15}$$

where δ = variational operator.

The deflection and axial displacements of the layered beam, which satisfy Eq. (4.15), can be approximated with the finite element form of the Rayleigh-Ritz procedure. An approximate minimization of the functional allows a direct solution of the differential equation (4.15).

The finite element solution technique is formulated by dividing the beam into a series of one-dimensional elements, as shown in Figure 4.3. This arrangement is sufficient since the variables y, the deflection of the beam, and u_i, the axial deformation of the i^{th} layer, vary only along the length of the beam. For each element of the beam, the variables y and u_i are approximated by polynomials in x. Piecewise linear approximating functions are used for the axial deformations u_i and a cubic approximating function is used for the deflections y.

The potential energy for any element, including the contributions from the external load, bending, axial deformations, and interlayer slip is approximated in terms of the nodal point values for the deflection y, the slope dy/dx, and the axial deformation u. Combining all the potential energy terms for the i^{th} element into a single term, J_i, the variation of the potential energy for a single element can be placed in the following form:

$$\delta J_i = \{\delta_s\}_i^T [k]_i \{s\}_i - \{\delta_s\}_i^T \{f\}_i \tag{4.16}$$

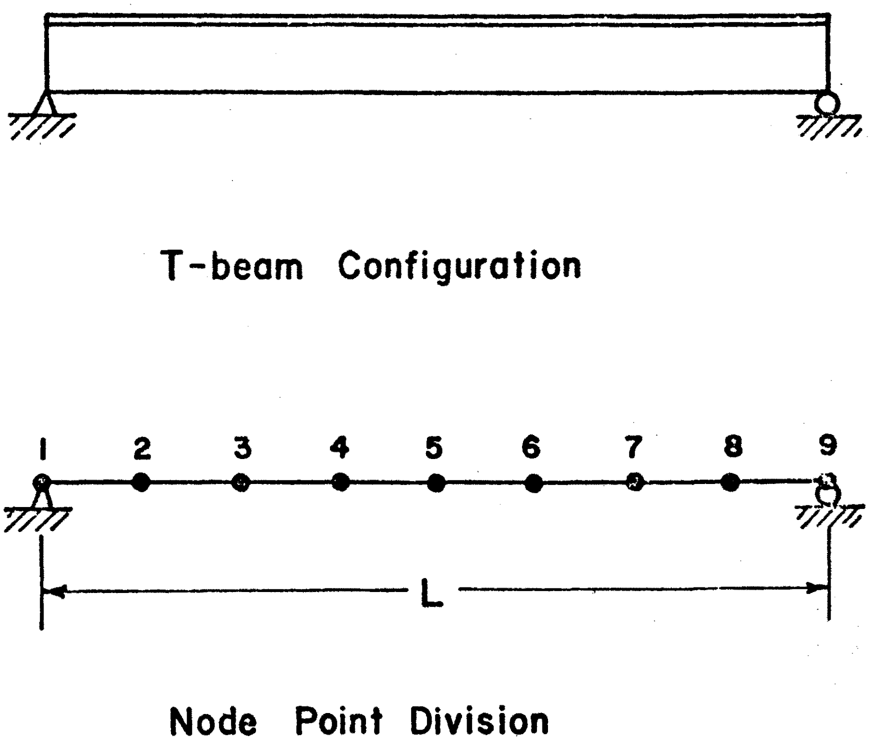

Figure 4.3 Finite element representations.

where $\{s\}_i$ = matrix combining all the generalized displacements for y, dy/dx, u_i,

$[k]_i$ = stiffness matrix for element i, and

$\{f\}_i$ = matrix combining all generalized external force corresponding to $\{s\}$.

The total variation of potential energy is obtained by the direct summation of the element matrices and leads to the general equilibrium equation for the entire beam

$$[K]\{S\} = \{F\} \tag{4.17}$$

where $[K]$, $\{S\}$ and $\{F\}$ are the system equivalents of $[k]_i$, $\{s\}_i$ and $\{f\}_i$.

By solving for the displacement matrix $\{S\}$ in Equation (4.17), the nodal point deflection y_i and slope dy/dx and the axial displacement u_i of each layer are obtained.

The solution technique presented by Thompson et al. (31) used the same mathematical model developed by Goodman (6) which is based on the assumption of a constant slip modulus along the length of the beam. To relieve the finite element method of this restrictive assumption, the nonlinear effect of the connector slip curve was introduced into the solution technique on an element by element basis using a stepwise linear numerical procedure.

Figure 4.4 shows a flow diagram of the computational procedure modified to treat the nonlinearity of the connector slip curve. A listing of the finite element computer program used in this study is presented in Appendix D. This finite element method program computes the nodal point

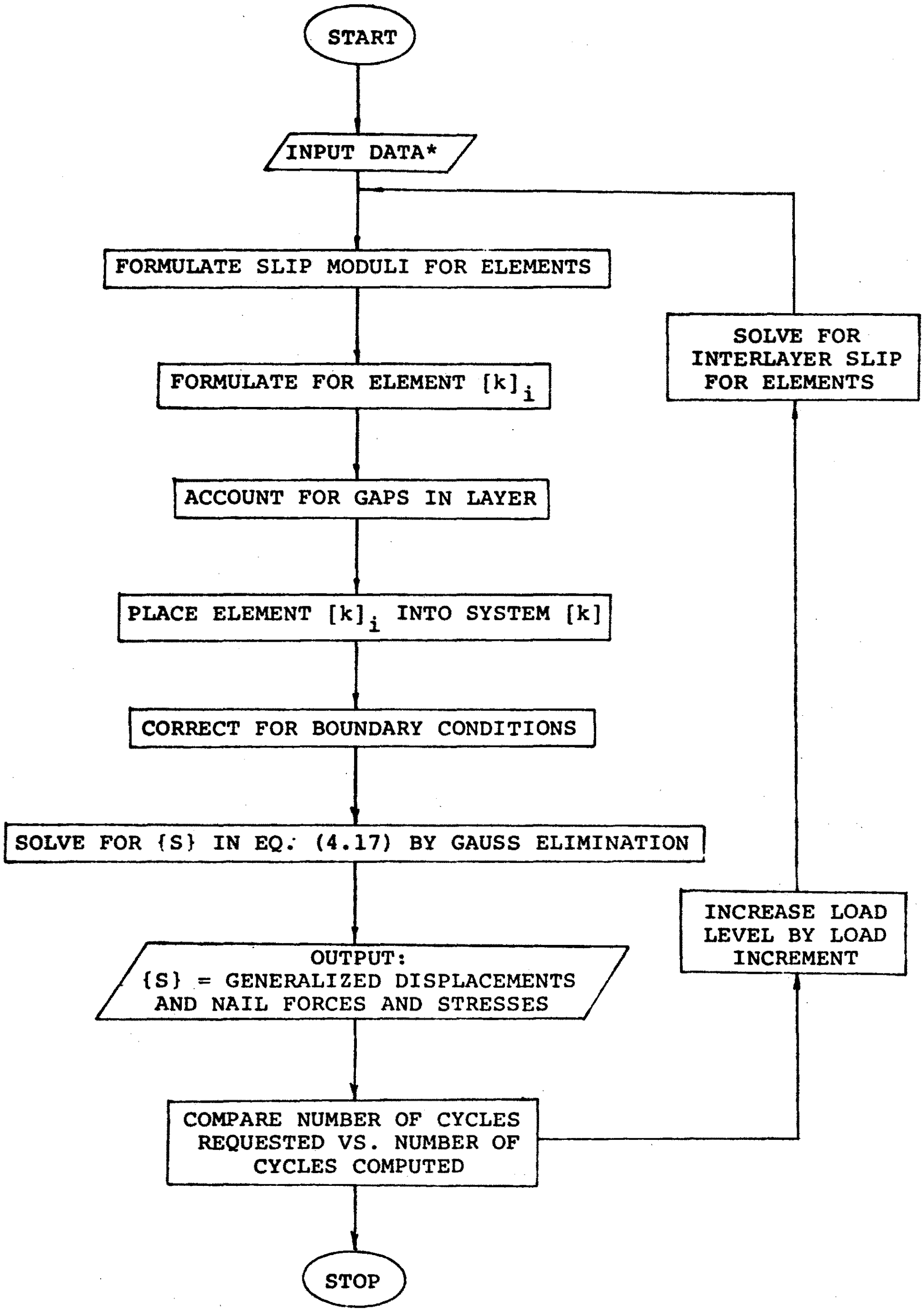

*Input data includes number of elements, layers, and gaps; modulus of elasticity values in bending and axial loading for each layer; dimensions of each layer and nodal point coordinates; connector spacing, and number of rows; load increment level and location.

Figure 4.4 Flow diagram for finite element solution.

deflection, slope and axial deformation of each layer. The slip modulus for each individual element is generated by an equation within the model. This equation is a polynomial expression describing the nonlinear load-slip relationship for the type of connector used in the model. The development of this equation is reviewed in Section 4.4.

A tangent slope value obtained from this equation as shown in Figure 4.3 represents the slip modulus and is a function of the average slip between the layers for each element for the first load increment.

The slip modulus is then reevaluated as a secant slope of the connector load-slip curve for an average slip value for each element. The solution proceeds to the next load increment using the total applied load value and the slip moduli from the preceding calculations (see Figure 4.5).

Discussion of the closeness of the finite element method to the exact (closed form) solution and its advantages is presented in Section 4.5.

4.4 Mathematical Model Slip Curve and Its Curve-fit Solution

To evaluate the slip modulus at varying load levels in the mathematical model, an equation to represent the connector load-slip curve is required. For the closed form solution, an equation used by Goodman (6) and Patterson (25) was selected to quantify the load-deformation behavior of the nailed and glued joints. This equation defines the deformation value in terms of the load variable.

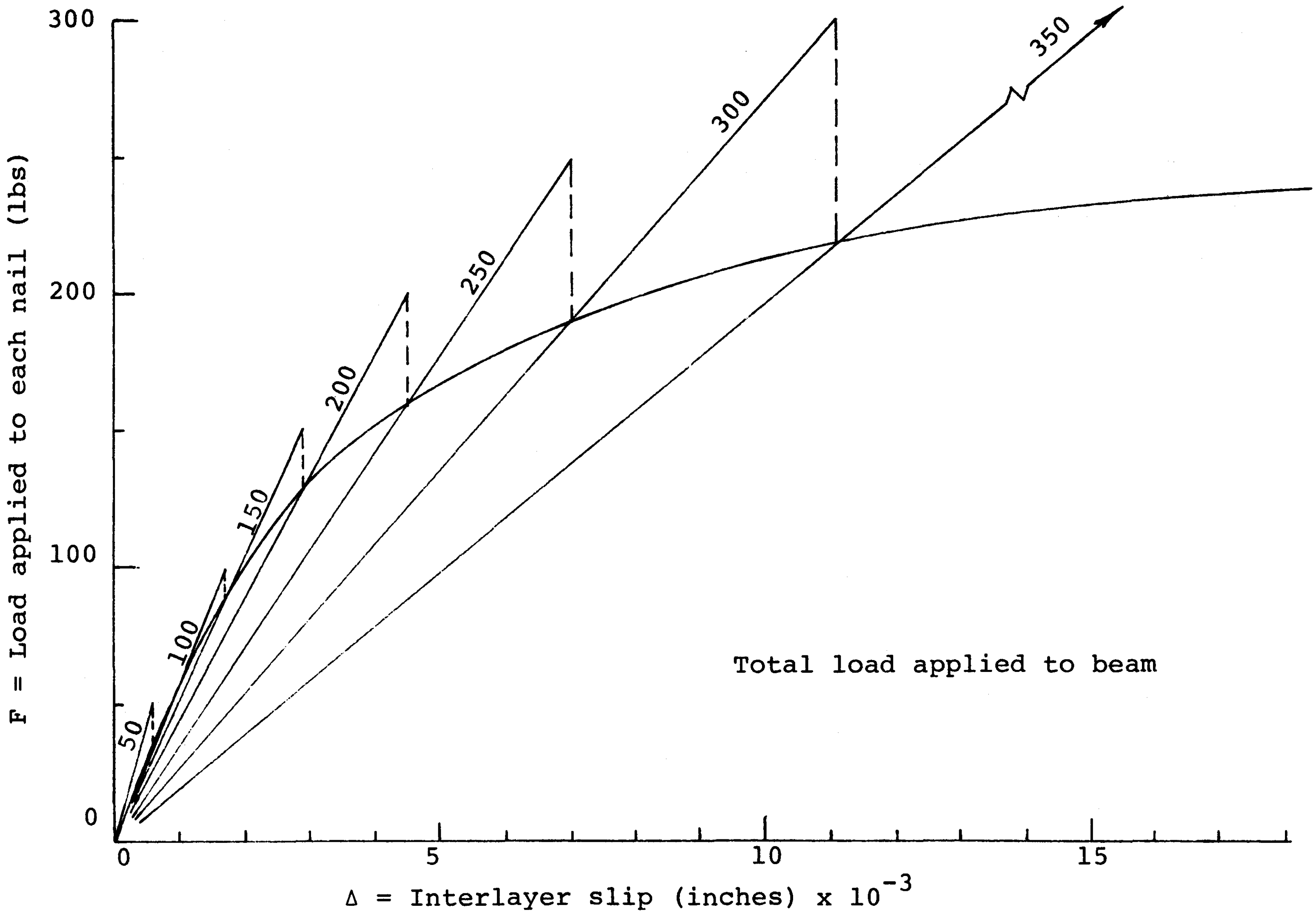

Figure 4.5 Step-wise nonlinear slip modulus procedure.

$$\Delta = C_1(e^{C_2F}-1) - C_3(e^{C_4F}-1) + C_5(e^{C_6F}-1) \qquad (4.18)$$

where Δ = connector deformation, in.,

F = force applied to each connector, lb.,

C_i = constants (i = 1 to 6).

The solution for each type of connector load-slip curves is accomplished by calculating different values for the six unknown constants. Solving for the six unknown constants, is simplified by assuming the values of C_2 to be 0.01, C_4 to be 0.002, and C_6 to be 0.0002. Taking the deformations at three load levels from the plot of the slip curve results in three simultaneous equations with three unknown constant values. Goodman (6) and Patterson (25) presented close curve-fits to the recorded curve to verify this approach.

Since calculations of the slip moduli in the finite element program required a load-slip curve equation defining the connector forces in terms of the solved slip deformation values and not the slip deformation in terms of the solved connector forces, a different curve fit approach to represent the connector load-slip relationship was needed. A least-squares curve fitting formulation was used. The general equation for fitting a set of data with a polynomial of m^{th} degree is conveniently expressed in the following matrix notation (15):

$$[A]\ \{k\} = \{B\}$$

where

$$[A] = \begin{bmatrix} n & \sum x_i & \sum x_i^{\,2} & \cdots & \sum x_i^{\,m} \\ \sum x_i & \sum x_i^{\,2} & \sum x_i^{\,3} & \cdots & \sum x_i^{\,m+1} \\ \vdots & & & & \\ \sum x_i^{\,m} & \sum x_i^{\,m+1} & \sum x_i^{\,m+2} & \cdots & \sum x_i^{\,2m} \end{bmatrix}$$

is a symmetric matrix, and

$$\{k\} = \begin{Bmatrix} k_o \\ k_1 \\ k_2 \\ \vdots \\ k_m \end{Bmatrix}, \qquad \{B\} = \begin{Bmatrix} \sum y_i \\ \sum y_i y_i \\ \sum x_i^{\,2} y_i \\ \vdots \\ \sum x_i^{\,m} y_i \end{Bmatrix}$$

x_i = deformation coordinate for the i^{th} point of the load-slip curve,

y_i = load coordinate for the i^{th} point of the load-slip curve, and

k_i = coefficient constants in the general equation.

Solving for the coefficient constants, the general polynomial equation is:

$$y = k_o + k_1 x + k_2 x^2 + k_3 x^3 + \ldots + k_m x^m$$

A very close curve fit to the connector load-slip curve using the least-squares method in a computer program is shown in Appendix E. A table presenting the coefficient constants in the general polynomial equation and the total summation of the square of the residuals is also shown.

4.5 The Capabilities of the Closed Form and Finite Element Solution Techniques

Although the closed form solution is an exact solution for the mathematical model, its application is limited by its basic assumptions. The assumption of constant section properties along the length of the beam excludes any consideration for gaps, knots, or any other type of weak sections or discontinuities in the beam's layers. The closed form solution also can consider only a constant connector slip modulus as a constant along the length of the beam. Since the slip between the layers varies along the length of the beam, the slip modulus also varies.

The finite element solution technique removes both of these restrictive assumptions of constant section properties and connector slip modulus along the length of the beam. Since these properties are handled on an element by element basis, they can vary for each element. Because of its closeness to the exact (closed form) solution as shown by Kuo (14) for the linear analysis, the finite element method was used to compute the theoretical deflections and other values in all of the subsequent verification calculations. The verification of the nonlinear mathematical model is presented in Chapter 5.

CHAPTER V

VERIFICATION OF A NONLINEAR MATHEMATICAL MODEL FOR T-BEAM BEHAVIOR

5.1 Introduction

A major objective of this part of the study is to assess the verification of the nonlinear mathematical model at high load levels. Verification of the developed nonlinear mathematical model will be based on the favorable comparison of the results of the specimens tested to failure or beyond the working load range. Although the intent of this study is to assess the reliability of the nonlinear mathematical model at overload levels, a study of the effect of gaps on the reliability of the mathematical model in the working load range is also presented. The selection of material parameters such as MOE of the joists and sheathing materials used in the finite element solution of the nonlinear mathematical model is discussed in Section 5.2. Comparison of the deflections measured during the T-beam tests and those computed using the nonlinear mathematical model are presented in Section 5.3.

5.2 Computation of Deflections Using the Mathematical Model

The variable parameters utilized in the mathematical model are the geometrical and mechanical properties of the materials and connectors used in the T-beam specimens. Descriptions of the procedures used to obtain the mechanical properties of the components and the connectors are presented in Chapter III. A short discussion of the input data is presented in Chapter III. A short discussion of the input data is presented to illustrate how the mathematical model handles the specimen variables in the theoretical deflection calculations.

The material properties of each piece of lumber and sheathing were individually determined before and during the T-beam construction. The dimensions of the joists and MOE values of the sheathing material used were those measured in the Wood Science Laboratory (19). To obtain a better estimate of the actual MOE for the joists, the MOE value obtained from edgewise orientation of the joist was measured during the construction of the specimens and used as an input variable. The sheathing MOE values as determined by McLain (19) in the directions parallel and perpendicular to the face grain were used.

For the joists, the MOE values were assumed to be constant along the joist length and equivalent for both bending and axial loading throughout the joist depth and length. This is equivalent to assuming the material to be homogeneous. This assumption cannot be made for the sheathing material since the effect of ply thickness and orientation on the bending and axial stiffness is significant. A detailed discussion of this problem is presented by Liu (18).

The mechanical properties in the two principal directions of plywood are different due to the orthotropic nature of wood and the orthotropic orientation of the adjacent plies of the plywood. The MOE values determined by McLain (19) were given as gross values valid for bending only and were based on the moment of inertia of the nominal thicknesses of the plywood. These values are different from those valid for use with the transformed sections. A conversion factor, k*, which converts the effective bending MOE values to the effective axial MOE values can be determined for each plywood species and thickness. The value of k* is computed by the following relationship:

$$k^* = \frac{I_{gr} A_{tr}}{I_{tr} A_{gr}}$$

where A_{gr} = gross cross section area of the material, in.^{2}

A_{tr} = transformed cross section area, in.^{2}

I_{tr} = moment of inertia based on the transformed section, in.^{4}, and

I_{gr} = the moment of inertia of the material based on gross dimension, in.^{4}

The analysis program was written for input of the gross axial and bending MOE values based on the nominal section dimensions and utilizing the k* factor to adjust, as necessary, for axial or bending stress.

As a result of the production process of the particleboard (21), the MOE values differ in the lengthwise and the crosswise directions. The MOE values of particleboard for bending and for axial loading in the same direction were assumed to be equal.

The slip modulus for both the nails and elastomeric adhesive connectors is handled by using the nonlinear equation derived by a least-squares curve fit process for an average slip curve determined by the Wood Science Laboratory (26), as discussed in Chapter IV. This slip modulus equation is incorporated in the finite element program to provide the input data for the mechanical behavior of the interlayer connection. The geometric property values for the connectors required as input data include the type of connection used (nails or glue), the connector spacing, and the number of rows of connectors.

A description of all parameters used in the computation of the deflections for each T-beam are included in the beam configuration diagrams in Appendix C.

The remainder of the input variables for the finite element solution concern the T-beam configuration with appropriate gap data and the loading arrangement. The element division of a typical T-beam analyzed by the finite element method solution is shown in Figure 5.1.

Since the introduction of gaps significantly increased the deflections in the experimental study, the effects of the sheathing joints present in all the specimens were important and had to be carefully modeled. The comparison of theoretical deflections computed with and without the assumption that the sheathing layers are continuous presented in Kuo's work (14) demonstrates that the gap effect

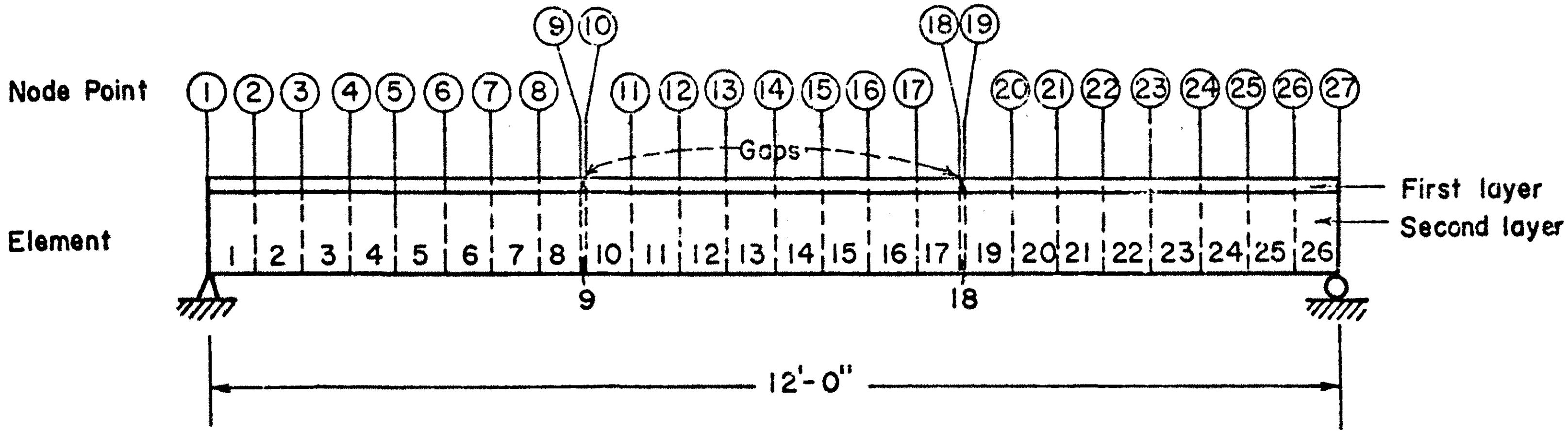

Figure 5.1 Typical T-beam elements used in computer program input.

can be sizable. The completely open gap is easily handled by the finite element solution technique. The length of an open gap element is assumed to be zero. The open gap is accounted for by using discontinuous linear functions to approximate the deflection. Thus, when an open gap is encountered in a given layer, the axial displacement in that layer is assumed no longer continuous and the axial force becomes zero.

In most of the experimental specimens, a glued or tightly butted sheathing joint was constructed. To properly model this sheathing joint, a flexible gap was introduced. These joint elements were assumed to have a finite length (about 1/8 in.) and a low joint stiffness. To handle the joint stiffnesses, MOE values for the joint elements were assumed ranging from 500 psi for tightly butted joints to about 5000 psi for glued joints. These values of MOE are based on the relative stiffness qualities of the joints in bending and axial loading. Since these values are very low compared to the plywood MOE, their numerical values are not as critical as their relative values.

The configuration of all the T-beam model elements is described in the finite element program by defining coordinates of the nodal points along the length of the beam and at the location of the gap elements.

Since the finite element solution is handled by a stepwise linear type procedure as shown in Figure 4.6, the number of increments desired is input along with the load increment applied at each nodal point.

5.3 Comparison of Experimental and Theoretical Values

Comparisons of the deflections observed during the experimental tests and the computed deflections are presented in Appendix C for the sixteen two- and three-layered T-beam specimens and will be discussed in length in this section. This discussion is handled by presenting a general example of a typical specimen comparison as shown in Appendix C followed by general comments concerning these results. Additional comments regarding each specimen's results will also be presented. A concentrated load at the midspan of the specimen was selected as the loading case for each of the specimens.

The figures in Appendix C include a load-deflection plot for each specimen for midspan of each joist and a deflection profile along the length of each joist for a selected loading case. Results from a typical two-layered nailed T-beam specimen are presented in Figure 5.2. This specimen, T7-8D16-1, was constructed with 2 x 8 Douglas-fir joists and 3/4 inch thick Douglas-fir plywood nailed with 8d common nails spaced 2 inches apart. The sheathing joints were tongue and groove and tightly butted together. This T-beam specimen was loaded to failure. The failure occurred in joist J-01. The load-deflection plot shows good agreement between the measured and predicted values beyond the working load range for the joist loaded to

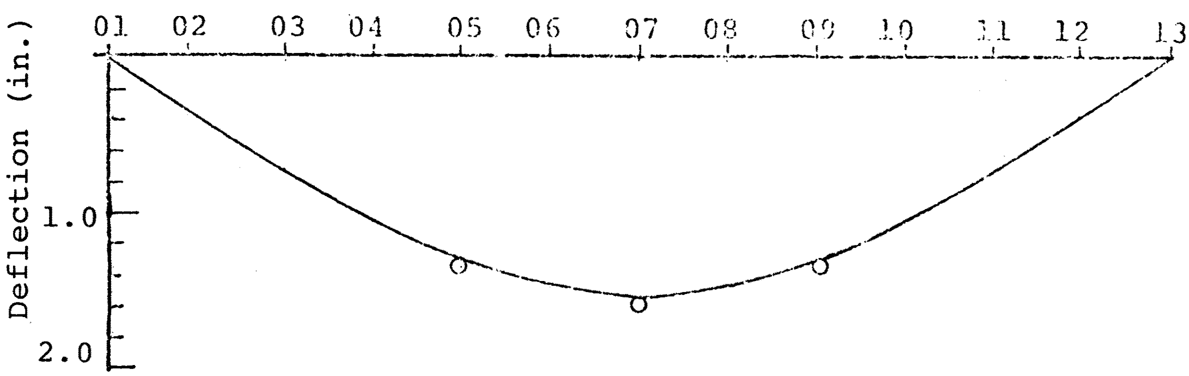

a) Deflection Profile at 3500 lbs.
Load at Midspan

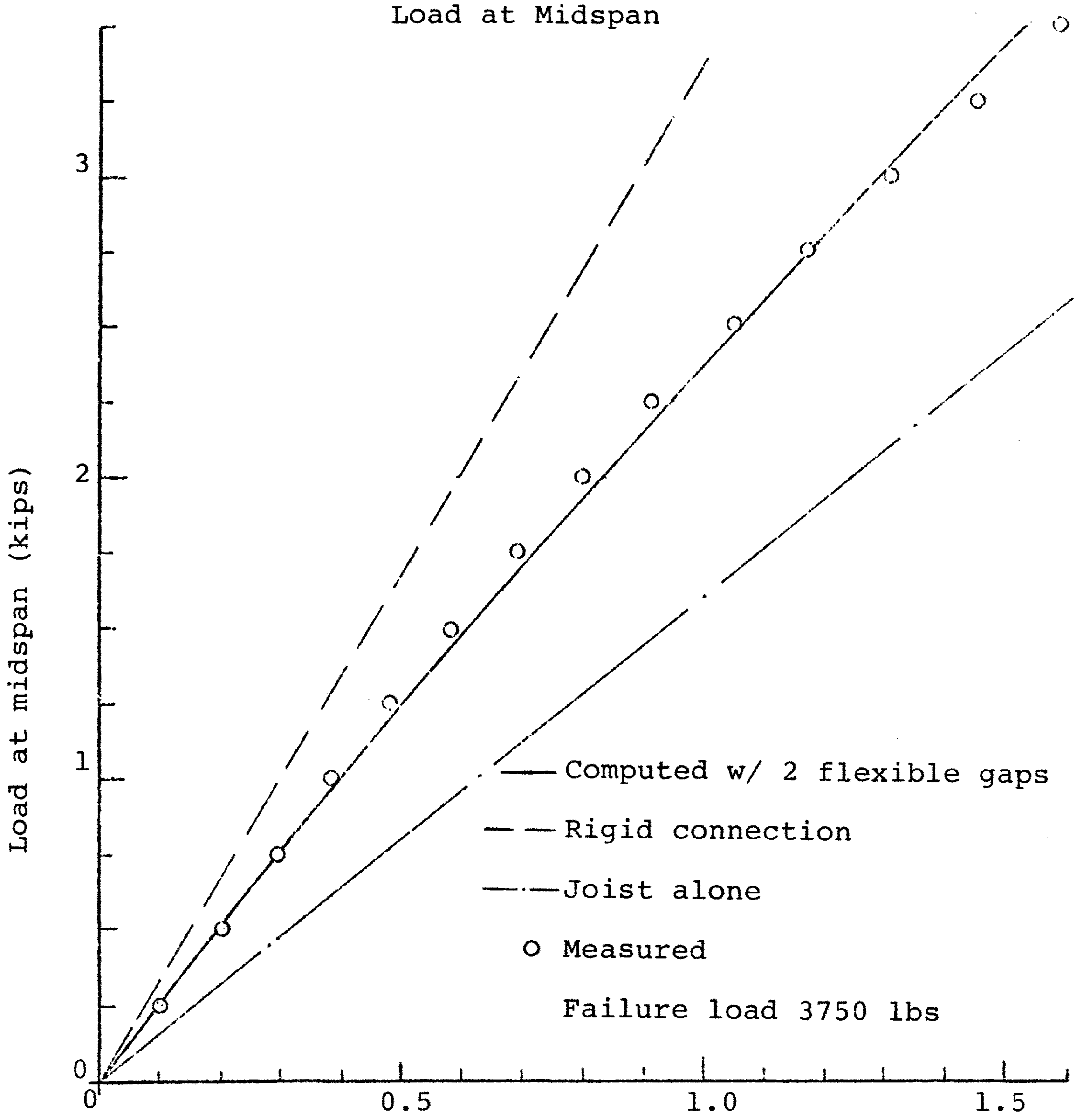

b) Load-Deflection Behavior

Figure 5.2 Example of beam verification T7-8D16-1 Joist J01 failure. This plot displays the nonlinear load-deflection behavior typical for the T-beam specimens. The deflection profile presented shows good agreement between the computed and measured deflections along the length of the beam.

5.3.1 Results of Verification Study for Beams Tested Beyond the Working Load Range

Verification of the nonlinear model for loadings above the working load range is discussed in this section. The reason for utilizing the nonlinear mathematical model to assess the behavior of the T-beam to failure is the need to handle the nonlinear slip characteristic of the connection between the layers beyond the working load range. In the construction procedure of the test specimens, a double T-beam configuration was used to provide the specimens with stability during the testing procedure. Both joists in each specimen were selected to have similar MOE values. Since both T-beam joists in each specimen had similar stiffnesses and were loaded to the same load level, it may be assumed that when one of the T-beam joists failed, the other joist in the specimen was near its ultimate capacity.

The comparison of the measured and predicted midspan deflections for all of the T-beams tested beyond the working load range is presented in Table 5.1. With the exception of a few cases that will be discussed later. good agreement was generally obtained. The average absolute difference and the average algebraic difference between the predicted

Table 5.1 Comparison of Measured and Predicted Midspan Deflections for T-Beams Tested Beyond Working Load Range

Specimen	Joist No.	Joist Description	Sheathing Description	Connector Description	Load Level** (lbs)	Observed Deflection Δm (in.)	Computed Deflection Δc (in.)	Δc/Δm	Sheathing Remarks
T6-8D16-1	1*	2x8 Douglas-fir	3/4" Douglas-fir plywood	8d common nails @ 8" c-c	2750	1.59	1.390	.874	2 flexible gaps
	2				2750	1.44	1.428	.992	
T7-8D16-1	1*	2x8 Douglas-fir	3/4" Douglas-fir plywood	8d common nails @ 2" c-c	3500	1.59	1.540	.969	2 flexible gaps
	2				3500	1.67	1.579	.946	
T8-8D16-1	1*	2x8 Douglas-fir	3/4" Douglas-fir plywood	glue & 8d common nails @ 8" c-c	2750	1.66	1.640	.988	2 open gaps
	2				2750	1.69	1.715	1.015	
T11-8D16-1	1*	2x8 Douglas-fir	3/4" Douglas-fir plywood	glued	1750	1.69	1.590	.941	1 open gap @ center-line
	2				1750	1.67	1.556	.932	
T14-12D24-2	1[a]*	2x12 Douglas-fir	1/2" Douglas-fir plywood & 1/2" particle board	8d common nails @ 8" c-c & 6d common nails @ 8" c-c	4000	.79	.736	.932	3 open gaps
	2[a]				4000	.816	.788	.965	
T15-8E19.2-2	1*	2x8 Engelmann spruce	1/2" Engelmann spruce plywood & 1/2" particle board	8d common nails @ 8" c-c & 6d common nails @ 8" c-c	2000	2.07	2.140	1.034	5 open gaps
	2				2000	2.00	2.140	1.070	
T16-8E19.2-2	1	2x8 Engelmann spruce	1/2 Engelmann spruce plywood & 1/2" particle board	8d common nails @ 8" c-c & 6d common nails @ 8" c-c (2 rows)	1500	1.23	1.255	1.020	3 flexible gaps
	2*				1500	1.49	1.477	.991	
T17-8D16-1	1	2x8 Douglas-fir	3/4" Douglas-fir plywood	8d common nails @ 8" c-c	3000[b]	1.58	1.469	.930	2 flexible gaps
	2*				5000	3.04	2.690	.885	
T18-8D16-1	1	2x8 Douglas-fir	3/4" Douglas-fir plywood	glue	3500	1.62	1.205	.744	2 flexible gaps
	2*				3500	1.94	1.313	.677	

* tested to ultimate failure
** last load level at which deflections were recorded before failure
[a] failed by local failure but sustained additional load before ultimate failure
[b] see discussion in Section 5.3.3.

Table 5.2 Comparison of Measured and Predicted Deflections for T-Beams Tested to Failure

Specimen		Row No. (dial gage location along the beam length)			Sheathing Remark	Connection Type	Midspan Load Level
		05*	07*	09*			
T6-8D16-1 Joist J-01	Measured, in.	1.36	1.59	1.33	2 flexible gaps	8d common nails @ 8" c-c	2750 lbs.
	Predicted, in.	1.183	1.390	1.183			
	Difference, %	-13.0	-12.6	-11.0			
T7-8D16-1 Joist J-01	Measured, in.	1.37	1.59	1.34	2 flexible gaps	8d common nails @ 2" c-c	3500 lbs.
	Predicted, in.	1.311	1.540	1.311			
	Difference, %	- 4.3	- 3.1	- 2.2			
T8-8D16-1 Joist J-01	Measured, in.	1.42	1.66	1.41	2 open gaps	glue & 8d common nails @ 8" c-c	2750 lbs.
	Predicted, in.	1.402	1.640	1.402			
	Difference, %	- 1.3	- 1.2	- 0.6			
T11-8D16-1 Joist J-01	Measured, in.	1.36	1.69	1.34	1 open gap @ centerline	glue	1750 lbs.
	Predicted, in.	1.304	1.594	1.304			
	Difference, %	- 4.1	- 5.9	- 2.7			
T14-12D24-2 Joist J-01	Measured, in.	0.68	0.79	0.69	3 open gaps	8d common nails @ 8" c-c & 6d common nails @ 8" c-c	4000 lbs.
	Predicted, in.	0.627	0.737	0.627			
	Difference, %	- 9.3	- 6.7	- 9.1			
T15-8E19.2-2 Joist J-01	Measured, in.	1.37	1.64	1.39	5 open gaps	8d common nails @ 8" c-c & 6d common nails @ 8" c-c	1500 lbs.
	Predicted, in.	1.295	1.520	1.295			
	Difference, %	- 5.5	- 7.3	- 6.8			
T16-8E19.2-2 Joist J-02	Measured, in.	1.34	1.49	1.39	3 flexible gaps	8d common nails @ 8" c-c & 6d common nails @ 8" c-c (2 rows)	1500 lbs.
	Predicted, in.	1.257	1.477	1.257			
	Difference, %	- 6.2	- 0.9	- 9.6			
		04*	07*	09*			
T17-8D16-1 Joist J-02	Measured, in.	1.061	1.580	1.077	2 flexible gaps	8d common nails @ 8" c-c	3000 lbs.
	Predicted, in.	1.049	1.528	1.049			
	Difference, %	- 1.8	- 3.3	- 2.6			
T18-8D16-1 Joist J-02	Measured, in.	1.01	1.52	0.98	2 flexible gaps	glue	3000 lbs.
	Predicted, in.	0.763	1.095	0.763			
	Difference, %	-24.5	-30.0	-22.1			

* See Figure 2.4 for deflection locations

values and the observed values at maximum load for the nailed connectors are 5.4 and 3.3 percent, respectively.

Only three T-beams with glued connections were tested, thus the large differences between the predicted values and the observed values for T-beam T18 (refer to Table 5.2) greatly effect the average differences calculated for all of the glued specimens. Since it appears that the model predicts a considerably stiffer behavior than observed for T-beam T18, this beam seems to be a special case. Possibly the slip modulus used for the glued connection in the mathematical model of specimen T18 overestimates the value actually effective in this specimen. Thus, the average absolute difference and the average algebraic difference between the predicted values and the observed values for the T-beams with glued connectors excluding the T18 specimen are 4.0 and 3.1 percent, respectively, and, including the T18 specimen's results, 12.1 and 11.7 percent, respectively. For the average absolute difference and average algebraic difference for all of the T-beams tested beyond the working load range, the values are 7.6 and 6.1 percent, respectively.

An inspection of Appendix C indicates that the deflection profiles show good agreement between the computed and measured deflections not only at midspan but along the length of the beam when the specimens were loaded to near failure. Table 5.2 compares the predicted and measured deflections for three locations along the length of these

T-beam specimens. With the exception of T-beam specimen T18-8D16-1 the computed and observed deflections for the joist that failed at ultimate load agree within 13.0 percent for these specimens listed in Table 5.2. The discrepancy in T-beam T18-8D16-1 will be discussed later.

The efficiency of each type of connector used in each T-beam specimens tested to failure can be seen in Appendix C. The T-beams constructed with glued and/or nailed types of connectors display deflections between those calculated with and without rigid connectors. Glued connectors show a higher degree of rigidity than do the nailed connectors as can be seen by comparing the load-deflection plot of the glued T-beam specimen T18 with that from a nailed specimen with otherwise similar material properties such as T6. As would be expected, the closer the nails were spaced in the nailed connectors, the higher the resulting rigidity. In general, good agreement exists between the predicted and measured deflections for the nailed connectors. For the glued connections, the model generally predicts a stiffer beam behavior than measured, possibly due to insufficient evaluation of the slip modulus for the glued connections, particularly for shear stresses beyond the working load range.

As shown in the discussion of the results in this section, the nonlinear analysis with only the load-slip nonlinearity being considered, is able to fit the T-beam load-deflection curve up to maximum load. This nonlinear analysis did not consider the material nonlinear stress-strain relationship in compression because the compressive stresses do not generally reach the nonlinear level in the composite T-beam as they do in the rectangular beam as shown by Zakic (34).

5.3.2 Results for Beams Tested in the Working Load Range

A study of the behavior of T-beam specimens tested only in the working load range was conducted using the nonlinear mathematical model. Kuo (14) has presented a similar study in the working load range using a constant slip modulus. This study for the low load range was conducted to investigate the effectiveness of the nonlinear model in the working load range as compared to the linear model presented by Kuo (14). The nonlinear mathematical model shows no significant improvement over the linear model in the working load range. This study also served the important purpose of verifying the ability of the nonlinear model to handle the different cases of discontinuities in the sheathing joints. The significance of this verification will be evident in the study of the effect of gaps on fiber stresses and connector forces in the next chapter.

The significant effect of the sheathing joint conditions on the measured deflections and the deflections calculated by the nonlinear model is shown in Appendix C. Even though T-beam specimens T9, T10, and T12 were not used in the overload verification study for the mathematical model, comparisons of the effects on the actual T-beam specimen and the T-beam model of increasing numbers of open gaps in the T-beams is shown in the load-deflection plots for these specimens. As the number of gaps increase, the deflection also increases. For the extreme case of many gaps, the load applied may be considered to be carried primarily by the joist alone since the effect of composite action is minimal.

Comparison of the measured and predicted midspan deflections for the T-beams tested only within the working load range is presented in Table 5.3. These specimens were not included in the verification study, but rather were included to study the effects of gaps on the behavior of the T-beam specimens. Comparison of these measured and predicted midspan deflections shows generally good agreement, but this correlation is no better than the correlation existing in Kuo's work (14). Thus, in the working load range the nonlinear mathematical model shows no significant improvement over the linear model since the calculated and actual deflection correlation is not improved significantly and increased computer time used by the iteration technique does not justify the small improvement. However, by comparing the midspan deflection values for the T-beams tested to failure, the linear model predicts the beams behavior to be too stiff by an average algebraic difference of 16.7 percent as compared to 6.1 percent for the nonlinear model. By comparison of these differences and by inspection of the typical T-beam specimen in Figure 5.3, the improvement of the nonlinear mathematical model over the linear model in

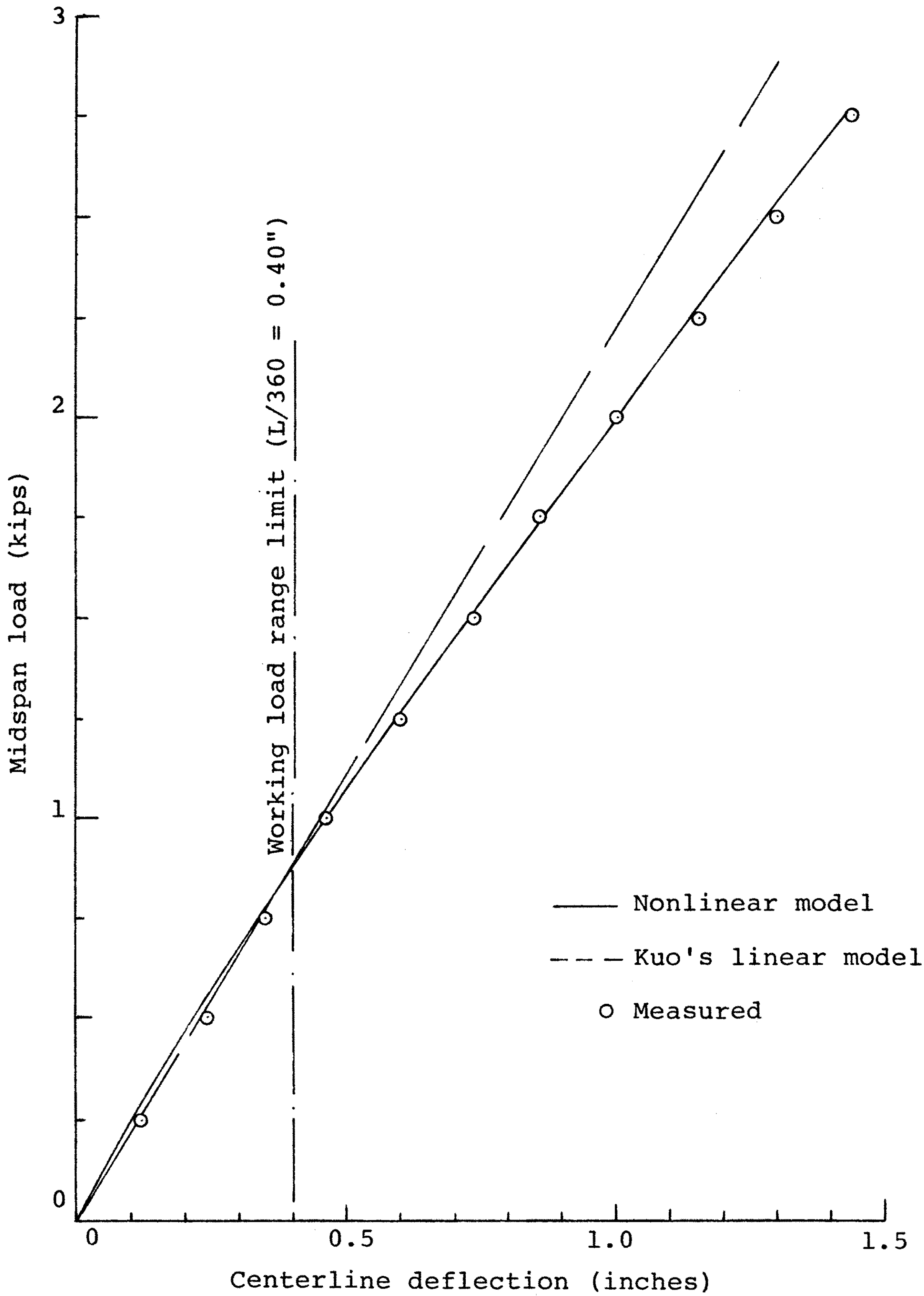

Figure 5.3 Results for T6-8D16-1 J-02.

the ultimate load range is significant, thus proving the advantage of the nonlinear model over the linear model in the ultimate load range and its effectiveness in predicting the T-beam failure loads.

5.3.3 Discussion of T-beam Specimens

For a detailed description of the results of the plots in Appendix C, a short discussion of each T-beam specimen and its results will now be presented.

T-beam specimen T3-8D16-1 and T5-8D16-1 (nails at 8 inch spacings

An inspection of the comparison of the observed deflections and the calculated deflections of the limiting case considering only the joist revealed a discrepancy. The recorded values for the actual deflections were larger than the corresponding calculated values for the deflection of the joist only. Since this relationship is erroneous, these specimens were not included in the verification study.

T-beam specimen T6-8D16-1 (nails at 8 inch spacings)

Good agreement between the observed and calculated deflections is exhibited by joist J-02, but for joist J-01, this agreement is not as favorable. An investigation of the load-deflection plot in Appendix C gives a clue to a probable cause for this discrepancy. The stiffness of the connectors decreases as the load exerted on them increases until the connectors have no significant increase in stiffness. This is equivalent to the limiting case of a constant connection force between the layers and the resulting deflections are computed using the stiffnesses of the joist only and the additional constant value transmitted to the joist by the sheathing through the connection. Thus the slope of the load-deflection plot of the T-beam specimens must always be greater than or equal to the slope of the limiting case of the joist only. The slope of the actual deflection plot is not greater than the slope of the joist only deflection plot in the higher load range. Thus it can be concluded that the stiffness value of the joist (MOE) used in the mathematical model for joist J-01 is slightly erroneous.

T-beam specimen T7-8D16-1 (nails at 2 inch spacings)

The load-deflection plot for both joists of this T-beam specimen show good agreement in Appendix C. This specimen is used in the verification study of the mathematical model.

T-beam specimen T9-8D16-1 (glued connector)

In the low load range, no favorable agreement exists for the comparison of the computed and observed values of the deflections of both joists. The computed deflection results of the mathematical model are significantly stiffer than the observed results in the low load range. This additional stiffness is attributed to the elastomeric adhesive connector. Due to a lack of thorough evaluation of the load-slip curve for the elastomeric adhesive connector, the load-slip curve for the glued connector showed a load-slip connection relationship that was too stiff. This caused the slip moduli to be significantly too stiff for the glued connector in the lower load range.

The abrupt change in the slope of the actual load-deflection curve for the T-beam specimens is due to the closure of the open gaps or the tightening up of the flexible gaps in the sheathing layer. Since this T-beam specimen was not tested to ultimate failure, it is not used in the verification study.

<u>T-beam specimen T8-8D16-1 (glue plus nails at 8 inch spacings)</u>

Although favorable agreement exists in the high load range for both joists of the T-beam specimen, this does not hold true for the low load range. The deflection results of the mathematical model are significantly stiffer than the observed results in the low load range (see graph in Appendix C). This discrepancy is caused by the combined glued and nailed connector. Since no study was conducted for the glue plus nail connector, the elastomeric adhesive connector was used in the mathematical model. As discussed in T-beam specimen T9-8D16-1 the use of the glued connector results in a significantly stiffer mathematical model than the actual specimen in the low load range.

<u>T-beam specimen T10-12E24-1 and T12-8D16-1 (nails of 8 inch and 6 inch spacings, respectively)</u>

Since these specimens were tested only in the elastic range, they could not be used in the verification study. But it can be observed in these specimens the effect of gaps on the deflection behavior of the T-beam. As the number of open gaps is increased, the performance of the T-beam specimen converges to that of the joist only.

T-beam specimen T11-8D16-1 (glued connector)

Favorable agreement is shown in the high load range for both joists of the T-beam specimen but not in the low load range. As discussed in T-beam specimen T9-8D16-1, this discrepancy is attributed to the use of the glued connector. Since this specimen was tested to failure, it is used in the verification study.

T-beam specimen T13-8D16-1 (nails at 4 inch spacing), T15-8E19.2-1 and T16-8E19.2-1 (nails at 8 inch spacings)

Although favorable agreement exists for both joists of the T-beam specimen, it was not used in the verification study because it was tested only in the elastic range.

T-beam specimen T14-12024-2 (nails at 8 inch spacing)

During the testing procedure of this specimen, initial failure occurred at the load level of 8000 pounds evenly distributed between each joist. This failure was an initial crack in joist J-01 but the specimen sustained additional loading until ultimate failure occurred at 14,000 pounds. For the verification study, the failure load is considered to be that load which caused the initial crack in joist J-01 since this caused an abrupt deflection in joist J-01, a change in the stiffness property of that joist and an uneven distribution of the load to each joist of the T-beam specimen. In the load range preceding the initial failure load, good agreement exists for both joists of the T-beam specimen.

T-beam specimen T15-8E19.2-2 and T16-8E19.2-2 (nails at 8 inch spacings)

The load-deflection plot for both joists of this T-beam specimen showed good agreement as shown in Appendix C. This specimen is used in the verification study of the mathematical model.

T-beam specimen T17-8D16-1 (nails at 8 inch spacings)

Favorable agreement exists for the load-deflection plots for joist J-01 of this specimen. Deflection measurements for joist J-01 were recorded only in the load range up to 3000 pounds because the actual deflections exceeded the deflection range of the LVDT's beyond this load range. Deflections were recorded to failure for joist J-02. Inspection of the load-deflection plot for joist J-02 reveals a discrepancy in the actual deflection curve which indicates an actual deflection greater than the calculated deflection for the joist only in the high load range. This erroneous fact can be attributed to a miscalculated MOE value for joist J-02, a crushing effect at the joist support, or a twisting effect of the joist causing a larger deflection to be recorded. In the load range up to 3000 pounds, good agreement is shown in the load-deflection plots for joist J-02. But beyond this load range, the correlation between the load-deflection plots deteriorates.

T-beam specimen T18-8D16-1 (glued connector)

As discussed for T-beam specimen T9-8D16-1, the use of the glue connector in the mathematical model results in a stiffer T-beam model than actually exists. The correlation between the computed deflections and the observed deflections follows this pattern of a T-beam model that is too stiff.

The favorable comparisons presented in Appendix C and discussed in this chapter demonstrate the general validity of the nonlinear mathematical model. This model has been shown to closely predict the behavior of nonrigidly connected composite beams over a wide range of conditions. Since the mathematical model has been verified a meaningful study of the fiber stresses and connector forces was possible. This study and its results are presented in the next chapter.

CHAPTER VI

MEMBER STRESSES AND CONNECTOR FORCES

6.1 Introduction

The mathematical model incorporating the nonlinear slip curve and verified in the previous chapter was used in the study of the member stresses and connector forces presented in this chapter. The governing equations incorporated in the model to allow calculation of the member stresses and connector forces will be presented in Section 6.2. A study of the stresses computed by the nonlinear mathematical model and the stresses obtained by using the limits of rigid connectors and no connectors is presented in Section 6.3 at load levels beyond the working load range. The effects of gaps on the maximum member stresses computed by the nonlinear model in the working load range are also studied in this section. The maximum values for the connector forces computed by the nonlinear model at load levels beyond the working load range and those obtained by using the upper limit of rigid connectors are compared in Section 6.4. A study of the effects of gaps on the maximum connector force and the connector force distribution along the length of the beam computed by the nonlinear model is also presented in Section 6.4. Comparisons of the predicted stresses and connector forces with those specified in the National Design Specifications (20) are presented in Sections 6.3 and 6.4.

6.2 Governing Equations for Member Stresses and Connector Forces in the Finite Element Solution Technique

The finite element solution of the mathematical model extended to incorporate nonlinear connector slip curve has also been extended to allow determination of the member stresses and the connector forces. These values are calculated on an element-by-element basis using the values of deflection, slope, and axial displacement at each nodal point obtained from the displacement matrix (see Section 4.3).

The stresses are caluculated at the top and bottom of each beam layer by utilizing the basic stress-strain equations for the system, resulting in

$$\sigma_{ij} = E_{ai}\varepsilon_{ai} + E_{bi}\varepsilon_{bj} \tag{6.1}$$

where σ_{ij} = stress in beam layer i at layer depth j,

ε_{ai} = axial strain in beam layer i,

ε_{bj} = bending strain in beam layer i at layer depth j,

E_{ai} = axial MOE, psi, and

E_{bi} = bending MOE, psi.

Since the values of E_a and E_b are input variables in the program, the only unknowns needed in the calculations are the values for ε_{ai} and ε_{bi}. Using the values for nodal point slope and axial deformation obtained from the finite element solution, the equations for the axial and bending strains are:

$$\varepsilon_{ai} = \frac{(u_{i,n+1} - u_{i,n})}{\ell} \tag{6.2}$$

and

$$\varepsilon_{bi} = \frac{(\frac{dy}{dx})_{n+1} - (\frac{dy}{dx})_n}{\ell} \tag{6.3}$$

where $u_{i,n}$ = axial deformation in i^{th} beam layer at the n^{th} nodal point, in., and

$(\frac{dy}{dx})_n$ = slope of all layers at the n^{th} nodal point,

ℓ = element length between nodal points n and $n+1$, in.

By substituting the values for strain from equations (6.2) and (6.3) into equation (6.1), the stresses can be obtained.

The connector forces are determined using the solution results for nodal point slope and axial deformation along with the least-squares fit curve describing the load-slip relationship. The value for the average interlayer slip between the layers for each element is required to solve for the connector forces and can be determined using the following equation:

$$\Delta_{i,i+1} = U_{ave}(i+1) - U_{ave}(i) - \frac{1}{2}(h_i + h_{i+1}) \left(\frac{dy}{dx}\right)_{ave} \tag{6.4}$$

where $\Delta_{i,i+1}$ = average interlayer slip between i^{th} and $i+1^{th}$ layers for the n^{th} element, in.,

$U_{ave}(i)$ = average axial deformation for the n^{th} element $(U_{ave} = \frac{1}{2}(U_n + U_{n+1}))$, in.,

h_i = depth of i^{th} layer, in., and

$(\frac{dy}{dx})_{ave}$ = average slope for the n^{th} element $[(\frac{dy}{dx})_{ave} = \frac{1}{2}(\frac{dy}{dx}(n) + \frac{dy}{dx}(n+1))]$.

Substitution of the value of the average interlayer slip from equation (6.4) into the connector load-slip curve equation determines the average connector force in each element.

The values for member stresses at the top and bottom of each layer and connector forces for each element is calculated by the computer program for each load increment. A study of typical values is presented in Sections 6.3 and 6.4.

6.3 Maximum Calculated Member Stresses by the Nonlinear Mathematical Model

The study of the member stresses was concentrated in the area of the maximum member stresses in tension since the normal mode of bending failure for wood beams is a tension failure occurring at the bottom of the beam. Discussions of the study of the maximum calculated member stresses in tension are presented in three parts. The first part concerns the comparisons of the maximum member stresses in tension calculated by the nonlinear mathematical model in the inelastic load range and the maximum member stresses in tension for the rigid connector upper limit condition. The second part compares the maximum calculated member stress values in tension for the T-beams tested to failure with the allowable unit stresses given in the National Design Specifications (20). The third part discusses the effect of gaps on the maximum member stresses in tension in the T-beams in the working load range.

6.3.1 Comparison of the Maximum Member Stresses in Tension for the Computed and the Upper and Lower Limits of Connector Effectiveness

Comparisons of the maximum member stresses in tension calculated by the nonlinear mathematical model and the maximum member stresses for the upper and lower limits of connector effectiveness are presented in Table 6.1 for the T-beam specimens tested beyond the working load range. As expected, the calculated values are greater than the maximum member stress values for the limiting connector condition of rigid connectors but less than the maximum member stress values obtained for the lower limit condition of no connectors.

The ratios of the maximum calculated member stresses in tension to the maximum member stresses for the rigid connector condition range from 1.57 to 1.01 for the T-beam specimens tested beyond the working load range. The stiffer connectors of glue or nails closely spaced generally produce lower ratios while the more flexible nailed connectors spaced at 8 inches produce ratios in the range of 1.35 to 1.55. Ratios of the maximum calculated member stresses to

Table 6.1 Comparison of Maximum Member Stresses in Tension for the Assumed Connector Conditions with the Calculated Values for T-Beams Tested Beyond the Working Load Range

Specimen	Joist No.	Layer Description	Connector Description	Load Level (lbs)	Max. Tensile Stress: Rigid Connector σ_R (psi)	Max. Tensile Stress: No Connector (Joist Only) σ_J (psi)	Max. Tensile Stress: Computed σ_c (psi)	σ_c/σ_R	σ_c/σ_J	Sheathing Remarks
T6-8D16-1	1*	2 x 8 Douglas-fir joist +	8d common nails@8"c-c	2750	4872.	7795.	6502.	1.335	.834	2 flexible gaps
	2	3/4" Douglas-fir plywood		2750	4989.	7993.	6647.	1.332	.832	
T7-8D16-1	1*	2 x 8 Douglas-fir joist +	8d common nails@2"c-c	3500	6119.	9664.	7091.	1.159	.734	2 flexible gaps
	2	3/4" Douglas-fir plywood		3500	6268.	9934.	7275.	1.161	.732	
T8-8D16-1	1*	2 x 8 Douglas-fir joist +	glue +	2750	4751.	7642.	5924.	1.247	.775	2 open gaps
	2	3/4" Douglas-fir plywood	8d common nails@8"c-c	2750	4741.	7677.	5941.	1.253	.774	
T11-8D16-1	1*	2 x 8 Douglas-fir joist +	glue	1750	2652.	4810.	4006.	1.511	.833	1 open gap @centerline
	2	3/4" Douglas-fir plywood		1750	2822.	5062.	4237.	1.501	.837	
T14-12D24-2	1*[a]	2 x 12 Douglas-fir joist +	8d common nails@8"c-c +	4000	2878.	4700.	4160.	1.448	.886	3 open gaps
	2[a]	1/2" Douglas-fir plywood + 1/2" particleboard	6d common nails@8"c-c	4000	2784.	4608.	4071.	1.461	.883	
T15-8E19.2-2	1*	2 x 8 Engelmann spruce joist +	8d common nails@8"c-c +	2000	3150.	5669.	4938.	1.568	.871	5 open gaps
	2	1/2" Engelmann spruce plywood + 1/2" particleboard	6d common nails@8"c-c	2000	3144.	5555.	4836.	1.538	.871	
T16-8E19.2-2	1	2 x 8 Engelmann spruce joist +	8d common nails@8"c-c +	1500	2464.	4398.	3718.	1.509	.845	3 flexible gaps
	2*	1/2" Engelmann spruce plywood + 1/2" particleboard	6d common nails@8"c-c (2 rows)	1500	2397.	4394.	3687.	1.538	.839	
T17-8D16-1	1	2 x 8 Douglas-fir joist +	8d common nails@8"c-c	3000[b]	5372.	8615.	7158.	1.332	.831	2 flexible gaps
	2*	3/4" Douglas-fir plywood		5000	8566.	13996.	11995.	1.400	.857	
T18-8D16-1	1	2 x 8 Douglas-fir joist +	glue	3500	5878.	9658.	5923.	1.008	.613	2 flexible gaps
	2*	3/4" Douglas-fir plywood		3500	5728.	9630.	5792.	1.011	.601	

*Joist controlling failure load
[a]Failed by local failure but sustained additional load before ultimate failure
[b]See discussion in Section 5.3.3.

the maximum member stresses for the joist only condition range from 0.60 to 0.90 for the T-beam specimens tested beyond the working load range. These ratios for the more flexible nailed connectors spaced at 8 inches ranged from 0.83 to 0.89 and for the stiffer connectors from 0.60 to 0.78. These ratios, of course, are also highly dependent on relative flange to joist areas and stiffnesses as well as connector properties.

Figure 6.1 presents a series of plots of stress in the beam cross-sections showing the development of stress distribution in a typical nailed T-beam system for incremental loads to failure. A similar series of plots is presented in Figure 6.2 for a typical glued T-beam system tested to failure. In both figures, the calculated bending stresses for the interlayer connection condition of no connectors are presented in parenthesis for each layer. Figure 6.3 presents a load-stress plot showing the nonlinear member stress development in the joist layer for a typical nailed T-beam. The nonlinear movement of the neutral axis is plotted in Figure 6.4 showing that the location of the neutral axis is dependent on the load level. Inspection of these plots show the nonlinear development of the cross-sectional stress distribution to failure. As an example of this nonlinear development, when the load applied to the typical nailed T-beam system shown in Figure 6.1 is doubled, the maximum member stress in tension increases by a factor greater than two.

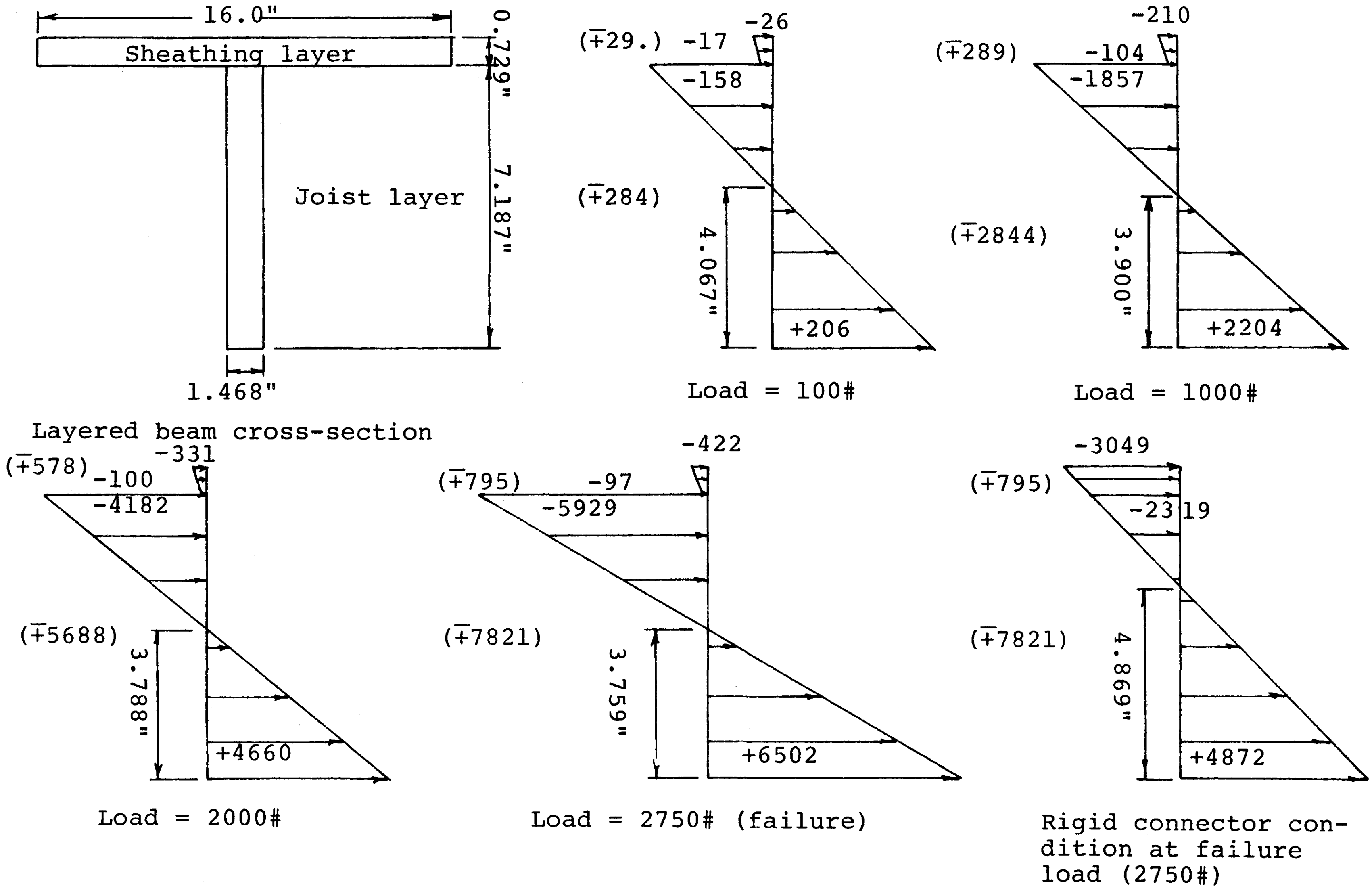

Figure 6.1 Development of stress distribution for a typical nailed T-beam T6-8D16-1 Joist J01.

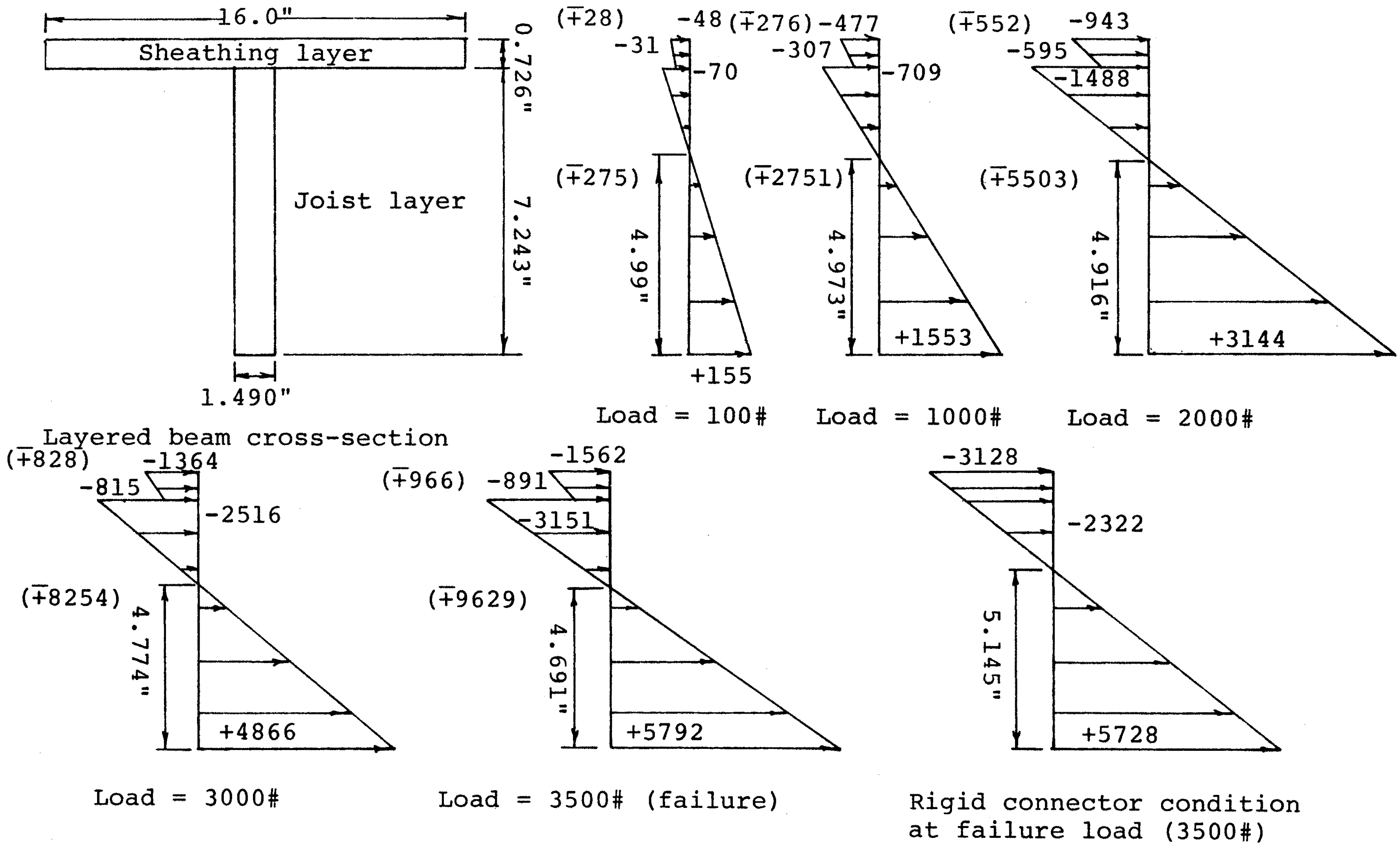

Figure 6.2 Development of stress distribution for a typical glued T-beam T18-8D16-1 Joist J02.

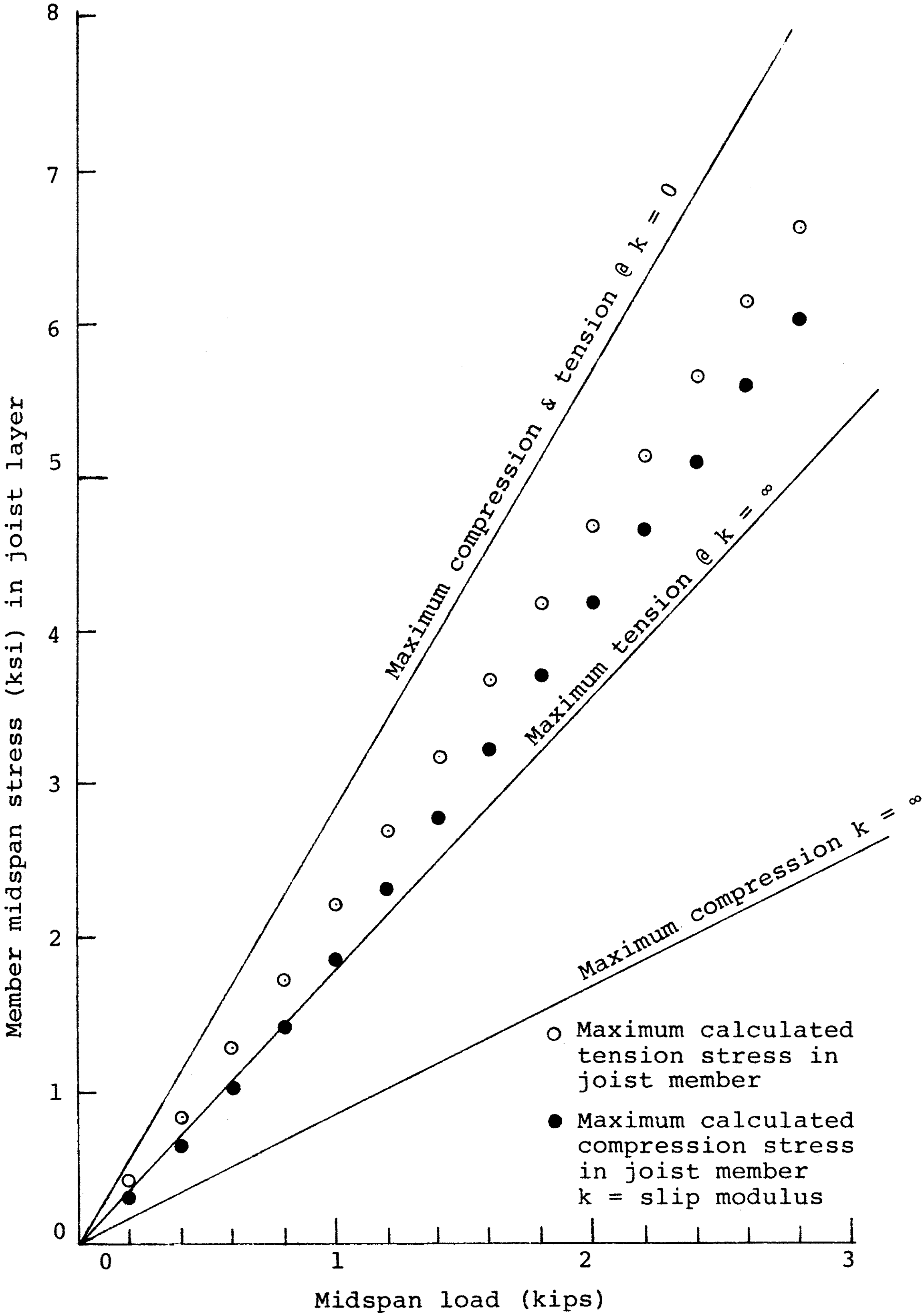

Figure 6.3 Load vs. stress plot for joist member T6-8D16-1 Joist J01.

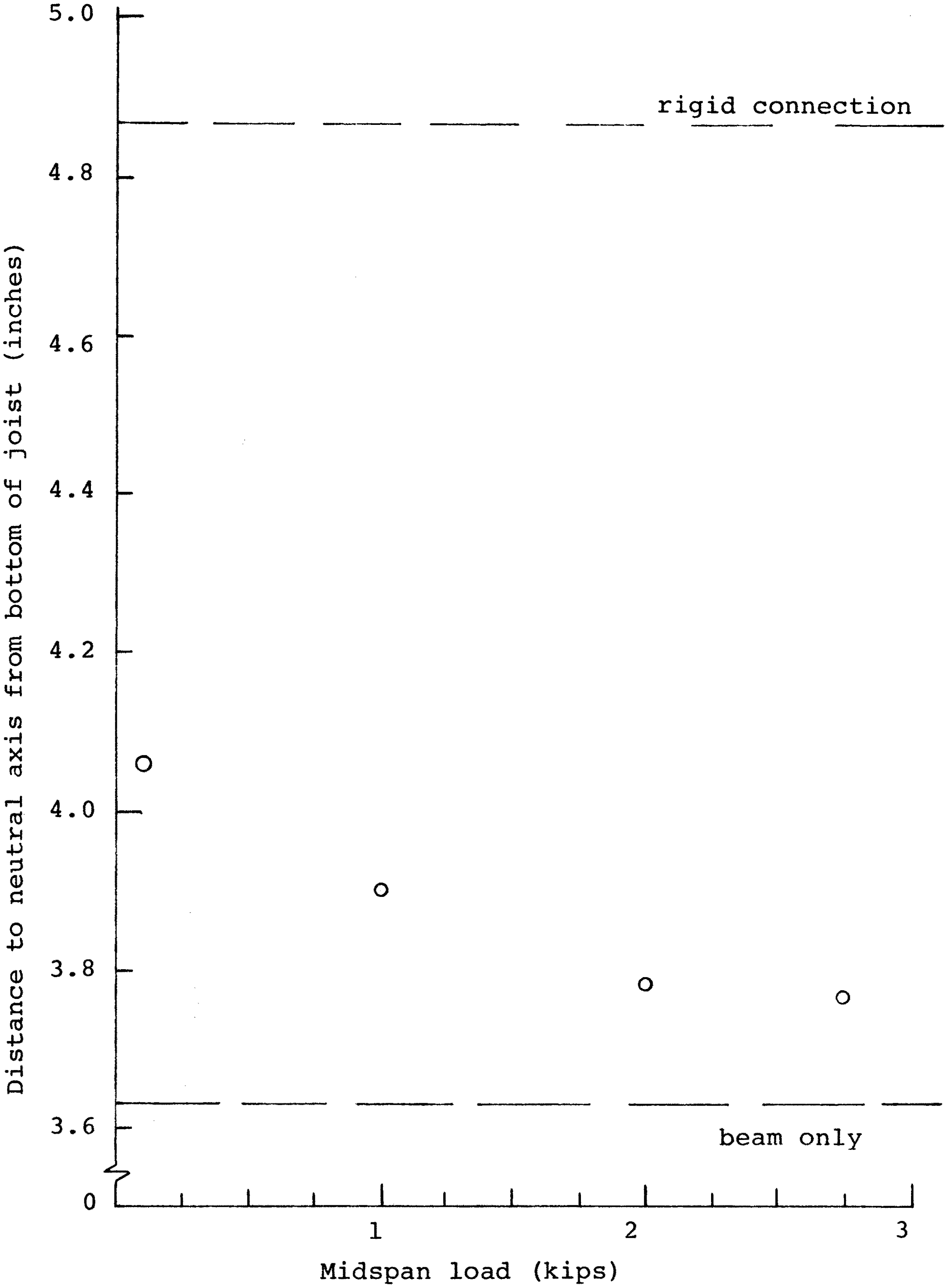

Figure 6.4 Neutral axis location vs. load for typical nailed T-beam T6-8D16-1 Joist J01.

6.3.2 Comparison of the Maximum Calculated Member Stress Values in Tension with the Allowable Unit Stresses from the National Design Specifications

A plot of the maximum calculated member stress in tension at the failure of the first joist versus the measured edgewise MOE value of each T-beam specimen tested to failure is shown in Figure 6.5. The National Design Specifications machine graded values for the allowable unit stresses in bending and tension parallel to grain (20) are also plotted. The 10 year duration values taken from NDS are adjusted for a load duration of approximately 5 minutes by a factor of 16/11 (4). From Figure 6.5 it can be observed that all of the points plotted for the maximum calculated member stress in tension are above the adjusted NDS machine graded values.

Tables 6.2 and 6.3 compare the ratios or factors of safety between the calculated values of maximum stress and the duration adjusted NDS visual and machine graded values for allowable unit stresses in bending and tension parallel to grain for the T-beam specimens tested to failure. For the visual graded values, the safety factor ranges from 1.6 to 5.4 for the allowable unit bending stresses and from 2.4 to 8.5 for the allowable unit tension stresses. For the machine graded values, this safety factor ranges from 1.3 to 3.3 for the allowable unit bending stresses and from 1.7 to 5.7 for the allowable unit tension stresses. For all of the T-beams tested to failure, the safety factor for the allowable unit tension stresses is greater than the factor

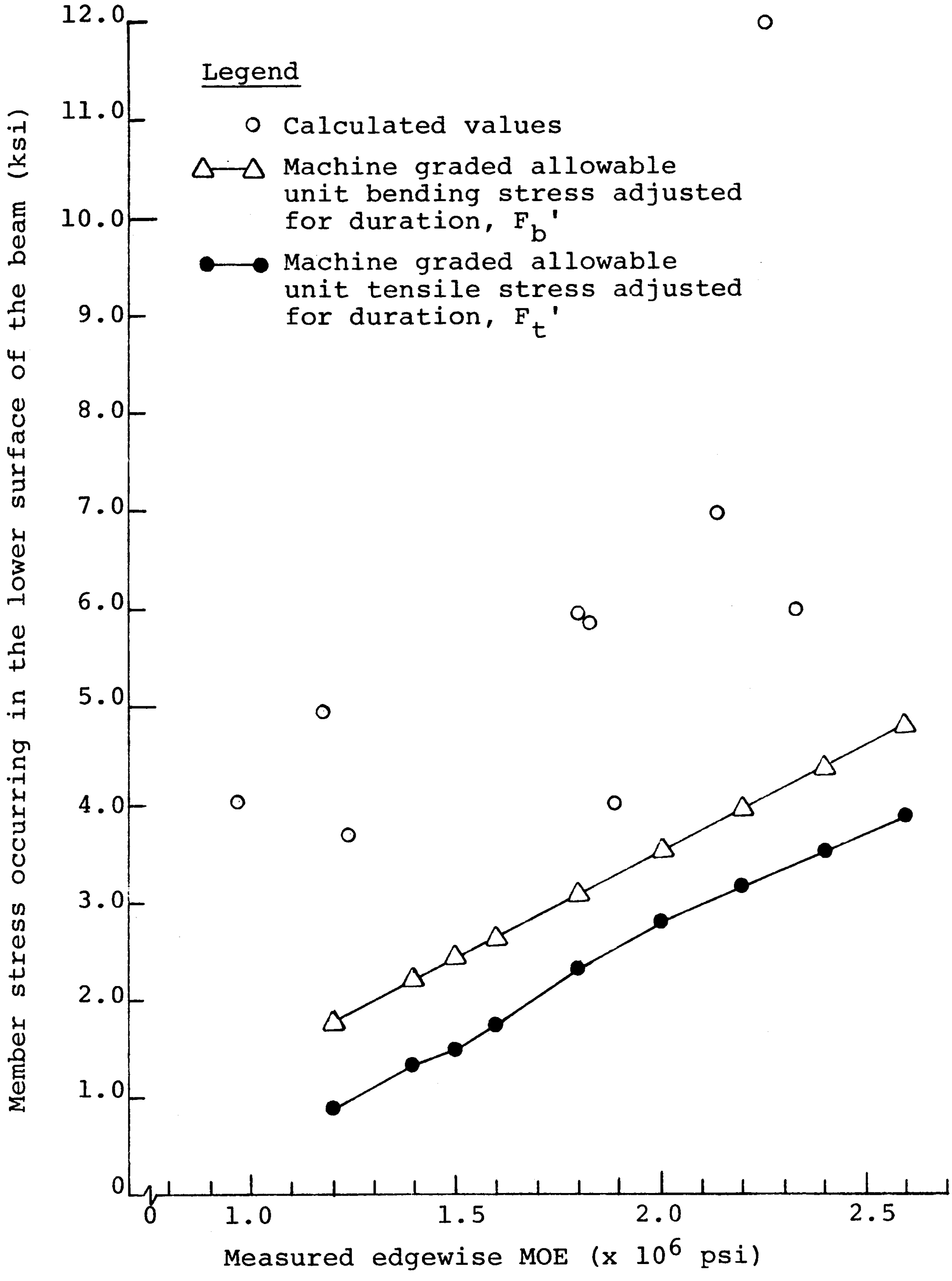

Figure 6.5 Member stress in lower surface vs. measured edgewise MOE plot.

Table 6.2 Factors of Safety for the Maximum Calculated Stress Values and the Visual Graded Allowable Unit Stress Values by the NDS for T-Beams Tested to Failure

T-Beam Specimen	Joist No.	Computed F_b psi	Allowable Unit Bending Stress			Allowable Unit Tension Stress		
			F_b (psi)	Duration Adjusted F_b' (psi)	Safety Factor	F_t (psi)	Duration Adjusted F_t' (psi)	Safety Factor
T6-8D16-1	J-01	6502.	1800	2618.	2.48	1200	1746.	3.73
T7-8D16-1	J-01	7091.	1800	2618.	2.71	1200	1746.	4.06
T8-8D16-1	J-01	5924.	1800	2618.	2.26	1200	1746.	3.39
T11-8D16-1	J-01	4006.	725	1055.	3.80	475	691.	5.80
T14-12D24-2	J-01	4160.	1800	2618.	1.59	1200	1746.	2.38
T15-8E19.2-2	J-01	4938.	1150	1673.	2.95	775	1128.	4.38
T16-8E19.2-2	J-02	3687.	475	691.	5.34	300	437.	8.43
T17-8D16-1	J-02	11995.	1800	2618.	4.58	1200	1746.	6.87
T18-8D16-1	J-02	5792.	1800	2618.	2.21	1200	1746.	3.31

Table 6.3 Factors of Safety for the Maximum Calculated Stresses and the Machine Graded Allowable Unit Stress Values by the NDS for T-Beams Tested to Failure

T-Beam Specimen	Joist No.	Edgewise MOE 10^6 psi	Computed F_b (psi)	Allowable Unit Bending Stress: F_b (psi)	Allowable Unit Bending Stress: Duration Adjusted F_b' (psi)	Allowable Unit Bending Stress: Safety Factor	Allowable Unit Tension Stress: F_t (psi)	Allowable Unit Tension Stress: Duration Adjusted F_t' (psi)	Allowable Unit Tension Stress: Safety Factor
T6-8D16-1	J-01	2.330	6502.	2890.	4205.	1.55	2310.	3360.	1.94
T7-8D16-1	J-01	2.141	7091.	2605.	3790.	1.87	2090.	3040.	2.33
T8-8D16-1	J-01	1.805	5924.	2110.	3070.	1.93	1588.	2310.	2.57
T11-8D16-1	J-01	0.975	4006.	1200.	1746.	2.29	600.	873.	4.60
T14-12D24-2	J-01	1.883	4160.	2230.	3245.	1.28	1718.	2500.	1.67
T15-8E19.2-2	J-01	1.191	4938.	1200.	1746.	2.83	600.	873.	5.66
T16-8E19.2-2	J-02	1.261	3687.	1300.	1892.	1.95	687.	1000.	3.69
T17-8D16-1	J-02	2.275	11995.	2810.	4089.	2.93	2240.	3260.	3.68
T18-8D16-1	J-02	1.819	5792.	2120.	3090.	1.87	1600.	2330.	2.49

of safety for the allowable unit bending stresses since the allowable unit bending stresses are greater than the allowable unit tension stresses. The range of safety factor values for the allowable unit tension stresses is greater than for the allowable unit bending stress. Since the calculation of the maximum member stress value in tension is neither a pure bending nor axial stress problem, but rather a combination of the two stress conditions, a study of the computed stresses and allowable unit stresses must include comparisons of both allowable stress values with the computed stress value. It is difficult to summarize any trend from the visual graded values used for comparison, but the machine graded values show a definite trend in Table 6.3. This trend is that stiffer connectors show a higher factor of safety and the three-layered systems show a higher factor of safety than the two-layered systems. Thus, the stiffer systems show a higher safety factor.

6.3.3 Study of the Effects of Gaps on the Maximum Calculated Member Stresses in Tension

In Table 6.4, comparisons of the maximum calculated member stresses in tension are made for the T-beam specimens tested in the working load range. These results are included to show the effect of gaps on the maximum joist tensile stresses which occur at the midspan. The range of ratios of the maximum calculated member stresses and the maximum tension stresses for the upper and lower limits of connector effectiveness are the same as those for the T-beam specimens tested beyond the working load range.

Table 6.4 Comparison of Maximum Calculated Tensile Stresses for T-Beams Tested in the Working Load Range

Specimen	Joist No.	Layer Description	Connector Description	Load Level (lbs)	Max. Tensile Stress: Rigid Connector σ_R (psi)	Max. Tensile Stress: No Connector (Joist Only) σ_J (psi)	Max. Tensile Stress: Computed σ_c (psi)	σ_c/σ_R	σ_c/σ_J	Sheathing Remarks
T9-8D16-1	1	2 x 8 Douglas-fir joist +	glue	1250	2210.	3460.	2231.	1.010	.645	2 flexible gaps
	2	3/4" Douglas-fir plywood		1250	2377.	3675.	2410.	1.014	.656	
T9-8D16-1	1	2 x 8 Douglas-fir joist +	glue	1250	2210.	3460.	2387.	1.080	.690	2 open gaps
	2	3/4" Douglas-fir plywood		1250	2377.	3675.	2577.	1.084	.701	
T10-12E24-1	1	2 x 12 Engelmann spruce joist +	8d common nails@8"c-c	2000	1376.	2302.	1807.	1.313	.785	2 flexible gaps
	2	3/4" Douglas-fir plywood		2000	1356.	2287.	1796.	1.324	.785	
T10-12E24-1	1	2 x 12 Engelmann spruce joist +	8d common nails@8"c-c	2000	1376.	2302.	2039.	1.482	.886	2 open gaps
	2	3/4" Douglas-fir plywood		2000	1356.	2287.	2026	1.494	.886	
T10-12E24-1	1	2 x 12 Engelmann spruce joist +	8d common nails@8"c-c	2000	1376.	2302.	2089.	1.518	.907	5 open gaps
	2	3/4" Douglas-fir plywood		2000	1356.	2287.	2075.	1.530	.907	
T12-8D16-1	1	2 x 8 Douglas-fir joist +	8d common nails@6"c-c	625	1036.	1831.	1164.	1.124	.636	2 flexible gaps
	2	3/4" Douglas-fir plywood		625	985.	1726.	1105.	1.122	.640	
T12-8D16-1	1	2 x 8 Douglas-fir joist +	8d common nails@6"c-c	500	828.	1465.	1275.	1.540.	.870	1 open gap @centerline + 2 flexible gaps
	2	3/4" Douglas-fir plywood		500	788.	1381.	1203.	1.527	.871	
T12-8D16-1	1	2 x 8 Douglas-fir joist +	8d common nails@6"c-c	500	828.	1465.	1289.	1.557	.880	3 open gaps
	2	3/4" Douglas-fir plywood		500	780.	1381.	1217.	1.544	.881	
T12-8D16-1	1	2 x 8 Douglas-fir joist +	8d common nails@6"c-c	500	828.	1465.	1289.	1.557	.880	5 open gaps
	2	3/4" Douglas-fir plywood		500	788.	1381.	1217.	1.544	.881	
T13-8D16-1	1	2 x 8 Douglas-fir joist +	8d common nails@4"c-c	500	859.	1383.	1062.	1.236	.768	2 open gaps
	2	5/8" Douglas-fir plywood		500	816.	1366.	1028.	1.260	.753	
T14-12D24-1	1	2 x 12 Engelmann spruce joist +	8d common nails@8"c-c	1000	810.	1175.	1025.	1.265	.872	2 open gaps
	2	1/2" Engelmann spruce plywood		1000	783.	1152.	1003.	1.281	.871	
T15-8E19.2-1	1	2 x 8 Engelmann spruce joist +	8d common nails@8"c-c	300	519.	850.	707.	1.362	.832	2 open gaps
	2	1/2" Engelmann spruce plywood		300	504.	833.	692.	1.373	.831	
T16-8E19.2-1	1	2 x 8 Engelmann spruce joist +	8d common nails@8"c-c	400	733.	1173.	921.	1.256	.785	2 flexible gaps
	2	1/2" Engelmann spruce plywood		400	712.	1172.	903.	1.268.	.770	

General observations can be made from the comparisons presented in Table 6.4. The introduction of gaps in the sheathing layer causes a significant increase in the maximum tension stress in the T-beam joist, the tensile stress increasing as the number of gaps increase. These increases are more significant for nails spaced at 8 inches than for the stiffer glued connection.

Figure 6.6 presents a series of plots of stresses in the beam cross-section showing the effects of gaps on the development of the stress distribution in a typical nailed T-beam system for a specific load. As shown, the effect of the first open gap significantly increases the stress values and lowers the neutral axis while additional open gaps do not affect the stress values and neutral axis location as much.

6.4 Study of the Maximum Calculated Connector Forces for the Nonlinear Mathematical Model

Results from the study of the maximum predicted connector forces are presented in three discussion areas. The first presents the comparisons of the maximum connector forces calculated by the nonlinear mathematical model in the inelastic load range and the corresponding forces assuming rigid connectors existed. The second area compares the maximum calculated nail forces and the ultimate lateral load capacity for nails as specified in the National Design Specifications (20) for the T-beams tested to failure and in the working load range. The third area discusses the effect

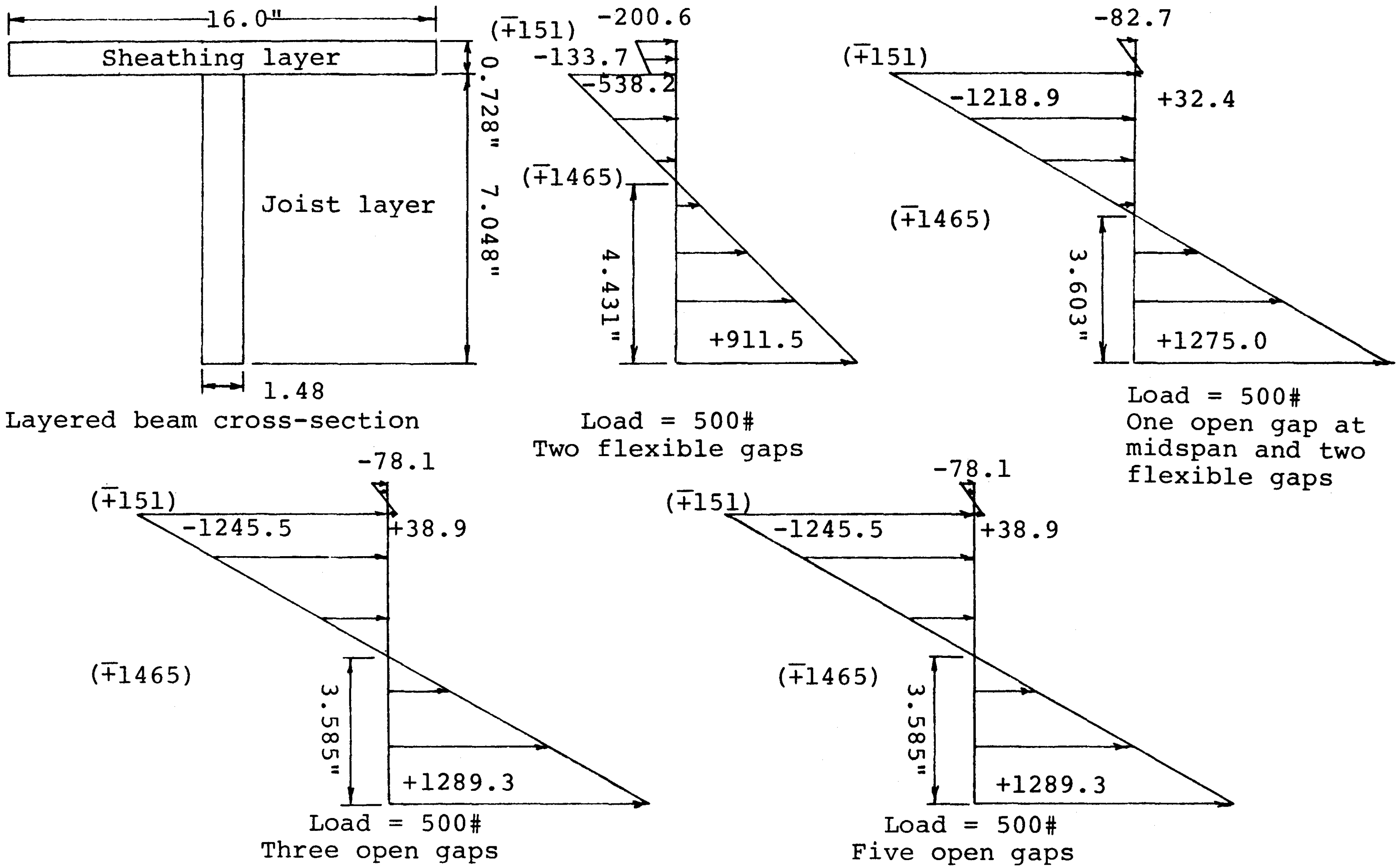

Figure 6.6 Effects of gaps on the development of the stress distribution
T12-8D16-1 Joist J01.

of gaps on the maximum predicted connector forces in the T-beams in the working load range.

6.4.1 Comparison of Maximum Connector Forces for the Calculated and the Rigid Connector Conditions.

Comparison of the maximum connector forces calculated by the finite element mathematical model and the maximum connector forces for the rigid connector condition is presented in Table 6.5 for the T-beam specimens tested beyond the working load range. The connector forces for the rigid connector condition is calculated by using the basic elastic beam equation for shear flow, q. That is:

$$q = \frac{VQ}{I} .$$

For the nailed connectors, this shear flow is multiplied by the nail spacing to get the load per nail. The connector force for glued beams is expressed as a shear stress by dividing the shear flow by the joist thickness.

The location of the maximum connector force will be discussed in Section 6.4.3 since the presence of gaps has a major effect on the connector force distribution. The ratios of the maximum connector force to the rigid connector force for the nailed connector T-beam specimens tested beyond the working load range ranges from 0.16 to 0.28 for the nails spaced at 8 inches. For the nailed connectors spaced at 2 inches this ratio is approximately 0.6. As expected, nails more closely spaced give a more rigid connector than nails spaced farther apart. For the glued connection, these ratios are in the range of 1.35 to 1.80.

Table 6.5 Comparison of Connector Forces for the T-Beams Tested Beyond the Working Load Range

Specimen	Joist No.	Layer Description	Connector Description	Load Level (lbs)	Rigid Connector Force f_R (#/nail or in. of glue)	Predicted Connector Force f_P (#/nail or in. of glue)	f_P/f_R	Remarks
T6-8D16-1	1*	2 x 8 Douglas-fir joist + 3/4" Douglas-fir plywood	8d common nails@8"c-c	2750	1495.5 lbs/nail	421.4 lbs/nail	.282	2 flexible gaps
	2			2750	1510.0 lbs/nail	426.1 lbs/nail	.282	
T7-8D16-1	1*	2 x 8 Douglas-fir joist + 3/4" Douglas-fir plywood	8d common nails@2"c-c	3500	462.4 lbs/nail	280.2 lbs/nail	.606	2 flexible gaps
	2			3500	467.5 lbs/nail	282.7 lbs/nail	.605	
T8-8D16-1	1*	2 x 8 Douglas-fir joist + 3/4" Douglas-fir plywood	glue + 8d common nails@8"c-c	2750	126.4 psi of glue	171.9 psi of glue	1.360	2 open gaps
	2			2750	127.3 psi of glue	172.9 psi of glue	1.358	
T11-8D16-1	1*	2 x 8 Douglas-fir joist + 3/4" Douglas-fir plywood	glue	1750	93.7 psi of glue	167.2 psi of glue	1.784	1 open gap @centerline
	2			1750	95.4 psi of glue	166.3 psi of glue	1.743	
T14-12D24-2	1*[a]	2 x 12 Douglas-fir joist + 1/2" Douglas-fir plywood + 1/2" particleboard	8d common nails@8"c-c + 6d common nails@8"c-c	4000	1486.4 lbs/nail	284.6 lbs/nail	.191	3 open gaps
	2[a]			4000	1512.2 lbs/nail	293.8 lbs/nail	.194	
T15-8E19.2-2	1*	2 x 8 Engelmann spruce joist + 1/2" Engelmann spruce plywood 1/2" particleboard	8d common nails@8"c-c + 6d common nails@8"c-c	2000	1361.7 lbs/nail	270.6 lbs/nail	.199	5 open gaps
	2			2000	1211.0 lbs/nail	271.5 lbs/nail	.224	
T16-8E19.2-2	1	2 x 8 Engelmann spruce joist + 1/2" Engelmann spruce plywood 1/2" particleboard	8d common nails@8"c-c + 6d common nails@8"c-c	1500	951.6 lbs/nail	237.7 lbs/nail	.250	3 flexible gaps
	2*			1500	985.7 lbs/nail	246.6 lbs/nail	.250	
T17-8D16-1	1	2 x 8 Douglas-fir joist + 3/4" Douglas-fir plywood	8d common nails@8"c-c	3000[b]	1641.3 lbs/nail	440.0 lbs/nail	.268	2 flexible gaps
	2*			5000	2739.3 lbs/nail	440.0 lbs/nail	.161	
T18-8D16-1	1	2 x 8 Douglas-fir joist + 3/4" Douglas-fir plywood	glue	3500	165.4 psi of glue	159.8 psi of glue	.966	2 flexible gaps
	2*			3500	171.4 psi of glue	162.0 psi of glue	.945	

*Joist controlling failure load
[a]Failed by local failure but sustained additional load before ultimate failure
[b]See discussion in Section 5.3.3.

The unexpected result of this range being larger than unity is attributed to the presence of discontinuities (open gaps) in the sheathing layer.

6.4.2 Comparison of Maximum Calculated Connector Forces and the Allowable Nail Force by the National Design Specifications

Comparisons of the maximum calculated nail forces and the ultimate and allowable nail forces specified by the National Design Specification for the T-beams tested to failure are presented in Table 6.6. Ratios of the NDS allowable nail capacity to the maximum calculated nail force range from 0.18 to 0.28 and the NDS ultimate capacity to the maximum calculated nail force range from 1.06 to 1.67.

Similar comparison of maximum nail forces are made for all of the T-beams in the working load range in Table 6.7. Ratios of the ultimate lateral load capacity of nails specified by NDS and the maximum calculated nail force in the elastic load range defined as the load producing a computed T-beam midspan deflection of L/360 range from 1.0 to 3.5. Similar ratios of the ultimate lateral load capacity of nails in the elastic load range for the load defined by the limit of visual graded allowable bending stress in the T-beam adjusted for duration range from 1.0 to 3.35 and are generally lower by 5 to 15 percent. Since the allowable nail capacity specified by the NDS is equal to 1/6 (36) of the ultimate nail capacity, comparison of the allowable lateral load nail capacities and the maximum calculated nail forces are equal to 1/6 of the aforementioned ratios.

Table 6.6 Safety Factors for the Maximum Calculated Nail Forces and the NDS Allowable and Ultimate Nail Capacities for T-Beams Tested to Failure

T-Beam Specimen	Joist No.	Maximum Computed Nail Force (lbs)	Allowable Lateral Load Capacity		Ultimate Lateral Load Capacity	
			Nail Force (lbs)	Safety Factor	Nail Force (lbs)	Safety Factor
T6-8D16-1	J-01	421.	78	0.185	468	1.11
T7-8D16-1	J-01	280.	78	0.279	468	1.67
T14-12D24-2	J-01	285.	78	0.274	468	1.64
T15-8E19.2-2	J-01	271.	51	0.188	306	1.13
T16-8E19.2-2	J-02	247.	51	0.206	306	1.24
T17-8D16-1	J-02	440.	78	0.177	468	1.06

Note: The ultimate lateral load capacity equals the NDS allowable lateral load capacity times a safety factor of six.

Table 6.7 Ratios of NDS Allowable and Ultimate Nail Capacities to Maximum Calculated Nail Forces at T-Beam Working Loads

T-beam Specimen	Joist No.	Sheathing Joint	Allowable Lateral Load Capacity (lbs)	$\Delta_{T\text{-beam}} = L/360$ Computed Nail Force (lbs)	$\Delta_{T\text{-beam}} = L/360$ Allowable/computed	$\Delta_{T\text{-beam}} = L/360$ Ultimate/Computed	$f_{b\ T\text{-beam}} = F_b'$ Computed Nail Force (lbs)	$f_{b\ T\text{-beam}} = F_b'$ Allowable/Computed	$f_{b\ T\text{-beam}} = F_b'$ Ultimate/Computed
T6-8D16-1	J-01	2 flexible gaps	78	203	.385	2.31	231	.338	2.03
	J-02			201	.400	2.38	231	.338	2.03
T7-8D16-1	J-01	2 flexible gaps	78	164	.477	2.86	191	.408	2.45
	J-02			163	.478	2.87	192	.407	2.44
T10-12E24-1	J-01	2 flexible gaps	51	313	.164	0.98	312	.164	0.98
	J-02			313	.164	0.98	313	.164	0.98
T10-12E24-1	J-01	2 open gaps	51	212	.240	1.44	222	.230	1.38
	J-02			212	.240	1.44	223	.228	1.37
T10-12E24-1	J-01	5 open gaps	51	126	.405	2.43	132	.387	2.32
	J-02			126	.405	2.43	132	.387	2.32
T12-8D16-1	J-01	2 flexible gaps	78	194	.402	2.41	177	.440	2.64
	J-02			198	.394	2.36	180	.433	2.60
T12-8D16-1	J-01	1 open gap @centerline + 2 flex. gaps	78	201	.388	2.33	196	.398	2.39
	J-02			203	.385	2.31	201	.388	2.33
T12-8D16-1	J-01	3 open gaps	78	140	.558	3.35	144	.540	3.24
	J-02			140	.558	3.35	141	.562	3.31
T12-8D16-1	J-01	5 open gaps	78	134	.582	3.49	140	.558	3.35
	J-02			135	.578	3.47	138	.565	3.39
T13-8D16-1	J-01	2 open gaps	78	193	.405	2.43	193	.405	2.43
	J-02			190	.410	2.46	208	.375	2.25
T14-12D24-1	J-01	2 open gaps	78	228	.342	2.05	240	.325	1.95
	J-02			227	.343	2.06	247	.315	1.89
T14-12D24-2	J-01	3 open gaps	78	226	.345	2.07	238	.328	1.97
	J-02			226	.345	2.07	245	.318	1.91
T15-8E19.2-1	J-01	2 open gaps	51	153	.333	2.00	201	.253	1.52
	J-02			151	.338	2.03	205	.248	1.49
T15-8E19.2-2	J-01	5 open gaps	51	149	.342	2.05	197	.258	1.55
	J-02			149	.342	2.05	200	.255	1.53
T16-8E19.2-1	J-01	2 flexible gaps	51	142	.358	2.15	167	.305	1.83
	J-02			141	.362	2.17	115	.443	2.66
T16-8E19.2-2	J-01	3 flexible gaps	51	147	.347	2.08	175	.292	1.75
	J-02			147	.347	2.08	120	.425	2.55
T17-8D16-1	J-01	2 flexible gaps	78	223	.350	2.10	253	.308	1.85
	J-02			225	.347	2.08	259	.302	1.81

Note: The ultimate lateral load capacity equals the NDS allowable lateral load capacity times a safety factor of 6.

Table 6.8 presents the maximum glue shear stresses calculated by the mathematical model at the elastic load range limits which are defined by both midspan deflection and maximum bending stress. These shear stress values for the glued connector range from 99 psi to 146 psi.

6.4.3 Study of the Effect of Gaps on the Maximum Predicted Connector Forces

In Table 6.9, similar comparisons of the maximum calculated connector forces and the rigid connector forces are made for the T-beam specimens tested only in the working load range. These results are tabulated to show the effects of gaps on the maximum connector force. The range of ratios of maximum calculated and rigid connector forces are higher for the T-beam specimens tested only in the working load range than for those tested beyond the working load range. This relationship of ratios is attributed to the higher degree of rigidity exhibited by the connector load-slip curves in the working load range as discussed in Section 5.3.

General observations can be made from the comparisons presented in Table 6.9. The introduction of one gap in the sheathing layer at the midspan of the T-beam causes a significant increase in the maximum nail force as shown in Table 6.7 (T12). But the introduction of additional gaps at any other location in the sheathing layer causes a significant decrease in the maximum nail force. This observation can be attributed to the fact that gaps in the sheathing layer disrupt the continuous interaction between

Table 6.8 Maximum Calculated Glued Connection Stresses for T-Beams Tested in the Working Load Range

T-Beam Specimen	Joist No.	Sheathing Joint	Computed Glue Stress @ $\Delta_{T\text{-Beam}}$ = 4360	Load Level (lbs)	Computed Glue Stress @ f_b T-Beam = F_b'	Load Level (lbs)
T8-8D16-1	J-01	2 open gaps	118. psi	840	145. psi	1375
	J-02		116. psi	800	146. psi	1375
T9-8D16-1	J-01	2 flexible gaps	108. psi	1120	122. psi	1450
	J-02		110. psi	1150	118. psi	1350
T9-8D16-1	J-01	2 open gaps	121. psi	1000	137. psi	1350
	J-02		122. psi	1020	133. psi	1275
T11-8D16-1	J-01	1 open gap @ centerline	109. psi	525	109. psi	525
	J-02		109. psi	535	105. psi	500
T18-8D16-1	J-01	2 flexible gaps	100. psi	1300	116. psi	1635
	J-02		99. psi	1200	120. psi	1675

Table 6.9 Comparison of the Rigid Connector Force and the Maximum Calculated Connector Force for the T-Beams Tested in the Working Load Range

Specimen	Joist No.	Layer Description	Connector Description	Load Level (lbs)	Rigid Connector Connector Force f_R (#/nail or in. of glue)	Predicted Connector Force f_P (#/nail or in. of glue)	f_P/f_R	Remarks
T9-8D16-1	1	2 x 8 Douglas-fir joist +	glue	1250	54.3 psi of glue	72.0 psi of glue	1.326	2 flexible gaps
	2	3/4" Douglas-fir plywood		1250	55.5 psi of glue	71.7 psi of glue	1.292	
T9-8D16-1	1	2 x 8 Douglas-fir joist +	glue	1250	54.3 psi of glue	132.6 psi of glue	2.442	2 open gaps
	2	3/4" Douglas-fir plywood		1250	55.5 psi of glue	131.9 psi of glue	2.377	
T10-12E24-1	1	2 x 12 Engelmann spruce joist +	8d common nails@8"c-c	2000	775.9 lbs/nail	319.1 lbs/nail	.411	2 flexible gaps
	2	3/4" Douglas-fir plywood		2000	793.2 lbs/nail	319.1 lbs/nail	.402	
T10-12E24-1	1	2 x 12 Engelmann spruce joist +	8d common nails@8"c-c	2000	775.9 lbs/nail	240.8 lbs/nail	.310	2 open gaps
	2	3/4" Douglas-fir plywood		2000	793.2 lbs/nail	240.7 lbs/nail	.303	
T10-12E24-1	1	2 x 12 Engelmann spruce joist +	8d common nails@8"c-c	2000	775.9 lbs/nail	147.0 lbs/nail	.189	5 open gaps
	2	3/4" Douglas-fir plywood		2000	793.2 lbs/nail	147.0 lbs/nail	.185	
T12-8D16-1	1	2 x 8 Douglas-fir joist +	8d common nails@6"c-c	625	299.1 lbs/nail	190.6 lbs/nail	.637	2 flexible gaps
	2	3/4" Douglas-fir plywood		625	289.0 lbs/nail	185.3 lbs/nail	.641	
T12-8D16-1	1	2 x 8 Douglas-fir joist +	8d common nails@6"c-c	500	239.3 lbs/nail	211.9 lbs/nail	.885	1 open gap @centerline + 2 flexible gaps
	2	3/4" Douglas-fir plywood		500	231.2 lbs/nail	207.9 lbs/nail	.899	
T12-8D16-1	1	2 x 8 Douglas-fir joist +	8d common nails@6"c-c	500	239.3 lbs/nail	160.7 lbs/nail	.672	3 open gaps
	2	3/4" Douglas-fir plywood		500	231.2 lbs/nail	155.7 lbs/nail	.673	
T12-8D16-1	1	2 x 8 Douglas-fir joist +	8d common nails@6"c-c	500	239.3 lbs/nail	152.7 lbs/nail	.638	5 open gaps
	2	3/4" Douglas-fir plywood		500	231.2 lbs/nail	148.1 lbs/nail	.641	
T13-8D16-1	1	2 x 8 Douglas-fir joist +	8d common nails@4"c-c	500	138.0 lbs/nail	193.3 lbs/nail	1.401	2 open gaps
	2	3/4" Douglas-fir plywood		500	145.6 lbs/nail	205.6 lbs/nail	1.412	
T14-12D24-1	1	2 x 12 Douglas-fir joist +	8d common nails@8"c-c	1000	314.0 lbs/nail	176.5 lbs/nail	.562	2 open gaps
	2	1/2" Douglas-fir plywood		1000	322.0 lbs/nail	181.9 lbs/nail	.565	
T15-8E19.2-1	1	2 x 8 Engelmann spruce joist +	8d common nails@8"c-c	300	179.2 lbs/nail	132.0 lbs/nail	.737	2 open gaps
	2	1/2" Engelmann spruce plywood		300	181.1 lbs/nail	132.6 lbs/nail	.732	
T16-8E19.2-1	1	2 x 8 Engelmann spruce joist +	8d common nails@8"c-c	400	321.7 lbs/nail	123.1 lbs/nail	.531	2 flexible gaps
	2	1/2" Engelmann spruce plywood		400	243.5 lbs/nail	131.1 lbs/nail	.538	

the layers along the length of the beam causing less shear force to be transmitted between the layers by the nails. The gap located at the midspan does not follow this theory because the shear force to be transmitted between the layers at the midspan section is zero for the loading used. The effect of gaps on the glued connector result in a significant increase in the maximum shear stress because the continuous connection effect of the glue is not disrupted as much by a few gaps as it is for nailed connection.

Figure 6.7 presents a series of connector force profiles along the length of a typical layer T-beam for different sheathing joint conditions. These profiles indicate the effect that gaps have on the connector distribution along the length of the beam.

For the T-beams tested as a part of this project, the calculated stresses and connector forces computed with the developed mathematical model indicate relative trends for different types of connector and sheathing conditions. Additional investigation must be performed to develop specific criteria to predict the ultimate failure of the T-beam by means of a knowledge of the member stresses or connector forces.

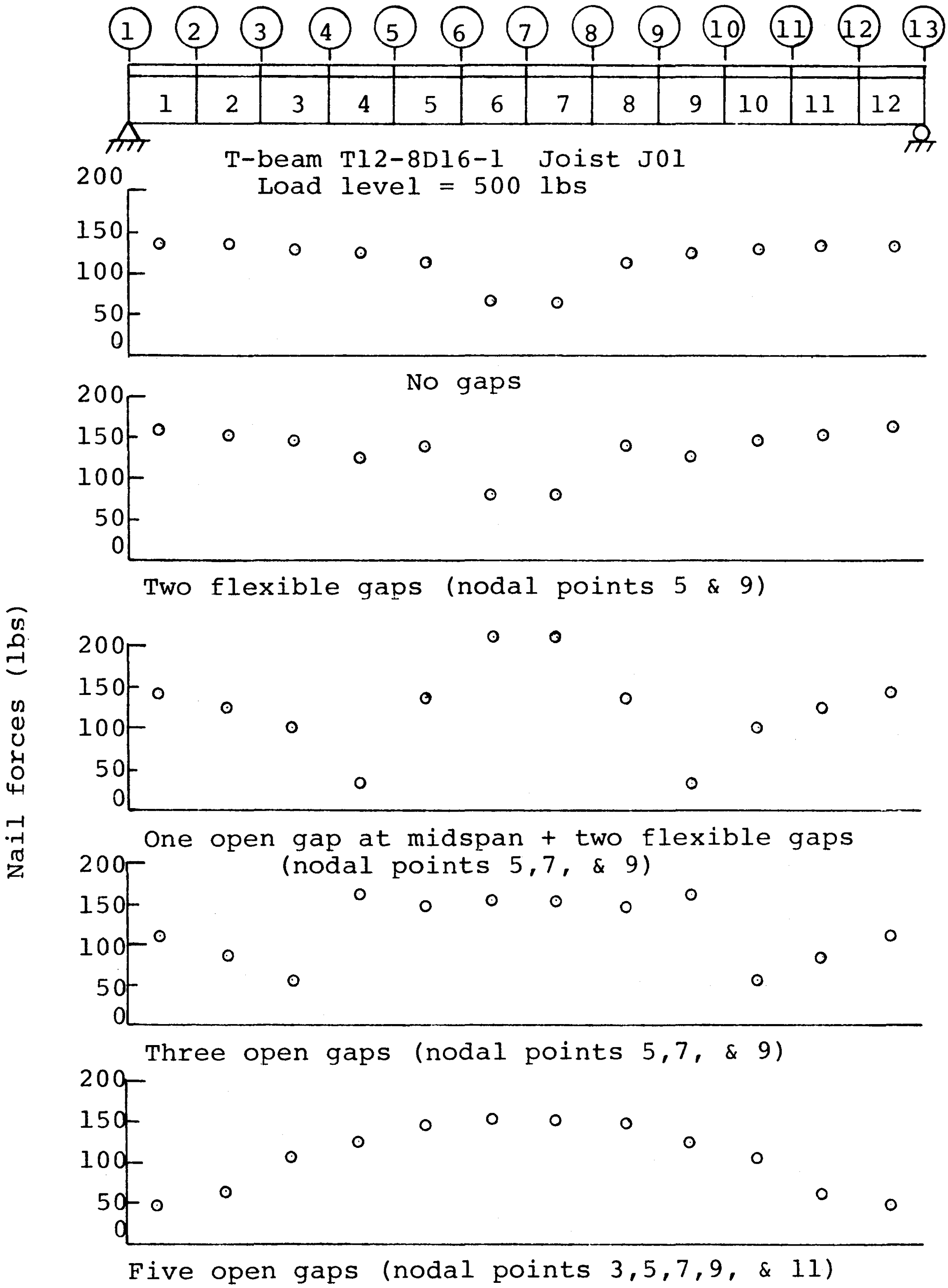

Figure 6.7 Effect of gaps on nail forces along beam length.

CHAPTER VII

SUMMARY AND CONCLUSIONS

This study has presented a discussion on the development of a nonlinear mathematical model used to predict the deflections, member stresses, and connector forces of wood joist T-beam systems tested to failure. In comparison to past studies, especially Kuo's work (14), the unique aspect of this study is the fact that the nonlinear connector load-slip relationship is taken into account, thus enabling the model to predict the behavior of the layer system to failure with a higher degree of accuracy. A finite element solution technique was developed during the overall research effort on joist floor systems and modified to include consideration of this nonlinearity and to compute the theoretical deflections, fiber stresses, and connector forces for two- and three-layered systems with variable properties along the length of the beam.

Development and verification of this nonlinear mathematical model was a primary objective of this study. Sixteen double T-beam specimens provided experimental data for the verification of the model. The specimens were constructed using a variety of material, connection, and configuration combinations. Properties for each piece of lumber and sheathing material were individually determined by the Wood Science Laboratory of Colorado State University. The joist modulus of elasticity values were also determined in the edgewise orientation during the specimen construction. Load-deformation curves for each type of connector used in this series of T-beam tests were determined by the Wood Science Laboratory. Of the T-beams constructed and tested, thirteen T-beams were two-layered systems and three were three-layered systems. Nine of these T-beams were tested to failure while the other T-beams were tested with varying combinations of gap locations and types in the working load range. Twelve T-beams were constructed with nailed connectors while four T-beams used an elastomeric adhesive connection.

The T-beam specimens were tested in the working load range by applying a concentrated load at selected locations along the beam. Deflections were obtained from dial gages mounted underneath the joists at selected locations. Upon conclusion of the elastic load tests, several of the T-beams were tested to failure by applying a concentrated load at the midspan of the beam. Engineering scales were attached to the joists and deflections were recorded at various locations along the joist by using a precise level.

Verification of the developed nonlinear mathematical model was based on the favorable comparison between the measured deflections and those computed by the nonlinear model loaded beyond the working load range. Studies of the member stresses and connector forces were made with the verified nonlinear model. Comparisons of the maximum calculated member stress and connector force values and the values obtained for the upper and lower limits of connector effectiveness and specified by the National Design Specifications were studied.

In general, test results showed good agreement with the predicted deflection values from the nonlinear mathematical model for the T-beam specimens tested beyond the working load range and to failure. The predicted values of deflection for the specimens with glued connections deviated some from the experimental results. The nonlinear model predicted significantly stiffer behavior for the T-beams with glued connections than was actually exhibited by the experimental specimens. This difference is probably due to insufficient evaluation of the slip modulus for the glued connection, particularly for the shear stress beyond the working load range. Additional evaluation of the load-deformation relationship for the glued connection is recommended and could result in theoretical values which better match the experimental results in the inelastic load range. Lack of quality control of the thickness of the glue line in the T-beam specimens could have also contributed to the discrepancy in the comparisons for the glued T-beams.

The predicted values for some specimens with nailed connectors, especially those spaced at 8 inches, deviated some from the experimental results in the high load range. This difference is probably due to insufficient evaluation of the slip modulus for the nailed connection beyond the working load range. Further investigation of the load-deflection relationship beyond the working load range for the nailed connection is recommended and would also improve the reliability of the nonlinear mathematical model.

Test results showed good agreement with the predicted deflection values from the nonlinear mathematical model in the working load range, but this correlation is no better than the correlation shown in Kuo's work (14). Thus, in the working load range, the nonlinear mathematical model shows no significant improvement over the linear model. However, this improvement is significant in the inelastic load range, thus demonstrating the advantages and the effectiveness of the nonlinear model in predicting the T-beam deflections to failure. It can also be concluded from studying the improvement of the nonlinear model over the linear model in the inelastic load range that the effect of the nonlinear slip between the layers of a layered beam has an important effect on the beam's performance; even more important than other nonlinear effects such as the inelastic stress-strain relationship of the beam.

The study of the maximum member stresses and connector forces generally showed consistent results with relative trends being evident. The presence of gaps significantly increases the maximum member stress in tension and connector force in a typical T-beam. The predicted values for maximum member stress in tension and the connector forces calculated with the model were between the values computed for the limiting cases of rigid connection and no connection for all the layered systems except the glued T-beam specimens. The presence of gaps in the glued T-beam specimen caused the maximum shear stress in the glued connection to exceed the value calculated by the basic elastic beam equation for shear flow ($q = VQ/I$) for a rigid connection and continuous sheathing layer.

Comparison of the maximum member stresses in tension and the NDS allowable unit stresses demonstrates the range of safety factors present in the specifications. The safety factors for the allowable unit bending stress and allowable unit tension stress parallel to the grain for the visual grading method range from 1.6 to 5.4 and from 2.4 to 8.5, respectively. For the machine grading method, a smaller range of safety factors for the allowable bending and tension stresses of 1.3 to 3.3 and 1.7 to 5.7, respectively, is evident.

Comparison of the maximum predicted nail forces at the T-beam failure loads and the NDS ultimate lateral load capacity for nails shows a ratio of the ultimate lateral load capacity by NDS and the maximum computed force for the nails ranging from 1.06 to 1.67. Nail forces generally exceeded the allowable lateral load capacity of nails specified by NDS when the T-beams were loaded to the working load limit defined by the deflection equal to L/360 or the maximum tensile stress equal to the allowable unit bending stress. Values ranged from 99 psi to 146 psi for the maximum predicted glue connection stress for the T-beams tested in the working load range, defined as occurring when the deflection and stresses computed for the composite system reached L/360 or F_b', respectively.

An extension of this research effort of the analysis of member stresses and connector forces is recommended and would result in the evaluation of a failure criteria for layered beam systems.

In conclusion, the verification study demonstrated that the nonlinear mathematical model for multilayered beams with interlayer slip closely predicts the behavior of two- and three-layered T-beam systems up to an undetermined failure load for a wide range of material and configuration combinations. Further development and use of this model for wood joist structural systems with the composite nature being properly recognized will allow for more economical design and more efficient use of materials.

REFERENCES

1. Amana, E.J. and Booth, L.G., "Theoretical and Experimental Studies on Nailed and Glued Plywood Stressed-Skin Components: Part I. Theoretical Study," Journal of the Institute of Wood Science, Vol. 4, No. 19, September 1967.

2. Amana, E.J. and Booth, L.G., "Theoretical and Experimental Studies on Nailed and Glued Plywood Stressed-Skin Components: Part II. Experimental Study," Journal of the Institute of Wood Science, Vol. 4, No. 20, April 1967.

3. American Society for Testing and Materials, 1972 Annual Book of ASTM Standards, Part 16, "Structural Sandwich Construction; Wood; Adhesives," ASTM, Philadelphia, Pennsylvania, 1972.

4. Bodig, J. and Troxell, H.E., "Working Stresses for Mechanically Rated Engelmann Spruce," Agricultural Experimental Station General Series 847, Colorado State University, April 1967.

5. Clark, L.G., "Deflections of Laminated Beams," Transactions, American Society of Civil Engineers, Vol. 119, 1954.

6. Goodman, J.R., "Layered Wood Systems with Interlayer Slip," Ph.D. Dissertation, University of California, Berkeley, 1967.

7. Goodman, J.R. and Popov, E.P., "Layered Beam Systems with Interlayer Slip," Journal of Structural Division, American Society of Civil Engineering, Vol. 94, No. ST 11, November 1968.

8. Granholm, H., "Om Sammansatta Balkar Och Pelare Med Sarkilo Hansyn Till Sapikade Trakonstrukioner" ("On Composite Beams and Columns with Particular Regard to Nailed Timber Structures"), Chalmers Tekniska Hogskoas Handlingar, No. 88, 1949.

9. Henghold, W.M., "Layered Beam Vibrations Including Slip," Ph.D. Dissertation, Colorado State University, Fort Collins, Colorado, June 1972.

10. Hilbrand, H.D. and Miller, D.G., "Machine Grading Theory and Practice," Forest Products Journal, Vol. 16 Nos. 11 and 12, November and December 1966.

11. Hoyle, R.J., Jr., "Deflections of Twenty Experimental Wood Beams Using Design Method of Kuenzi and Wilkinson," Unpublished report, Washington State University, College of Engineering Research Division, September 1972.

12. Hoyle, R.J., Jr., "Behavior of Wood I-Beams Bonded with Elastomeric Adhesive," Bulletin 328, College of Engineering Research Division, Washington State University, Pullman, Washington, 1973.

13. Ko, M.F., "Layered Beam Systems with Interlayer Slip," M.S. Thesis, Colorado State University, Fort Collins, Colorado, December 1972.

14. Kuo, M.L., "Verification of a Mathematical Model for Layered T-Beams," M.S. Thesis, Colorado State University, Fort Collins, Colorado, 1974.

15. Kuo, Shan S., Numerical Methods and Computers, Addison-Wesley Publishing Company, London, 1965.

16. Krueger, G.P. and Sandberg, L.B., "Ultimate-Strength Design of Reinforced Timber-Evaluation of Design Parameters," Wood Science, Vol. 6, No. 4, April 1974.

17. Kuenzi, E.W. and Wilkinson, T.L., "Composite Beams--Effect of Adhesive on Fastener Rigidity," USDA Forest Service Research Paper FPL 152, 1971.

18. Liu, J.S., "Verification of Mathematical Model for Wood Joist Floor Systems," Ph.D. Dissertation, August 1974.

19. McLain, T.E., "Nondestructive Evaluation of Full Size Wood Composite Panels," M.S. Thesis, Colorado State University, Fort Collins, Colorado, May 1973.

20. National Design Specification for Stress-Grade Lumber and Its Fasteners, National Lumber Manufacturers Association, 1973 Edition.

21. National Particleboard Association, "Particleboard Design and Use Manual," AIA file No. 23-L, 1967.

22. Newmark, N.M., Seiss, C.P., and Viest, I.M., "Tests and Analysis of Composite Beams with Incomplete Interaction," Proceedings, Society for Experimental Stress Analysis, Vol. 09, No. 1, 1951.

23. Norris, C.B., Erickson, W.S., and Kommers, Wm. J., "Flexural Rigidity of a Rectangular Strip of Sandwich Construction--Comparison between Mathematical Analysis and Results of Tests," Forest Products Laboratory Report 1505A, May 1952.

24. O'Halloran, M.R., "Nondestructive Parameters for Lodgepole Pine Dimension Lumber," M.S. Thesis, Colorado State University, Fort Collins, Colorado, 1969.

25. Patterson, D.W., "Nailed Wood Joist under Lateral Loads," M.S. Thesis, Colorado State University, Fort Collins, Colorado, April 1973.

26. Penner, B.G., "Experimental Behavior of Wood Flooring Systems," M.S. Thesis, Colorado State University, Fort Collins, Colorado, December 1972.

27. Pleshkov, P.F., Teoriia Rashceta Depeviannykh (Theoretical Studies of Composite Wood Structures), Moscow, 1952.

28. Rassam, H.Y., "Layered Columns with Interlayer Slip," Ph.D. Dissertation, Colorado State University, Fort Collins, Colorado, March 1969.

29. Rose, J.D., "Field-Glued Plywood Floor Tests," Report 118, American Plywood Association Laboratory, Revised, May 1970.

30. Seiss, C.P., Viest, I.M., and Newmark, N.M., "Small Scale Tests of Shear Connectors of Composite T-Beams," Bulletin 396, University of Illinois Engineering Experimental Station, Vol. 49, No. 45, February 1952.

31. Thompson, E.G., Goodman, J.R., and Vanderbilt, M.D., "Analysis of Layered Wood Systems with Gaps at Joints," to be published.

32. Western Wood Products Association, Western Woods Use Book, WWPA, Portland, Oregon, 1973.

33. Wolfe, R.W., "Upgrading of Dimension Lumber by Finger Jointing," M.S. Thesis, Colorado State University, Fort Collins, Colorado, May 1972.

34. Wood Handbook, The Forest Products Laboratory Forest Service, U.S. Department of Agriculture, Handbook No. 72, 1955.

35. Zakic, Borislav D., "Inelastic Bending of Wood Beams," Journal of the Structural Division, Proceedings of the American Society of Civil Engineers, October 1973.

36. Zienkiewicz, O.C., The Finite Element Method in Engineering Science, McGraw-Hill Publishing Company, London, 1971.

APPENDIX A

PROPERTIES OF JOISTS

APPENDIX A PROPERTIES OF JOISTS

Specimen No.	Joist No.	Joist Dimension		*Average Flat-wise MOE 10^6 psi	**Edgewise MOE 10^6 psi		
		w in	h in		No lat. supp.	With Header 1 nail	With Header 3-nail
T3-8D16-1	DW-S-08-33	1.495	7.153	1.938	2.402		2.320
	DW-S-08-39	1.475	7.190	1.964	1.850		1.811
T4-8D16-1	DW-S-08-37	1.468	7.145	1.766	2.206		2.429
	DW-S-08-43	1.488	7.210	1.696	2.131		2.269
T5-8D16-1	DW-S-08-27	1.490	7.137	1.481	1.656		1.847
	DW-S-08-34	1.491	7.163	1.448	1.765		1.774
T6-8D16-1	DW-S-08-15	1.468	7.187	1.799	2.181		2.330
	DW-S-08-23	1.475	7.092	1.798	2.062		2.349
T7-8D16-1	DW-S-08-45	1.503	7.209	1.787	1.883		2.141
	DW-S-08-58	1.478	7.170	1.791	2.027		2.152
T8-8D16-1	DW-S-08-22	1.476	7.251	1.739	1.757	1.628	1.805
	DW-S-08-29	1.429	7.195	1.793	1.879	1.535	1.744
T9-8D16-1	DW-S-08-12	1.496	7.217	1.880	1.981	2.074	2.269
	DW-S-08-05	1.443	7.130	1.830	2.395	2.478	2.566
T10-12E24-1	EC-S-12-05	1.492	11.210	1.068	1.124	1.076	1.269

APPENDIX A (Continued)

Specimen No.	Joist No.	Joist Dimension w in	Joist Dimension h in	*Average Flat-wise MOE 10^6 psi	**Edgewise MOE 10^6 psi No lat. supp.	With Header 1 nail	With Header 3-nail
T10-12E24-1	EC-S-12-04	1.503	11.205	0.988	1.243	1.217	1.261
T11-8D16-1	DW-N-08-52	1.500	7.231	0.853	0.929	0.968	0.975
	DW-N-08-47	1.480	7.092	0.933	0.993	1.074	1.088
T12-8D16-1	DW-N-08-51	1.480	7.048	0.838	1.178	1.249	1.249
	DW-N-08-55	1.491	7.232	0.937	1.222	1.261	1.261
T13-8D16-1	DW-N-08-21	1.494	7.226	1.174	1.357		1.342
	DW-N-08-49	1.496	7.268	1.021	1.055		1.077
T14-12D24-1	DW-S-12-21	1.488	11.115	1.296	1.740	1.845	1.883
	DW-S-12-23	1.507	11.156	1.290	1.586	1.667	1.715
T15-8E19.2-1	EK-S-08-01	1.494	7.139	0.769	1.051	1.161	1.191
	EK-S-08-09	1.500	7.197	0.781	1.054	1.106	1.151
T16-8E19.2-1	EC-S-08-06	1.454	7.115	1.033	1.425		1.500
	EK-N-08-13	1.465	7.091	1.026	1.261		1.261

APPENDIX A (Continued)

Specimen No.	Joist No.	Joist Dimension w in	Joist Dimension h in	*Average Flatwise MOE 10^6 psi	**Edgewise MOE 10^6 psi No lat. supp.	With Header 1 nail	With Header 3-nail
T17-8D16-1	DW-S-08-31	1.470	7.143	2.015	2.362	-	2.445
	DW-S-08-53	1.497	7.169	2.117	2.237	-	2.275
T18-8D16-1	DW-S-08-59	1.495	7.222	1.813	-	-	2.071
	DW-S-08-63	1.490	7.243	2.091	-	-	1.819

*Determined by the Wood Science Laboratory. Refer to Section 3.2.1 for description of tests.
**Determined during the specimen construction. Refer to Section 3.2.2 for description of tests.

APPENDIX B

PROPERTIES OF SHEATH

APPENDIX B PROPERTIES OF SHEATHING*

Specimen No.	Sheet No.	Nominal Dimension	$E_{\parallel}$** 10^6 psi	$E_{\perp}$** 10^5 psi	G 10^5 psi	Grade
T3-8D16-1	DP-34-27	4'x8'x3/4"	1.341	4.870	0.7870	Tongue and groove, STD-INT
	DP-34-28	4'x8'x3/4"	1.133	5.418	0.8184	Tongue and groove, STD-INT
T4-8D16-1	DP-34-25	4'x8'x3/4"	1.283	5.5 0	0.8829	Tongue and groove, STD-INT
T5-8D16-1	DP-34-21	4'x8'x3/4"	1.499	5.390	0.8613	Tongue and groove, STD-INT
T6-8D16-1	DP-34-20	4'x8'x3/4"	1.249	6.008	0.8872	Tongue and groove, STD-INT
T7-8D16-1	DP-34-22	4'x8'x3/4"	1.369	5.300	0.8641	Tongue and groove, STD-INT
T8-8D16-1	DP-34-17	4'x8'x3/4"	1.243	4.912	0.8901	Tongue and groove, STD-INT
T9-8D16-1	DP-34-18	4'x8'x3/4"	1.270	5.352	0.8389	Tongue and groove, STD-INT
T10-12E24-1	DP-34-10	4'x8'x3/4"	1.235	5.463	0.8025	Tongue and groove, STD-INT
	DP-34-13	4'x8'x3/4"	1.513	5.516	0.9863	Tongue and groove, STD-INT
T11-8D16-1	DP-34-8	4'x8'x3/4"	1.247	5.326	0.7421	Tongue and groove, STD-INT
T12-8D16-1	DP-34-12	4'x8'x3/4"	1.513	5.581	0.8251	Tongue and groove, STD-INT
T13-8D16-1	EP-58-28	4'x8'x3/4"	1.281	4.323	0.9537	Tongue and groove, STD-INT (exterior glue)
T14-12D-24-1	DP-12-02	4'x8'x1/2"	1.721	2.563	1.351	STD-INT (intermed. glue)
	DP-12-03	4'x8'x1/2"	1.664	2.236	1.504	STD-INT (intermed. glue)
T14-12D-24-2	DB-12-19	4'x8'x1/2"	.5782	4.494	1.719	Floor underlayment
	DB-12-20	4'x8'x1/2"	.5837	4.367	1.806	Floor underlayment
T15-8E19.2-1	EP-12-02	4'x8'x1/2"	1.411	2.221	2.224	STD-INT (exterior glue)
	EP-12-03	4'x8'x1/2"	1.390	2.157	2.246	STD-INT (exterior glue)

APPENDIX B* (Continued)

Specimen No.	Sheet No.	Nominal Dimension	$E_{\parallel}$** 10^6 psi	$E_{\perp}$** 10^5 psi	G 10^5 psi	Grade
T15-8E19.2-2	DB-12-19	4'x8'x1/2"	0.5782	4.494	1.719	Floor underlayment
	DB-12-20	4'x8'x1/2"	0.5837	4.367	1.806	Floor underlayment
	DB-12-21	4'x8'x1/2"	0.5447	4.290	1.702	Floor underlayment
T16-8E19.2-1	EP-12-03	4'x8'x1/2"	1.390	2.157	2.246	STD-INT (exterior glue)
	EP-12-04	4'x8'x1/2"	1.360	2.287	2.058	STD-INT (exterior glue)
T16-8E19.2-2	DB-12-7	4'x8'x1/2"	0.4486	3.331	1.773	Floor underlayment
	DB-12-10	4'x8'x1/2"	0.4869	3.808	1.657	Floor underlayment
T17-8D16-1	DP-34-01	4'x8'x3/4"	1.356	4.655	0.666	Tongue and groove, STD-INT
	DP-34-02	4'x8'x3/4"	1.333	5.152	0.693	Tongue and groove, STD-INT
T18-8D16-1	DP-34-01	4'x8'x3/4"	1.356	4.655	0.666	Tongue and groove, STD-INT
	DP-34-24	4'x8'x3/4"	1.362	5.253	0.920	Tongue and groove, STD-INT

*See Section 3.2.1 for description of testing procedure.
**E values are valid for bending and based on gross section dimensions, see Section 5.
$\parallel$=Face grain parallel to bending; $\perp$=Face grain perpendicular to bending.

APPENDIX C

SPECIMEN CONFIGURATION AND COMPARISONS OF PREDICTED AND OBSERVED DEFLECTIONS

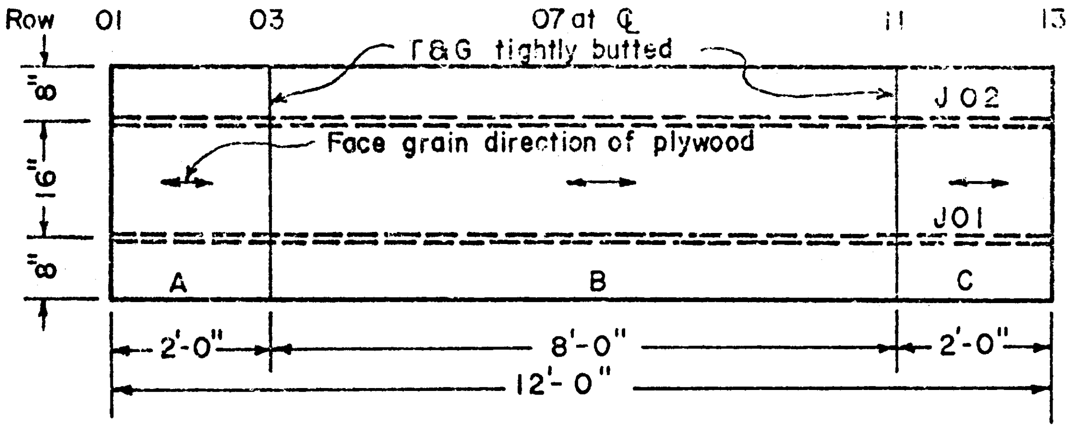

TOP VIEW

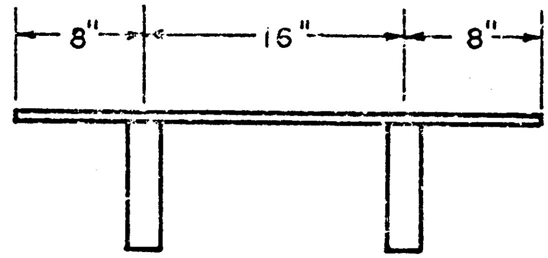

CROSS SECTION

Description of specimen

Joist: 2x8 Douglas fir

J01	DW-S-08-33	$E = 2.32\mathrm{x}10^6$ psi
J02	DW-S-08-39	$E = 1.811\mathrm{x}10^6$ psi

Sheathing: 3/4" D.F. Plywood

A	DP-34-28	$E_{\perp} = 1.133\mathrm{x}10^6$ psi
B	DP-34-27	$E_{\perp} = 1.341\mathrm{x}10^6$
C	DP-34-28	

Connector: Franklin Construction Adhesive

Sheathing Joints: T&G tightly butted

Test sequence

1. Loaded at row 07 with ΔP = 250 lb up to P = 1000 lb
2. Loaded at row 09 with loads same in 1
3. Loaded at row 11 with loads same as in 1
4. Cut gaps at rows 03 and 11, repeated test 1.

Figure C.1 Configuration and Properties of Specimen T3-8D16-1.

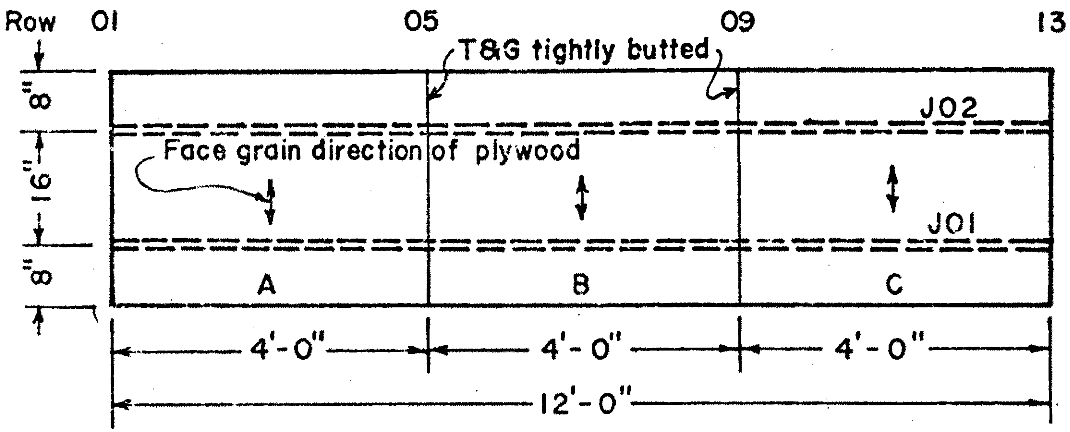

TOP VIEW

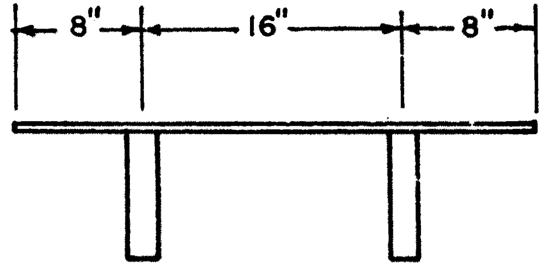

CROSS SECTION

Description of Specimen:

Joist: 2x8 Douglas fir

J01	DW-S-08-37	$E = 2.429 \times 10^6$ psi
J02	DW-S-08-43	$E = 1.694 \times 10^6$ psi

Sheathing: 3/4" D. F. Plywood

A	DP-34-25	$E_{\perp} = 5.50 \times 10^5$ psi
B	DP-34-25	
C	DP-34-25	

Connector: 8-d common nails, spacing @ 8"

Sheathing joints: Tongue & groove, tightly butted.

Test sequence:

1. Loaded at row 07 with $\Delta P = 250$ lb up to $P = 1000$
2. Loaded at row 09 with loads same in 1
3. Loaded at row 11 with loads same in 1
4. Cut gaps at rows 05 and 09; repeated tests 1, 2 and 3
5. Failure test: loaded at row 07; J02 failed at $P = 4000$ lbs.

Figure C.2 Configuration and Properties of Specimen T4-8D16-1.

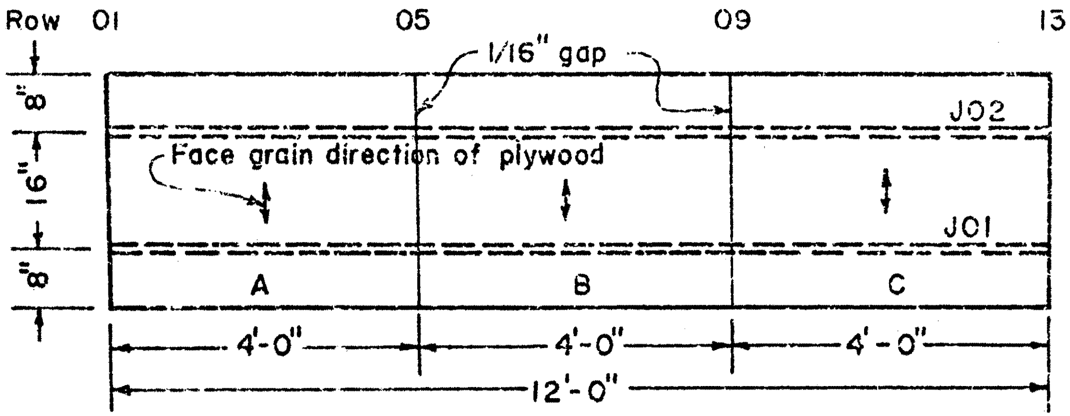

TOP VIEW

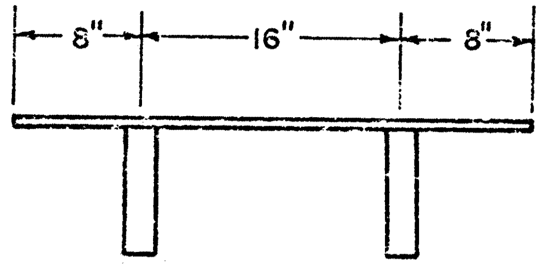

CROSS SECTION

Description of specimen:

Joist: 2x8 Douglas fir

J01	DW-S-08-27	$E = 1.847 \times 10^6$ psi
J02	DW-S-08-34	$E = 1.774 \times 10^6$

Sheathing: 3/4" D.F. Plywood

A	DP-34-21	$E_{\perp} = 5.39 \times 10^5$ psi
B	DP-34-21	
C	DP-34-21	

Connector: 8-d common nail spacing at 8"

Sheathing Joints: T&G with 1/16" gap

Test sequence

1. Loaded at row 07 with $\Delta P = 250$ lb up to $P = 1000$ lbs.
2. Loaded at row 09 with loads same in 1
3. Loaded at row 11 with loads same in 1
4. Cut gaps at rows 05 and 09; repeated tests from 1 to 3
5. Failure test: P at row 07; J01 failed at $P = 5500$ lbs.

Figure C.3 Configuration and Properties of Specimen T5-8D16-1.

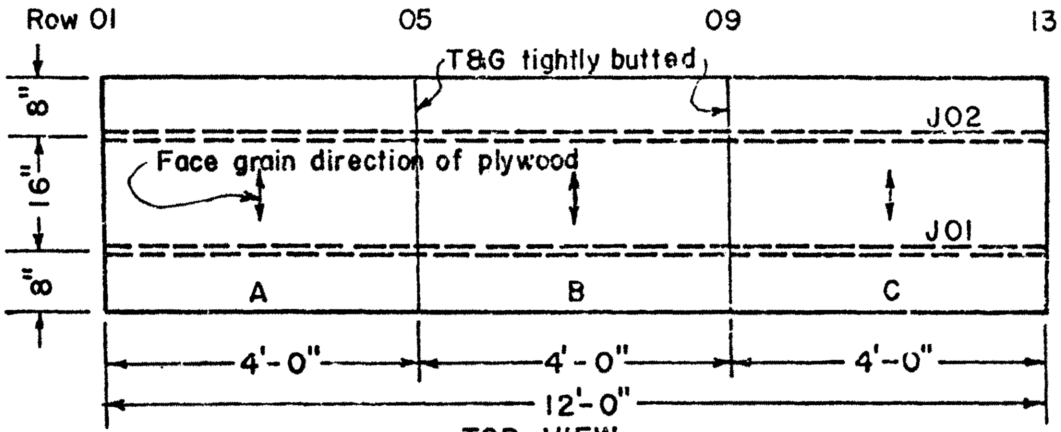

TOP VIEW

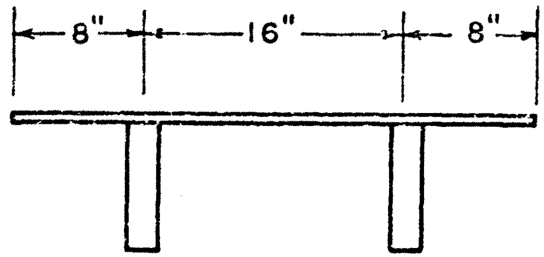

CROSS SECTION

<u>Description of specimen:</u>

Joist: 2x8 Douglas fir

J01	DW-S-08-15	E = 2.330×10^6 psi
J02	DW-S-08-23	E = 2.349×10^6 psi

Sheathing: 3/4" D.F. Plywood

A	DP-34-20	$E_{\perp} = 6.008 \times 10^5$ psi
B	DP-34-20	
C	DP-34-20	

Connector: 8-d common nails spacing at 8"

Sheathing Joints: T&G tightly butted

<u>Test sequence</u>

1. Loaded at row 07 with controlling $\Delta = 0.1$" for each increment, up to $\Delta = 0.4$"
2. Repeated test 1 for five times
3. Failure test with P at row 07; J01 failed at P = 5900 lbs.

Figure C.4 Configuration and Properties of Specimen T6-8D16-1.

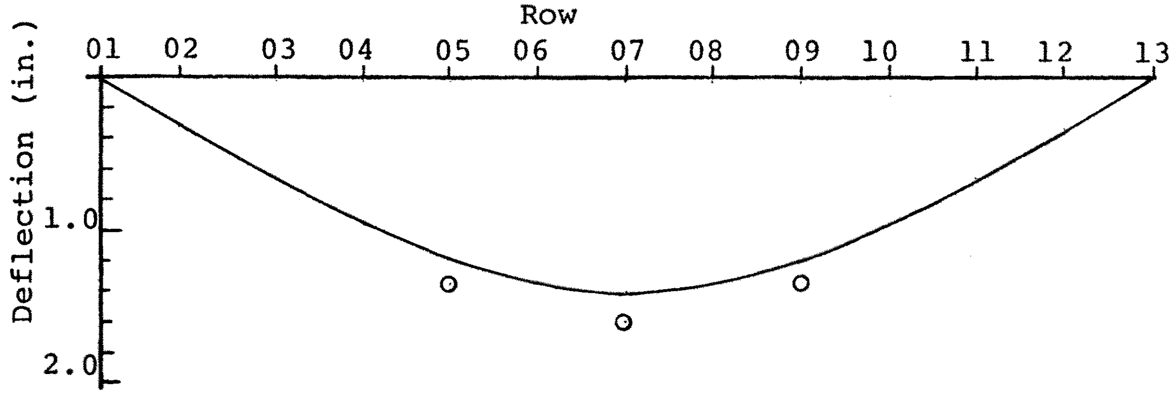

a) Deflection Profile at 2750 lbs. Load at Midspan

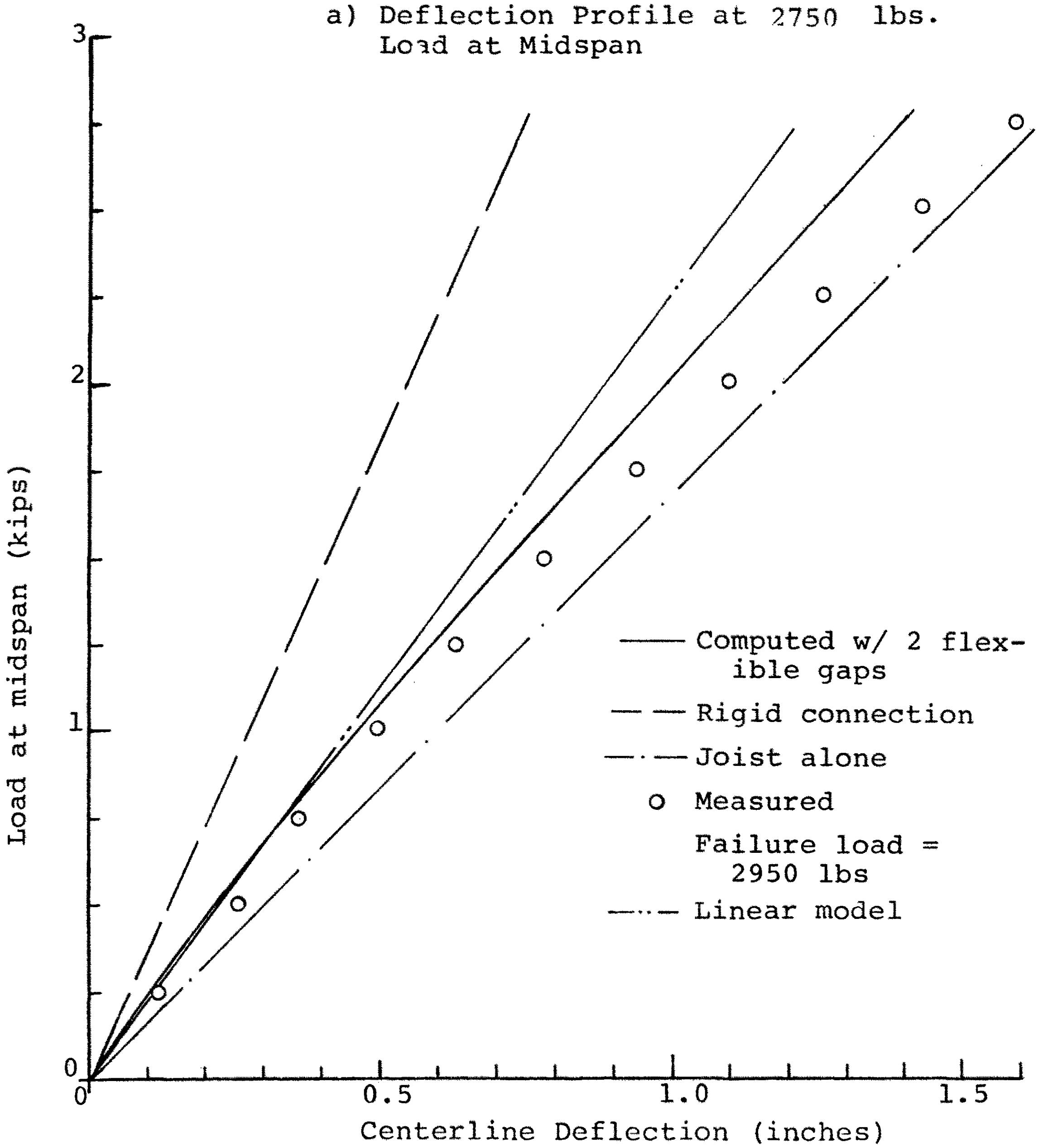

b) Load-Deflection Behavior

Figure C.5 Beam verification - T6-8D16-1 J01 with butted T & G joints.

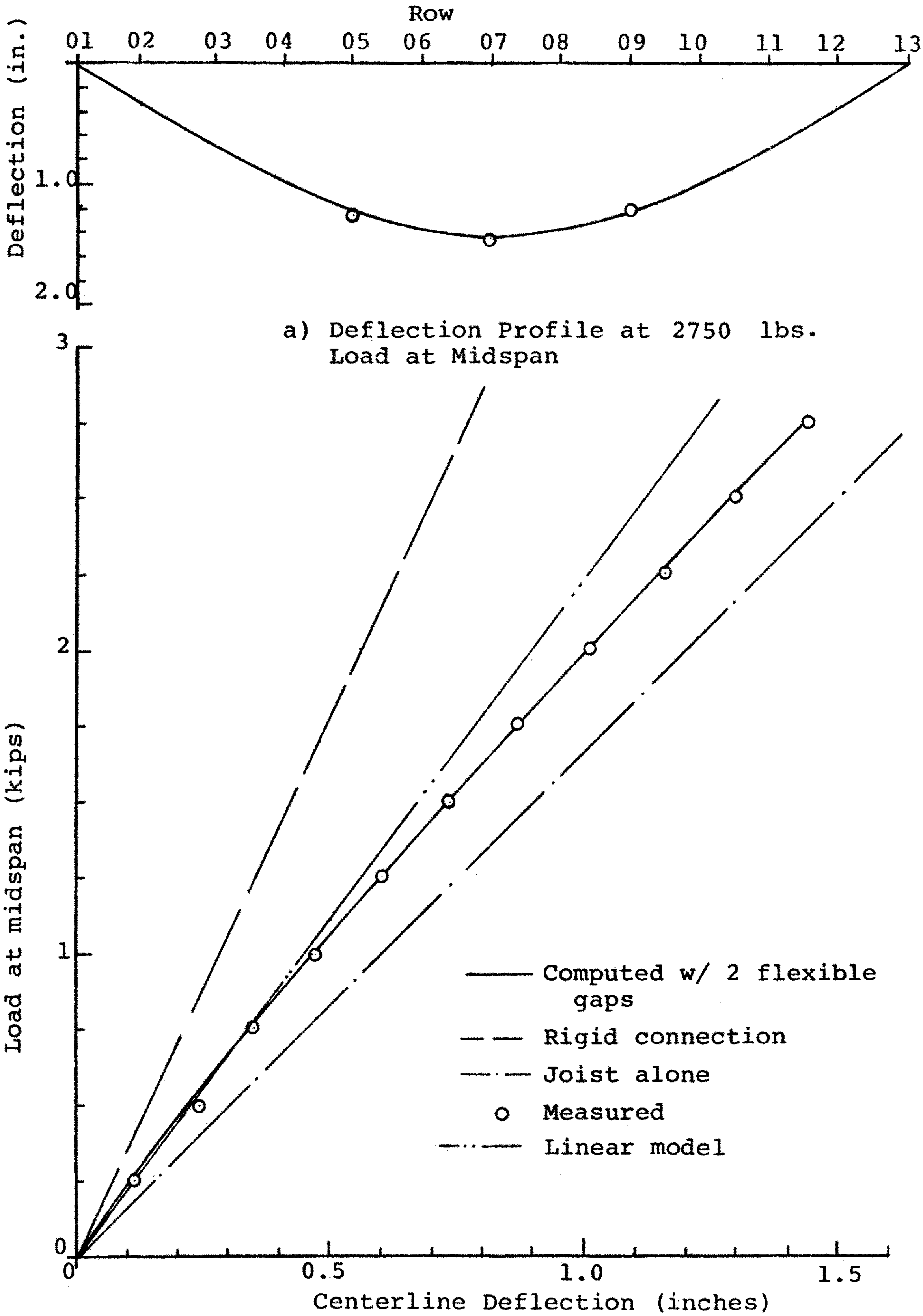

b) Load-Deflection Behavior

Figure C.6 Beam verification - T6-8D16-1 J02 with butted T & G joints.

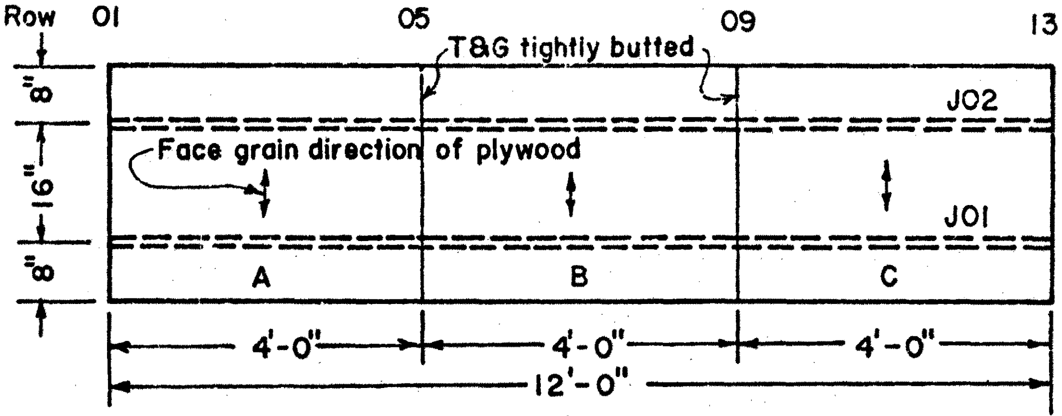

TOP VIEW

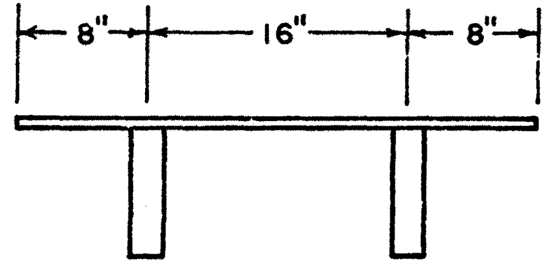

CROSS SECTION

Description of specimen:

Joist: 2x8 Douglas fir

J01	DW-S-08-45	$E = 2.141 \times 10^6$ psi
J02	DW-S-08-58	$E = 2.152 \times 10^6$ psi

Sheathing: 3/4" D.F. Pluwood

A	DP-34-22	$E_{\perp} = 5.30 \times 10^5$ psi
B	DP-34-22	
C	DP-34-22	

Connector: 8-d common nails spacing at 2"

Sheathing Joints: T&G tightly butted

Test sequence

1. Loaded at row 07 with controlling $\Delta = 0.1"$ for ecach increment, up to $\Delta = 0.4"$
2. Repeated test 1 for five times
3. Failure test with P at row 07; J01 failed at P = 7500 lbs.

Figure C.7 Configuration and Properties of Specimen T7-8D1601.

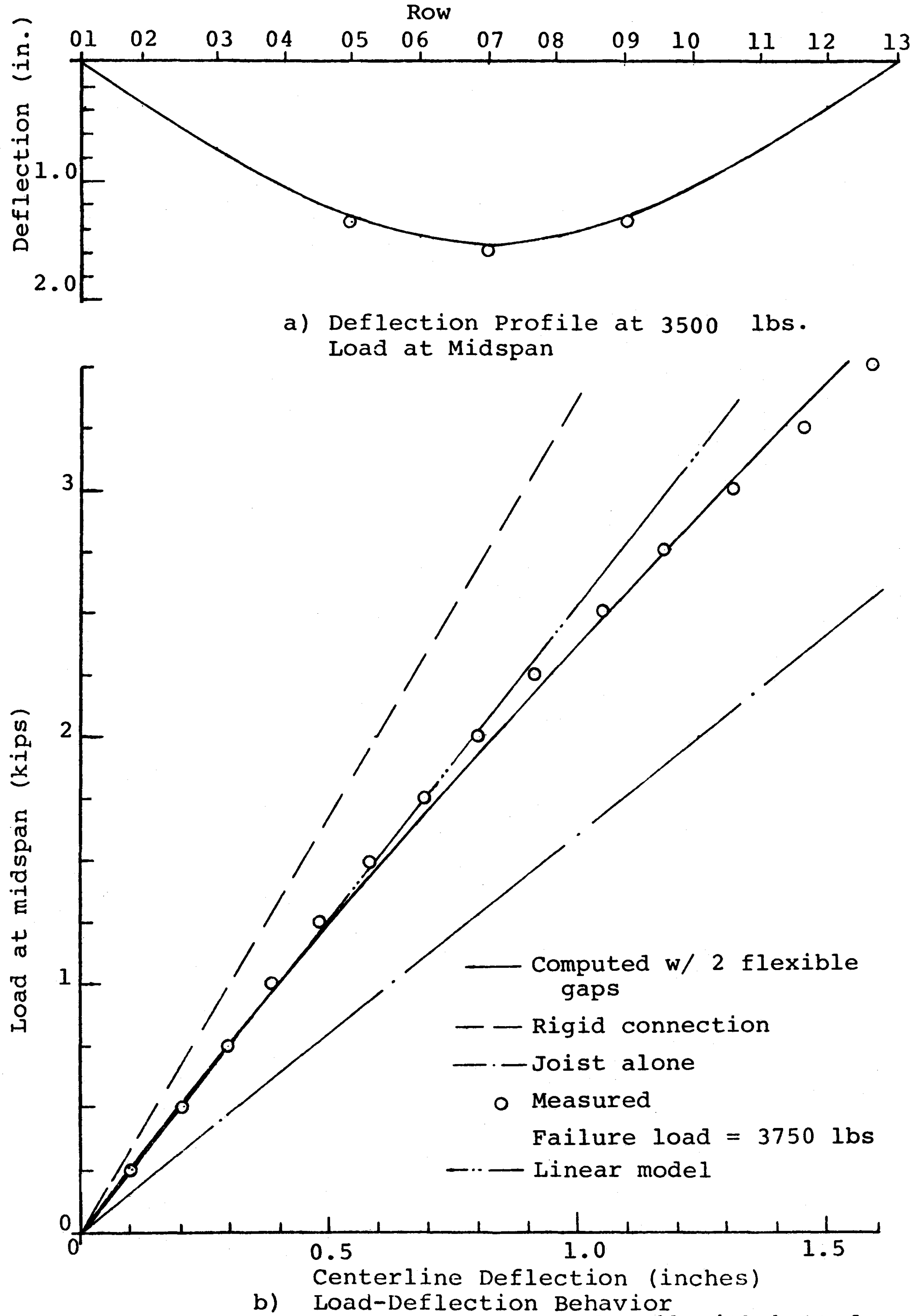

Figure C.8 Beam verification - T7-8D16-1 J01 with butted T & G joints.

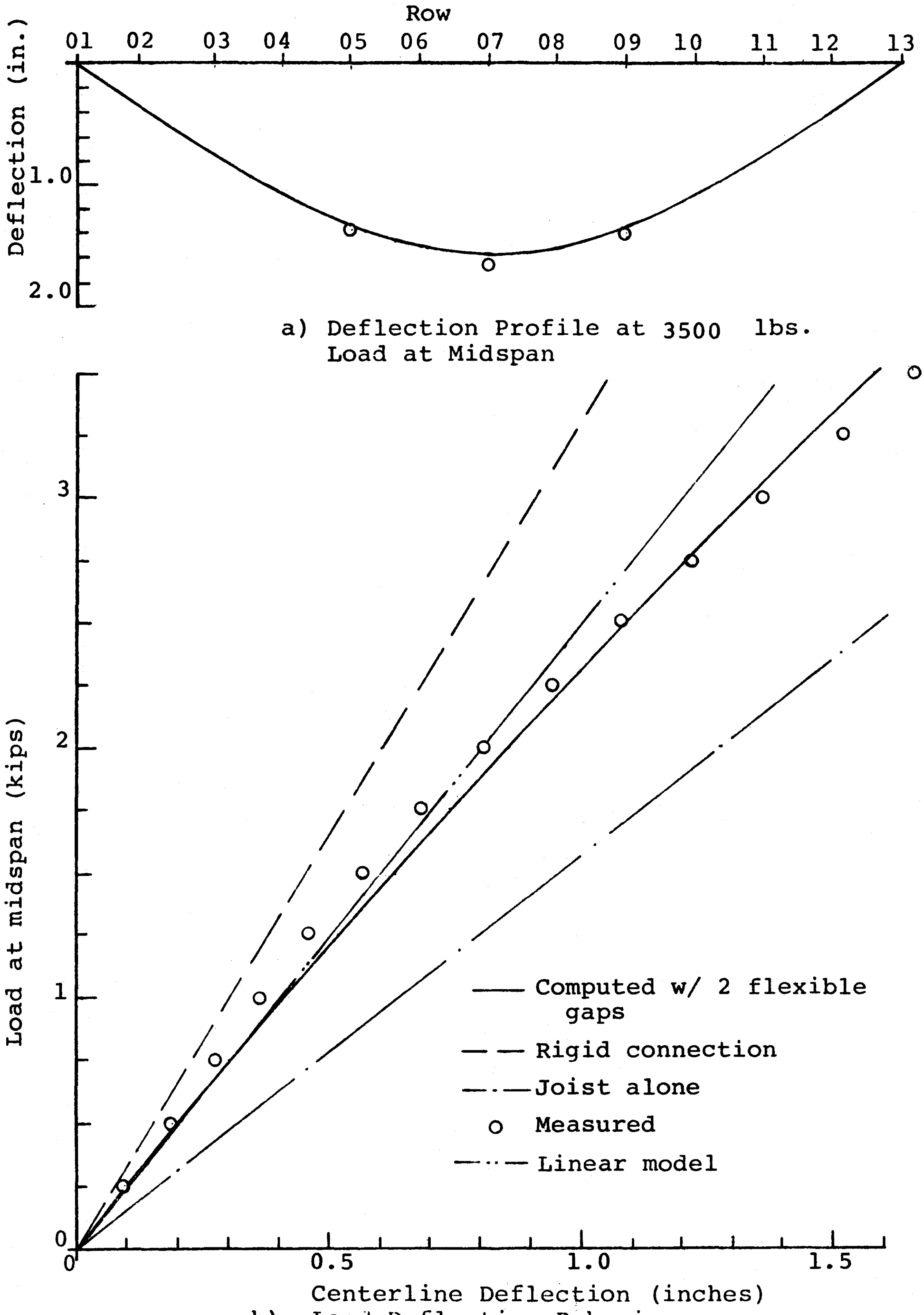

Figure C.9 Beam verification - T7-8D16-1 J02 with butted T & G joints.

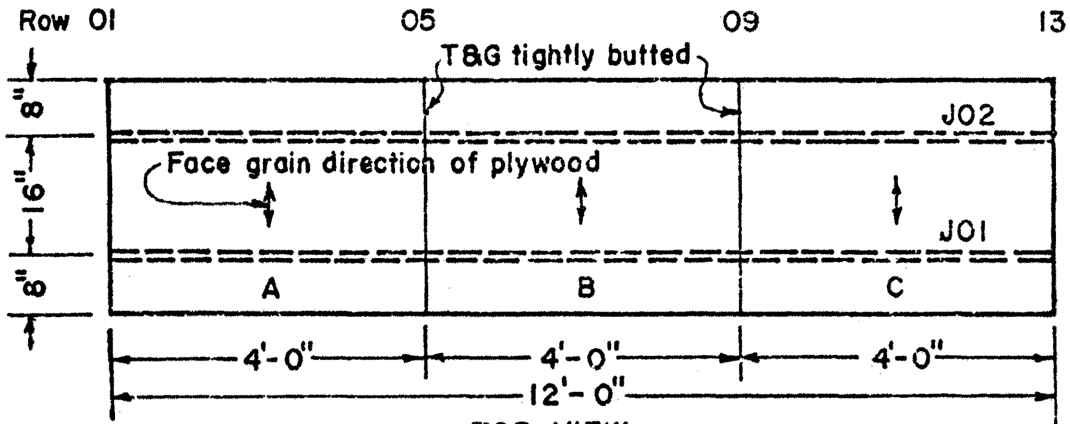

TOP VIEW

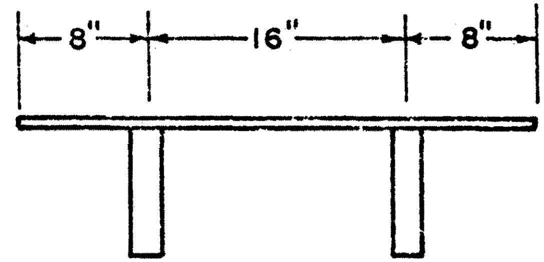

CROSS SECTION

Description of specimen:

Joist: 2x8 Douglas fir

J01	DW-S-08-22	$E = 1.805 \times 10^6$ psi
J02	DW-S-08-29	$E = 1.744 \times 10^6$ psi

Sheathing: 3/4" D.F. Plywood

A	DP-34-17	$E_{\perp} = 4.912 \times 10^5$ psi
B	DP-34-17	
C	DP-34-17	

Connector: Franklin Construction Adhesive and 8d common nails spaced at 8"

Sheathing Joints: T&G tightly butted

Test sequence

1. Loaded at row 07 with ΔP = 500 lb up to P = 2500 lbs
2. Repeated test 1 for three times
3. Cut gaps at rows 05 and 09; repeated test 1
4. Gaps filled with wood strip and repeated test 1
5. Test to failure: P at row 07; J01 failed at P = 5900 lbs.

Figure C.10 Configuration and Properties of Specimen T8-8D16-1.

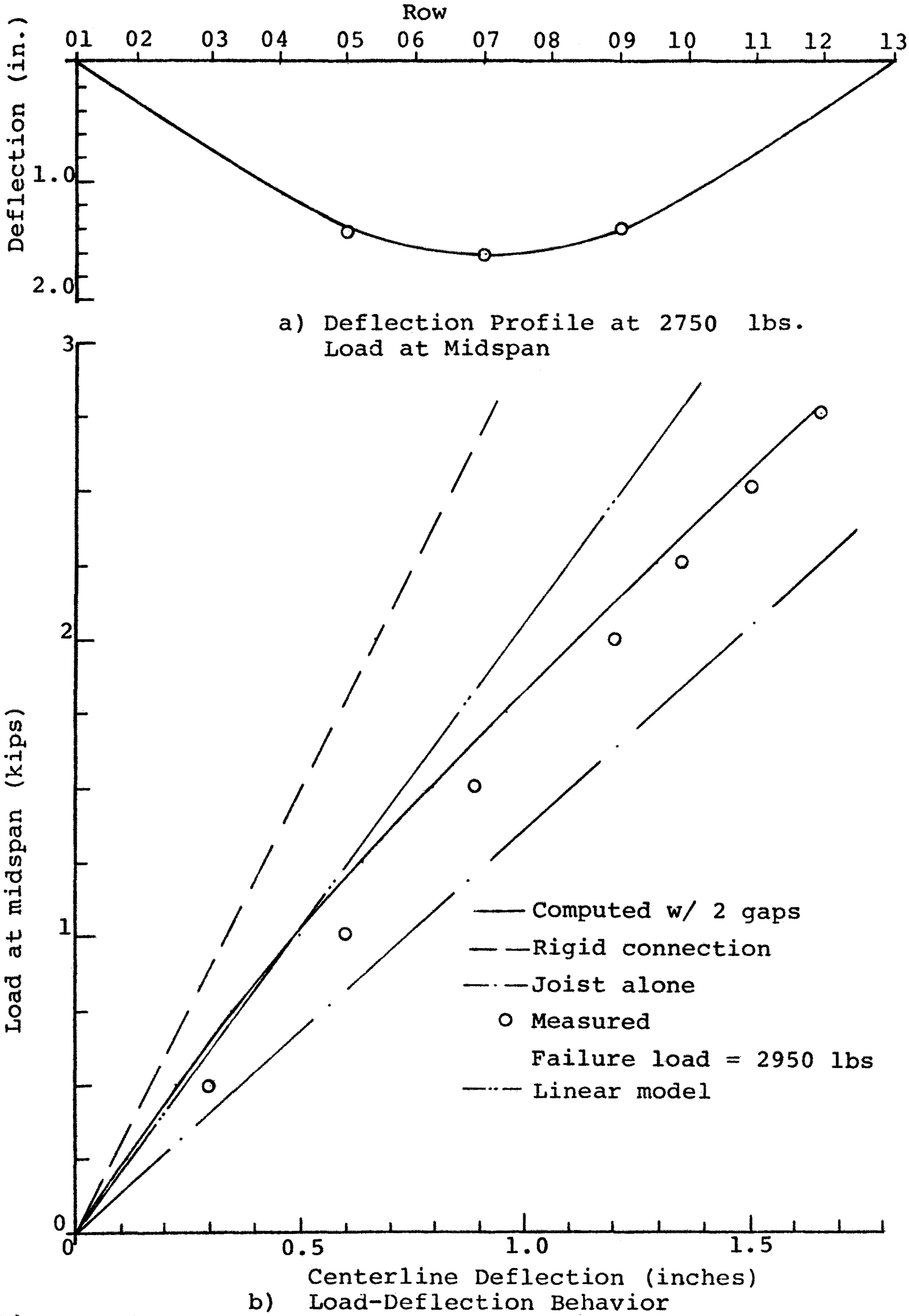

Figure C.11 Beam verification - T8-8D16-1 J01 with gaps.

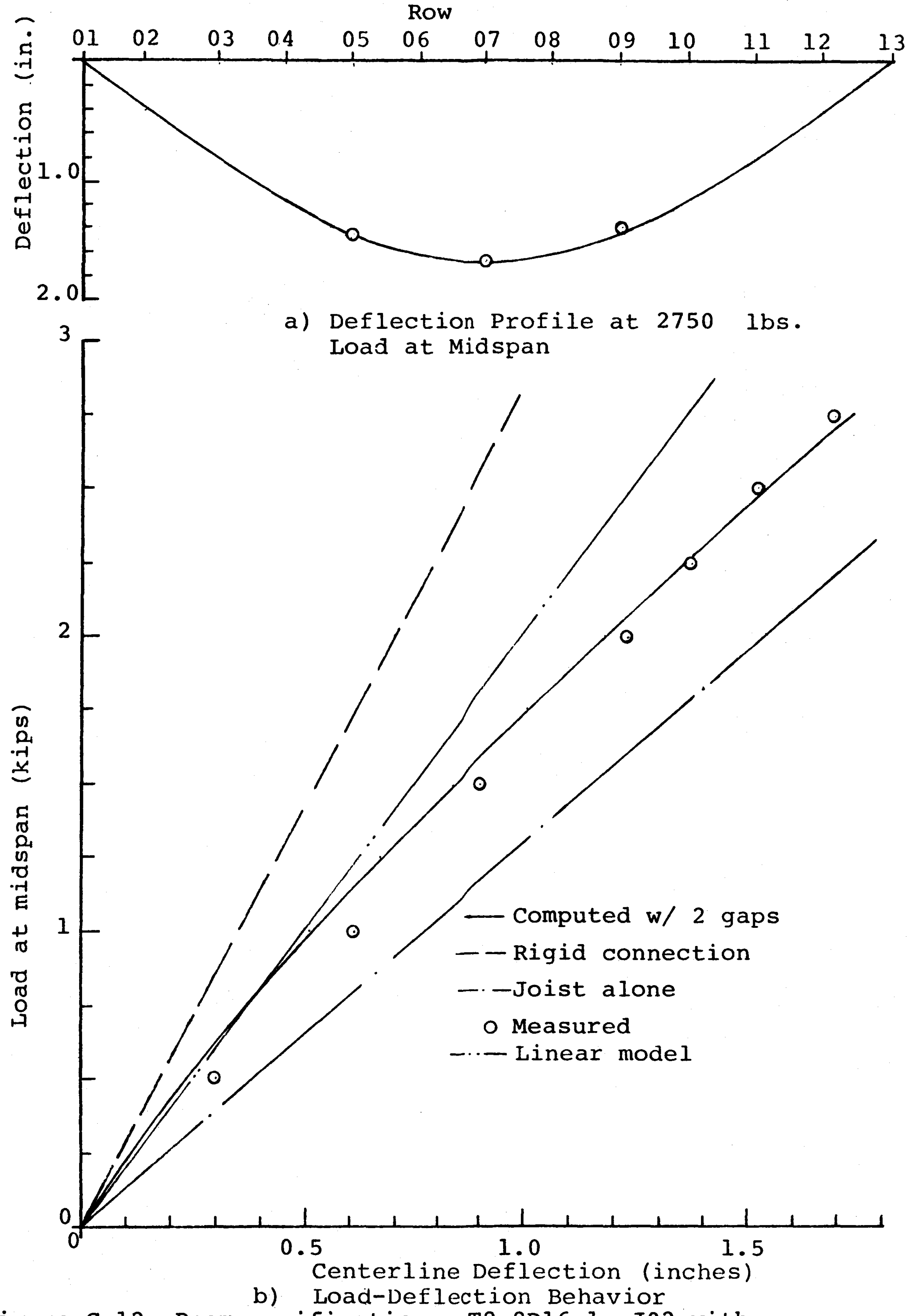

Figure C.12 Beam verification - T8-8D16-1 J02 with gaps.

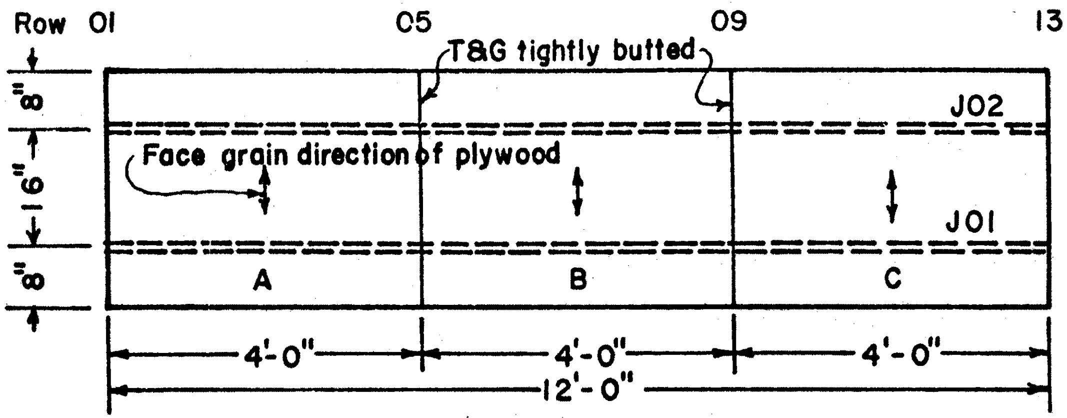

TOP VIEW

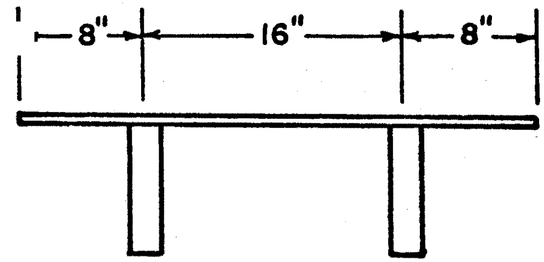

CROSS SECTION

Description of specimen:

Joist: 2x8 Douglas fir

J01	DW-S-08-12	$E = 2.269\times10^6$ psi
J02	DW-S-08-05	$E = 2.566\times10^6$

Sheathing: 3/4" D.F. Plywood

A	DP-34-18	$E_\perp = 5.352\times10^5$ psi
B	DP-34-18	$E_\perp = 5.352\times10^5$ psi
C	DP-34-18	$E_\perp = 5.352\times10^5$ psi

Connector: Franklin Construction Adhesive

Sheathing Joints: T&G tightly butted

Test sequence

1. Loaded at row 07 with ΔP = 500 lbs up to P = 2500 lbs
2. Repeated test 1 for five times
3. Cut gaps at rows 05 and 09; reloaded same as in 1
4. Gaps filled with wood strip; repeated test 1
5. Gaps filled; repeated test 1 up to P = 4000 lbs
6. Test to failure: P at row 07; J02 cracked and completely failed at P = 10,000 lbs.
7. Test to failure for single T, J01 failure load = 5000 lbs

Figure C.13 Configuration and Properties of Specimen T9-8D16-1.

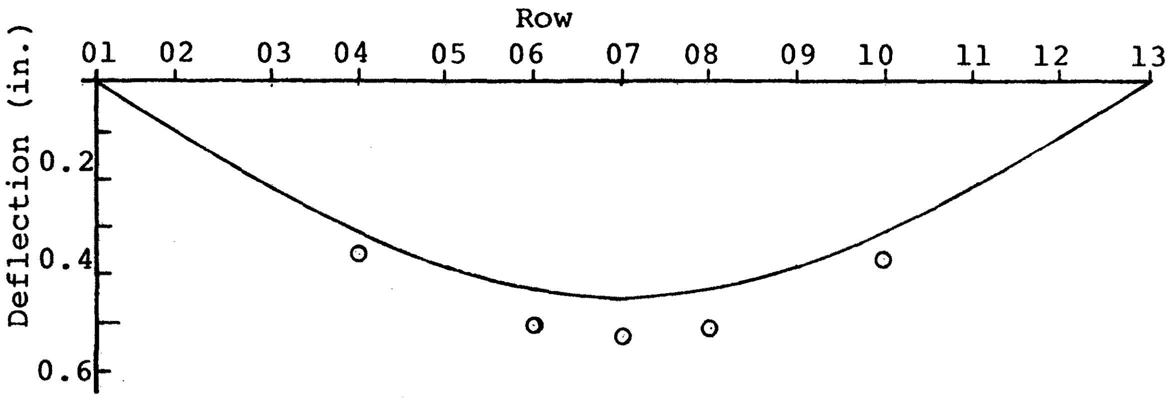

a) Deflection Profile at 1250 lbs.
Load at Midspan

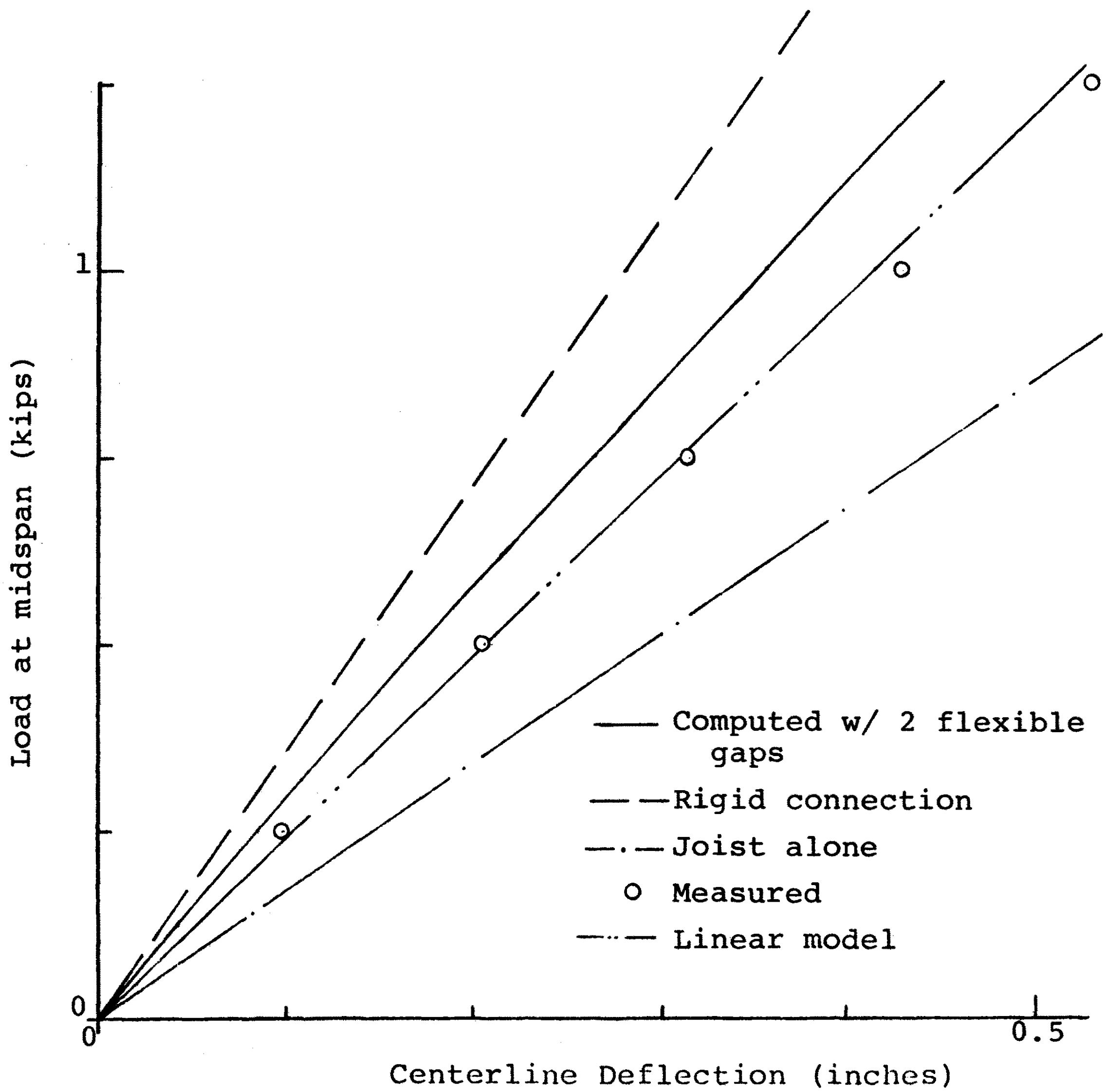

b) Load-Deflection Behavior

Figure C.14 Beam verification - T9-8D16-1 J01 with butted T & G joints.

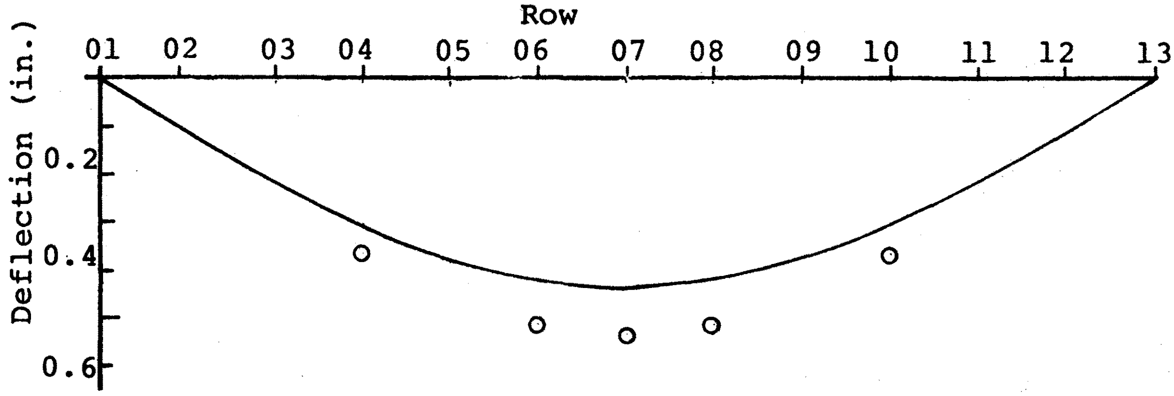

a) Deflection Profile at 1250 lbs. Load at Midspan

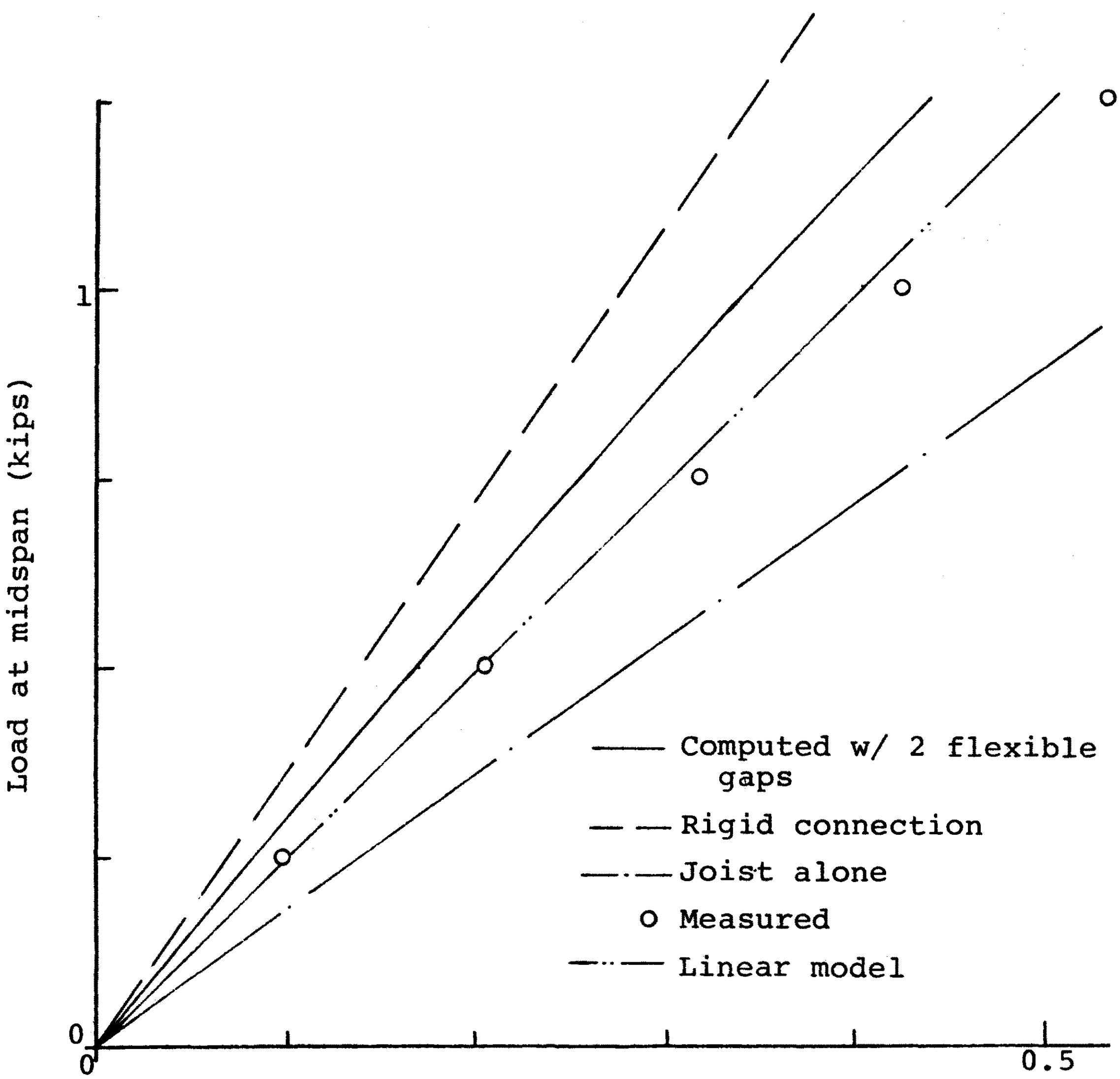

b) Load-Deflection Behavior

Figure C.15 Beam verification - T9-8D16-1 J02 with butted T & G joints.

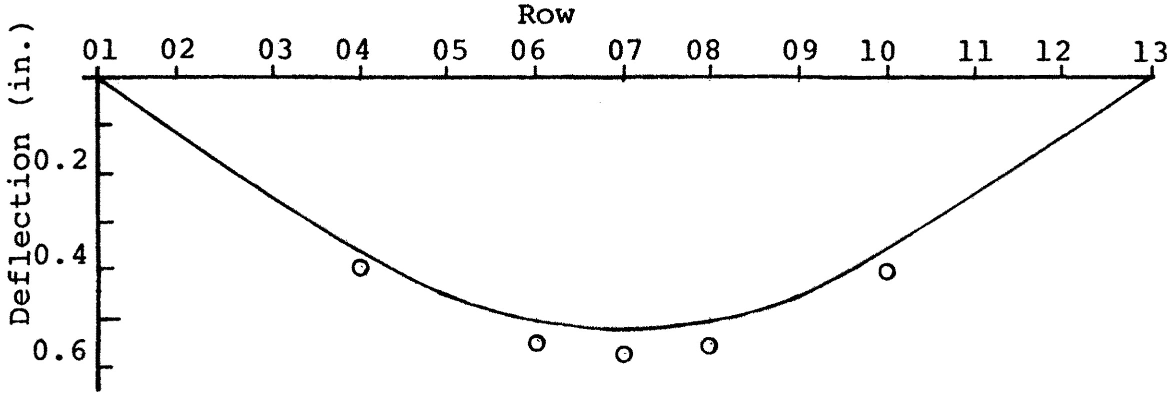

a) Deflection Profile at 1250 lbs.
Load at Midspan

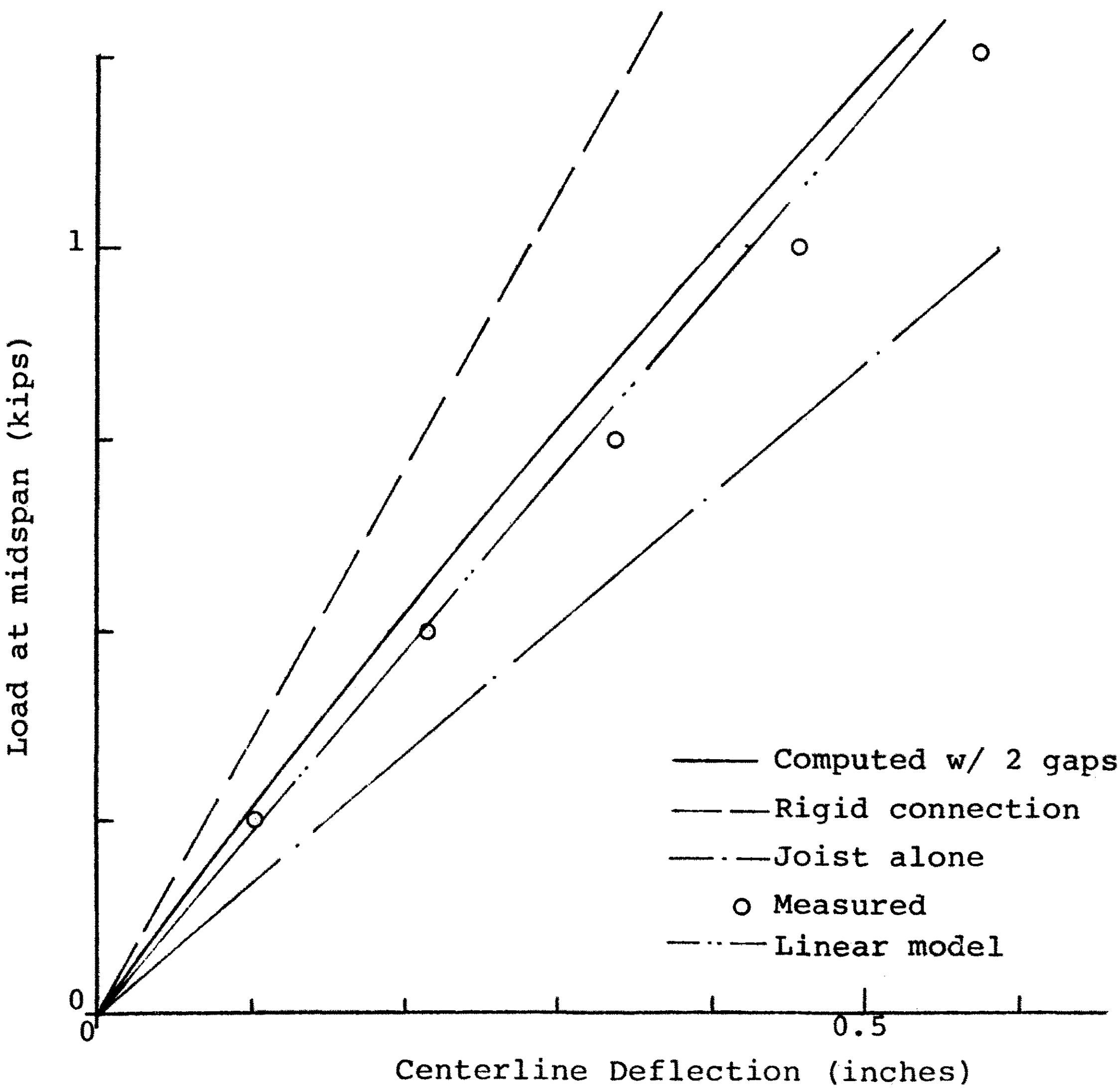

b) Load-Deflection Behavior

Figure C.16 Beam verification - T9-8D16-1 J01 with gaps.

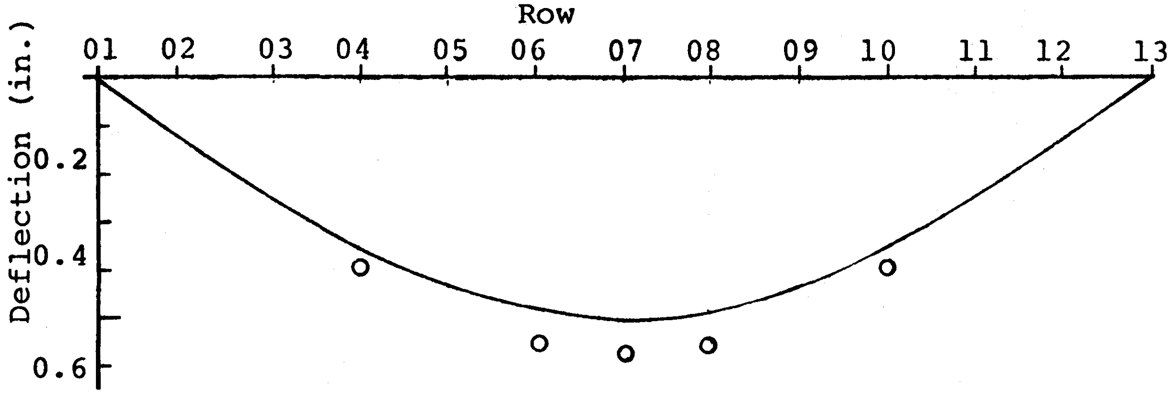

a) Deflection Profile at 1250 lbs.
Load at Midspan

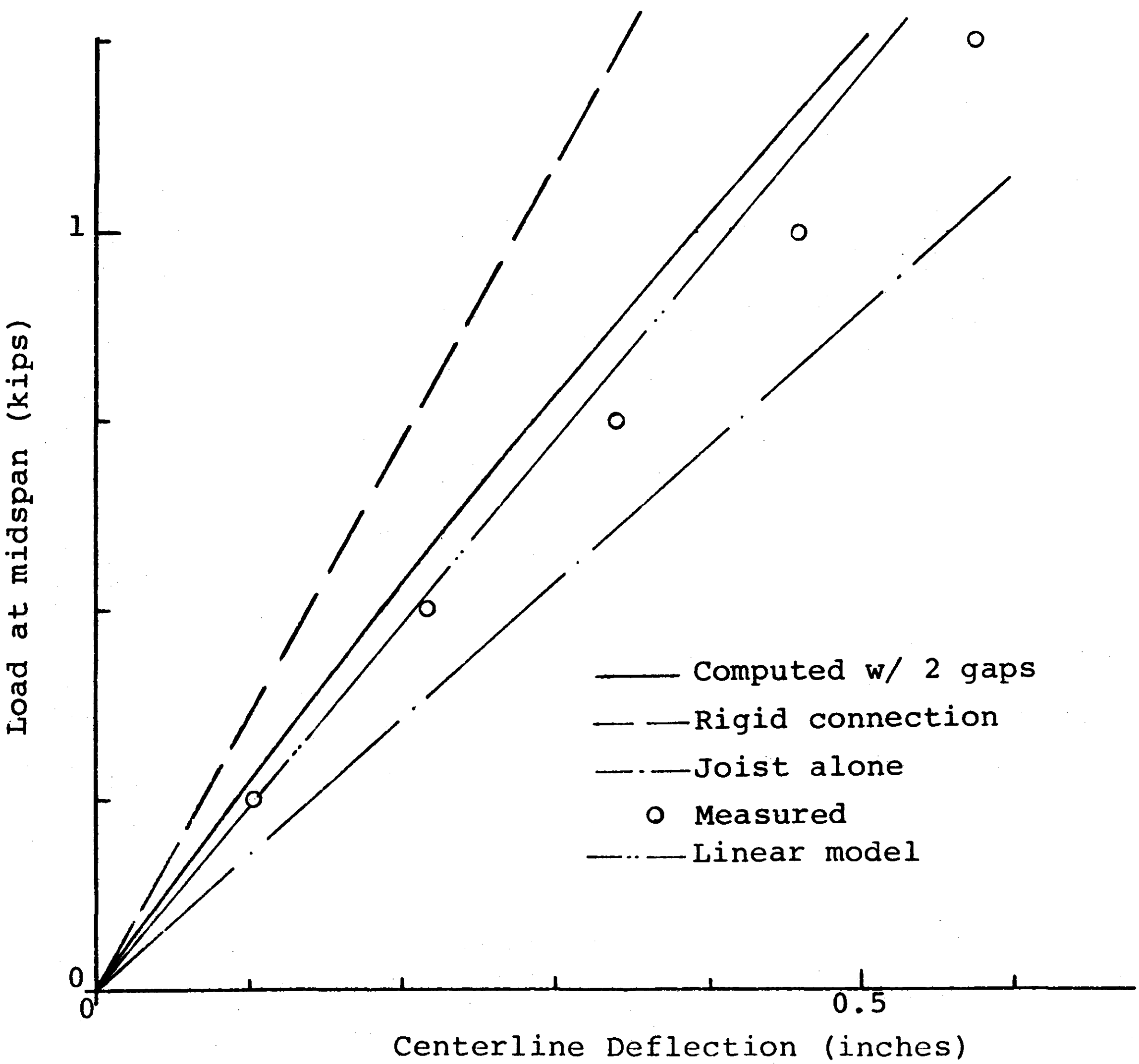

b) Load-Deflection Behavior

Figure C.17 Beam verification - T9-8D16-1 J02 with gaps.

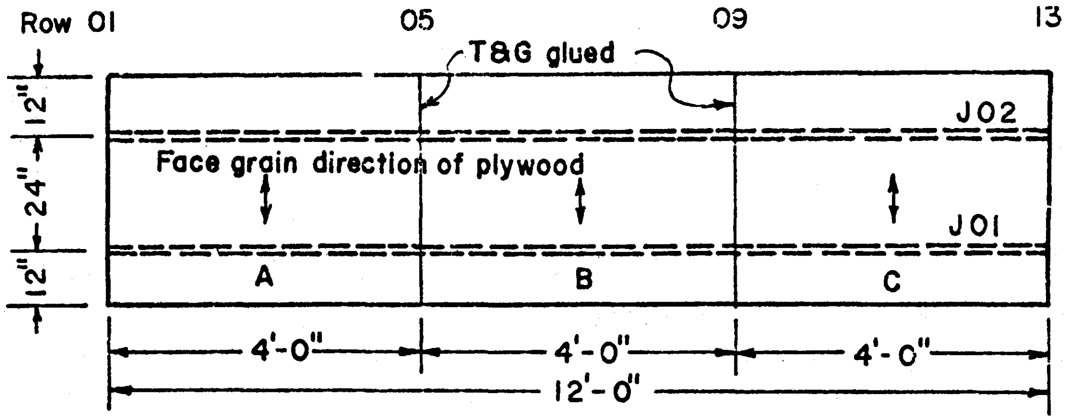

TOP VIEW

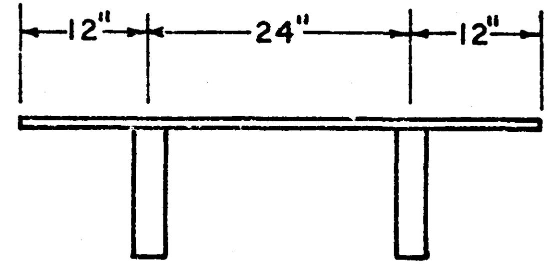

CROSS SECTION

Description of specimen:

Joist: 2x12 Engelmann spruce

J01	EC-S-12-05	$E = 1.269 \times 10^6$ psi
J02	EC-S-12-04	$E = 1.261 \times 10^6$

Sheathing: 3/4" D.F. Plywood

A	DP-34-10	$E_\perp = 5.463 \times 10^6$ psi
B	DP-34-13	$E_\perp = 5.516 \times 10^6$
C	DP-34-13	

Connector: 8-d common nails spaced at 8"

Sheathing Joints: glued T & G

Test sequence

1. Loaded at row 07 with $\Delta P = 1000$ lbs up to $P = 4000$ lbs. Repeated three times
2. Cut gaps at rows 05 and 09, loaded at row 07 with $\Delta P = 500$ up to $P = 2000$ lbs. Repeated twice.
3. Cut gaps at 2-foot intervals and loaded as in 2
4. Cut gaps at 1 foot intervals and loaded as in 2
5. Cut gaps at 6 in intervals and loaded as in 2 but $P_{max} = 3000$ lbs
6. Test to failure: loaded at row 07; both joists failed at $P = 5500$ lbs.

Figure C.18 Configuration and Properties of Specimen T10-12E24-1.

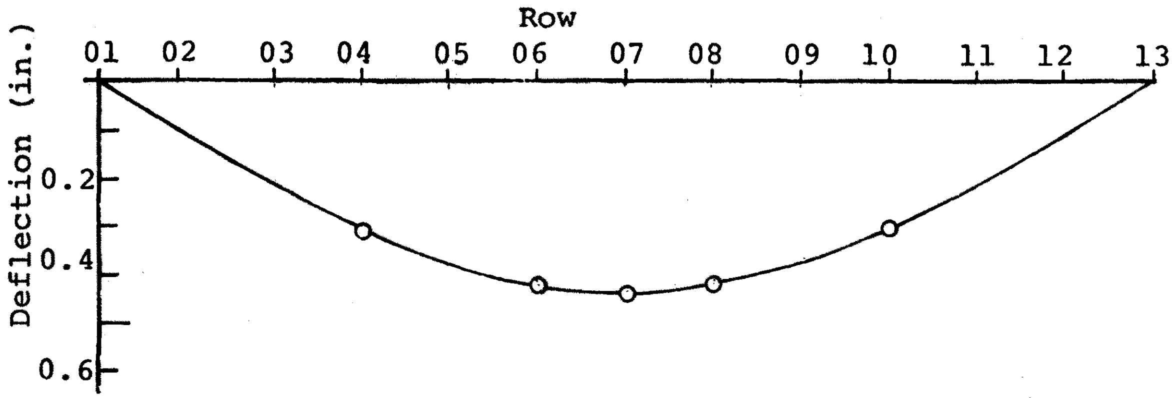

a) Deflection Profile at 2000 lbs. Load at Midspan

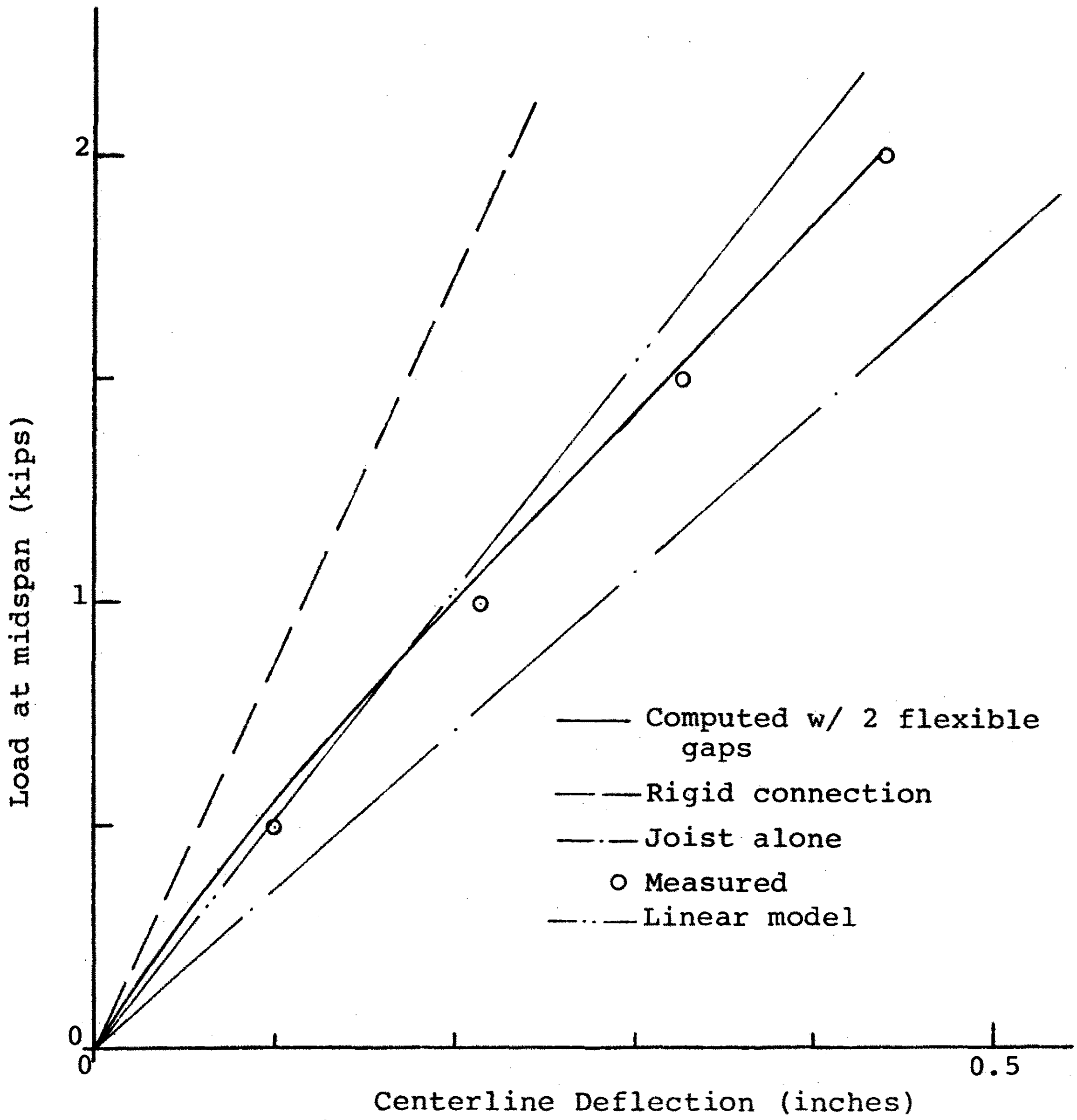

b) Load-Deflection Behavior

Figure C.19 Beam verification - T10-12E24-1 J01 with glued T & G joints.

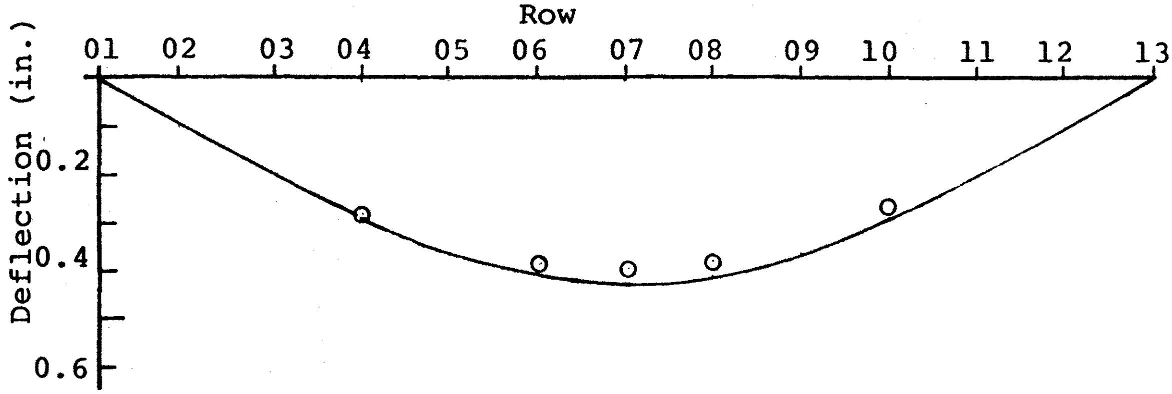

a) Deflection Profile at 2000 lbs.
Load at Midspan

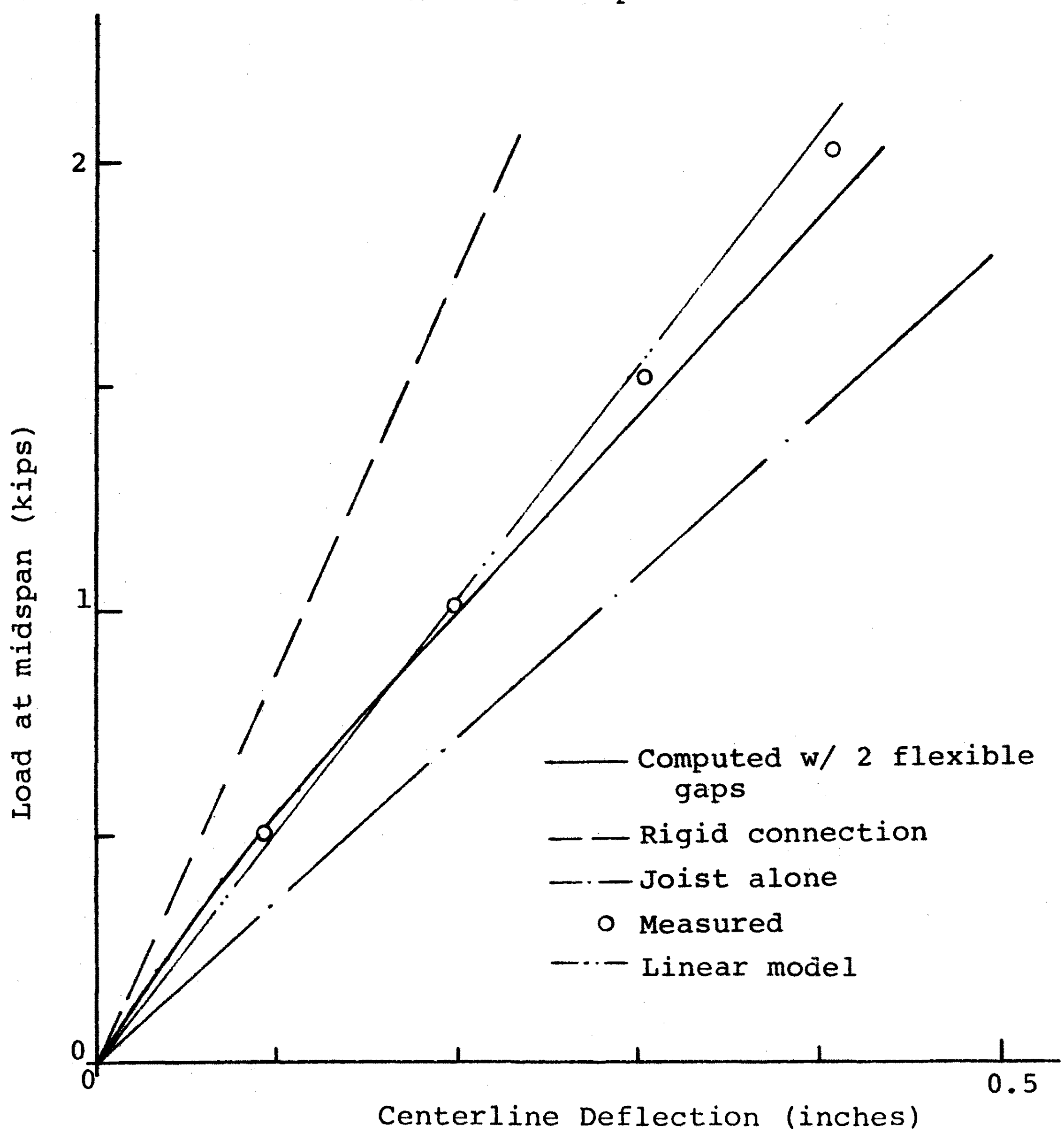

b) Load-Deflection Behavior

Figure C.20 Beam verification - T10-12E24-1 J02 with glued T & G joints.

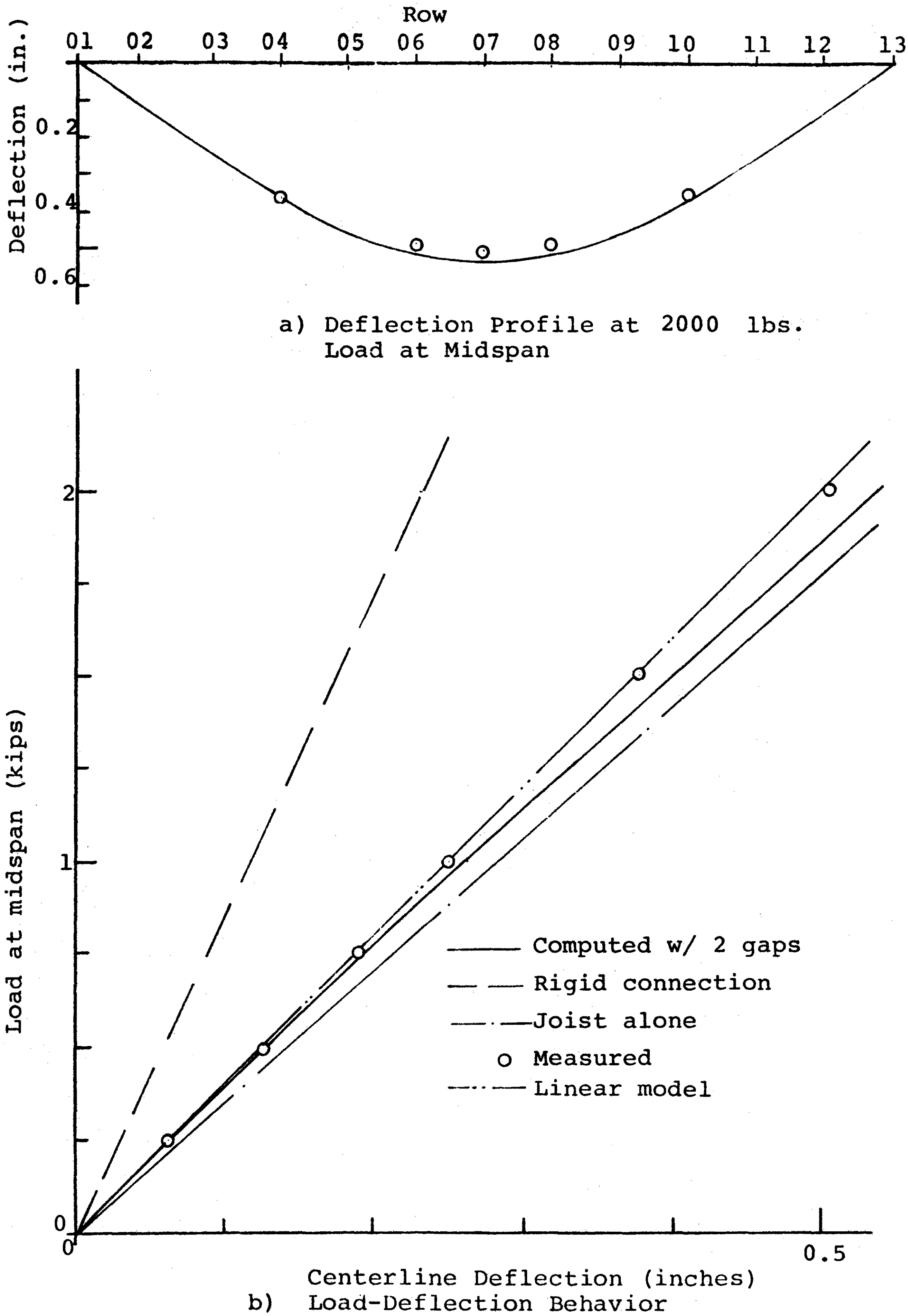

Figure C.21 Beam verification - T10-12E24-1 J01 with gaps.

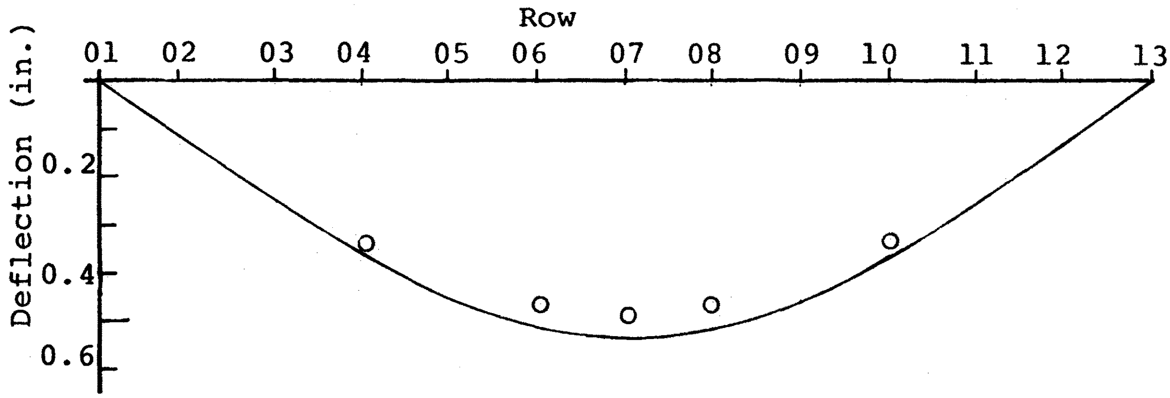

a) Deflection Profile at 2000 lbs. Load at Midspan

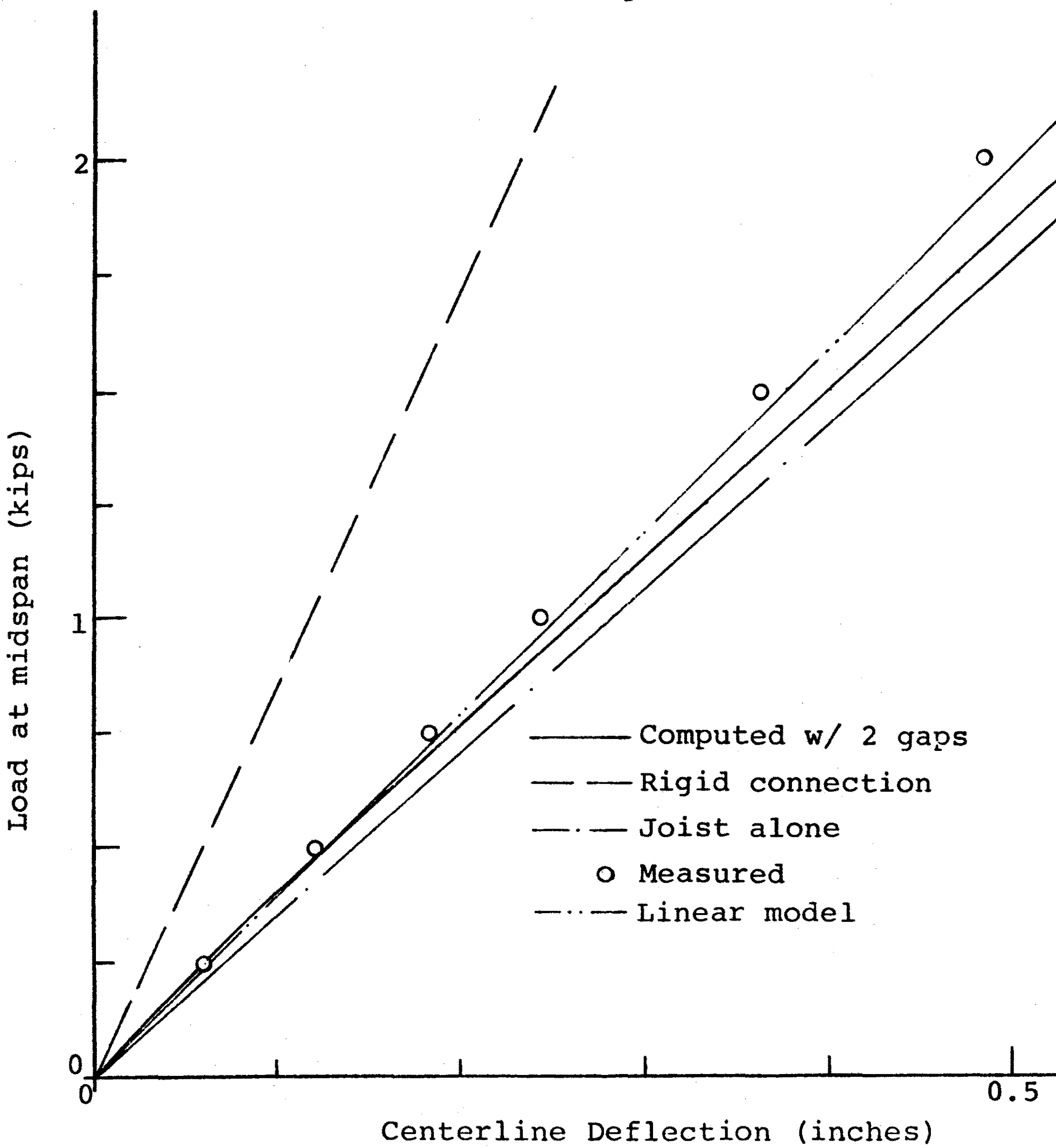

b) Load-Deflection Behavior

Figure C.22 Beam verification - T10-12E24-1 J02 with gaps.

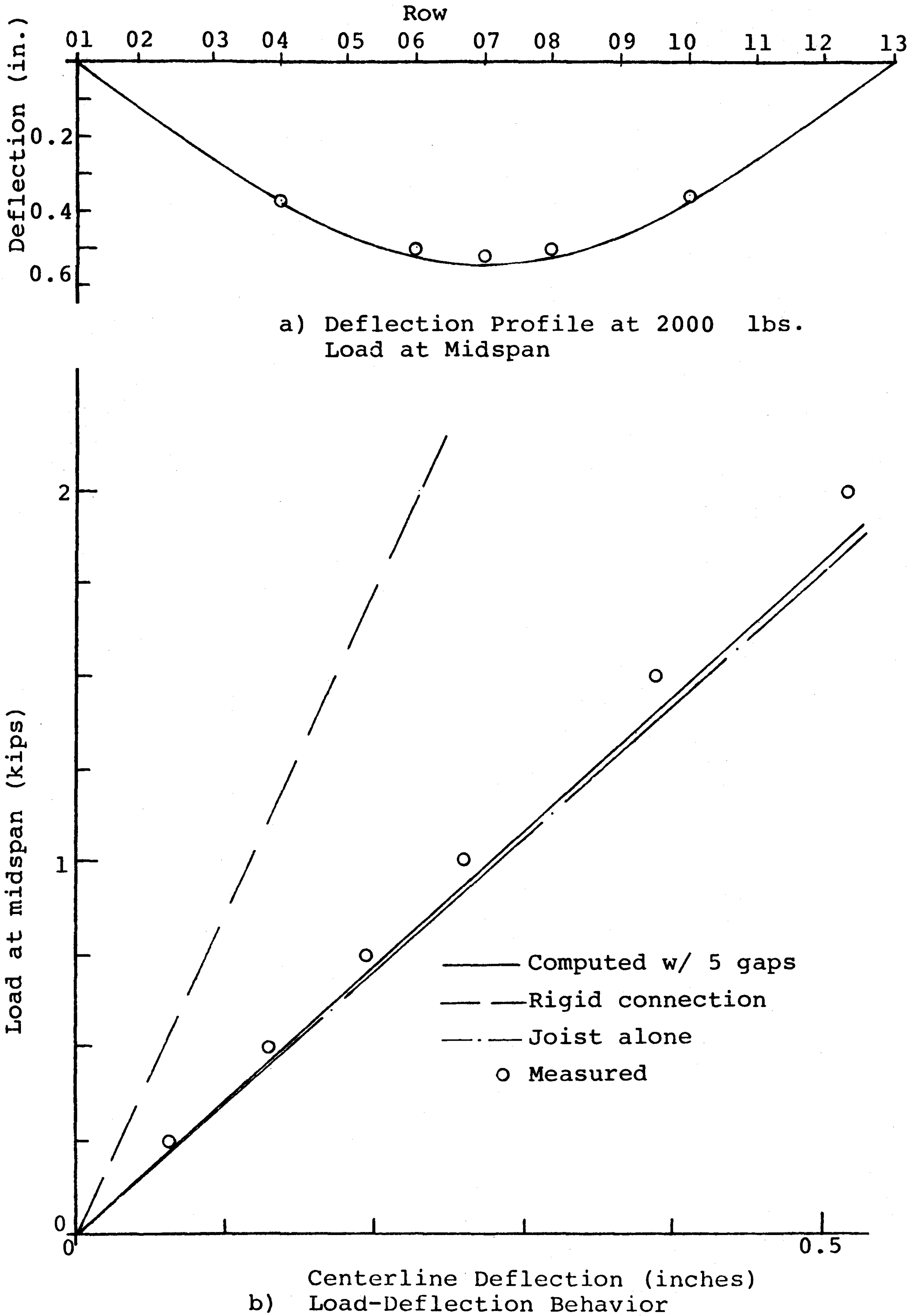

Figure C.23 Beam verification - T10-12E24-1 J01 with gaps.

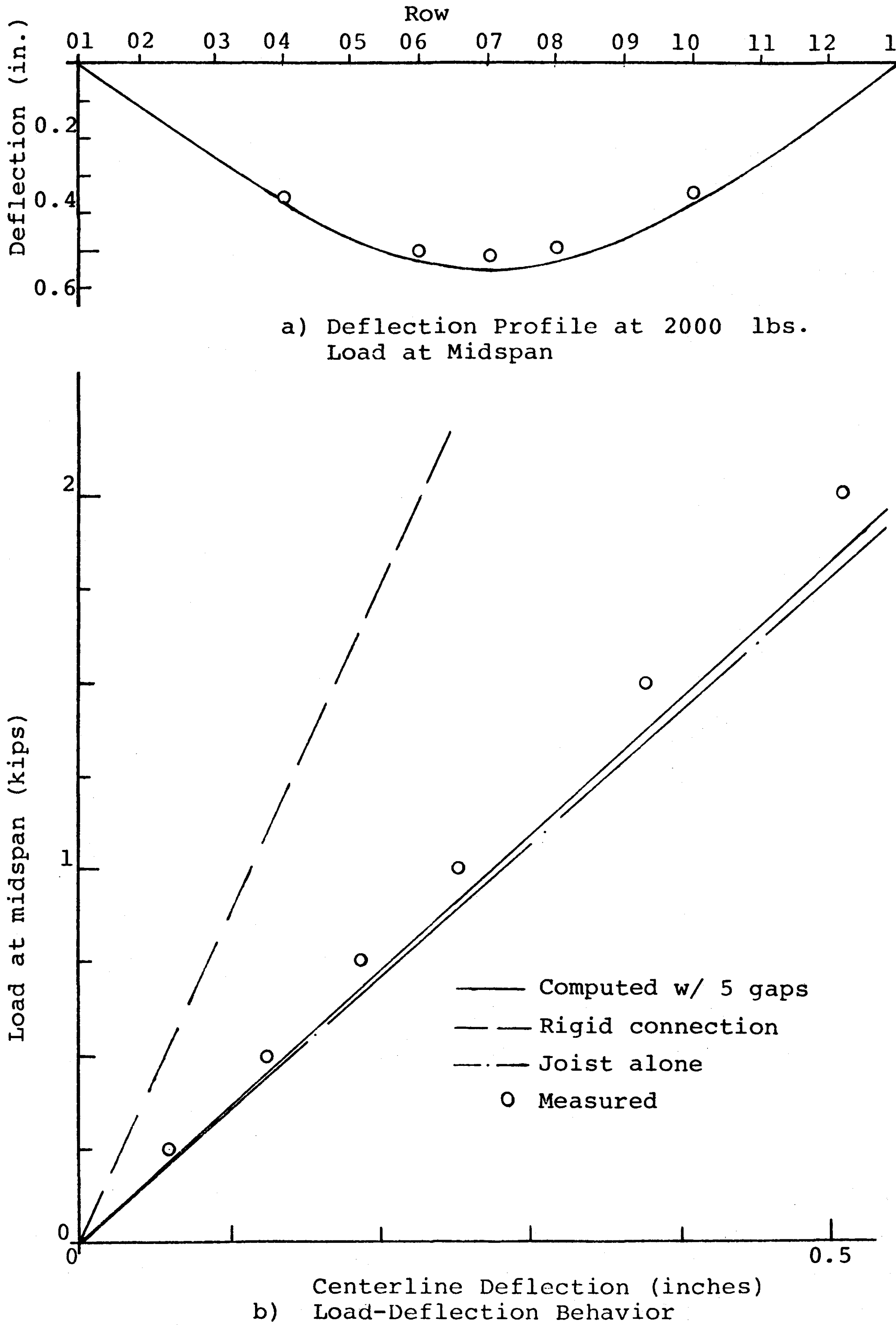

Figure C.24 Beam verification - T10-12E24-1 J02 with gaps.

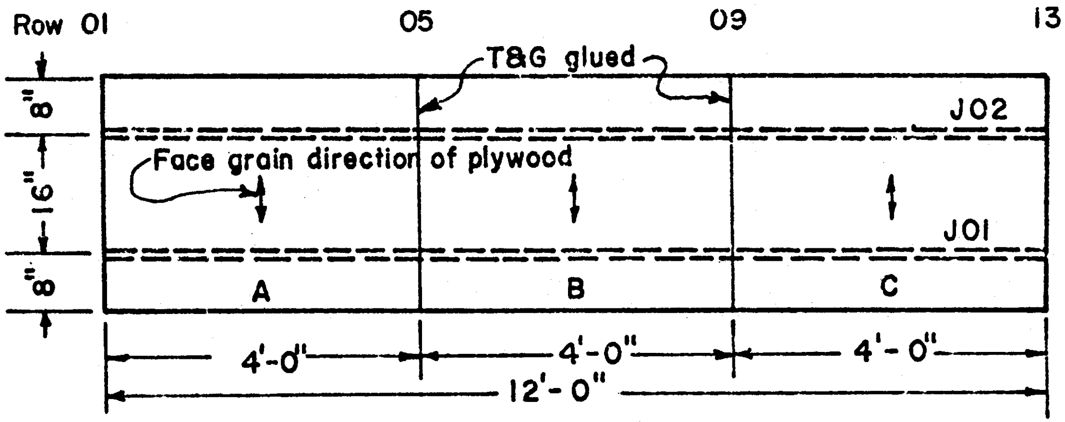

TOP VIEW

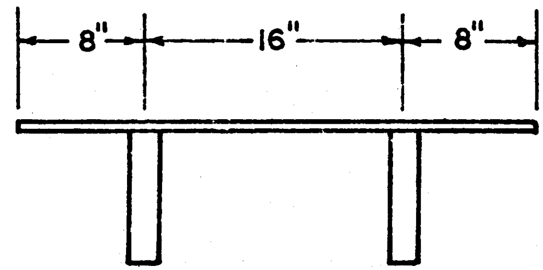

CROSS SECTION

Description of specimen:

Joist: 2x8 Douglas fir

J01	DW-N-08-52	$E = 0.975\times10^6$ psi
J01	DW-N-08-47	$E = 1.088\times10^6$

Sheathing: 3/4" D.F. Plywood

A	DP-34-8	$E_{\perp} = 5.326\times10^5$ psi
B	DP-34-8	$E_{\perp} = 5.326\times10^5$ psi
C	DP-34-8	$E_{\perp} = 5.326\times10^5$ psi

Connector: Franklin Construction Adhesive

Sheathing Joints: glued T&G

Test sequence

1. Loaded at row 07 with $\Delta P = 250$ lb up to $P = 1500$ lb. Repeated twice
2. Cut gap at midspan and loaded at row 07 with $\Delta P = 250$ up to $P = 1000$ lbs
3. Loaded at row 05 with $\Delta P = 250$ up to $P = 1250$ lbs
4. Test to failure: loaded at row 07 with $\Delta P = 500$ up to $P = 1500$ lbs.; then $\Delta P = 250$ up to failure. J01 failed at $P = 3750$ lbs.

Figure C.25 Configuration and Properties of Specimen T11-8D16-1.

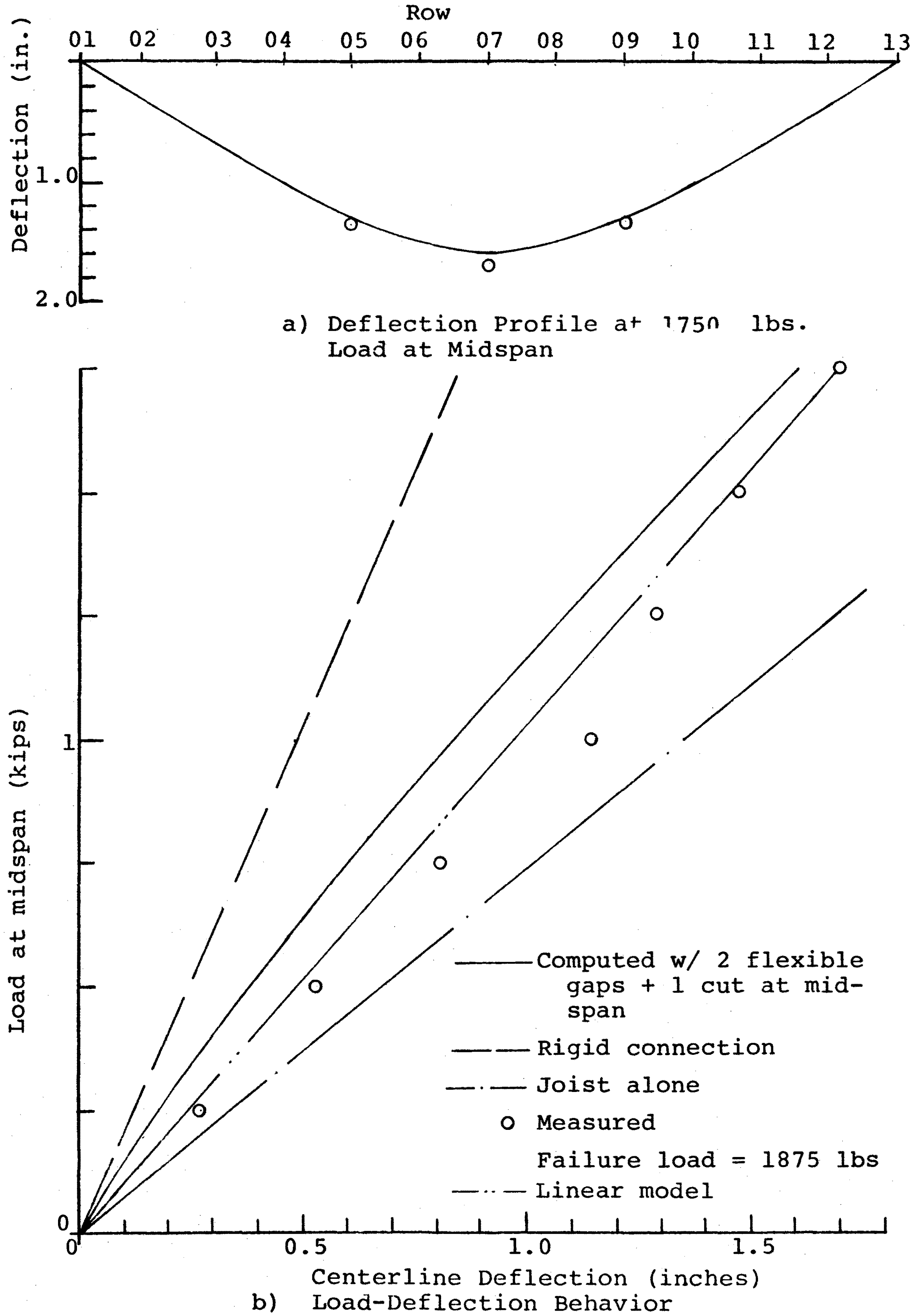

Figure C.26 Beam verification - T11-8D16-1 J01 with gaps.

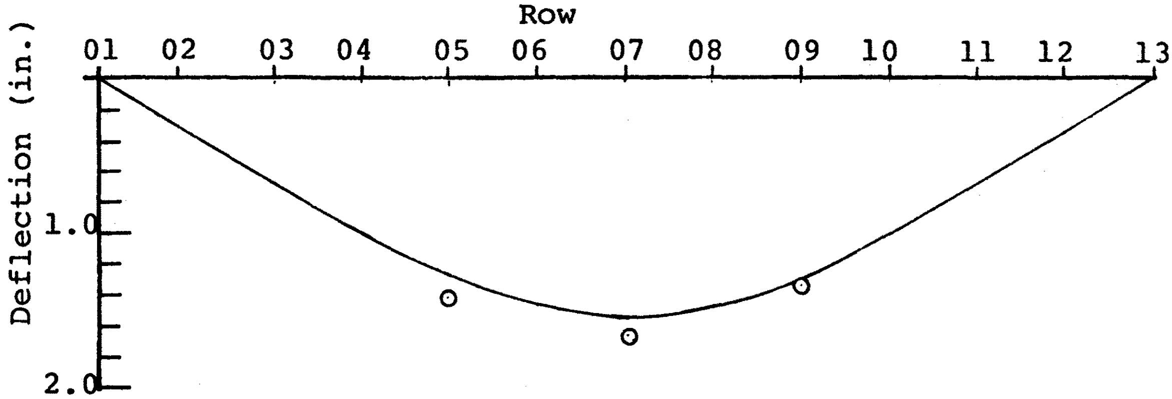

a) Deflection Profile at 1750 lbs. Load at Midspan

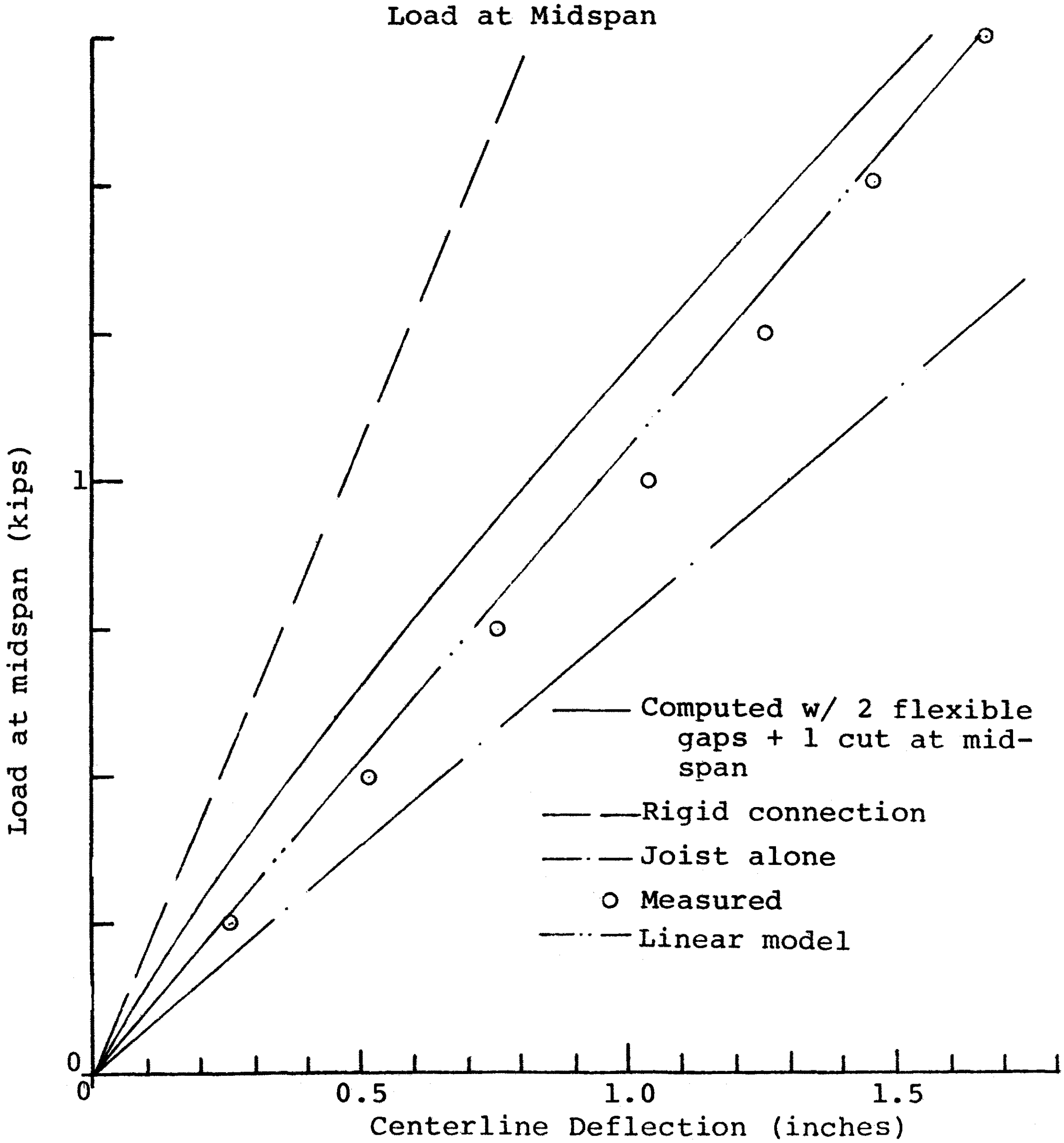

Centerline Deflection (inches)

b) Load-Deflection Behavior

Figure C.27 Beam verification - T11-8D16-1 J02 with gaps.

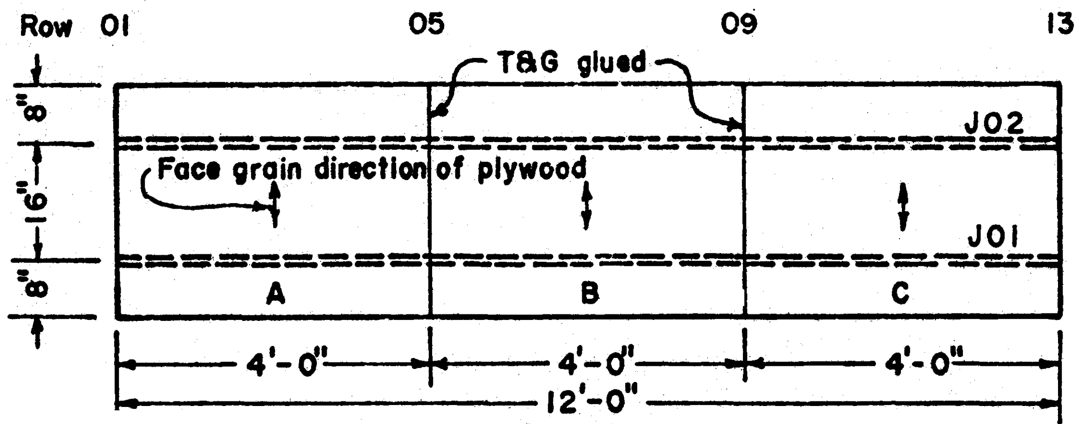

TOP VIEW

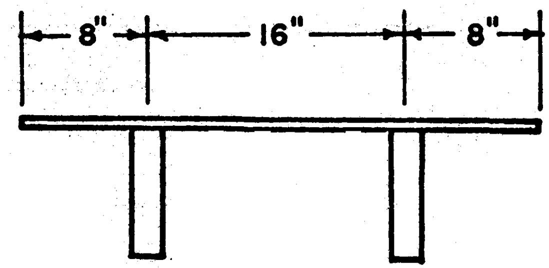

CROSS SECTION

Description of specimen:

Joist: 2x8 Douglas fir

J01	DW-N-08-51	$E = 1.249\times10^6$ psi
J02	DW-N-08-55	$E = 1.261\times10^6$

Sheathing: 3/4" D.F. Plywood

A	DP-34-12	$E_\perp = 5.581\times10^5$ psi
B	DP-34-12	$E_\perp = 5.581\times10^5$ psi
C	DP-34-12	$E_\perp = 5.581\times10^5$ psi

Connector: 8-d common nails spaced at 6"

Sheathing Joints: T&G glued

Test sequence

1. Loaded at row 07 with ΔP = 250 lb up to P = 1250 lbs. Repeated three times.
2. Cut gap at row 07 and tested as in 1
3. Cut gaps at rows 05 and 09 (total 3 cuts), loaded at row 07 with ΔP = 250 lb up to P = 1000 lbs
4. Loaded at rows 03 and 04 with center gap filled; P_{max} = 1000 lbs
5. Cut gaps at 2-foot intervals and loaded as in 3
6. Cut gaps at 1-foot intervals and loaded at row 07 with P = 750 lbs
7. Cut gaps at 6 in intervals and loaded as in 6.

Figure C.28 Configuration and Properties of Specimen T12-8D16-1.

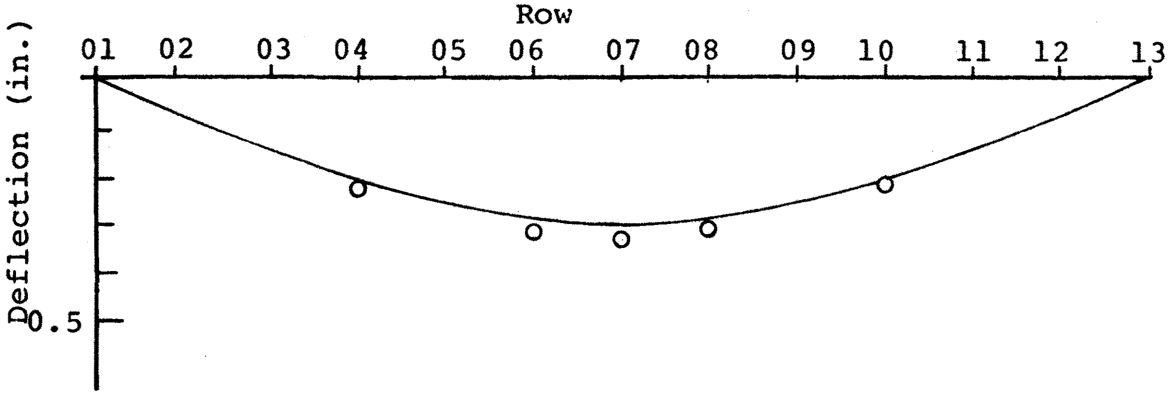

a) Deflection Profile at 500 lbs.
Load at Midspan

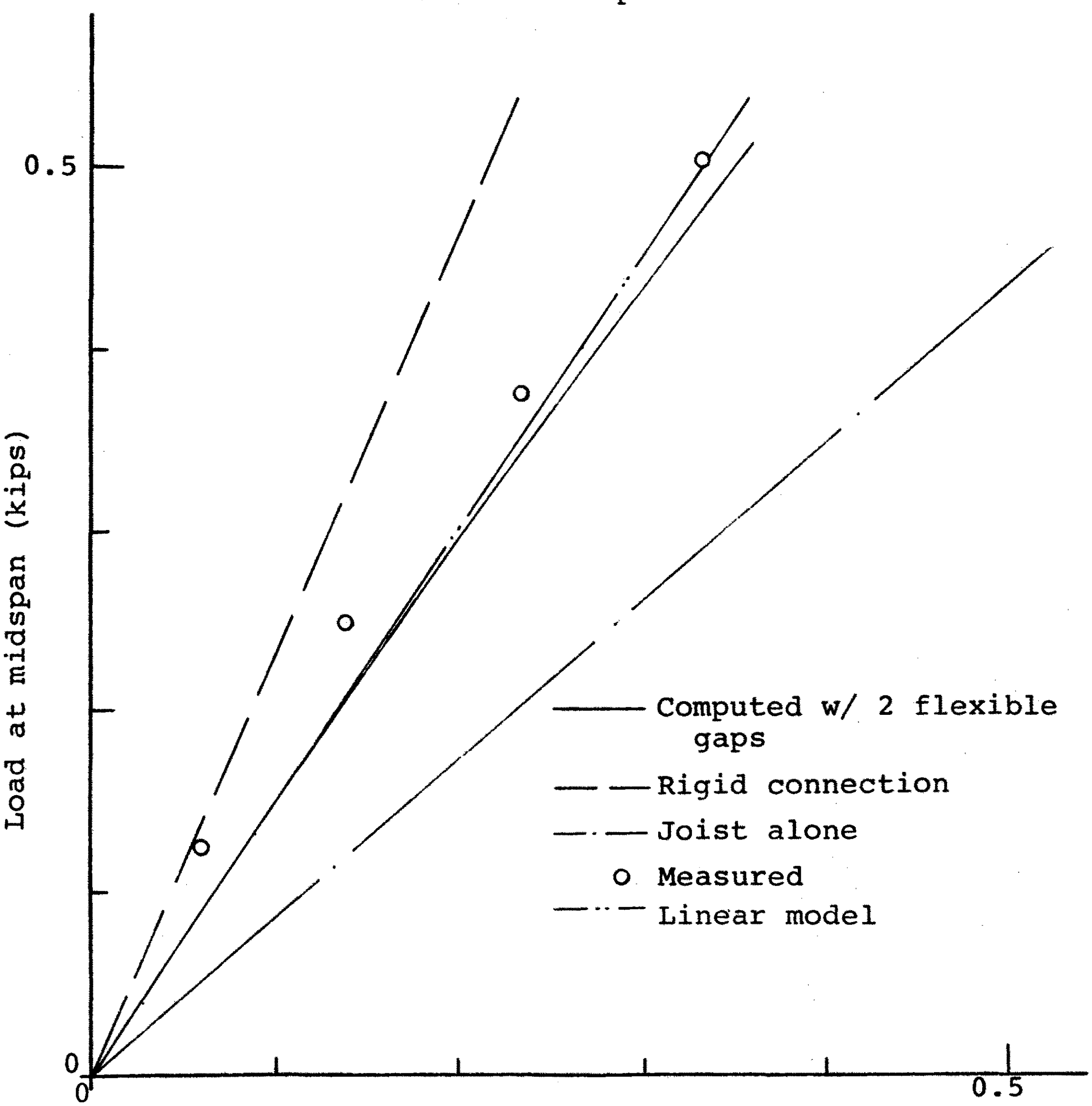

Centerline Deflection (inches)
b) Load-Deflection Behavior

Figure C.29 Beam verification - T12-8D16-1 J01 with glued T & G joints.

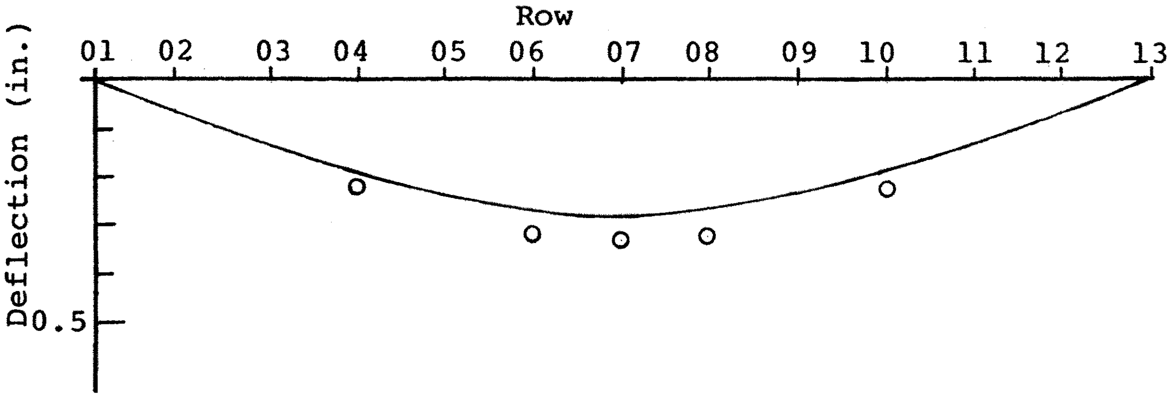

a) Deflection Profile at 500 lbs.
Load at Midspan

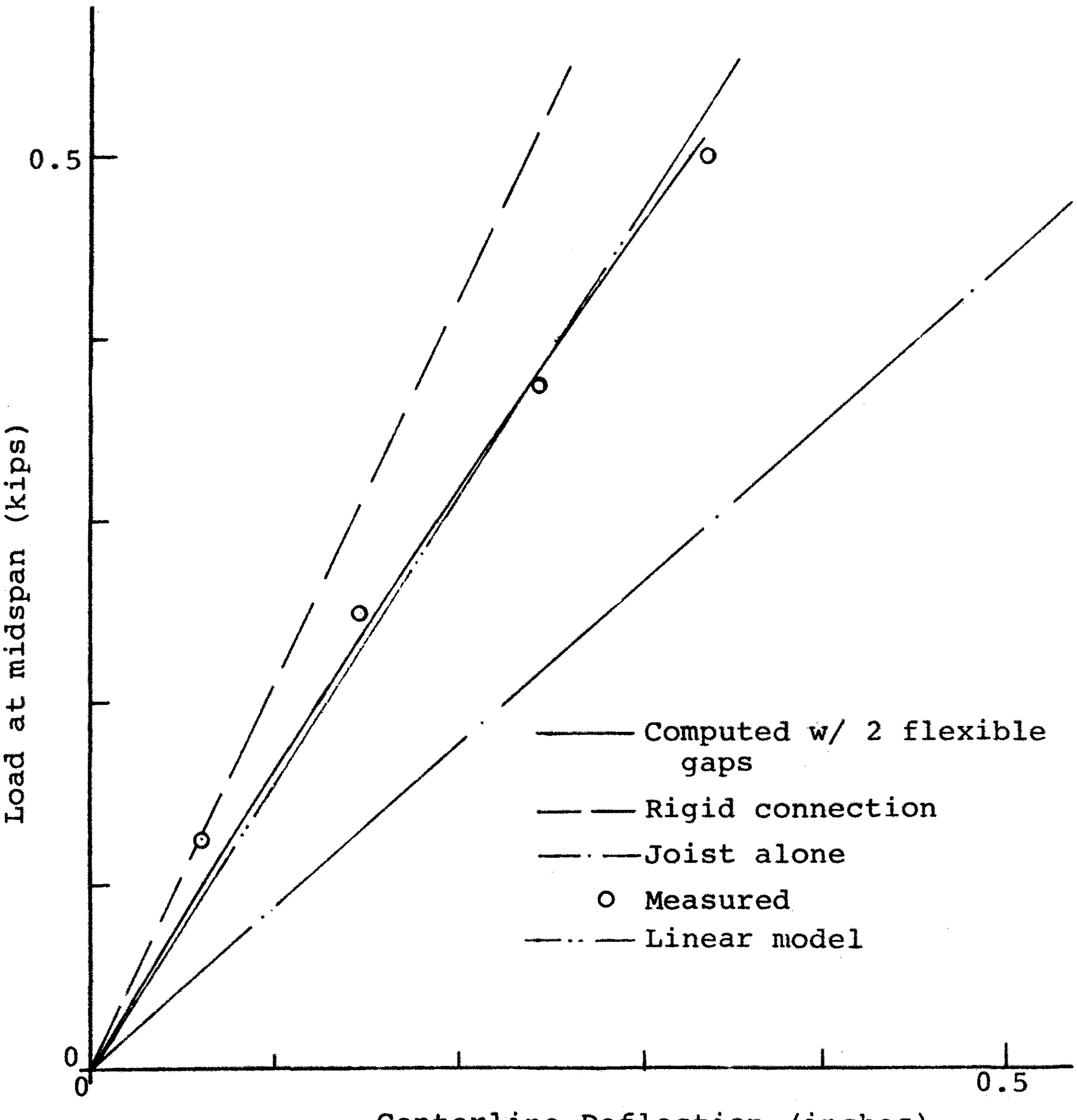

b) Load-Deflection Behavior

Figure C.30 Beam verification - T12-8D16-1 J02 with glued T & G joints.

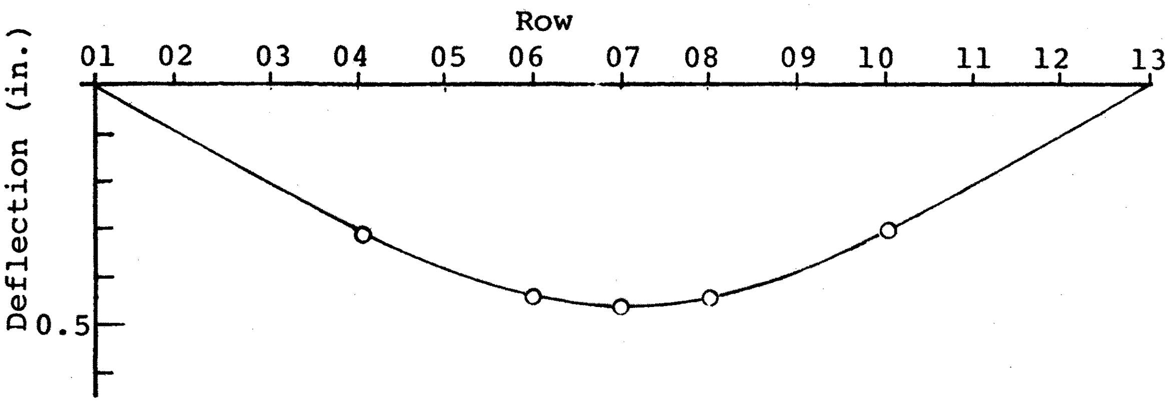

a) Deflection Profile at 500 lbs. Load at Midspan

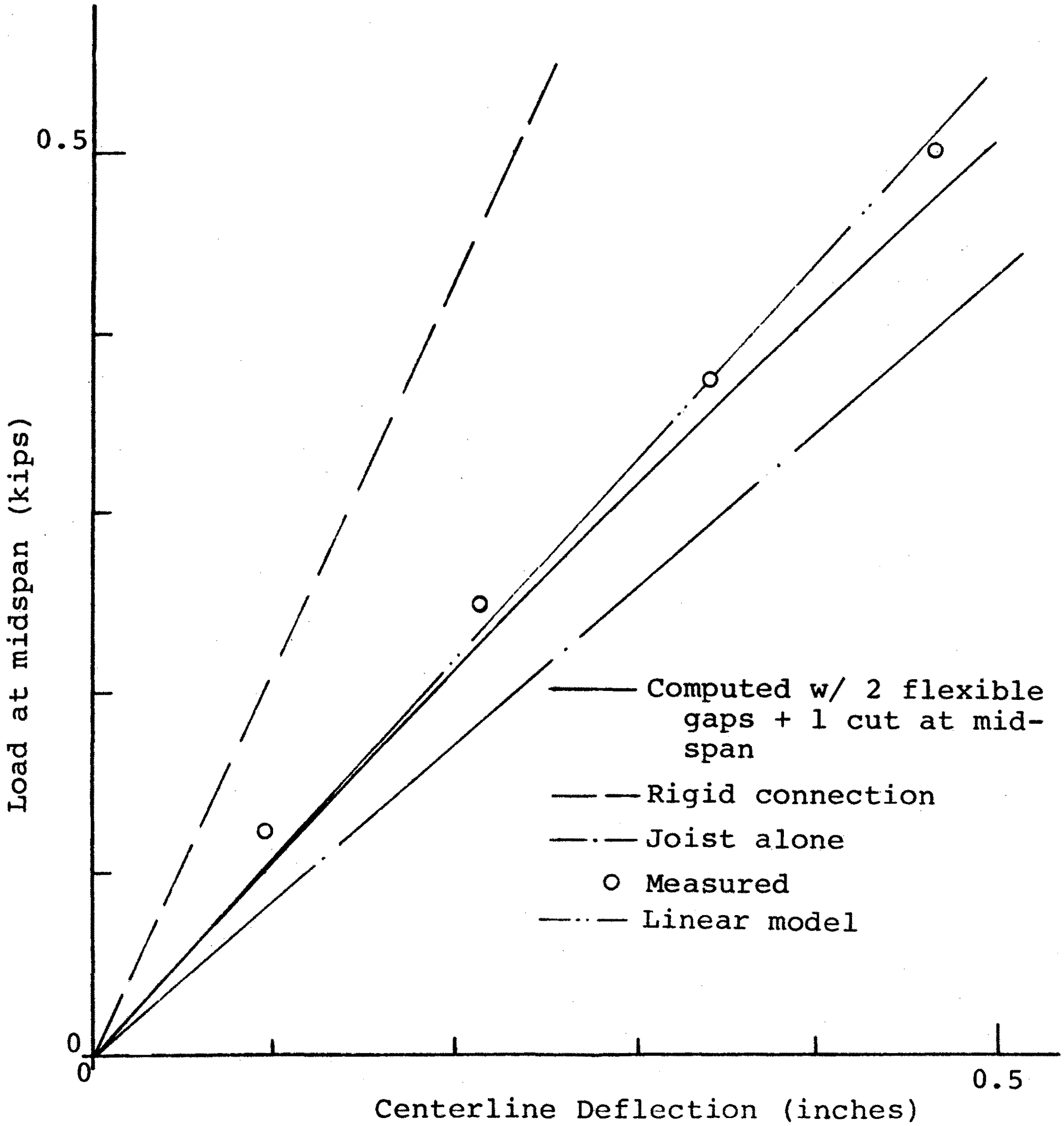

b) Load-Deflection Behavior

Figure C.31 Beam verification - T12-8D16-1 J01 with gaps.

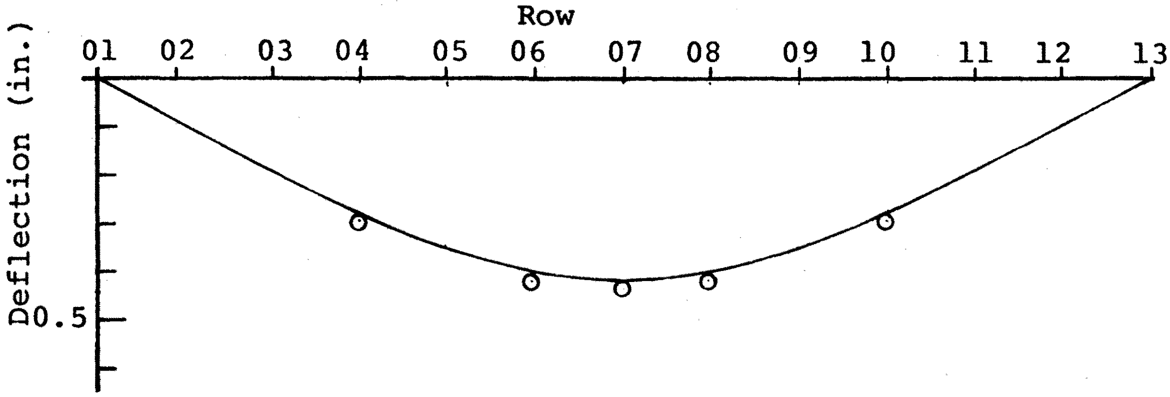

a) Deflection Profile at 500 lbs.
Load at Midspan

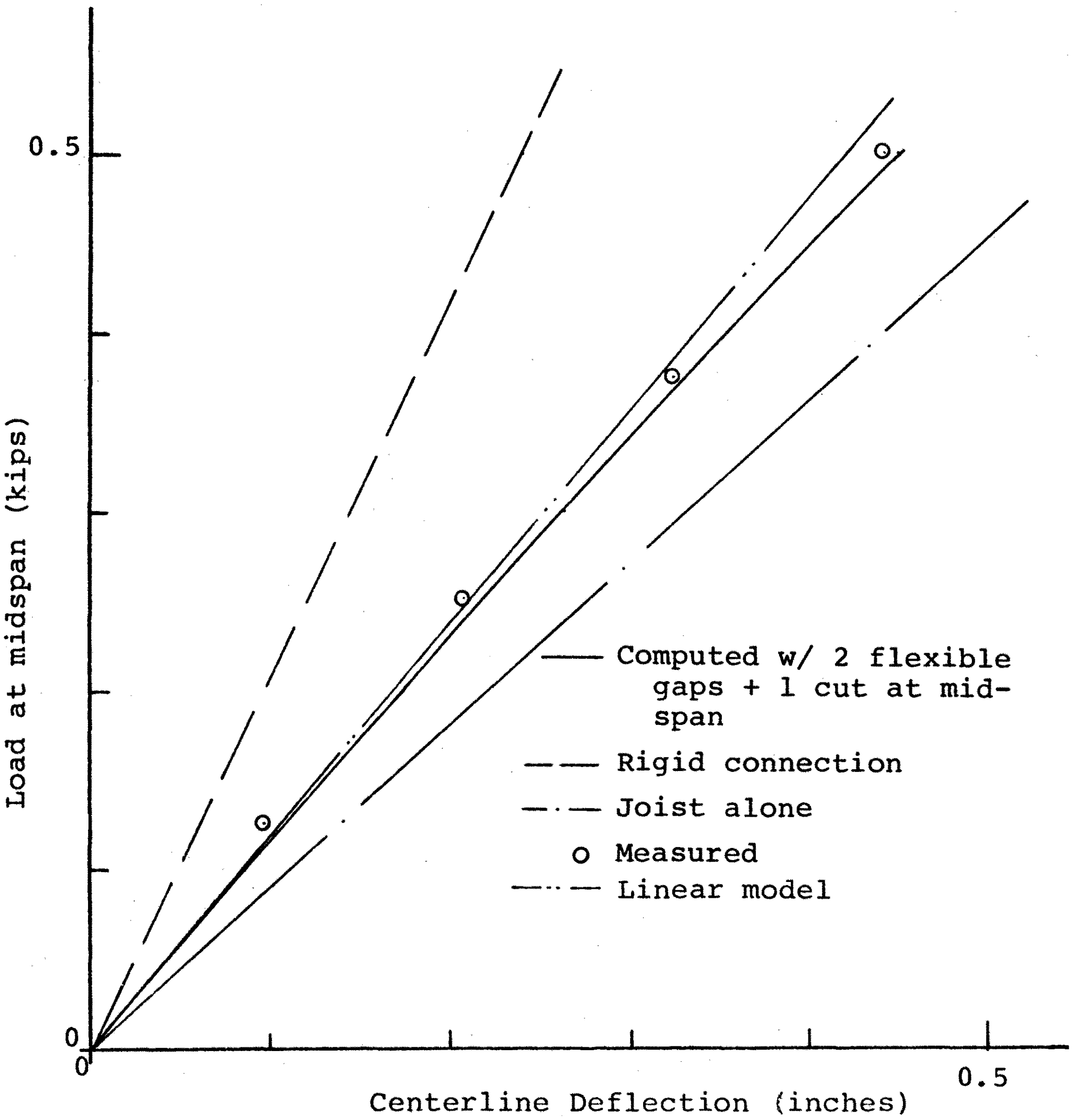

b) Load-Deflection Behavior

Figure C.32 Beam verification - T12-8D16-1 J02 with gaps.

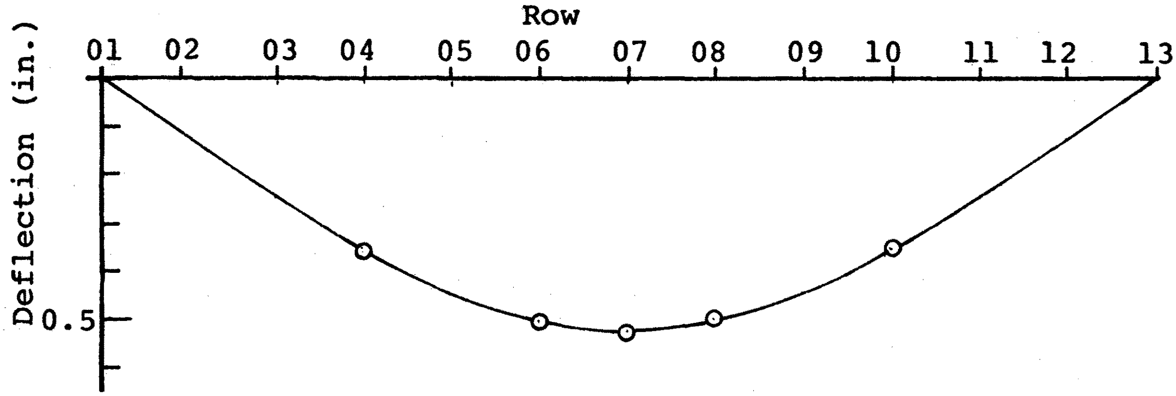

a) Deflection Profile at 500 lbs. Load at Midspan

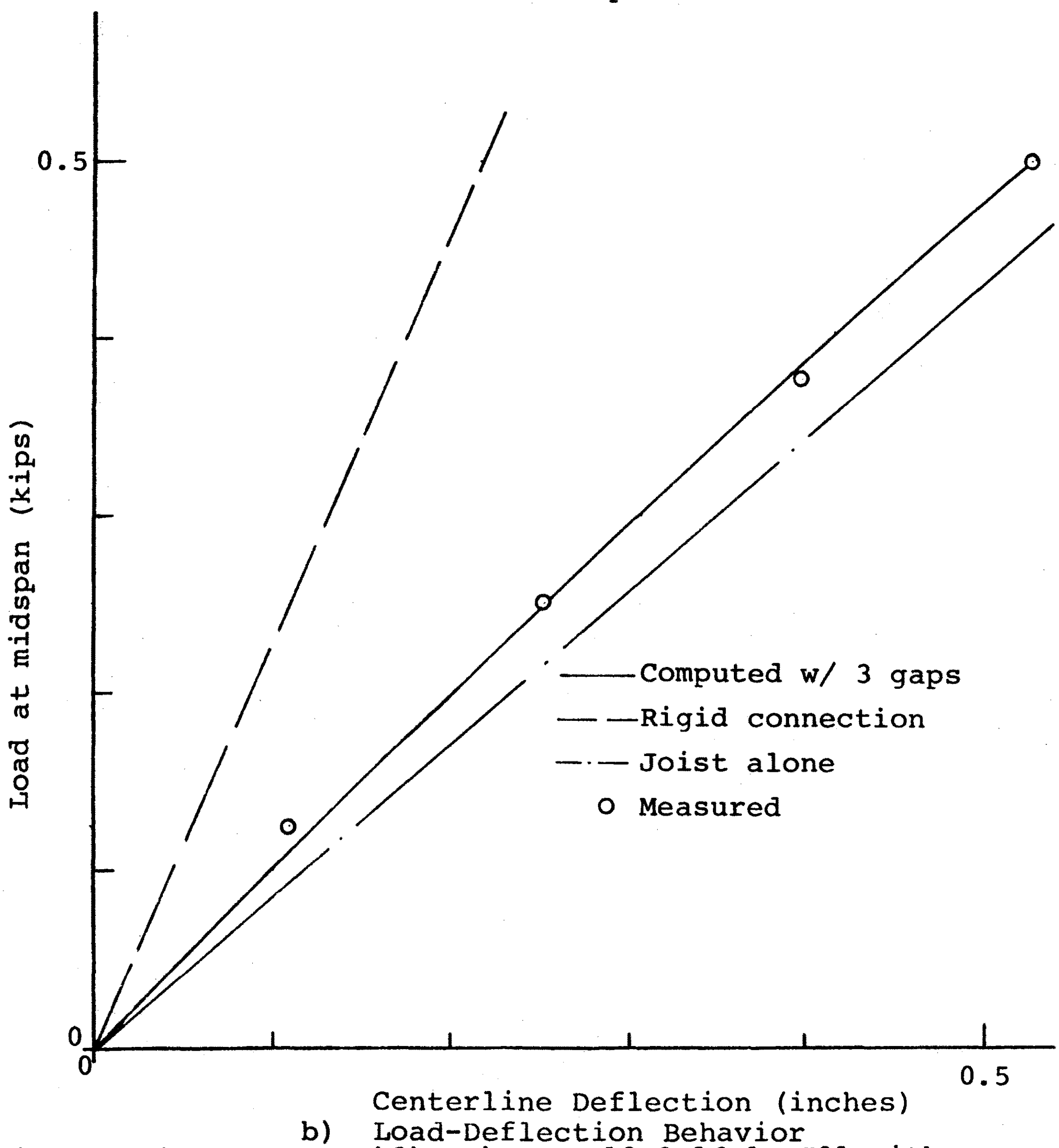

Centerline Deflection (inches)

b) Load-Deflection Behavior

Figure C.33 Beam verification - T12-8D16-1 J01 with gaps.

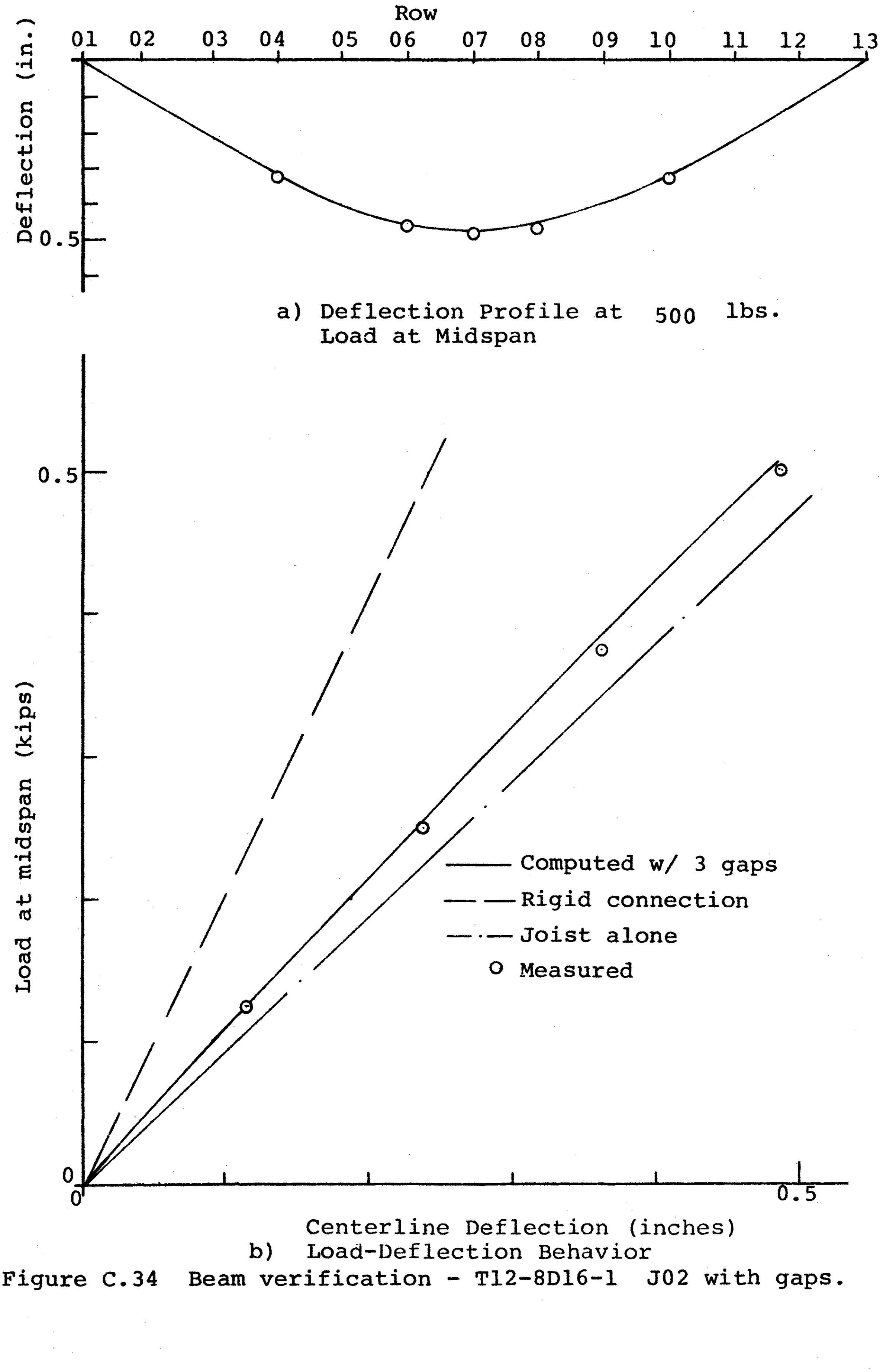

b) Load-Deflection Behavior

Figure C.34 Beam verification - T12-8D16-1 J02 with gaps.

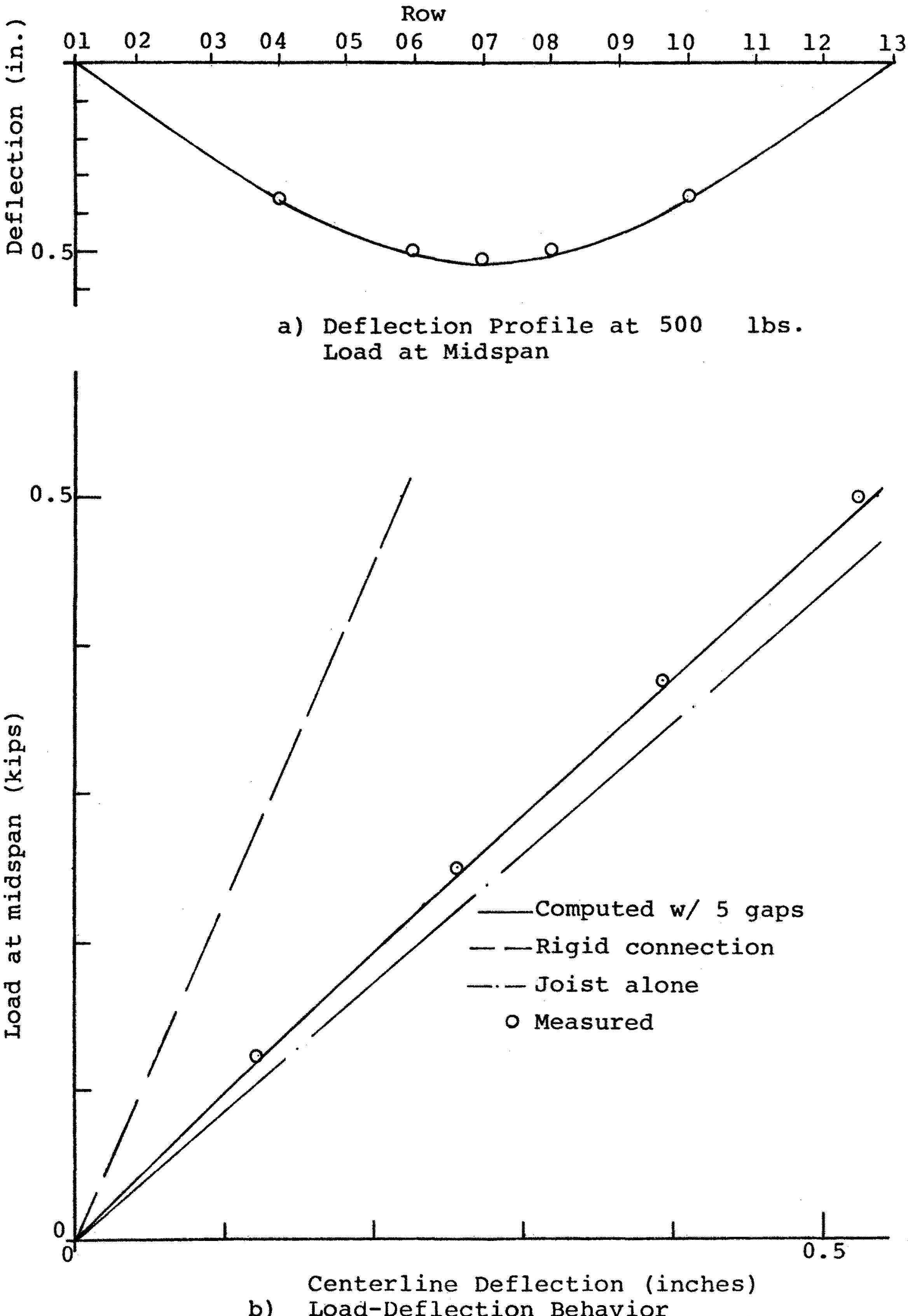

Figure C.35 Beam verification - T12-8D16-1 J01 with gaps.

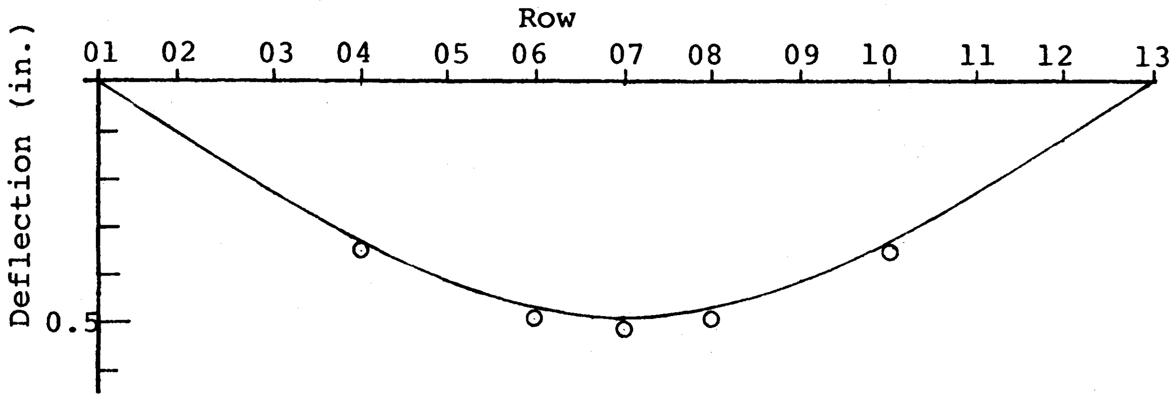

a) Deflection Profile at 500 lbs.
Load at Midspan

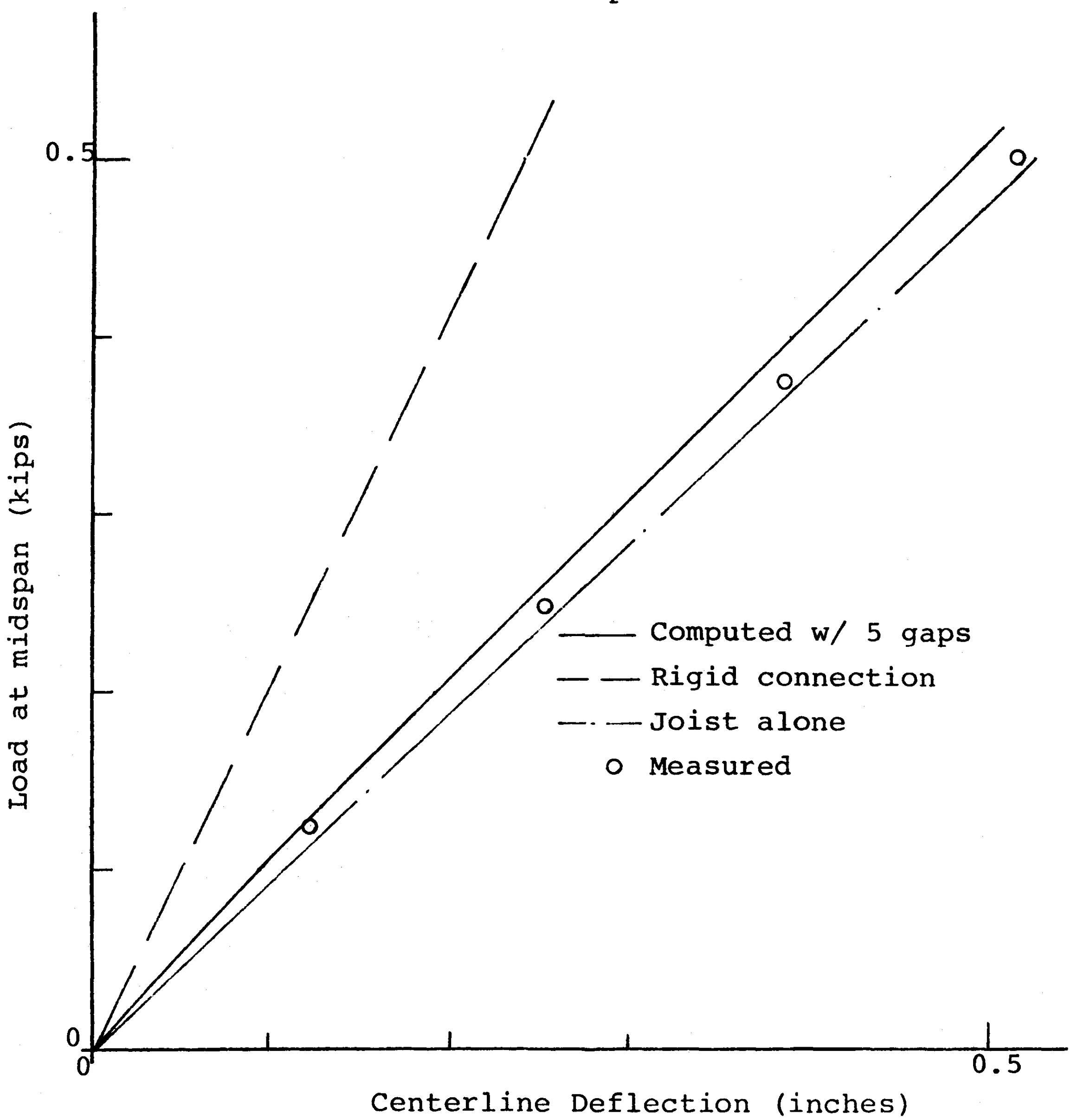

b) Load-Deflection Behavior

Figure C.36 Beam verification - T12-8D16-1 J02 with gaps.

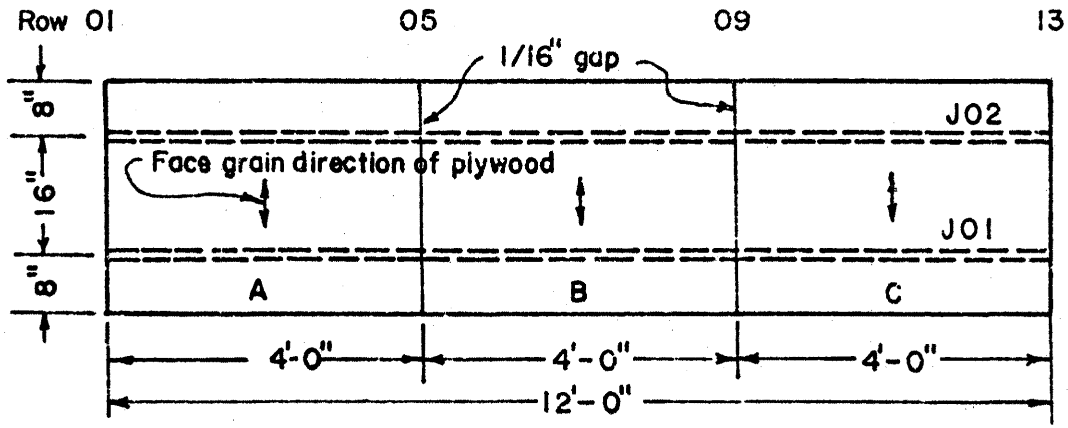

TOP VIEW

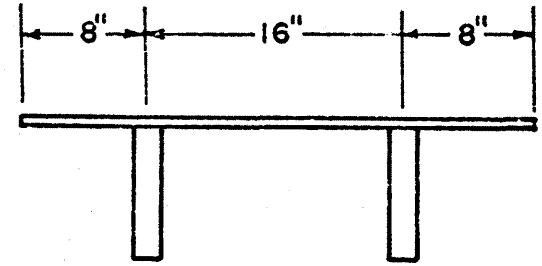

CROSS SECTION

Description of specimen:

Joist: 2x8 Douglas fir

J01	DW-N-08-21	$E = 1.342\times10^6$ psi
J02	DW-N-08-49	$E = 1.077\times10^6$

Sheathing: 3/4" E.S. Plywood

A	EP-58-28	$E_\perp = 4.323\times10^5$ psi
B	EP-58-28	$E_\perp = 4.323\times10^5$ psi
C	EP-58-28	$E_\perp = 4.323\times10^5$ psi

Connector: 8-d common nails spaced at 4"

Sheathing Joints: T&G with 1/16" gaps

Test sequence

1. Loaded at row 07 with ΔP = 250 up to P = 1000 lbs. Repeated twice.

2. Cyclic loading with load from 20 to 800 lbs. Ramp function with T = 80 sec., sustained for 850 cycles

3. Cyclic loading with load from 0 to 800 lbs. Ramp function with T = 40 sec., sustained for 750 cycles

4. Loaded at 07 with ΔP = 100 up to P = 1500 lbs.

Figure C.37 Configuration and Properties of Specimen T13-8D16-1.

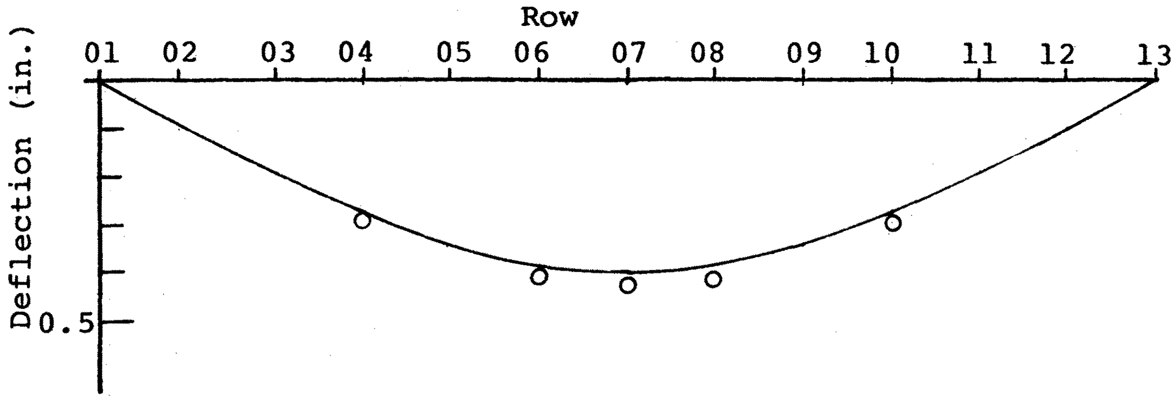

a) Deflection Profile at 500 lbs.
Load at Midspan

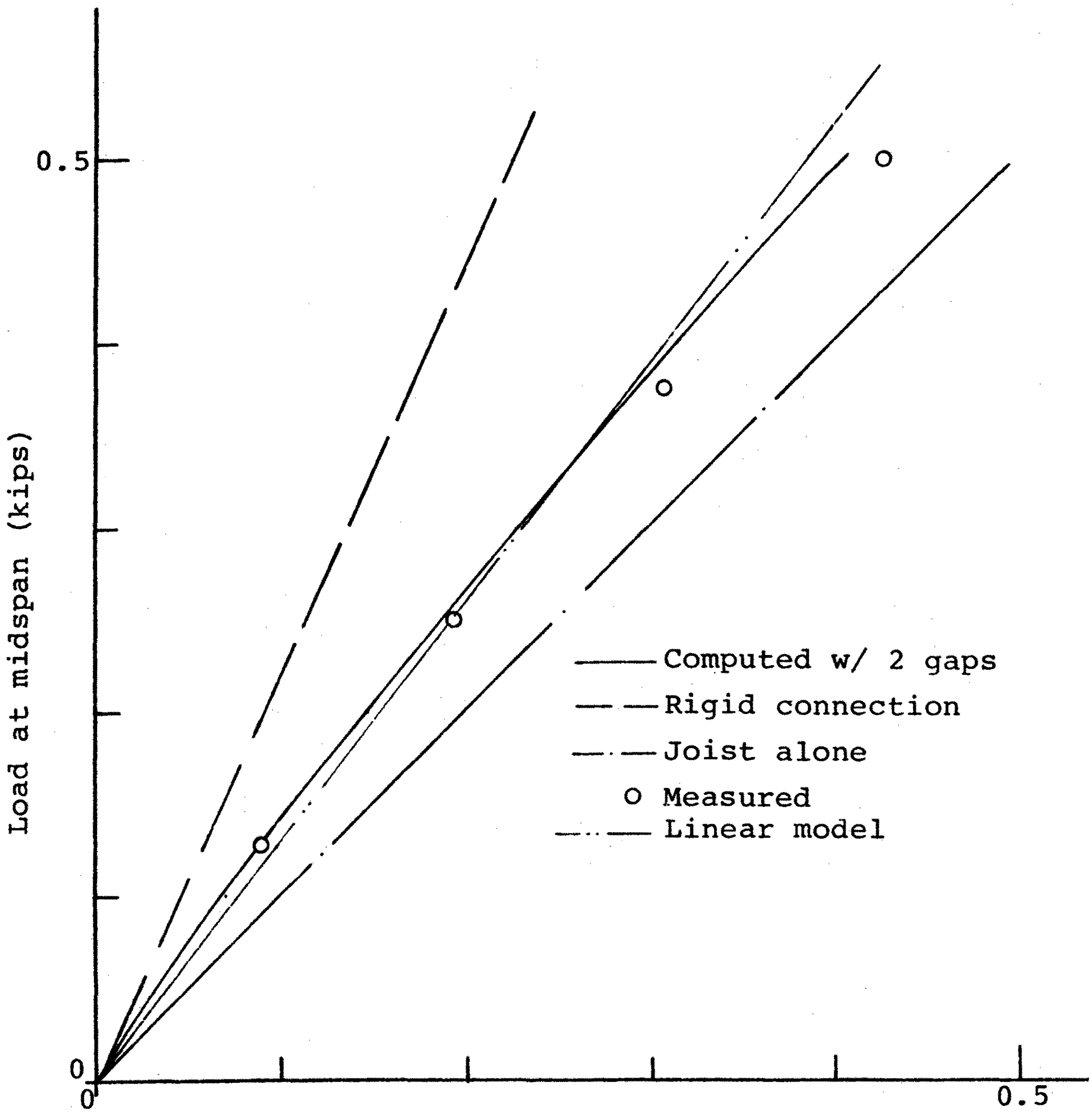

b) Load-Deflection Behavior

Figure C.38 Beam verification - T13-8D16-1 J01 with gaps.

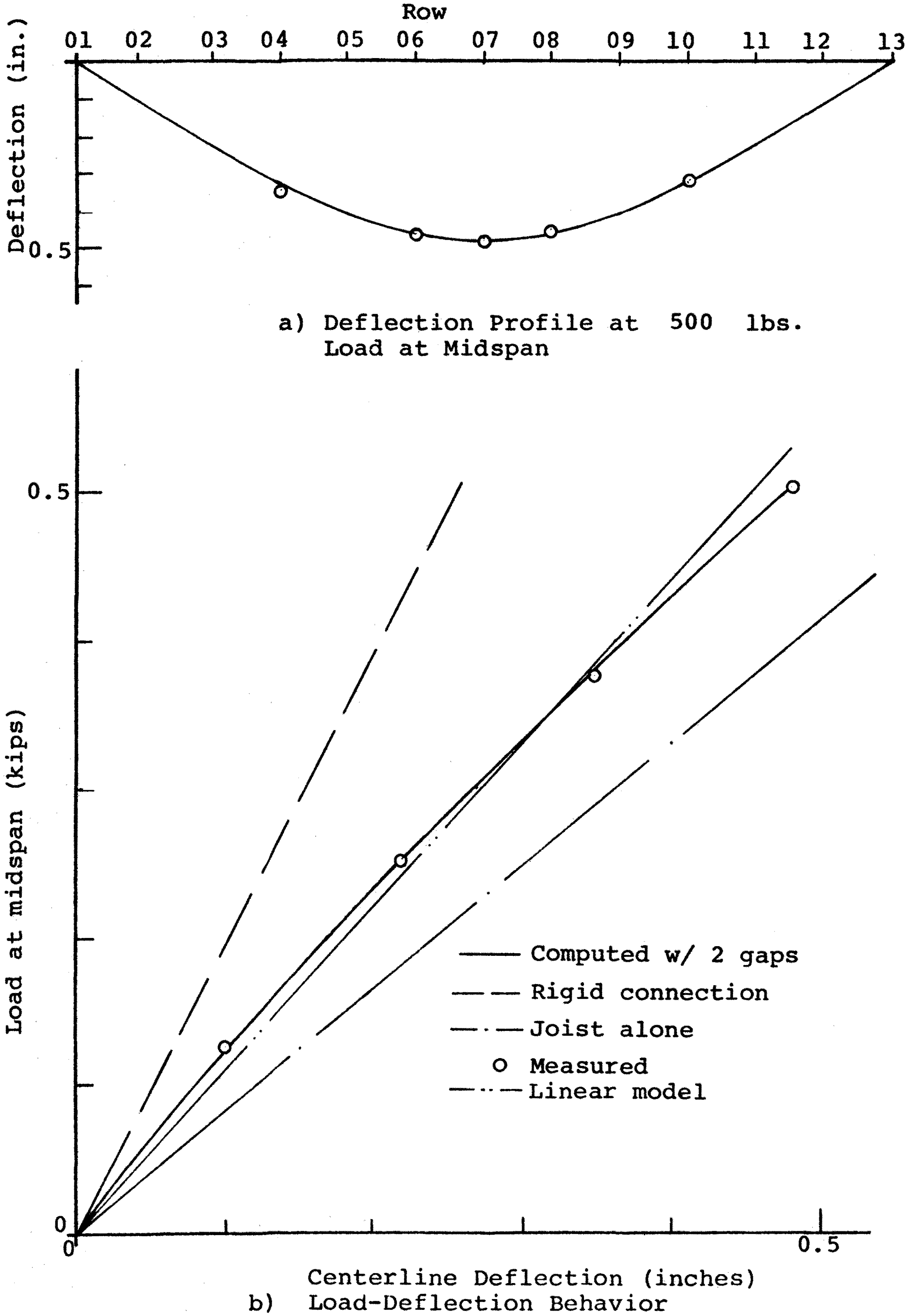

Figure C.39 Beam verification - T13-8D16-1 J02 with gaps.

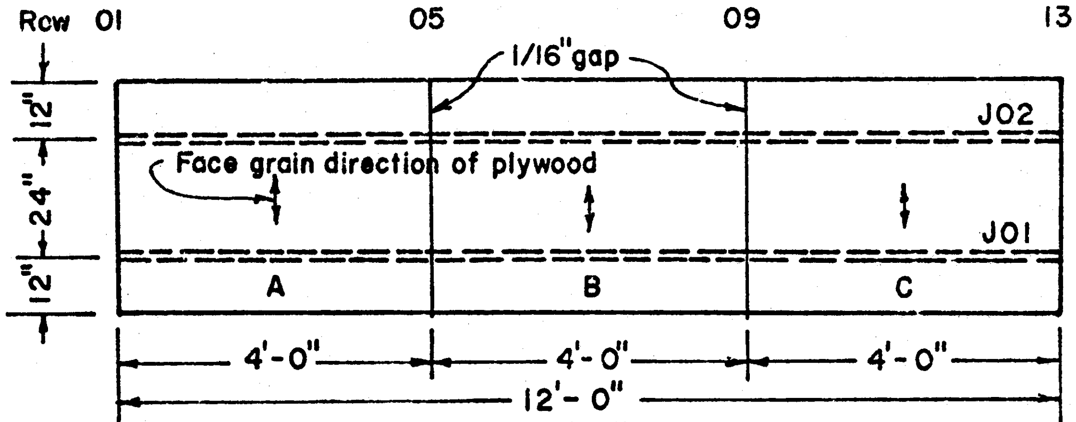

TOP VIEW

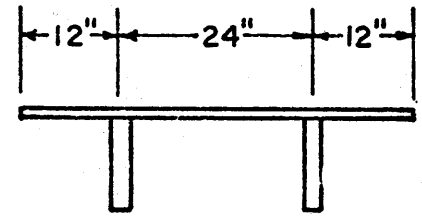

CROSS SECTION

Description of specimen:

Joist: 2x12 Douglas fir

J01	DW-S-12-21	$E = 1.883\text{x}10^6$ psi
J01	DW-S-12-23	$E = 1.715\text{x}10^6$

Sheathing: 1/2" D.F. Plywood

A	DP-12-02	$E_\perp = 2.563\text{x}10^5$ psi
B	DP-12-02	$E_\perp = 2.563\text{x}10^5$ psi
C	DP-12-03	$E_\perp = 2.236\text{x}10^5$ psi

Connector: 8-d common nails spaced at 8"

Sheathing Joints: left with 1/16" gaps

Test sequence

1. Loaded at row 07 with $\Delta P = 250$ up to $P = 1500$ lbs
2. Loaded at row 05 with loads same in 1
3. Loaded at row 03 with loads same in 1
4. Loaded at row 07 with P up to 2000 lbs.

Figure C.40 Configuration and Properties of Specimen T14-12D24-1.

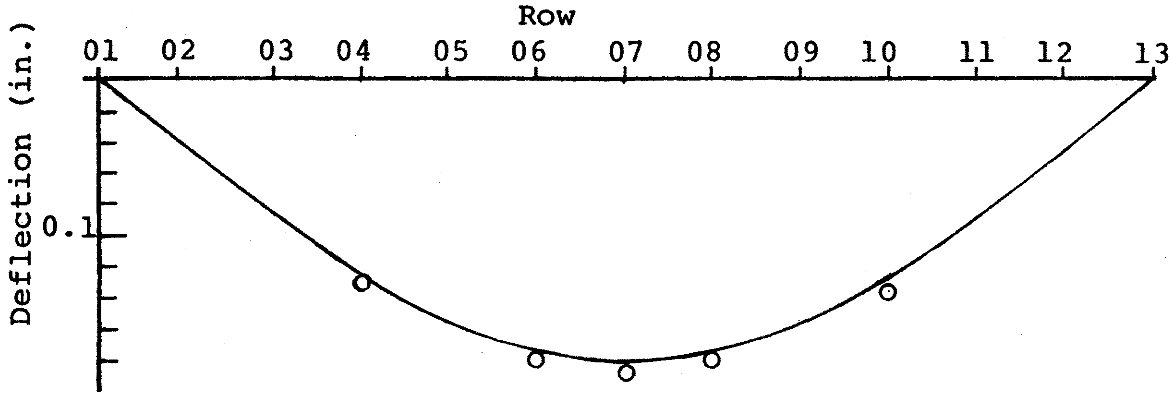

a) Deflection Profile at 1000 lbs.
Load at Midspan

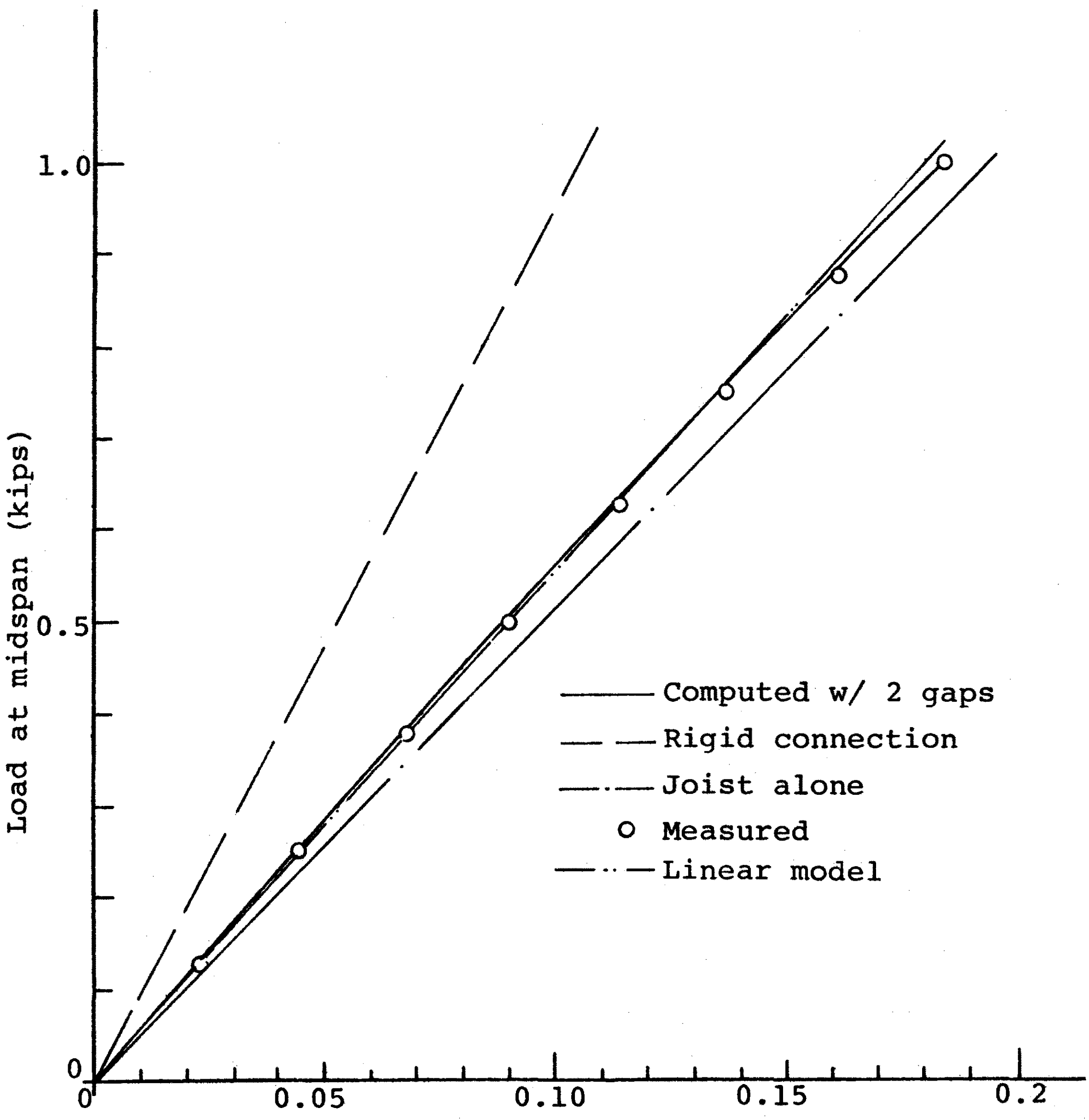

b) Load-Deflection Behavior

Figure C.41 Beam verification - T14-12D24-1 J01 with gaps.

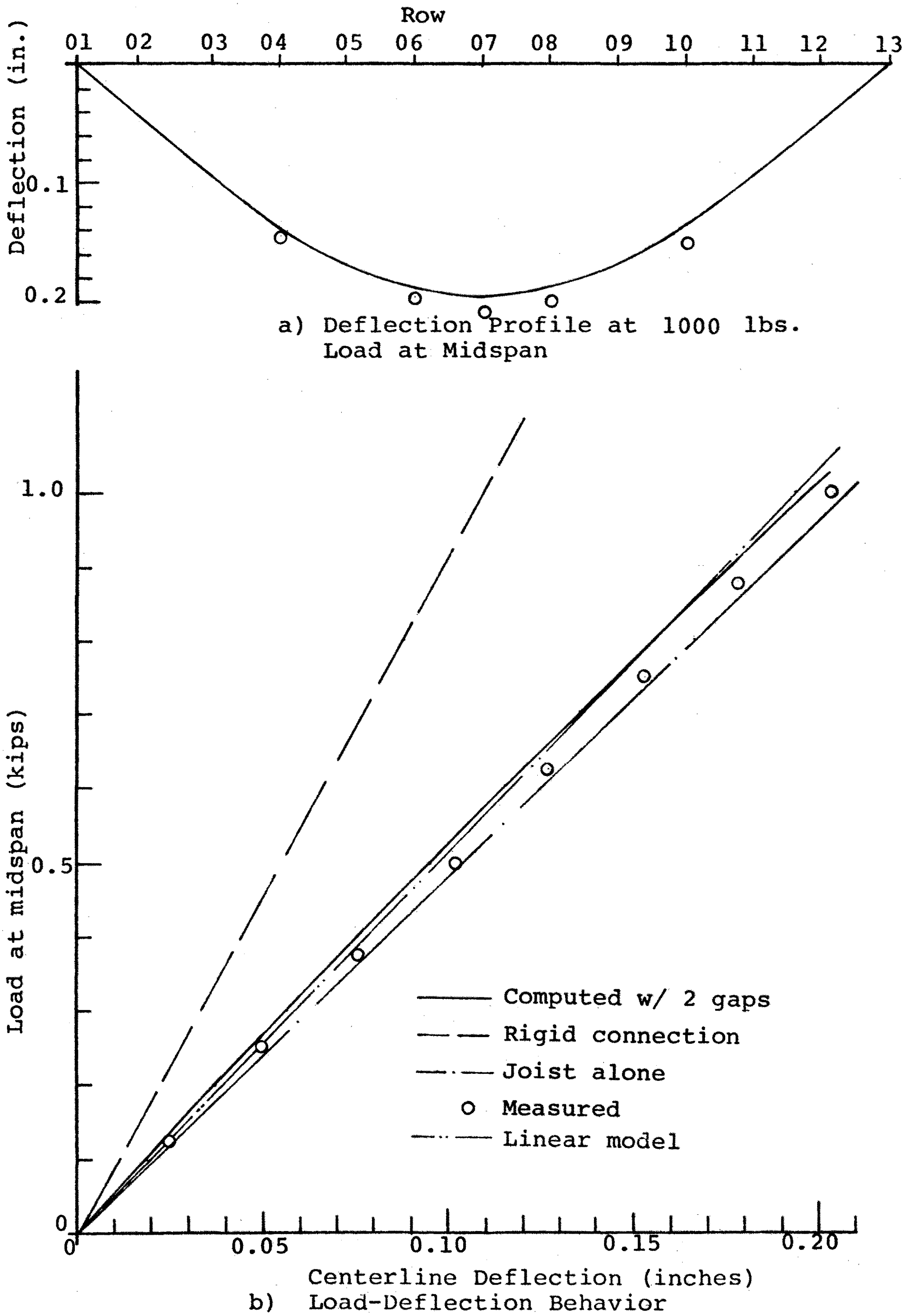

Figure C.42 Beam verification - T14-12D24-1
J02 with gaps.

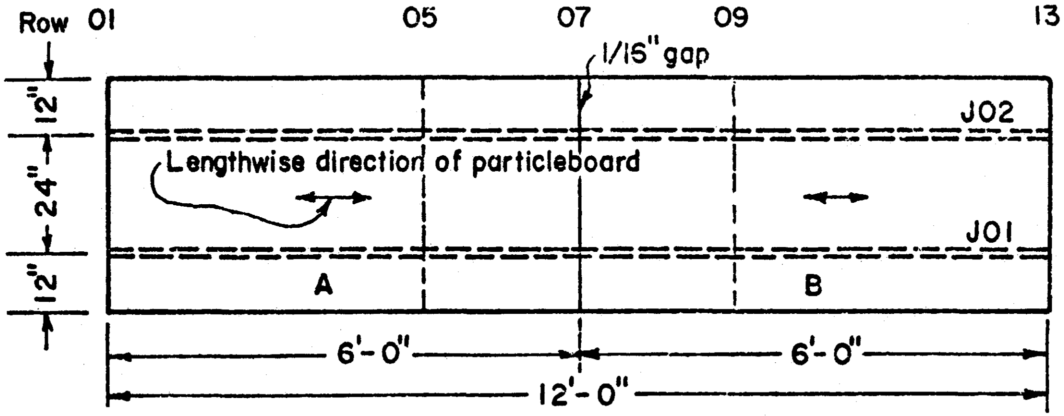

TOP VIEW

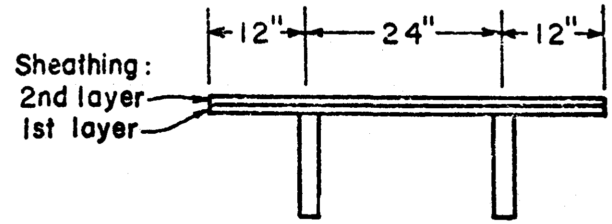

CROSS SECTION

Description of specimen:

Joist: 2x12 Douglas fir (see T14-12D24-1)

Sheathing: 1st layer (see T14-12D24-1)
2nd layer 1/2" particleboard

A	DB-12-20	$E_u = 5.837 \times 10^5$ psi
B	DB-12-19	$E_u = 5.782 \times 10^5$

Connector: 1st layer (see T14-12D24-1)
2nd layer 6d cement-coated nails spaced at 8"

Sheathing Joint: 1/16" gap

Test sequence

1. Loaded at row 07 with $\Delta P = 250$ to $P = 500$ and $\Delta P = 500$ up to $P = 2500$ lbs
2. Loaded at row 05 with loads same in 1
3. Loaded at row 03 with loads same in 1
4. Test to failure: loaded at row 07 with $\Delta P = 500$. J01 cracked at $P = 12500$ lbs and J02 failed at $P = 14,000$ lbs.

Figure C.43 Configuration and Properties of Specimen T14-12D24-2.

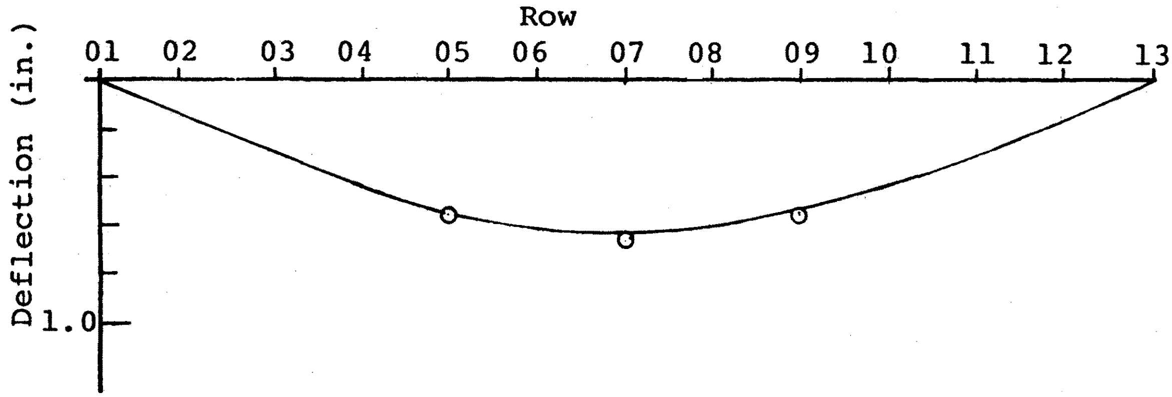

a) Deflection Profile at 3500 lbs. Load at Midspan

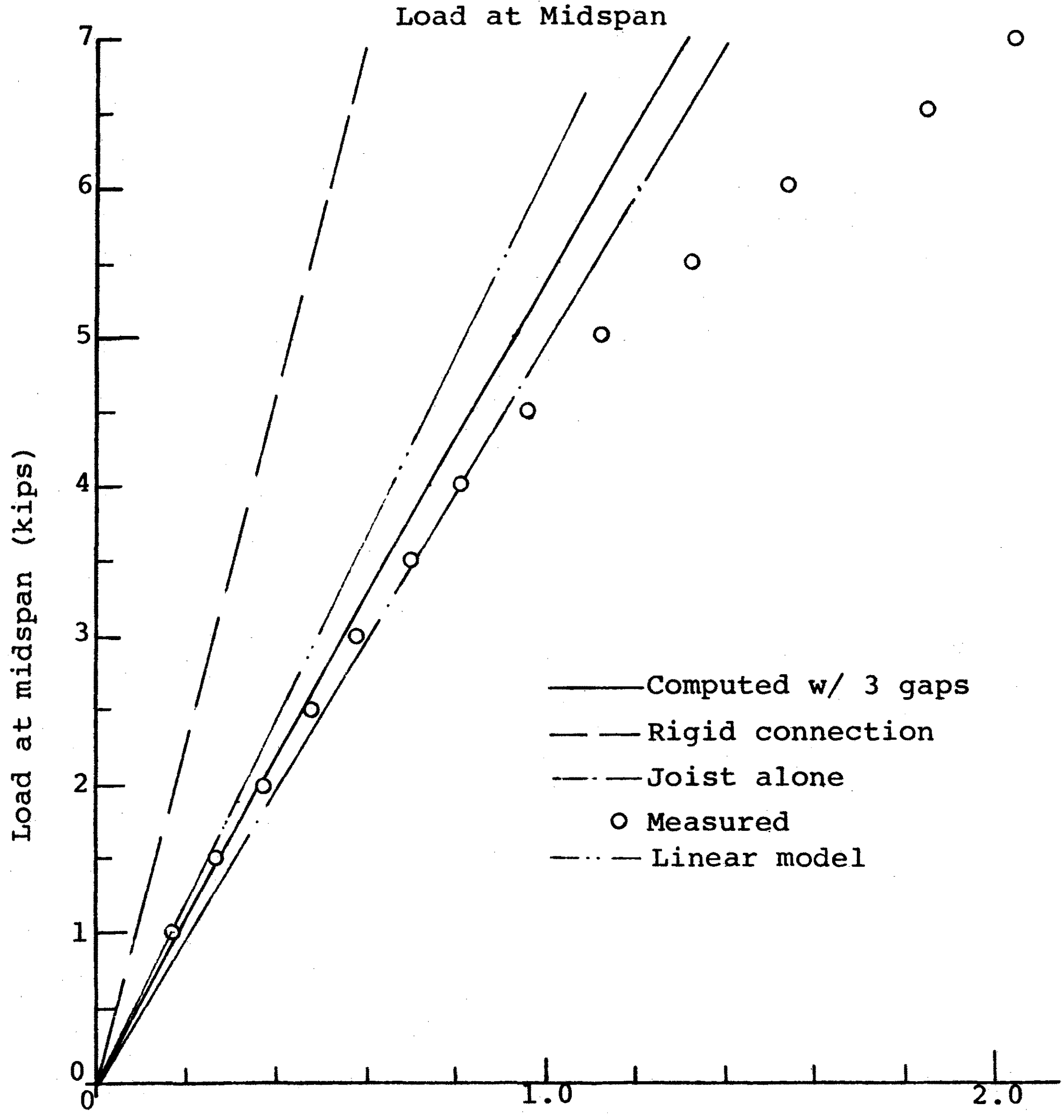

b) Load-Deflection Behavior

Figure C.44 Beam verification - T14-12D24-2 J01 with gaps.

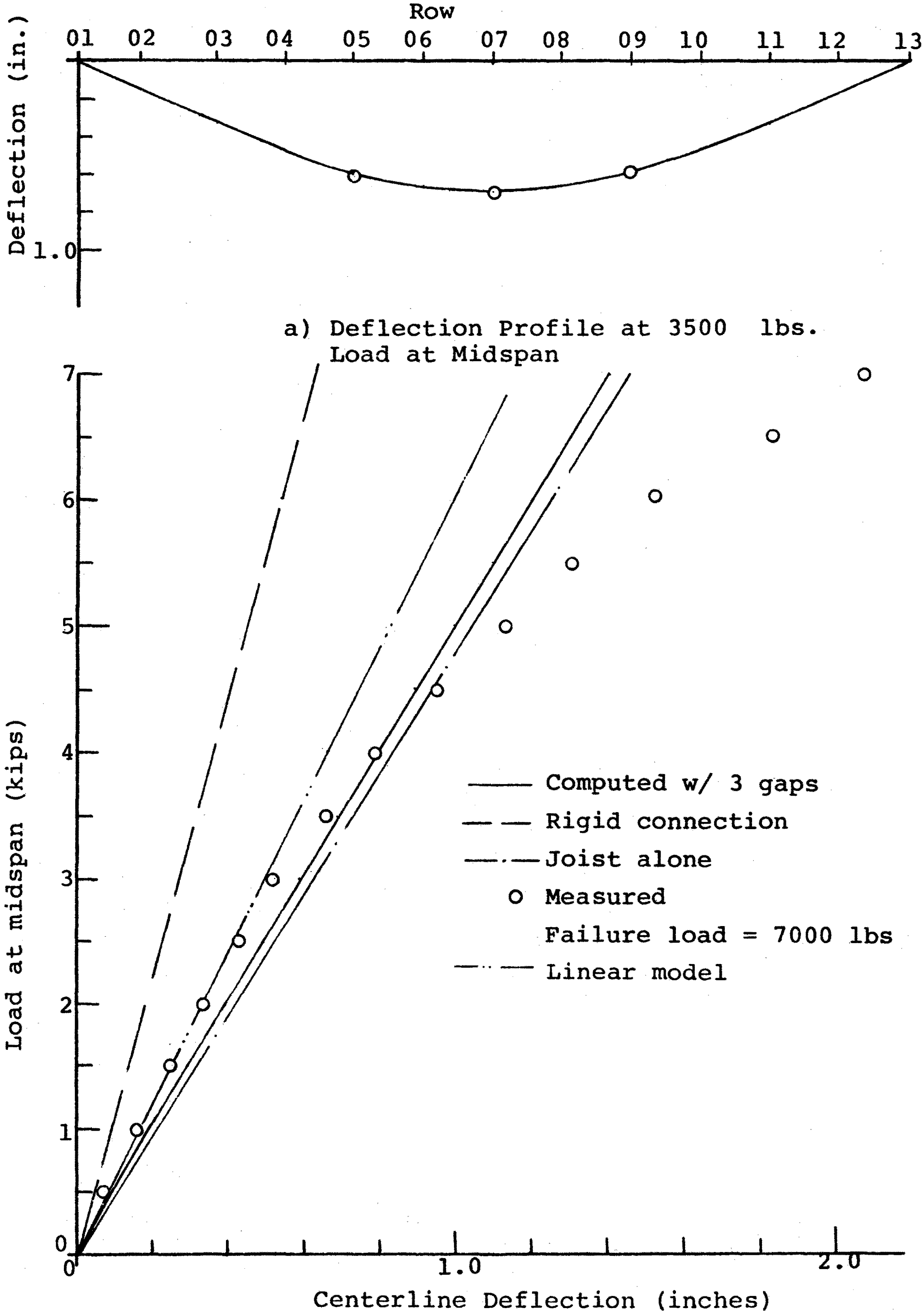

a) Deflection Profile at 3500 lbs. Load at Midspan

b) Load-Deflection Behavior

Figure C.45 Beam verification - T14-12D24-2 J02 with gaps.

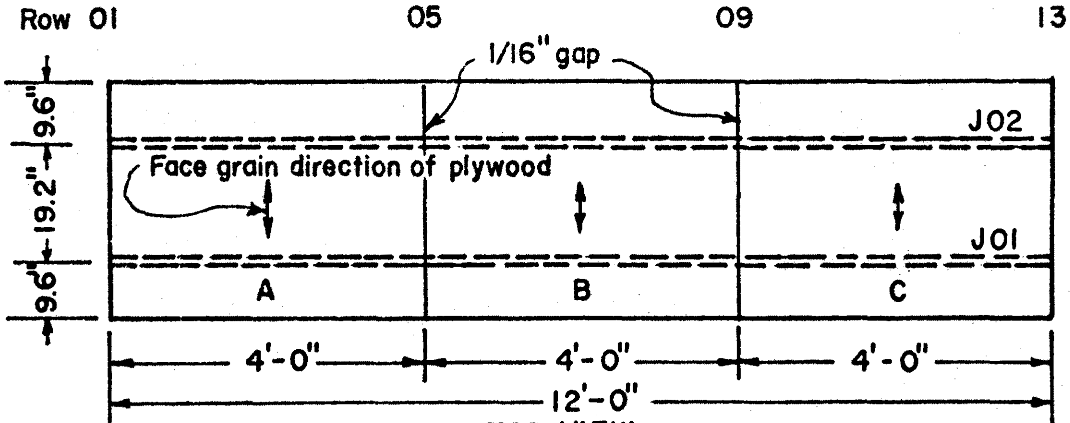

TOP VIEW

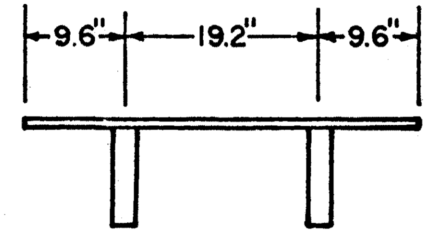

CROSS SECTION

Description of specimen:

Joist: 2x8 Engelmann spruce

J01	EK-S-08-01	$E = 1.191 \times 10^6$ psi
J02	EK-S-08-09	$E = 1.151 \times 10^6$

Sheathing: 1/2" E.S. Plywood

A	EP-12-03	$E_{\perp} = 2.221 \times 10^5$ psi
B	EP-12-02	$E_{\perp} = 2.157 \times 10^5$
C	EP-12-02	

Connector: 8-d common nails spaced at 8"

Sheathing Joints: left with 1/16" gaps

Test sequence

1. Loaded at row 07 with $\Delta P = 250$ up to $P = 750$ lbs
2. Repeated 1 with $\Delta P = 100$ up to $P = 600$ lbs
3. Loaded at row 05 with $\Delta P = 100$ up to $P = 700$ lbs
4. Loaded at row 03 with loads same in 2.

Figure C.46 Configuration and Properties of Specimen T15-8E19.2-1.

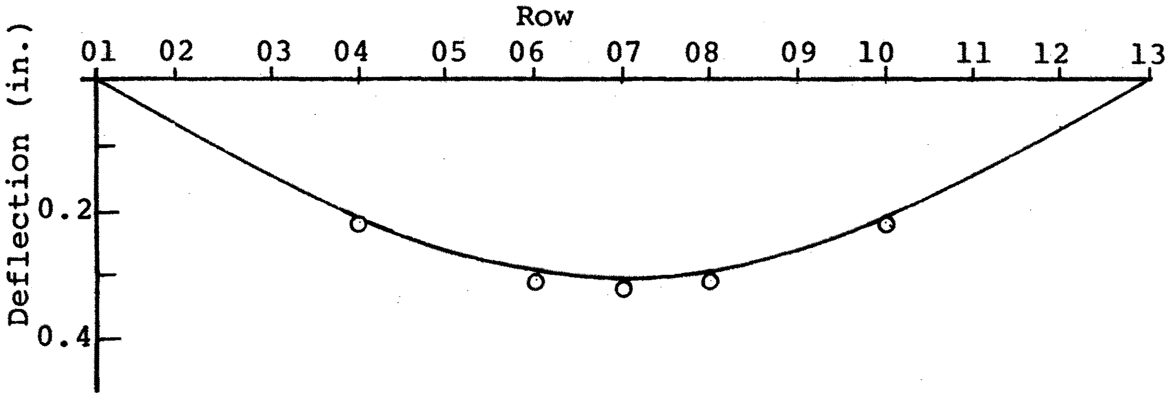

a) Deflection Profile at 300 lbs. Load at Midspan

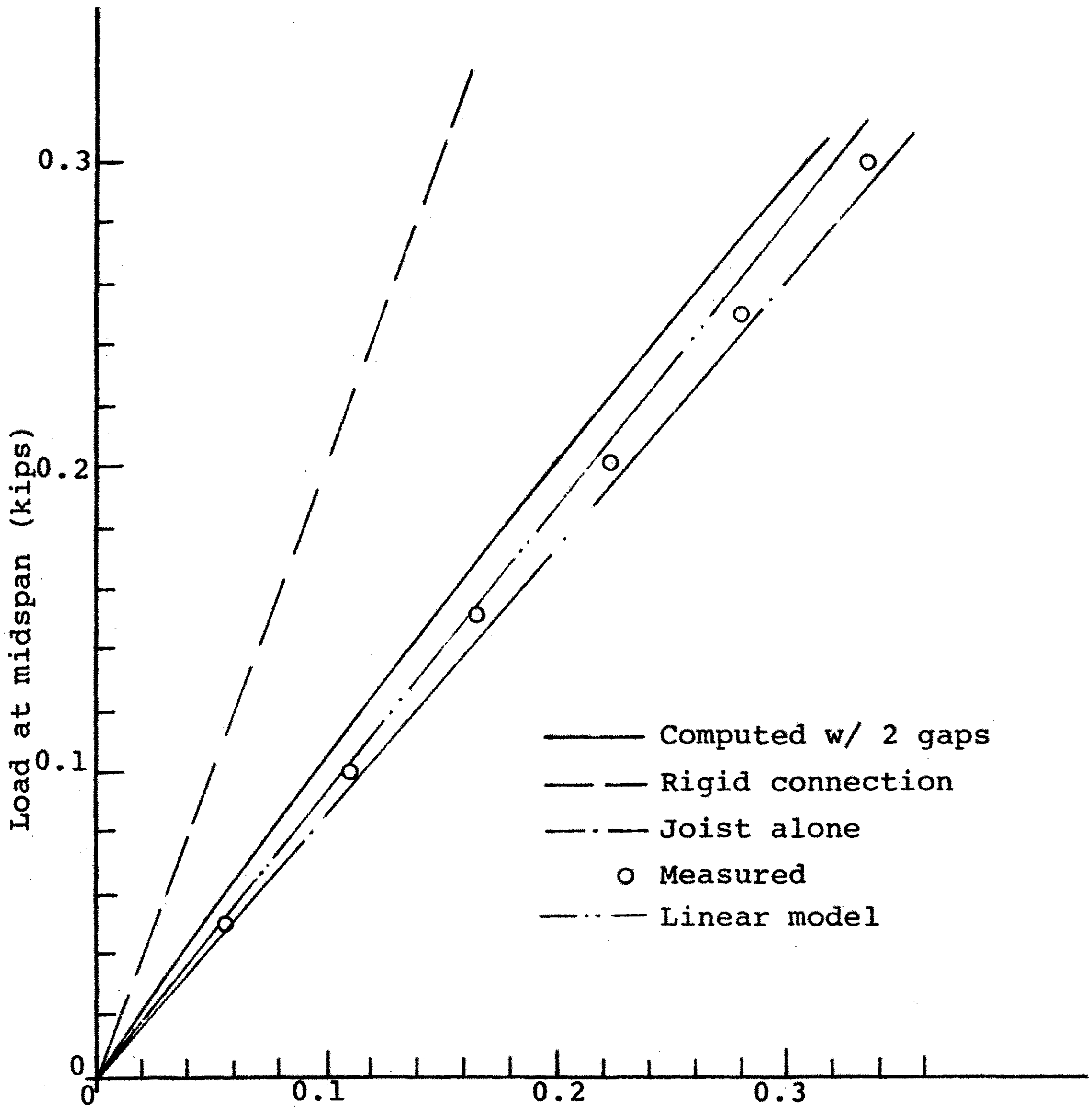

b) Load-Deflection Behavior

Figure C.47 Beam verification - T15-8E19.2-1 J01 with gaps.

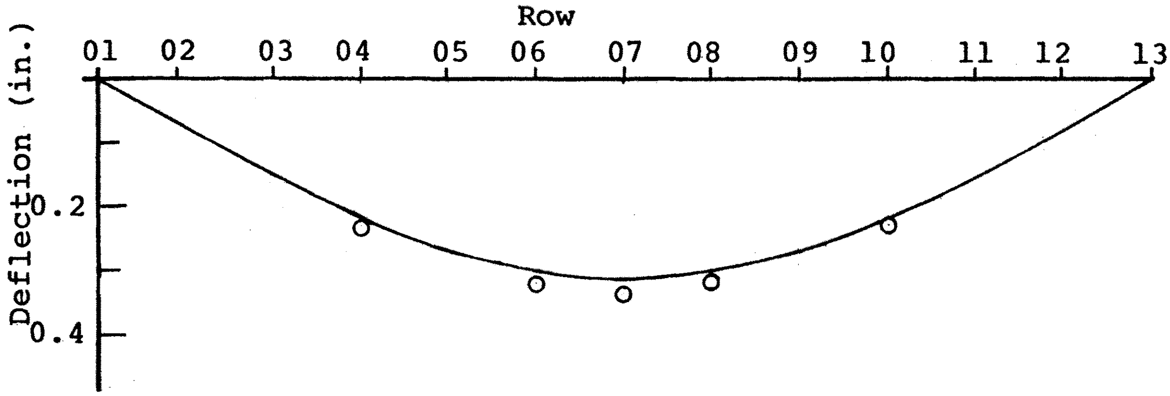

a) Deflection Profile at 300 lbs. Load at Midspan

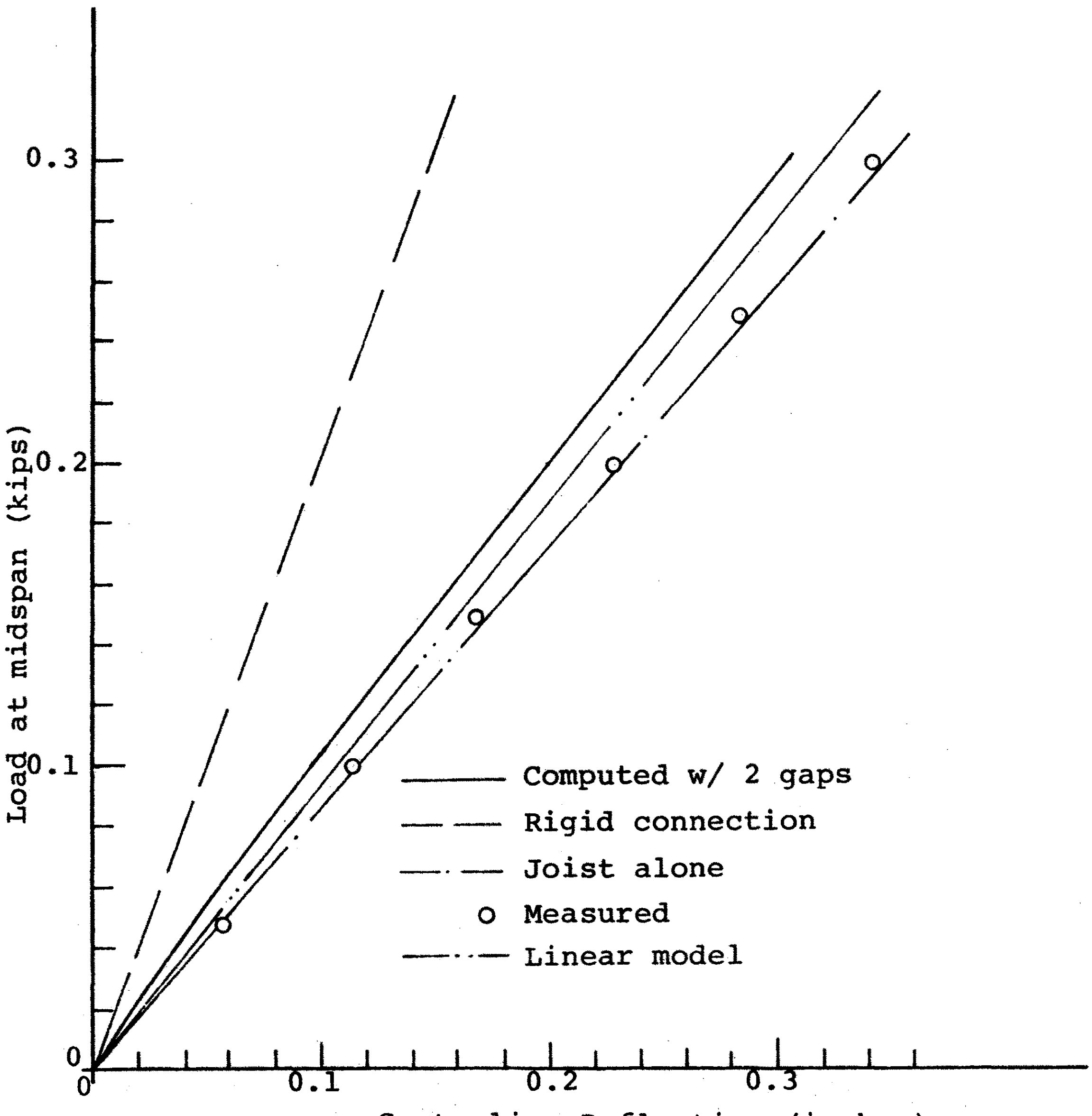

b) Load-Deflection Behavior

Figure C. 48 Beam verification - T15-8E19.2-1 J02 with gaps.

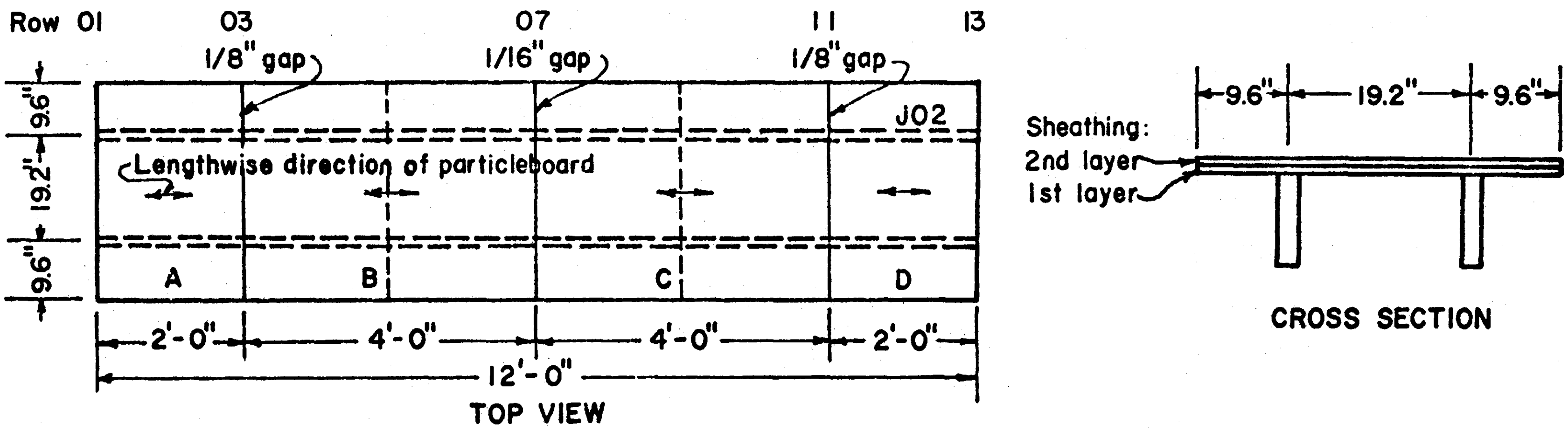

Description of specimen:

Joist: 2x8 Engelmann spruce (see T15-8E19.2-1)

Sheathing: 1st layer (see T15-8E19.2-1)
2nd layer 1/2" particleboard

A	DB-12-20	$E_{\parallel} = 5.837 \times 10^5$ psi
B	DB-12-21	$E_{\parallel} = 5.447 \times 10^5$
C	DB-12-21	$E_{\parallel} = 5.447 \times 10^5$
D	DB-12-19	$E_{\parallel} = 5.782 \times 10^5$

Connector: 1st layer (see T15-8E19.2-1)
2nd layer 6-d cement-coated nails spaced at 6"

Sheathing Joints: left with 1/16" and 1/8" gaps

Test sequence

1. Loaded at row 07 with $\Delta P = 100$ up to $P = 800$ lbs
2. Loaded at row 05 with $\Delta P = 200$ up to $P = 1000$ lbs
3. Loaded at row 03 with loads same in 2
4. Test to failure: loaded at row 07 with $\Delta P = 500$. J01 failed at $P = 4500$ lbs.

Figure C.49 Configuration and Properties of Specimen T15-8E19.2-2.

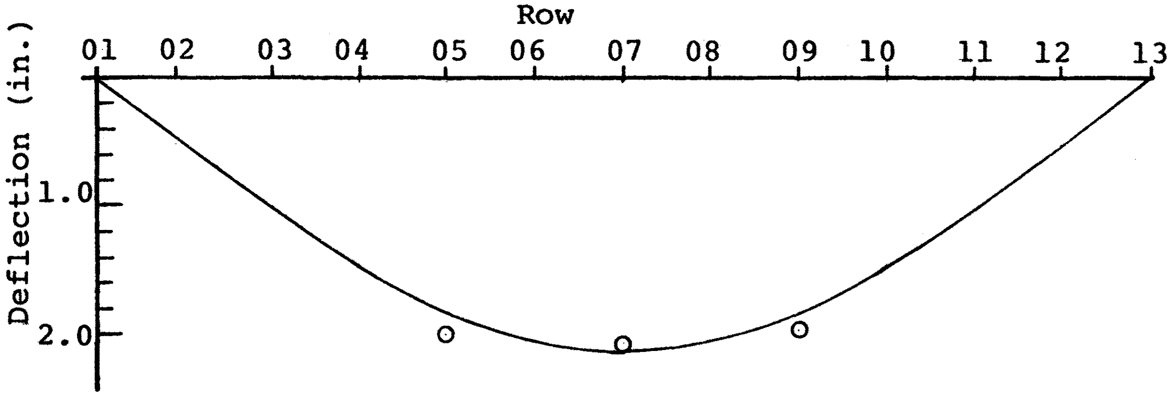

a) Deflection Profile at 2000 lbs.
Load at Midspan

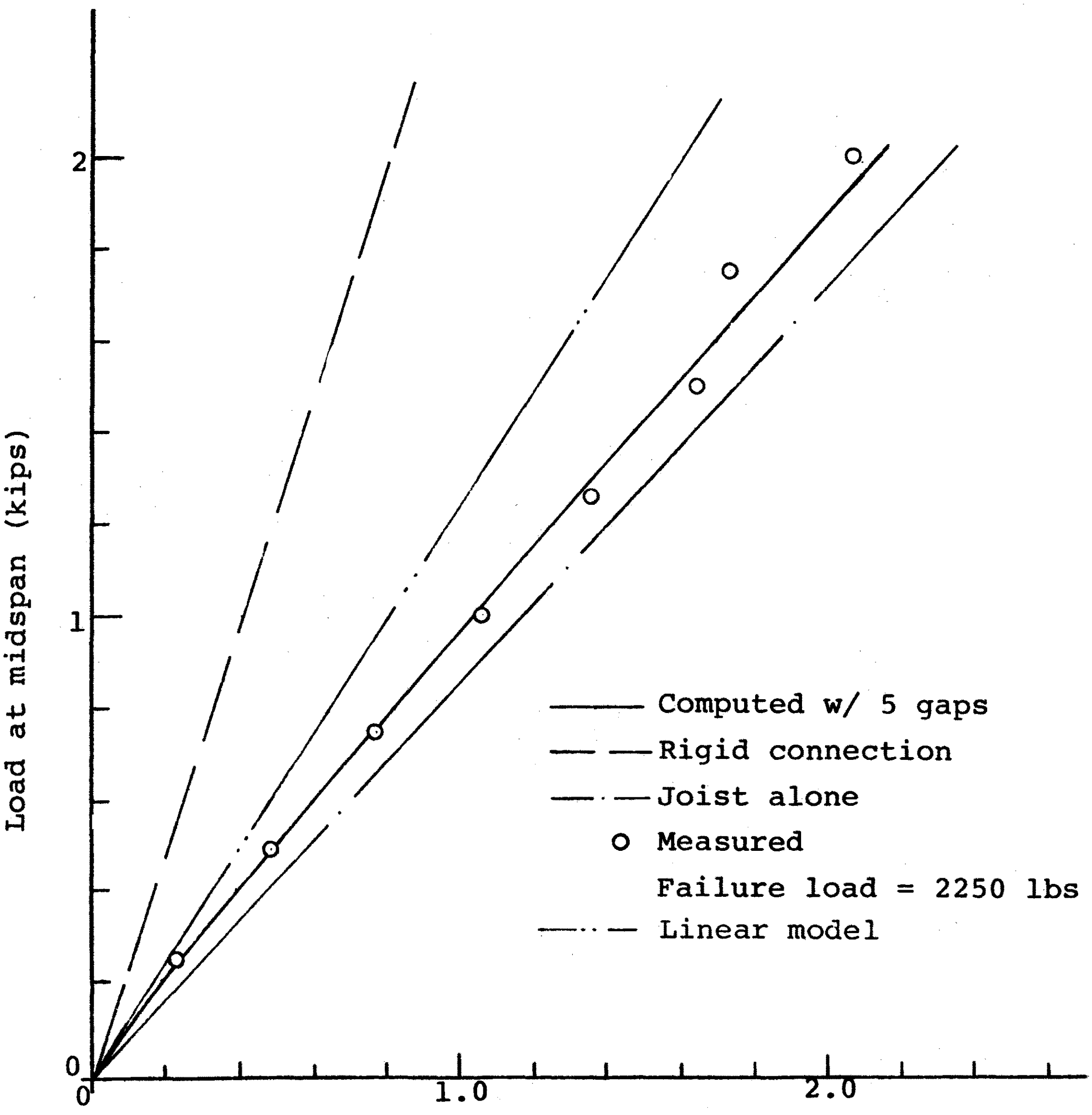

b) Load-Deflection Behavior

Figure C.50 Beam verification - T15-8E19.2-2 J01 with gaps.

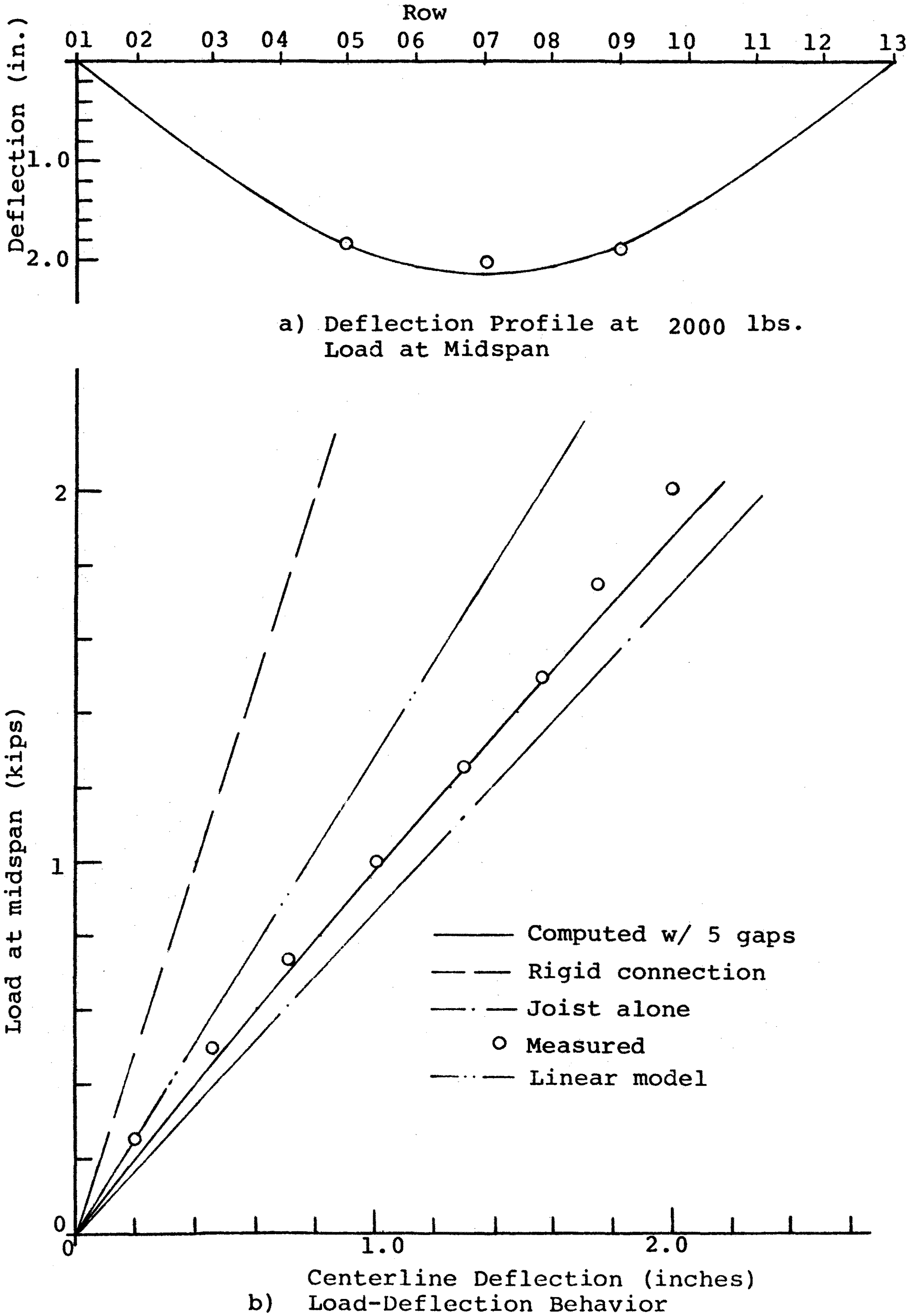

Figure C.51 Beam verification - T15-8E19.2-2 J02 with gaps.

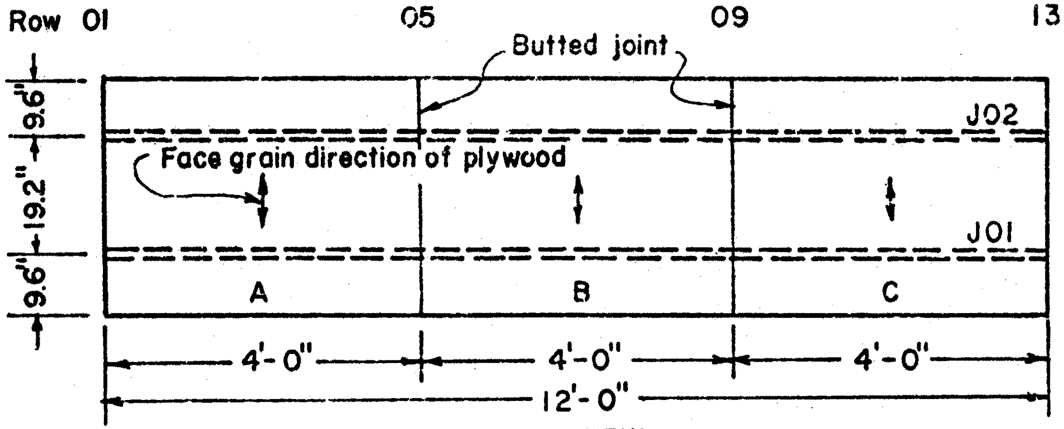

TOP VIEW

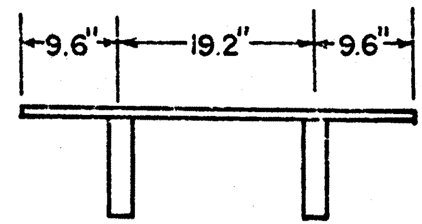

CROSS SECTION

Description of specimen:

Joist: 2x8 Engelmann spruce

J01	EC-S-08-06	$E = 1.410 \times 10^6$ psi
J02	EK-N-08-13	$E = 1.276 \times 10^6$

Sheathing: 1/2" E.S. Plywood

A	EP-12-04	$E_{\perp} = 2.287 \times 10^5$ psi
B	EP-12-04	$E_{\perp} = 2.287 \times 10^5$ psi
C	EP-12-03	$E_{\perp} = 2.157 \times 10^5$ psi

Connector: 8-d common nails spaced at 8"

Sheathing Joints: tightly butted

Test sequence

1. Loaded at row 07 with $\Delta P = 200$ up to $P = 800$ lbs
2. Loaded at row 05 with loads same in 1
3. Loaded at row 03 with loads same in 1.

Figure C.52 Configuration and Properties of Specimen T16-8E19.2-1.

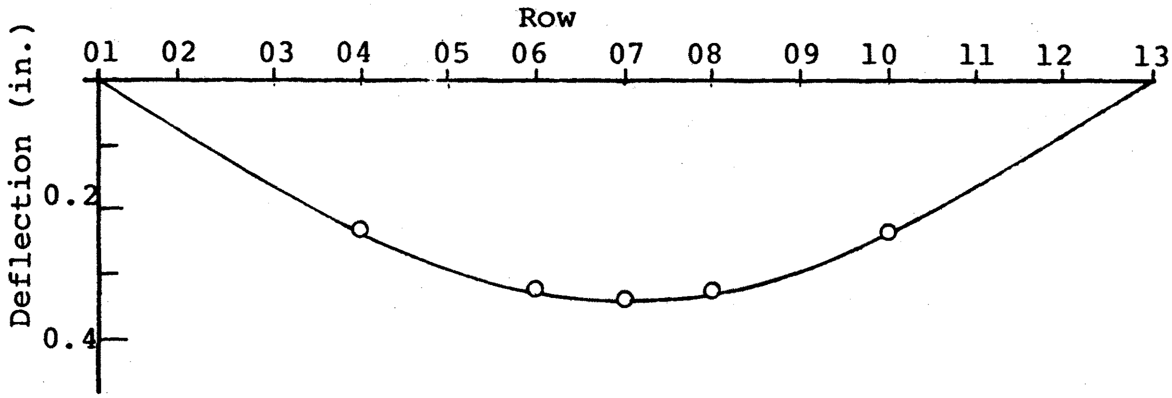

a) Deflection Profile at 400 lbs.
Load at Midspan

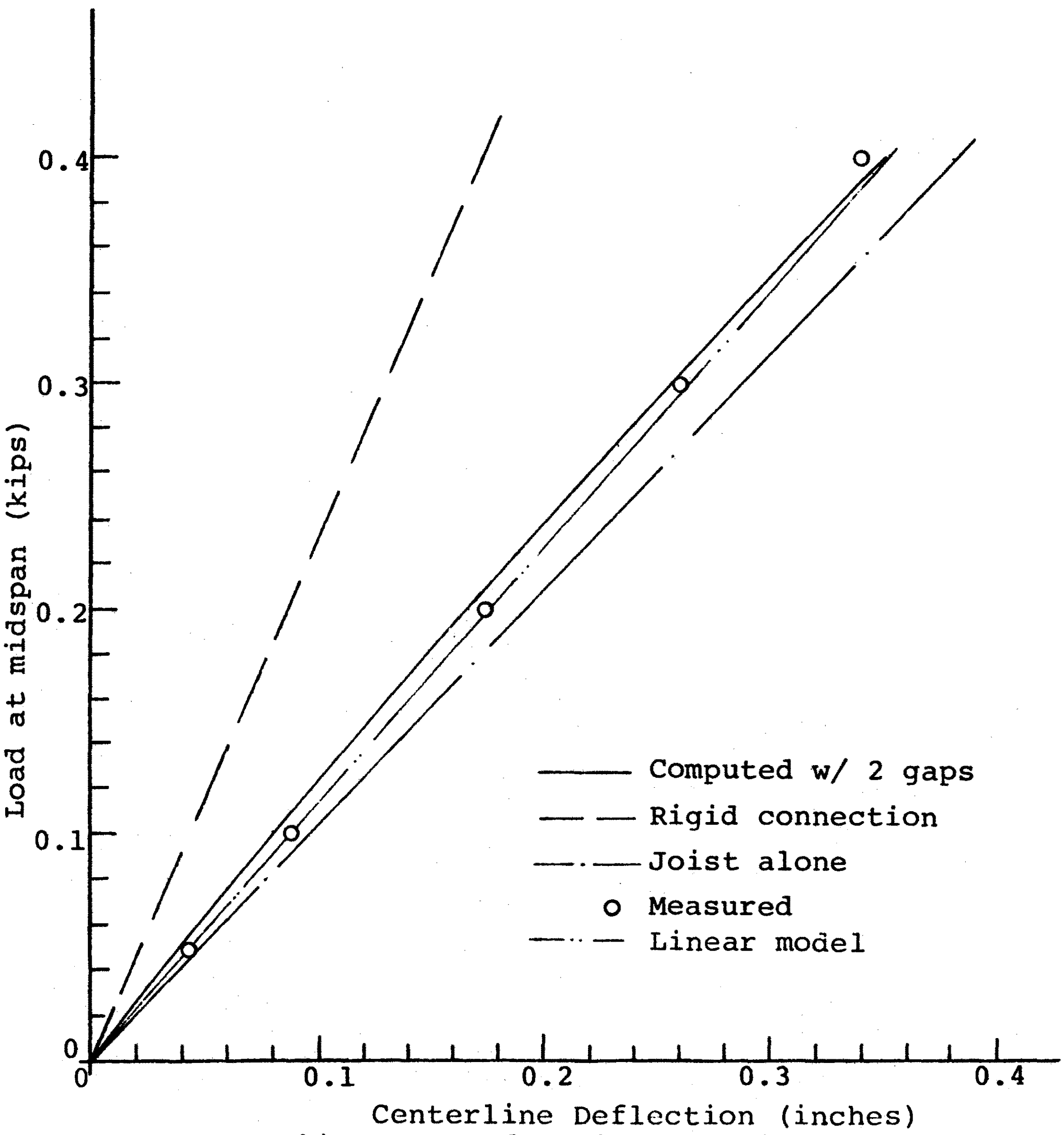

b) Load-Deflection Behavior

Figure C.53 Beam verification - T16-8E19.2-1 J01 with butted joints.

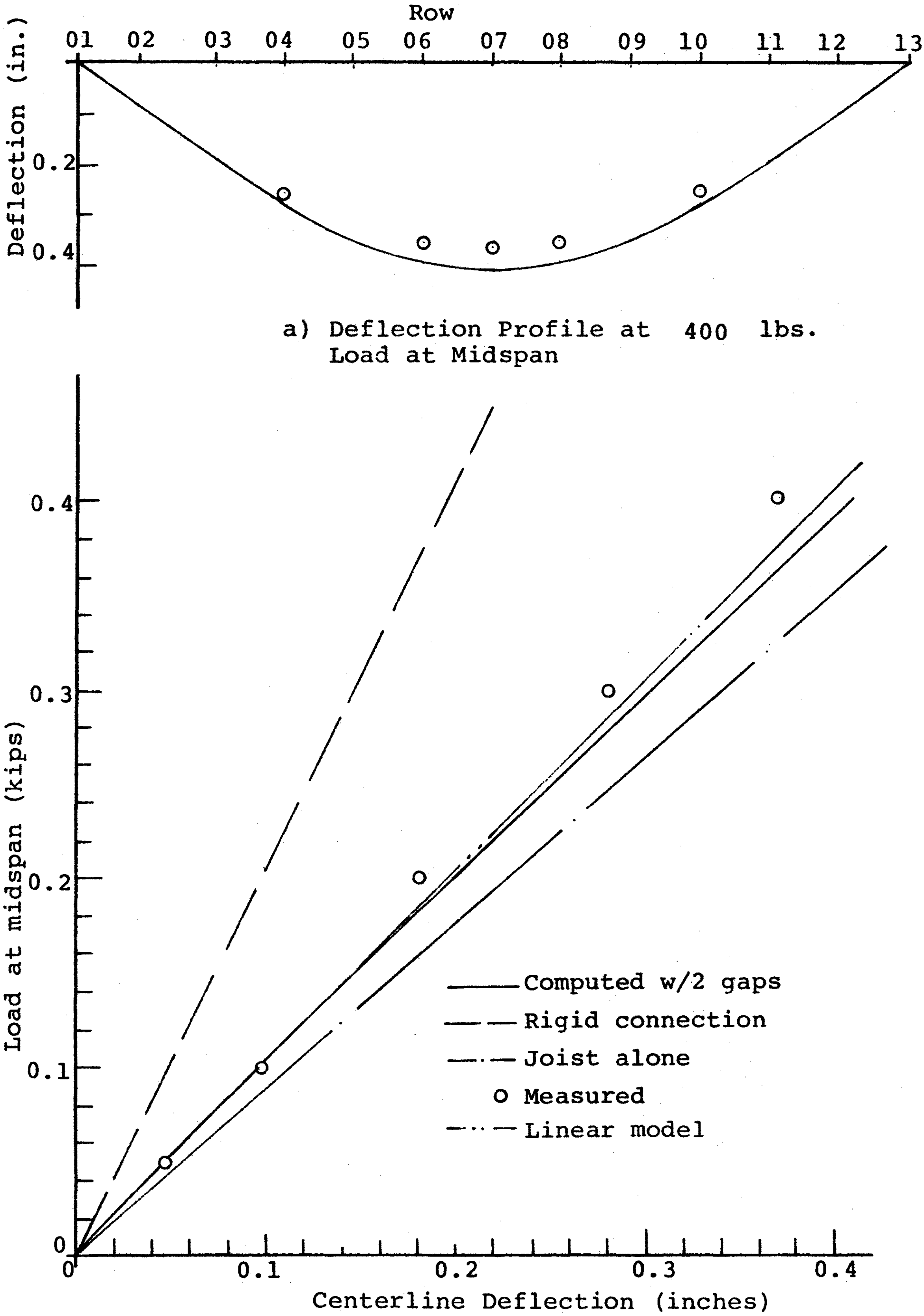

a) Deflection Profile at 400 lbs.
Load at Midspan

b) Load-Deflection Behavior

Figure C.54 Beam verification - T16-8E19.2-1 J02 with butted joints.

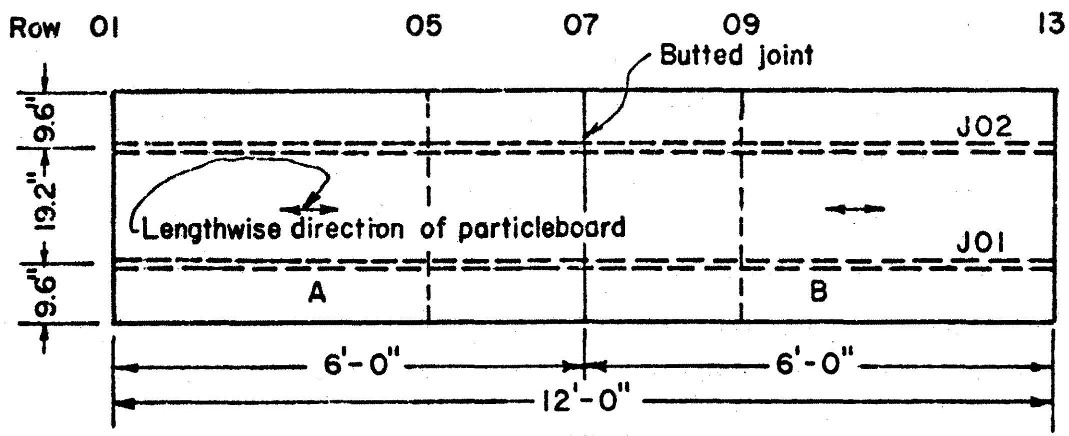

TOP VIEW

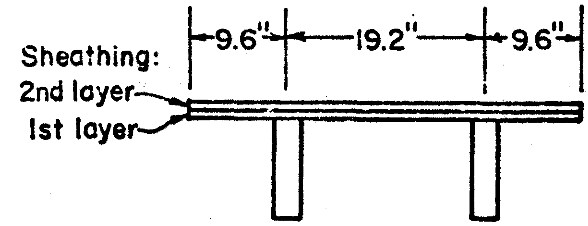

CROSS SECTION

Description of specimen:

Joist: 2x8 E.S. (see T16-8E19.2-1)

Sheathing: 1st layer (see T16-8E19.2-1)
2nd layer 1/2" particleboard

A	DB-12-10	$E_{\parallel} = 4.869 \times 10^5$ psi
B	DB-12-07	$E_{\parallel} = 4.486 \times 10^5$

Connector: 1st layer (see T16-8E19.2-1)
2nd layer 6-d common nails spaced at 8", 2 rows per joist (Nails not driven into joist)

Sheathing Joint: tightly butted

Test sequence

1. Loaded at row 07 with $\Delta P = 200$ up to $P = 1000$ lbs
2. Loaded at row 05 with loads same in 1
3. Loaded at row 03 with loads same in 1
4. Test to failure: loaded at row 07 with $\Delta P = 500$, J02 failed at $P = 3400$ lbs.

Figure C.55 Configuration and Properties of Specimen T16-8E19.2-2.

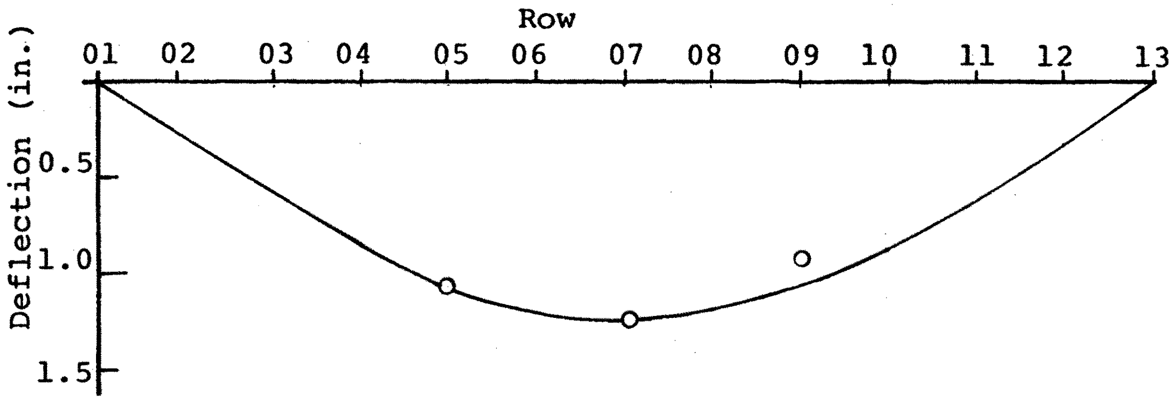

a) Deflection Profile at 1500 lbs. Load at Midspan

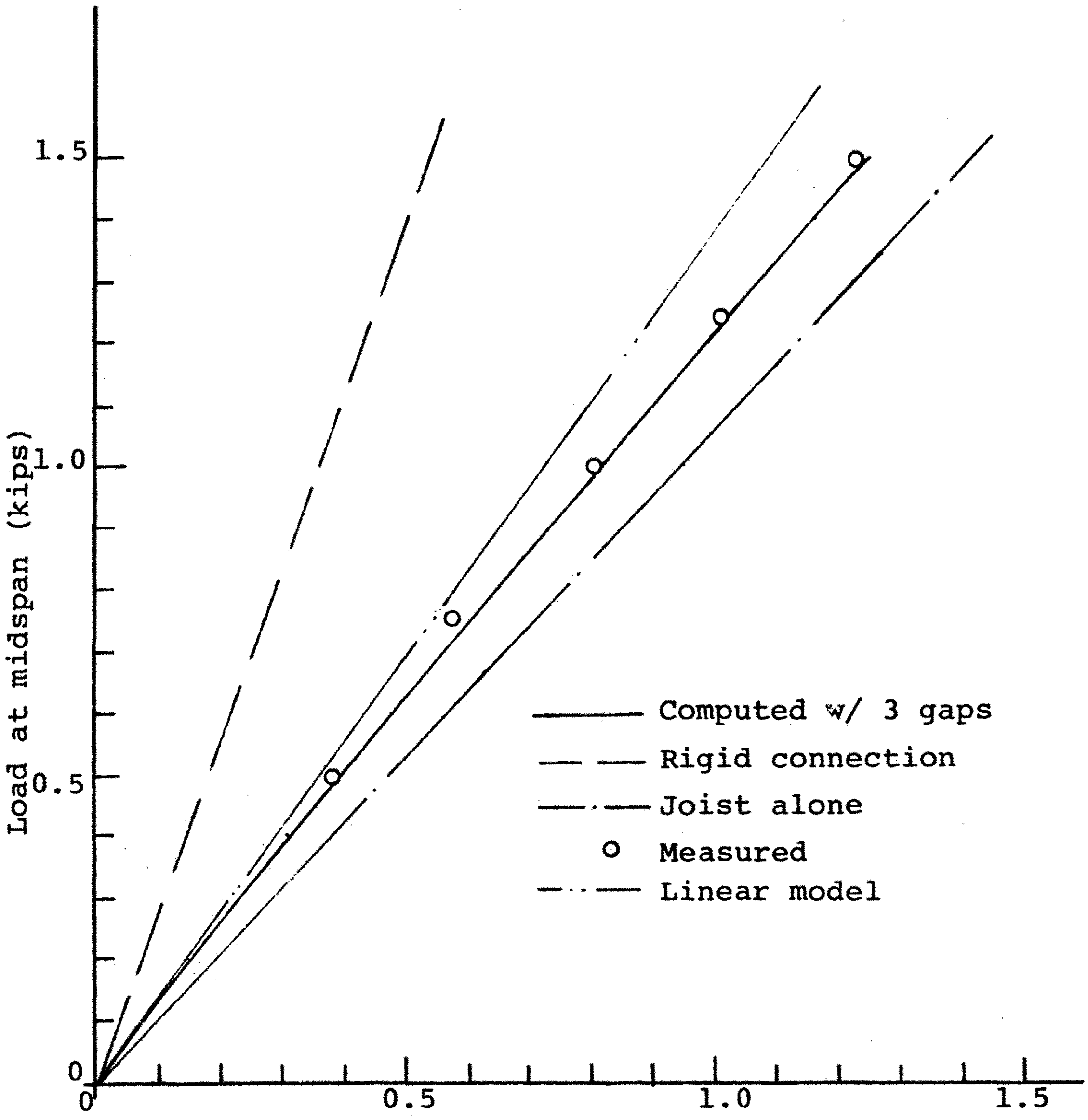

b) Load-Deflection Behavior

Figure C.56 Beam verification - T16-8E19.2-2 J01 with butted joints.

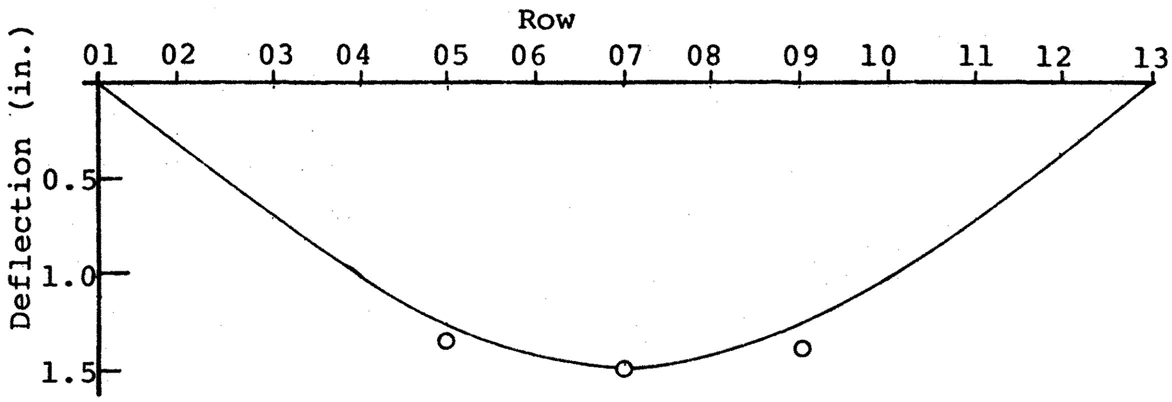

a) Deflection Profile at 1500 lbs. Load at Midspan

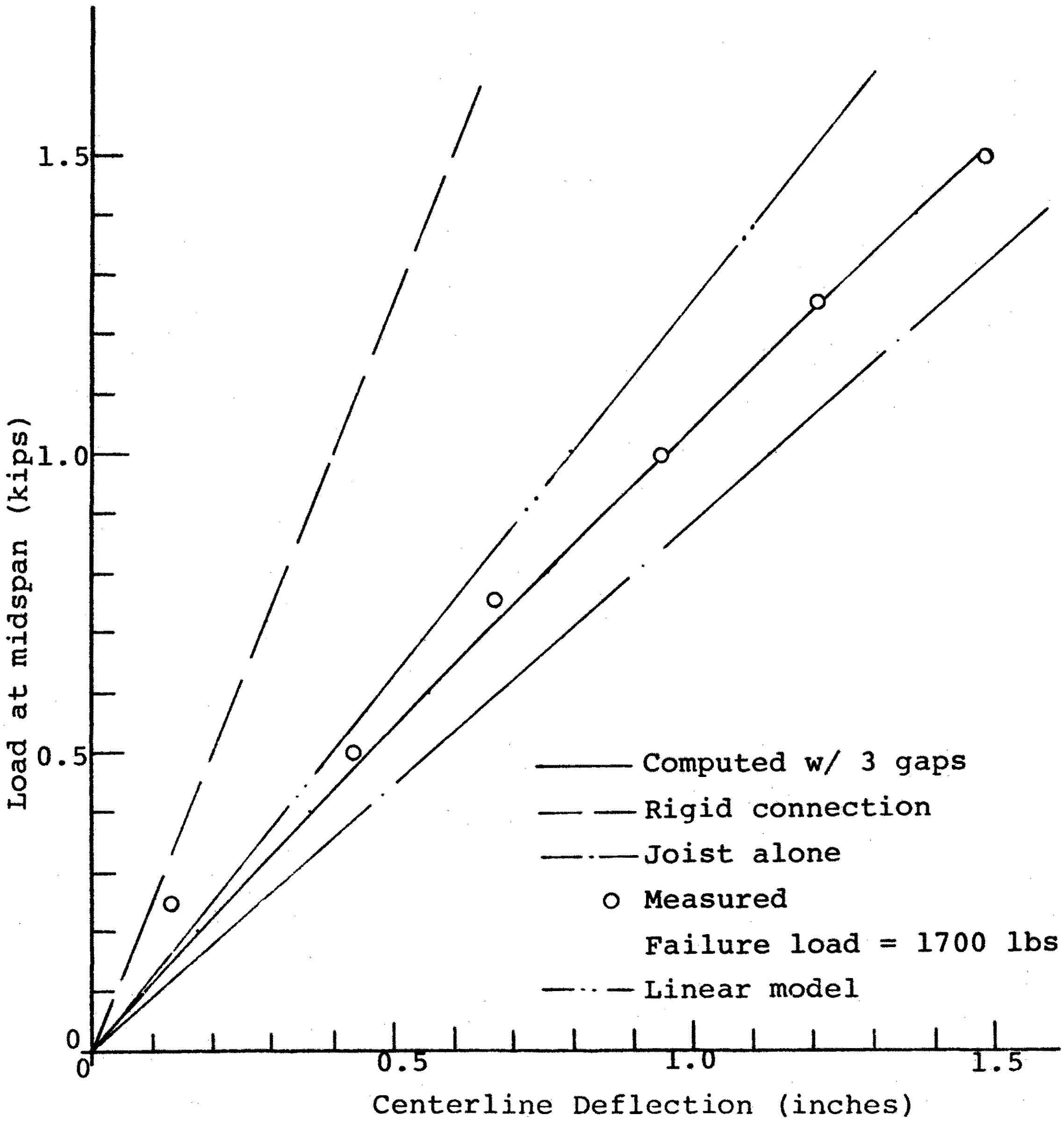

b) Load-Deflection Behavior

Figure C.57 Beam verification - T16-8E19.2-2 J02 with butted joints.

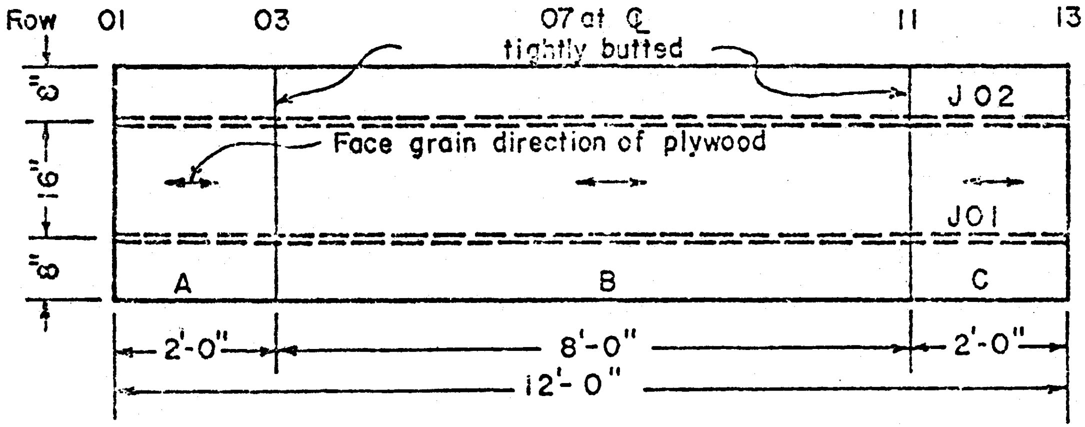

TOP VIEW

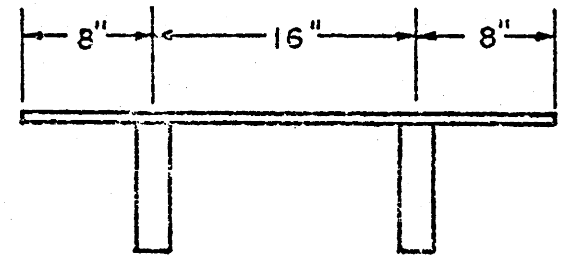

CROSS SECTION

<u>Description of specimen</u>:

Joist: 2x8 Douglas-fir

J01 DW-S-08-31 $E=2.44\times10^6$ psi
J02 DW-S-08-53 $E=2.275\times10^6$ psi

Sheathing: 3/4" D.F. Plywood

A DP-34-01 $E=1.356\times10^6$ psi
B DP-34-02 $E=1.333\times10^6$ psi
C DP-34-01 $E=1.356\times10^6$ psi

Connector: 8-d common nails spaced at 8"

Sheathing Joints: glued

<u>Test sequence</u>:

1. Loaded at row 07 with P=200 lbs up to P=1400 lbs
2. Loaded at row 04 with P=200 lbs up to P=1400 lbs
3. Loaded at row 10 with P=200 lbs up to P=1400 lbs
4. Test to failure: loaded at row 07; joist J02 failed at P=10,000 lbs

Figure C.58 Configuration and Properties of Specimen T17-8D16-1.

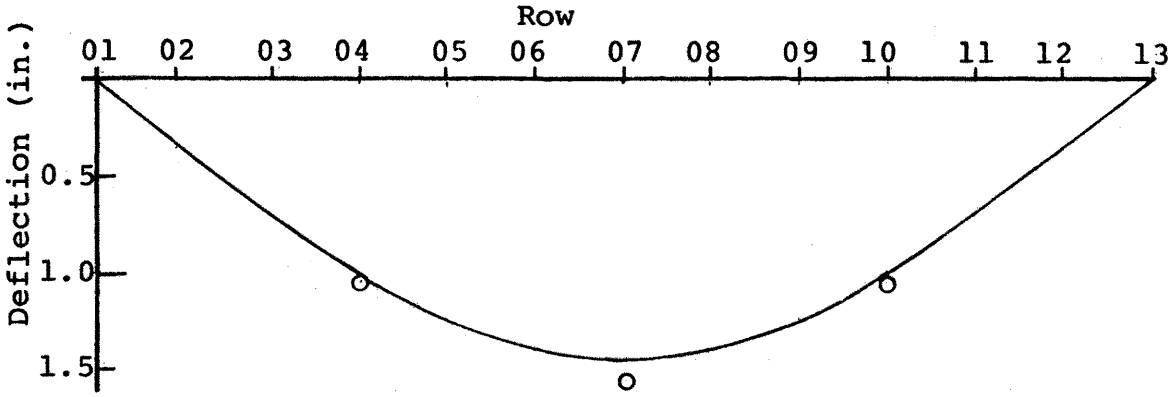

a) Deflection Profile at 3000 lbs.
Load at Midspan

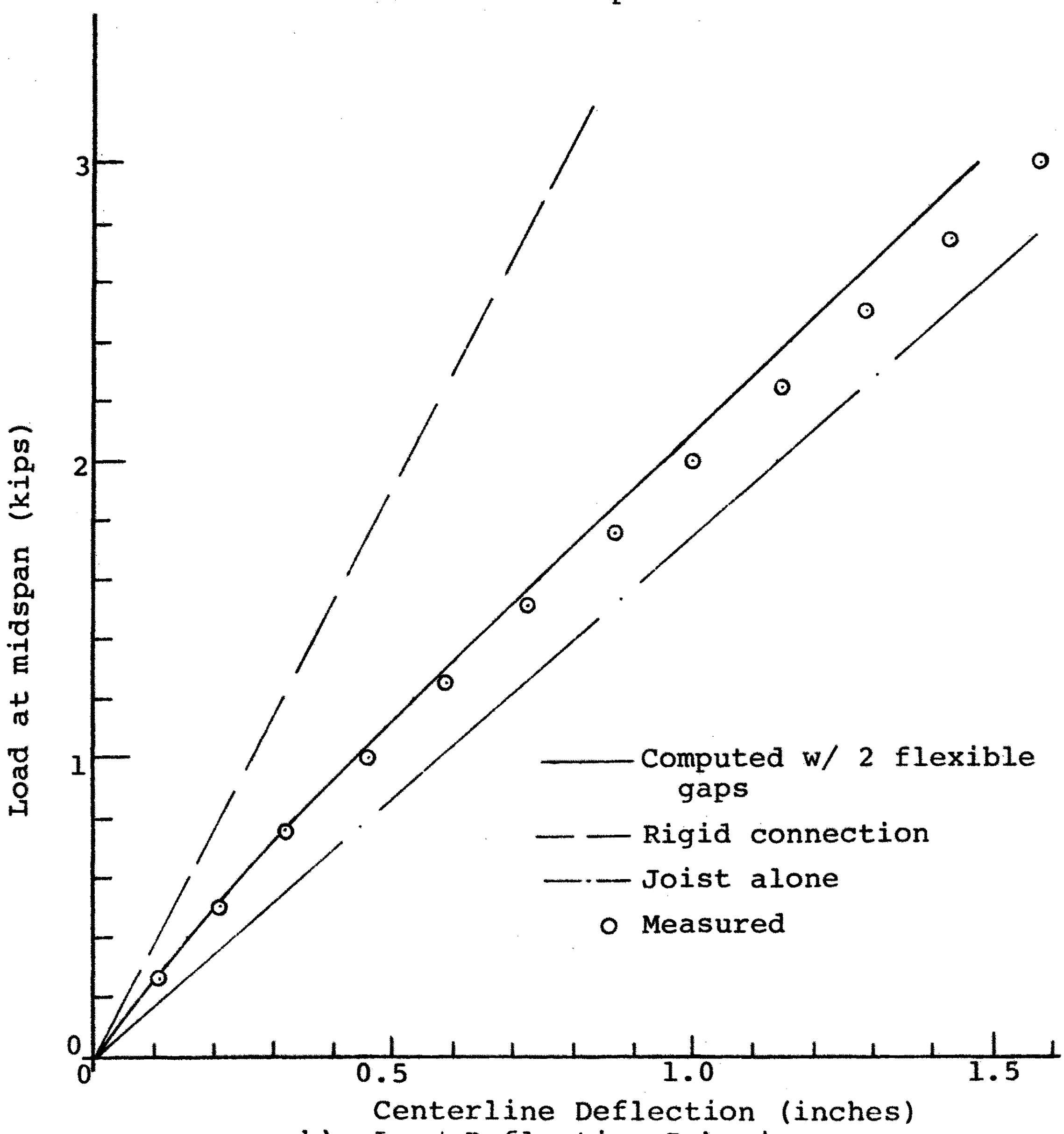

b) Load-Deflection Behavior

Figure C.59 Beam verification - T17-8D16-1 J01 with butted joints.

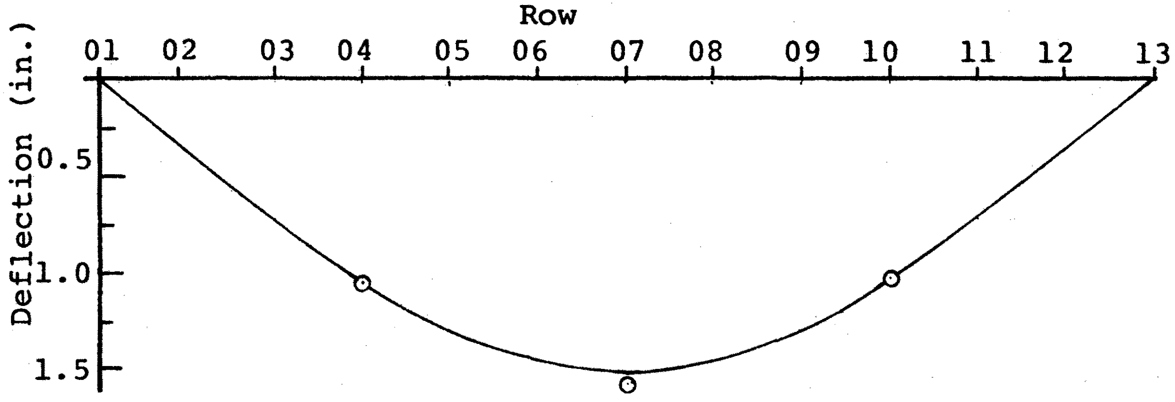

a) Deflection Profile at 3000 lbs. Load at Midspan

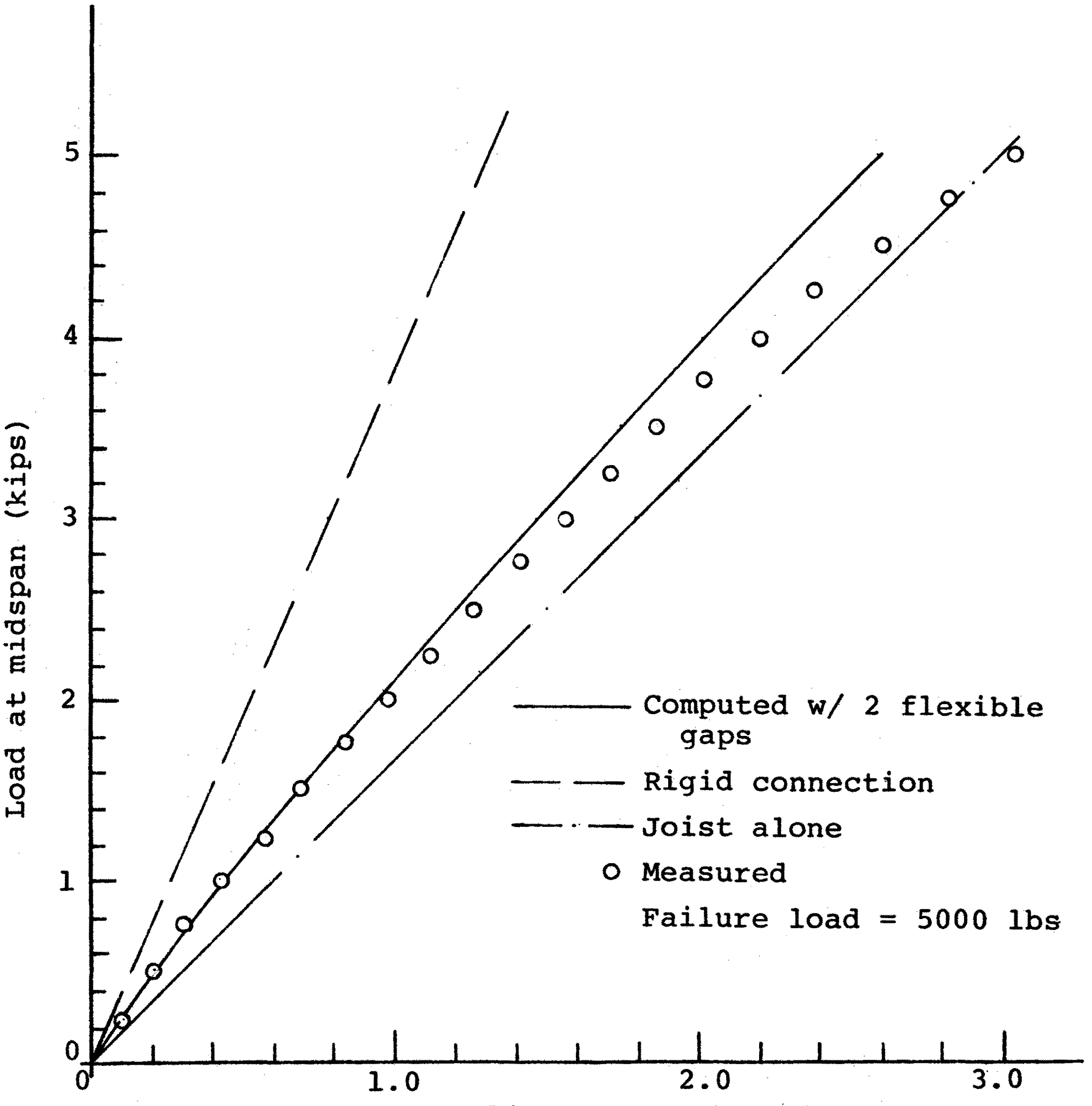

b) Load-Deflection Behavior

Figure C.60 Beam verification - T17-8D16-1 J02 with butted joints.

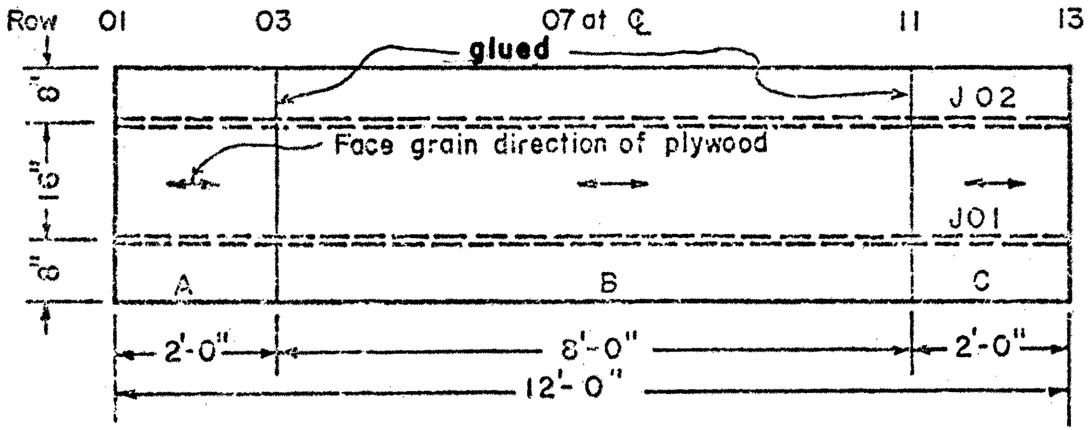

TOP VIEW

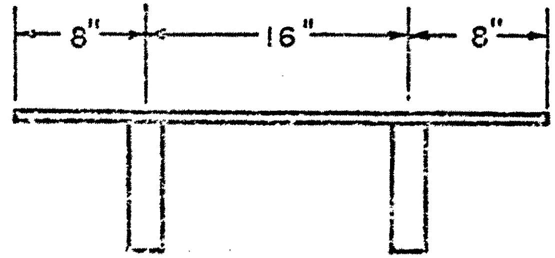

CROSS SECTION

<u>Description of specimen:</u>

Joist: 2x8 Douglas-fir

J01 DW-S-08-59 $E=2.07 \times 10^6$ psi
J02 DW-S-08-63 $E=1.819 \times 10^6$ psi

Sheathing: 3/4" D.F. Plywood

A DP-34-01 $E=1.356 \times 10^6$ psi
B DP-34-24 $E=1.362 \times 10^6$ psi
C DP-34-01 $E=1.356 \times 10^6$ psi

Connector: Franklin Construction Adhesive

Sheathing Joints: glued

<u>Test sequence:</u>

1. Test to failure: loaded at row 07; joist J02 failed at P=8000 lbs

Figure C.61 Configuration and Properties of Specimen T18-8D16-1.

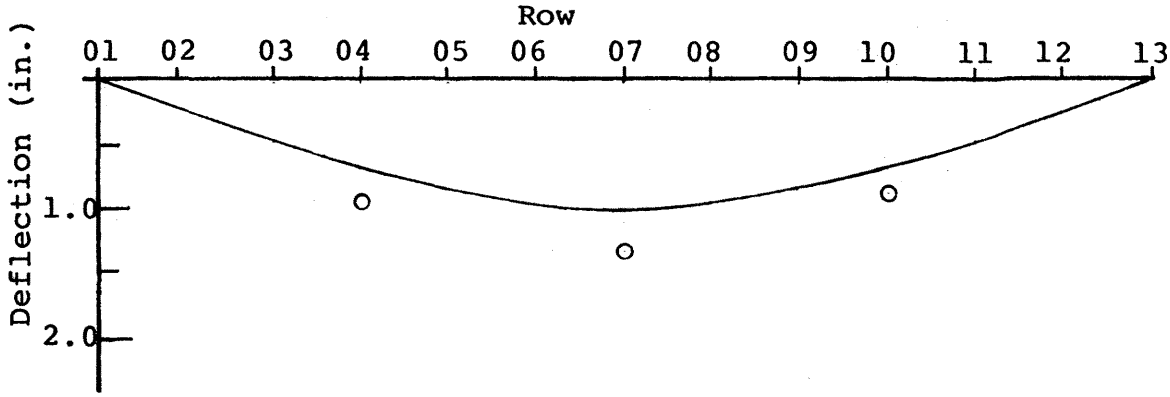

a) Deflection Profile at 3000 lbs. Load at Midspan

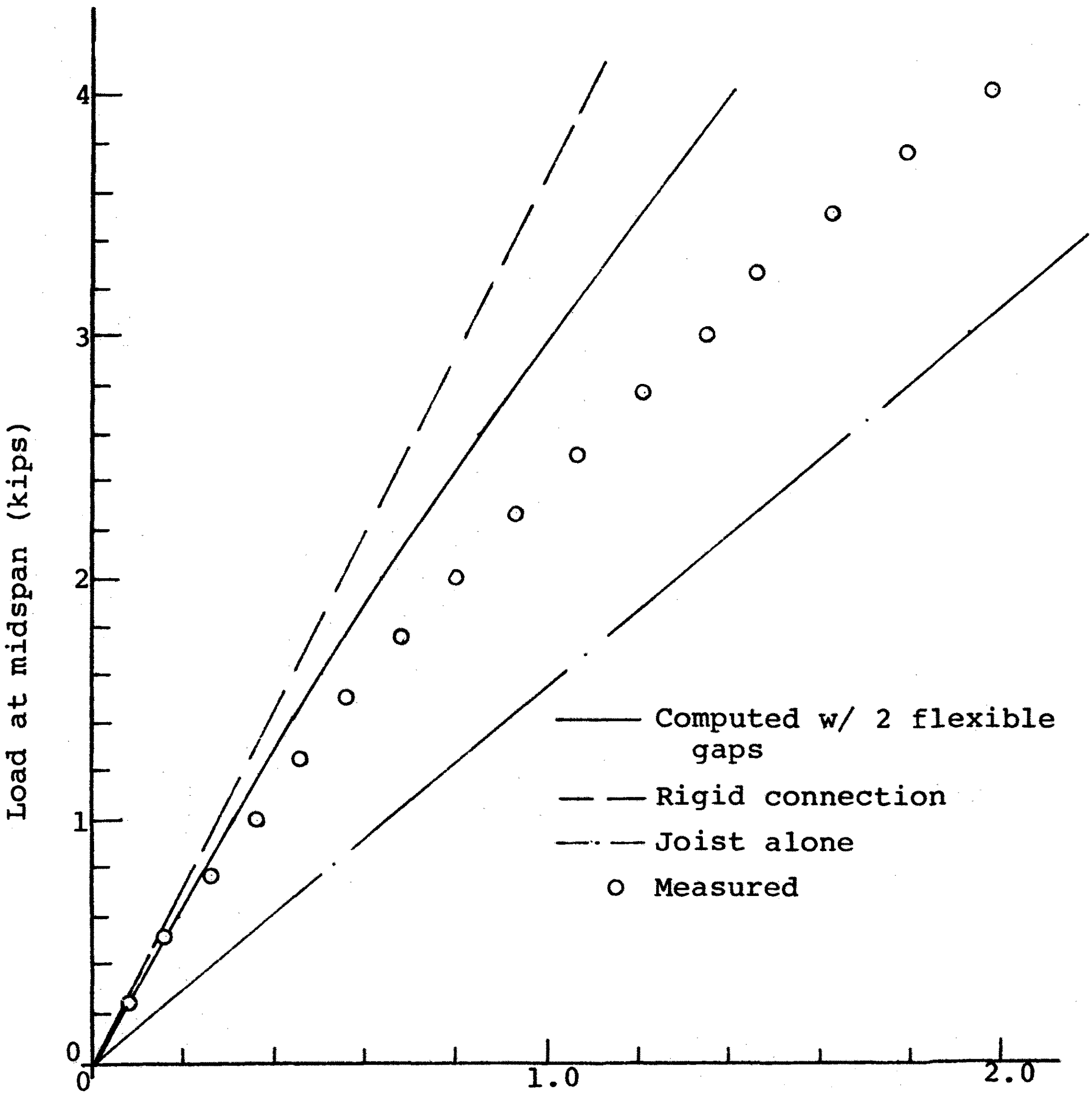

b) Load-Deflection Behavior

Figure C.62 Beam verification - T18-8D16-1 J01 with glued joints.

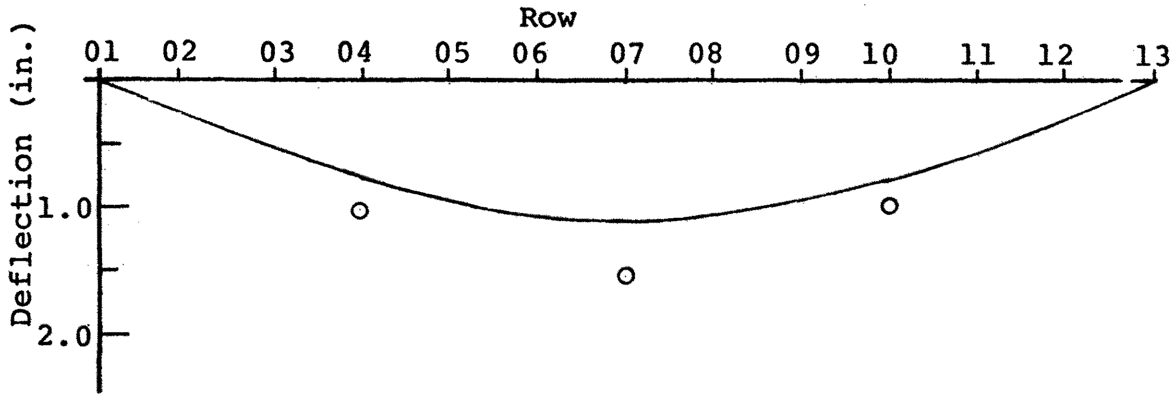

a) Deflection Profile at 3000 lbs.
Load at Midspan

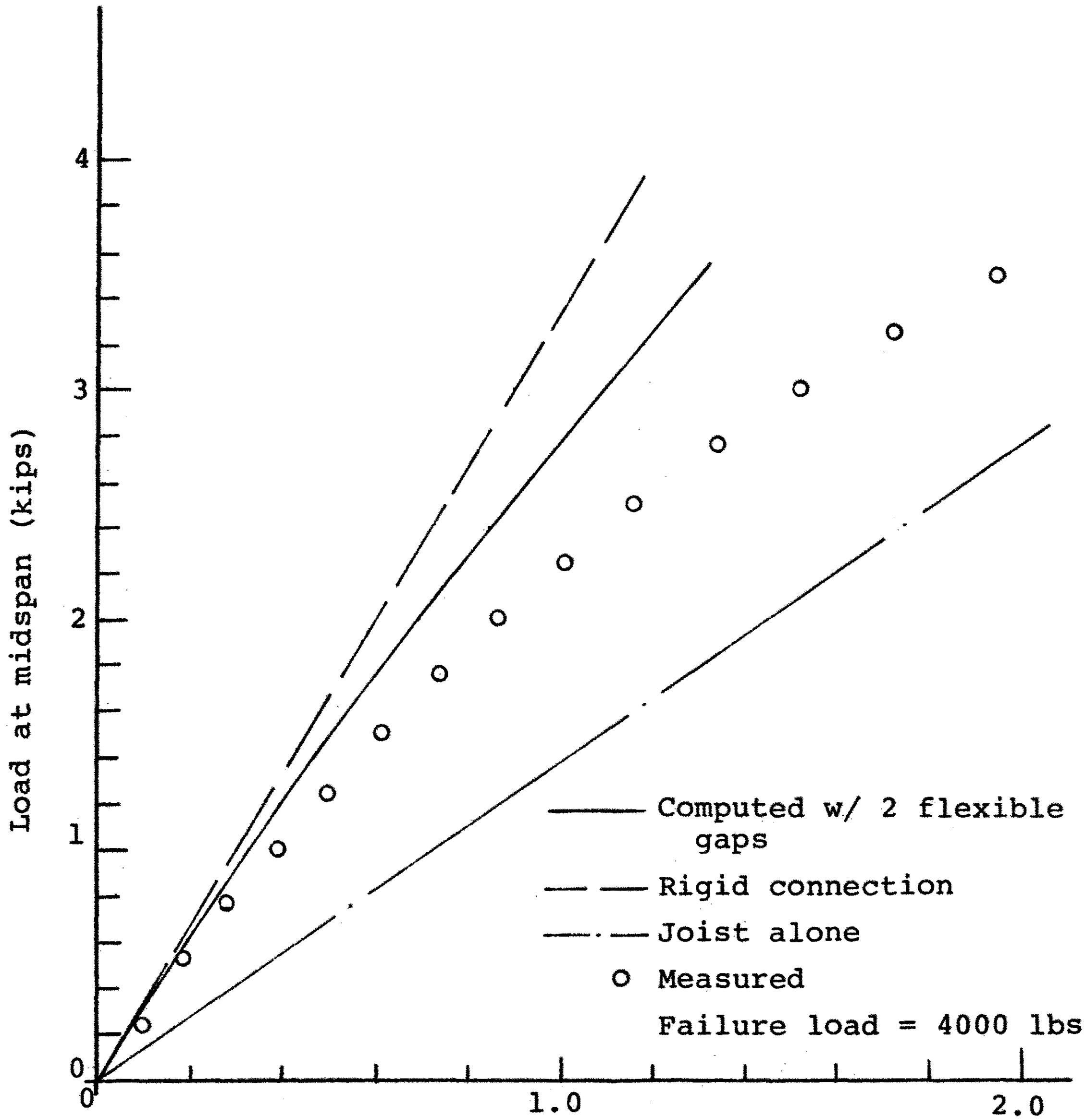

b) Load-Deflection Behavior

Figure C.63 Beam verification - T18-8D16-1 J02 with glued joints.

APPENDIX D

LISTING OF FINITE ELEMENT COMPUTER PROGRAM

PROGRAM ELM CDC 6400 FTN V3.0-P365 OPT=1 09/06/74 11.29.14.

```
      PROGRAM ELM
     1 (INPUT,OUTPUT,TAPE5=INPUT,TAPE6=OUTPUT)
C
C
C     FINITE ELEMENT PROGRAM FOR BEAMS WITH INTERLAYER SLIP
C     WRITTEN BY ERIK THOMPSON, JUNE 1973, FORT COLLINS.
C
C
      COMMON SUP(2,2),SUU(2,2),SXU(4,2),FINC(40),
     1 CORD(41),RN(2,40),S(2,40),RK(2,40),EGI(3,40),EGA(3,40),
     1 JCODE(14),JGAP(14),
     1 SK(205,15),ICOMM,NL,KCODE,
     1 Y(205),F(205),NUMEL,
     1 SKE(14,14),W(5),H(5),
     1 STRST(3,60),STRSB(3,60),FORCE(3,60)
C
C
C
C     READ AND INITIALIZATION
C
      ICHCK=0
C
      WRITE(6,24)
C     NPROB IS THE NUMBER OF PROBLEMS THAT HAVE DIFFERENT NODAL PT. COORDINATES
      READ(5,2) NPROB
      WRITE(6,2)NPROB
      DO 1050 NNN=1,NPROB
      READ(5,2) IFLAG
C     IFLAG DETERMINES THE NUMBER OF TIMES THE SAME COORDINATES CAN BE USED
C     FOR A GIVEN T-BEAM.
      DO 1050 NMN=1,IFLAG
      WRITE(6,27)
      READ(5,25)
      WRITE(6,25)
      WRITE(6,1)
      READ(5,2) LOCAT
      READ(5,2) NUMEL,NL,NGAP
      WRITE(6,2)NUMEL,NL,NGAP
C
      WRITE(6,3)
      READ(5,4) (J,W(J),H(J),I=1,NL)
      WRITE(6,4)(I,W(I),H(I),I=1,NL)
C
      WRITE(6,14)
C
      IEND=NUMEL
      JEND=NL
C
      NUMNP=NUMEL+1
      NUMEQ=(2+NL)*NUMNP
      IBAND=3*(2+NL)
C
      WRITE(6,20)
C
      DO 125 I=1,NL
      READ(5,2) MATL
      IF(MATL) 120,120,123
  120 READ(5,5) EGA1,EGI1
      DO 121 J=1,NUMEL
```

```
          EGA(I,J)=EGA1   $   EGI(I,J)=EGI1
      121 CONTINUE
          GO TO 125
      123 READ(5,9)   (EGA(I,J),J=1,NUMEL)
          READ(5,9)   (EGI(I,J),J=1,NUMEL)
      125 CONTINUE
C
C     CORRECTION FOR GAP ELEMENTS
C
          IF(NGAP) 135,135,132
      132 DO 133 I=1,NGAP
          READ(5,2) LL,NEL
C
C     INPUT GAP LOCATION
C
          DO 133 J=1,NL
          IF(J.EQ.LL) GO TO 133
          EGA(J,NEL)=-1.
      133 CONTINUE
     135  CONTINUE
          DO 126 I=1,NUMEL
          WRITE(6,2) I
          DO 126 J=1,NL
          WRITE (6,35) J,EGA(J,I),EGI(J,I)
       35 FORMAT (10X,I10,2E10.3)
      126 CONTINUE
C
          WRITE(6,22)
          IEND=NL-1
          DO 130 I=1,IEND
          READ (5,31) KCODE,RKI,SI,RNI
          WRITE(6,23)RKI,SI,RNI
          DO 130 J=1,NUMEL
          RK(I,J)=RKI
          S(I,J)=SI
          RN(I,J)=RNI
      130 CONTINUE
C
          WRITE(6,12)
          IF(NMN.GT.1) GO TO 138
          READ(5,9) (CORD(I),I=1,NUMNP)
      138 WRITE(6,9)(CORD(I),I=1,NUMNP)
C
C
C
          DO 1050 ME=1,LOCAT
          READ (5,2) NINC,MINC
          READ (5,9) (FINC(I),I=1,NUMNP)
          DO 137 I=1,205
          Y(I)=0.0
      137 CONTINUE
          KINC = 0
          INC = 1
      139 CONTINUE
          DO 140 I=1,NUMEQ
          F(I)=0.0
          DO 140 J=1,IBAND
          SK(I,J)=0.0
      140 CONTINUE
```

```
C
      JCODE(1)=1
      JCODE(2)=2
      JCODE(3)=(2+NL)+2
      JCODE(4)=(2+NL)+1
C
      I1=2
      I2=4+NL
      IBGN=5
      IEND=4+2*NL-1
C
      DO 160 I=IBGN,IEND,2
      IP1=I+1
      I1=I1+1
      I2=I2+1
      JCODE(I)=I1
      JCODE(IP1)=I2
  160 CONTINUE
C
C
C
C
C
C     FORMULATION OF SMALL K MATRIX
C
C
      DO 699 I=1,NUMEL
      ICOMM = I
C
C
C     INITIALIZE ARRAYS
C
      JEND=4+2*NL
      DO 310 J=1,JEND
      DO 310 K=1,JEND
      SKE(J,K)=0.0
  310 CONTINUE
C
C     CALCULATE PARAMETERS
C
C
      CALL STIFF
C
      RL=CORD(I+1)-CORD(I)
      IF(RL.EQ.0.0) GO TO 629
      EI=0.0
      DO 330 J=1,NL
      EI=EI+EGI(J,I)*W(J)*(H(J)**3)/12.0
  330 CONTINUE
C
      C2K=0.0
      NLM1=NL-1
      DO 340 J=1,NLM1
      C2K=C2K+(((H(J)+H(J+1))/2.0)**2)*RK(J,I)*RN(J,I)/S(J,I)
  340 CONTINUE
C
C
C     STRAIN PLUS CONNECTOR ENERGY DUE TO DEFLECTION
C
```

```
      SKE(1,1)=(12.00/(RL**3))*EI+(1.2/RL)*C2K
      SKE(1,2)=(6.00/(RL**2))*EI+(0.1)*C2K
      SKE(1,3)=+SKE(1,2)
      SKE(1,4)=-SKE(1,1)
      SKE(2,2)=(4.00/RL)*EI+(4.0*RL/30.0)*C2K
      SKE(2,3)=(2.00/RL)*EI-(RL/30.0)*C2K
      SKE(2,4)=-SKE(1,2)
      SKE(3,3)=+SKE(2,2)
      SKE(3,4)=-SKE(1,2)
      SKE(4,4)=+SKE(1,1)
C
C
C     STRAIN PLUS CONNECTOR ENERGY DUE TO AXIAL DEFORMATION
C
      SUP(1,1)=+1.0/RL
      SUP(1,2)=-1.0/RL
      SUP(2,2)=+1.0/RL
C
      SUU(1,1)=RL/3.0
      SUU(1,2)=RL/6.0
      SUU(2,1)=RL/6.0
      SUU(2,2)=RL/3.0
C
C
      DO 430 J=1,NL
      J1=5+2*(J-1)
      J2=J1+1
C
      FAC1=EGA(J,I)*W(J)*H(J)
      FAC2=0.0
      IF(J.NE.NL) FAC2=FAC2+RK(J,I)*RN(J,I)/S(J,I)
      IF(J.NE.1) FAC2=FAC2+RK(J-1,I)*RN(J-1,I)/S(J-1,I)
C
C
      SKE(J1,J1)=SUP(1,1)*FAC1+SUU(1,1)*FAC2
      SKE(J1,J2)=SUP(1,2)*FAC1+SUU(1,2)*FAC2
      SKE(J2,J2)=SUP(2,2)*FAC1+SUU(2,2)*FAC2
C
  430 CONTINUE
C
C
      DO 470 J=1,NLM1
C
      J1=5+2*(J-1)
      J2=J1+1
      J3=J1+2
      J4=J3+1
C
      FAC=RK(J,I)*RN(J,I)/S(J,I)
C
      SKE(J1,J3)=-SUU(1,1)*FAC
      SKE(J1,J4)=-SUU(1,2)*FAC
      SKE(J2,J3)=-SUU(2,1)*FAC
      SKE(J2,J4)=-SUU(2,2)*FAC
C
  470 CONTINUE
C
C
C     CONNECTOR ENERGY -- MIXED
```

```
C
      SXU(1,1)=-0.5
      SXU(1,2)=-0.5
      SXU(2,1)=+RL/12.0
      SXU(2,2)=-RL/12.0
      SXU(3,1)=-RL/12.0
      SXU(3,2)=+RL/12.0
      SXU(4,1)=+0.5
      SXU(4,2)=+0.5
C
      DO 530 J=1,NL
C
      J1=5+2*(J-1)
      J2=J1+1
      FAC=0.0
      IF(J.NE.NL)FAC=FAC+(RK(J,I)*RN(J,I)/S(J,I))*(H(J)+H(J+1))/2.0
      IF(J.NE.1) FAC=FAC-(RK(J-1,I)*RN(J-1,I)/S(J-1,I))*
     1                                          (H(J-1)+H(J))/2.0
C
      DO 515 K=1,4
      SKE(K,J1)=SXU(K,1)*FAC
      SKE(K,J2)=SXU(K,2)*FAC
  515 CONTINUE
  530 CONTINUE
C
C
C     FILL LOWER TRIANGULAR MATRIX
C
      JEND=4+2*NL
      DO 570 J=1,JEND
C
      KBGN=J+1
      KEND=JEND
      DO 570 K=KBGN,KEND
      SKE(K,J)=SKE(J,K)
  570 CONTINUE
C
C
C
C
C
C
C     ACCOUNT FOR GAPS
C
      JEND=4+2*NL
      DO 605 J=1,JEND
      JGAP(J)=JCODE(J)
  605 CONTINUE
C
      IF(I.EQ.1) GO TO 616
      ITEST=0
      DO 612 J=1,NL
      IF(EGA(J,I-1).GT.0.0) GO TO 612
      ITEST=1
      J1=5+2*(J-1)
      J2=JGAP(J1)
      SK(J2,1)=1.0E+50
      JGAP(J1)=JGAP(J1)-2-NL
```

```
  612 CONTINUE
      IF(ITEST.EQ.0) GO TO 616
      DO 615 J=1,2
      J1=JGAP(J)
      SK(J1,1)=1.0E+50
      JGAP(J)=JGAP(J)-2-NL
  615 CONTINUE
  616 CONTINUE
C
C     PLACEMENT IN LARGE SK MATRIX
C
      JEND=4+2*NL
      KEND=JEND
C
      DO 620 J=1,JEND
      J1=JGAP(J)
      DO 620 K=1,KEND
      K1=JGAP(K)
      IF(K1.LT.J1) GO TO 620
      K2=K1-J1+1
      SK(J1,K2)=SK(J1,K2)+SKE(J,K)
  620 CONTINUE
C
  629 CONTINUE
C
      JEND=4+2*NL
      DO 630 J=1,JEND
      JCODE(J)=JCODE(J)+2*NL
  630 CONTINUE
C
C
  699 CONTINUE
C
C     BOUNDARY
C
C
      SK(1,1)=SK(1,1)*(1.0E+50)
      ID=NUMEQ-1-NL
      SK(ID,1)=SK(ID,1)*(1.0E+50)
      ID=2+NL
      SK(ID,1)=SK(ID,1)*(1.0E+50)
C     NNODE DETERMINES WHERE THE NODE FORCE IS LOCATED IN THE FORCE VECTOR.
C     FF IS THE MAGNITUDE OF THE NODAL FORCE.
      WRITE(6,26)
C
      P = 0.
      DO 700 I=1,NUMNP
      I1 = (2+NL)*(I-1) + 1
      RI1 = INC
      F(I1) = FINC(I)*RI1
      PSET = ABS(F(I1))
      IF (P.GE.PSET) GO TO 700
      P = PSET
  700 CONTINUE
      WRITE (6,7) P
C
C
C     TRIANGULARIZATION
C
```

```
      NEM1=NUMEQ-1
C
      DO 950 I=1,NEM1
      D=1.0/SK(I,1)
      JEND=NUMEQ-I+1
      IF(JEND.GT.IBAND) JEND=IBAND
C
      DO 940 J=2,JEND
      IJ1=I+J-1
      FAC=SK(I,J)*D
C
      K1=0
      DO 930 K=J,JEND
      K1=K1+1
      SK(IJ1,K1)=SK(IJ1,K1)-SK(I,K)*FAC
  930 CONTINUE
C
      F(IJ1)=F(IJ1)-F(I)*FAC
      SK(I,J)=FAC
  940 CONTINUE
C
      F(I)=F(I)*D
C
  950 CONTINUE
C
      F(NUMEQ)=F(NUMEQ)/SK(NUMEQ,1)
C
C     BACK SUBSTITUTION
C
      Y(NUMEQ)=F(NUMEQ)
      DO 970 I=1,NEM1
      I1=NUMEQ-I
      JEND=NUMEQ-I1+1
      IF(JEND.GT.IBAND) JEND=IBAND
      RHS=F(I1)
      DO 960 J=2,JEND
      J1=I1+J-1
      RHS=RHS-SK(I1,J)*Y(J1)
  960 CONTINUE
      Y(I1)=RHS
  970 CONTINUE
C
      CALL STRES
C
C     WRITE STATEMENTS
C
C
C
      WRITE(6,19)
      DO 1020 I=1,NUMNP
      JBGN=1+(2+NL)*(I-1)
      JEND=JBGN+(1+NL)
      WRITE(6,18)I,(Y(J),J=JBGN,JEND)
 1020 CONTINUE
      WRITE (6,29)
      DO 1000 I=1,NUMEL
      WRITE(6,30) I,RK(1,I),FORCE(1,I),(STRST(J,I),STRSB(J,I),J=1,2)
 1000 CONTINUE
      IF (NL.EQ.2) GO TO 1011
```

```
      WRITE (6,32)
      DO 1010 I=1,NUMEL
      WRITE (6,30) I,RK(2,I),FORCE(2,I),STRST(3,I),STRSB(3,I)
 1010 CONTINUE
 1011 CONTINUE
C
      KINC = KINC + 1
      IF (INC.LT.NINC) GO TO 1049
      IF (KINC.LT.MINC) GO TO 139
      GO TO 1050
 1049 INC = INC + 1
      GO TO 139
C
 1050 CONTINUE
      STOP
C
C     FORMAT STATEMENTS
C
    1 FORMAT(30H0    NUMEL         NL      NGAPS     )
    2 FORMAT(3I10)
    3 FORMAT(30H0        LY          W          H    )
    4 FORMAT(I10,2E10.3)
    5 FORMAT(4E10.3)
    6 FORMAT(4E10.3)
    7 FORMAT(4F10.0)
    8 FORMAT(66H0    RK(J,I)   S(J,I) AND RN(J,I)   ARRAYS FOR EACH LAYER P
     1ER ELEMENT           ,/)
    9 FORMAT(6E10.3)
   10 FORMAT(10E10.3)
   11 FORMAT(18H1   SKE(I,J) MATRIX       ,/)
   12 FORMAT(16H0   XORD(I) ARRAY      ,/)
   13 FORMAT(1H0)
   14 FORMAT(57H0 EGA(I,J) AND EGI(I,J) ARRAYS FOR EACH LAYER PER ELEMEN
     1T      ,//)
   15 FORMAT(5E10.3)
   16 FORMAT(5E10.3)
   17 FORMAT(10E10.3)
   18 FORMAT(I10,7E15.5)
   19 FORMAT(115H           NP              Y            DY/DX              U1
     1           U2              U3              U4              U5    ,/)
   20 FORMAT(45H0   ELEMENT      LAYER          EA          EI       ,/)
   21 FORMAT(2E10.3)
   22 FORMAT(30H0        RKI          SI        RNI       ,/)
   23 FORMAT(3E10.3)
   24 FORMAT(15H0NO. PROB.        ,/)
   25 FORMAT(*
     1                                 *)
   26 FORMAT (*    LOAD *)
   27 FORMAT(1H1)
   28 FORMAT(I10,E10.3,I12//)
   29 FORMAT (//*        NUMEL          RK        NAIL FORCE          STRS1T
     1       STRS1B          STRS2T          STRS2B *)
   30 FORMAT (I10,6E15.5)
   31 FORMAT (I5,3E10.3)
   32 FORMAT (//*        NUMEL          RK         NAIL FORCE          STRS3T
     1        STRS3B */)
C
C
      END
```

```
C
      SUBROUTINE STIFF
      COMMON SUP(2,2),SUU(2,2),SXU(4,2),FINC(40),
     1 CORD(41),RN(2,40),S(2,40),RK(2,40),EGI(3,40),EGA(3,40),
     1 JCODE(14),JGAP(14),
     1 SK(205,15),ICOMM,NL,KCODE,
     1 Y(205),F(205),NUMEL,
     1 SKE(14,14),W(5),H(5),
     1 STRST(3,60),STRSB(3,60),FORCE(3,60)
      IC1 = (ICOMM-1)*(2+NL) +1
      ICP = 2+NL
      SLOPE = (Y(IC1+1) + Y(IC1+ICP+1))/2.0
      U1    = (Y(IC1+2) + Y(IC1+ICP+2))/2.0
      U2    = (Y(IC1+3) + Y(IC1+ICP+3))/2.0
      U3    = (Y(IC1+4) + Y(IC1+ICP+4))/2.0
      IF (ICOMM.EQ.NUMEL) GO TO 315
      IF (EGA(NL,ICOMM).NE.-1.0) GO TO 315
      SLOPE = Y(IC1+1)
      U1 = 0.0
      U2 = 0.
      U3 = 0.
      GO TO 320
  315 CONTINUE
      IF (ICOMM.EQ.1) GO TO 320
      IF (EGA(2,ICOMM-1).NE.-1.0) GO TO 322
      SLOPE = (Y(IC1-ICP+1) + Y(IC1+ICP+1))/2.0
      U2    = (Y(IC1-ICP+3) + Y(IC1+ICP+3))/2.0
      U3    = (Y(IC1-ICP+4) + Y(IC1+ICP+4))/2.0
      GO TO 320
  322 CONTINUE
      IF (EGA(1,ICOMM-1).NE.-1.0) GO TO 320
      SLOPE = (Y(IC1-ICP+1) + Y(IC1+ICP+1))/2.0
      U1    = (Y(IC1-ICP+2) + Y(IC1+ICP+2))/2.0
      U3    = (Y(IC1-ICP+4) + Y(IC1+ICP+4))/2.0
  320 CONTINUE
      DEL= (U2-U1) -(H(2)+H(1))/2.0 *SLOPE
      DEL1 = 1000. *ABS(DEL)
      DELL = (U3-U2) - (H(3) + H(2))/2.0 *SLOPE
      DEL2 = 1000. *ABS(DELL)
      IF (NL.EQ.2) GO TO 317
      IF(EGA((NL-1),ICOMM).EQ.-1.0) GO TO 317
      IF (EGA(1,ICOMM).EQ.-1.0) GO TO 325
      IF (DEL1.LE.130.) GO TO 318
      RK(1,ICOMM) = 240./DEL1
      GO TO 319
  318 RK(1,ICOMM) = 4.3900938 -0.083501913*DEL1 +0.0057424903*DEL1**2 -
     * 0.0002409156*DFL1**3 + 0.0000052880041*DEL1**4 - 0.65567654*DEL1*
     1*5/10000000. + 0.46573539*DEL1**6/1000000000. -0.17727098*DEL1**7/
     *10000000000.  + 0.002808726*DEL1**8/1000000000000.
  319 RK(1,ICOMM) = 1000.*RK(1,ICOMM)
      GO TO 323
  317 CONTINUE
      IF (EGA(2,ICOMM).EQ.-1.0) GO TO 325
  323 CONTINUE
      IF (NL.EQ.2) DEL2 = DEL1
      IF (DEL2.LE.60.0 ) GO TO 324
      RK((NL-1),ICOMM) = 178.0/DEL2
      GO TO 327
  324 CONTINUE
```

```
      SUBROUTINE  STIFF

                   RK((NL-1),ICOMM) = 44.521205 -7.2659378*DEL2 +0.70805607*DEL2**2 -
                  1 0.042044914*DEL2**3 +0.0015616336*DEL2**4 -0.000036410455*DEL2**5
                  1 + 0.51715645*DFL2**6/1000000. -0.40862412*DEL2**7/100000000. +
                  1 0.13761924*DEL2**8/10000000000.
               327 RK((NL-1),ICOMM) = 1000.*RK((NL-1),ICOMM)
                   IF (KCODE.EQ.1) GO TO 325
                   RK((NL-1),ICOMM) = RK((NL-1),ICOMM)*W(NL)
               325 CONTINUE
                   RETURN
                   END

      SYMBOLIC REFERENCE MAP

ENTRY POINTS
    1  STIFF

VARIABLES       SN  TYPE           RELOCATION
    70  CORD        REAL        ARRAY     / /           321  DEL         REAL
   323  DELL        REAL                                322  DEL1        REAL
   324  DEL2        REAL                                711  EGA         REAL        ARRAY     / /
   521  EGI         REAL        ARRAY     / /          7460  F           REAL        ARRAY     / /
    20  FINC        REAL        ARRAY     / /         11064  FORCE       REAL        ARRAY     / /
 10307  H           REAL        ARRAY     / /          7140  ICOMM       INTEGER               / /
   314  ICP         INTEGER                             313  IC1         INTEGER
  1101  JCODE       INTEGER     ARRAY     / /          1117  JGAP        INTEGER     ARRAY     / /
  7142  KCODE       INTEGER               / /          7141  NL          INTEGER               / /
  7775  NUMEL       INTEGER               / /           401  RK          REAL        ARRAY     / /
   141  RN          REAL        ARRAY     / /           261  S           REAL        ARRAY     / /
  1135  SK          REAL        ARRAY     / /          7776  SKE         REAL        ARRAY     / /
   315  SLOPE       REAL                              10600  STRSB       REAL        ARRAY     / /
 10314  STRST       REAL        ARRAY     / /             0  SUP         REAL        ARRAY     / /
     4  SUU         REAL        ARRAY     / /            10  SXU         REAL        ARRAY     / /
   316  U1          REAL                                317  U2          REAL
   320  U3          REAL                              10302  W           REAL        ARRAY     / /
  7143  Y           REAL        ARRAY     / /

INLINE FUNCTIONS    TYPE    ARGS
        ABS         REAL       1  INTRIN

STATEMENT LABELS
    40  315                        163  317                        142  318
   160  319                        103  320                         63  322
   167  323                        204  324                        242  325
   225  327

COMMON BLOCKS    LENGTH
        / /        4840

STATISTICS
  PROGRAM LENGTH     325B      213
    BLANK COMMON  113508B     4840
```

SUBROUTINE STRES

```
      SUBROUTINE STRES
      DIMENSION AX(3,60), BND(3,60)
      COMMON SUP(2,2),SUU(2,2),SXU(4,2),FINC(40),
     1 CORD(41),RN(2,40),S(2,40),RK(2,40),EGI(3,40),EGA(3,40),
     1 JCODE(14),JGAP(14),
     1 SK(205,15),ICOMM,NL,KCODE,
     1 Y(205),F(205),NUMEL,
     1 SKE(14,14),W(5),H(5),
     1 STRST(3,60),STRSB(3,60),FORCE(3,60)
      DO 390 I=1,NUMEL
      IC2 = (I-1)*(2+NL) + 1
      ICQ = 2+NL
      SLOP = (Y(IC2+1)+ Y(IC2+ICQ+1))/2.0
      U1F  = (Y(IC2+2)+ Y(IC2+ICQ+2))/2.0
      U2F  = (Y(IC2+3)+ Y(IC2+ICQ+3))/2.0
      U3F  = (Y(IC2+4)+ Y(IC2+ICQ+4))/2.0
      IF (I.EQ.NUMEL) GO TO 385
      IF (EGA(NL,I).NE.-1.0) GO TO 385
      SLOP = Y(IC2 +1)
      U1F = 0.0
      U2F = 0.0
      U3F = 0.0
  385 CONTINUE
      IF (I.EQ.1) GO TO 372
      IF (EGA(2,I-1).NE.-1.0) GO TO 370
      SLOP = (Y(IC2-ICQ+1) + Y(IC2+ICQ+1))/2.0
      U2F  = (Y(IC2-ICQ+3) + Y(IC2+ICQ+3))/2.0
      U3F  = (Y(IC2-ICQ+4) + Y(IC2+ICQ+4))/2.0
      GO TO 372
  370 CONTINUE
      IF (EGA(1,I-1).NE.-1.0) GO TO 372
      SLOP = (Y(IC2-ICQ+1) + Y(IC2+ICQ+1))/2.0
      U1F  = (Y(IC2-ICQ+2) + Y(IC2+ICQ+2))/2.0
      U3F  = (Y(IC2-ICQ+4) + Y(IC2+ICQ+4))/2.0
  372 CONTINUE
      DELF = U2F-U1F -(H(2) +H(1))/2.0*SLOP
      DELF1 = 1000.*ABS(DELF)
      DELG = U3F-U2F -(H(3) +H(2))/2.0 *SLOP
      DELF2 = 1000.*ABS(DELG)
      IF (NL.EQ.2) GO TO 395
      IF (DELF1.LE.130.) GO TO  393
      FORCE(1,I)      = 240.
      GO TO  395
  393 FORCE(1,I)      = 4.3900938*DELF1 -0.083501913*DELF1**2 +
     * 0.0057424903*DELF1**3 -0.0002409156*DELF1**4 + 0.0000052880041*
     1DELF1**5 -0.65567654*DELF1**6/10000000. + 0.46573539*DELF1**7/
     *1000000000. -0.17727098*DELF1**8/10000000000. +0.0028080726*DELF1
     1**9/100000000000.
  395 CONTINUE
      IF (NL.EQ.2) DELF2 = DELF1
      IF (DELF2.LE.60.0 ) GO TO 387
      FORCE((NL-1),I) = 178.0
      GO TO 389
  387 CONTINUE
      FORCE((NL-1),I) = 44.521205*DELF2 -7.2659378*DELF2**2 +
     1 0.70805607*DELF2**3 -0.042044914*DELF2**4+ 0.0015616336*DELF2**5-
     1 0.000036410455*DELF2**6 +0.51715645*DELF2**7/1000000.  -
     1 0.40862412*DELF2**8/100000000. + 0.13761924*DELF2**9/1000000000.
  389 CONTINUE
```

```
      SUBROUTINE  STRES

                  IF ((CORD(I+1)-CORD(I)).EQ.0.0) GO TO 381
                  SLOPE = (Y(IC2+ICQ+1)-Y(IC2+1))/(CORD(I+1)-CORD(I))
                  U1P   = (Y(IC2+ICQ+2)-Y(IC2+2))/(CORD(I+1)-CORD(I))
                  U2P   = (Y(IC2+ICQ+3)-Y(IC2+3))/(CORD(I+1)-CORD(I))
                  U3P   = (Y(IC2+ICQ+4)-Y(IC2+4))/(CORD(I+1)-CORD(I))
                  IF (EGA(NL,I-1).EQ.-1.0) GO TO 382
                  GO TO 380
              381 SLOPE = 0.0
                  U1P = 0.0
                  U2P = 0.0
                  U3P = 0.0
                  GO TO 380
              382 SLOPE =-(Y(IC2-ICQ+1) -Y(IC2+ICQ+1))/(CORD(I+1)- CORD(I))
                  IF (EGA(2,I-1).EQ.-1.0) GO TO 383
                  U1P   =-(Y(IC2-ICQ+2) -Y(IC2+ICQ+2))/(CORD(I+1)- CORD(I))
                  GO TO 384
              383 U2P   =-(Y(IC2-ICQ+3) -Y(IC2+ICQ+3))/(CORD(I+1)- CORD(I))
              384 U3P   =-(Y(IC2-ICQ+4) -Y(IC2+ICQ+4))/(CORD(I+1)- CORD(I))
              380 CONTINUE
                  AX(1,I) = U1P*EGA(1,I)
                  AX(2,I) = U2P*EGA(2,I)
                  BND(1,I) = H(1)/2.0*SLOPE*EGI(1,I)
                  BND(2,I) = H(2)/2.0*SLOPE*EGI(2,I)
                  STRST(1,I) = AX(1,I) - BND(1,I)
                  STRSB(1,I) = AX(1,I) + BND(1,I)
                  STRST(2,I) = AX(2,I) - BND(2,I)
                  STRSB(2,I) = AX(2,I) + BND(2,I)
                  IF (NL.EQ.2) GO TO 390
                  IF ((CORD(I+1)-CORD(I)).EQ.0.0) GO TO 396
                  IF (EGA(NL,I-1).EQ.-1.0) GO TO 397
                  U3P = (Y(IC2+ICQ+4) -Y(IC2+4))/(CORD(I+1)-CORD(I))
                  GO TO 397
              396 U3P = 0.0
              397 AX(3,I) = U3P*EGA(3,I)
                  BND(3,I) = H(3)/2.0*SLOPE*EGI(3,I)
                  STRST(3,I) = AX(3,I) - BND(3,I)
                  STRSB(3,I) = AX(3,I) + BND(3,I)
              390 CONTINUE
                  RETURN
                  END

      SYMBOLIC REFERENCE MAP

ENTRY POINTS
    1  STRES

VARIABLES       SN  TYPE             RELOCATION
  420  AX           REAL       ARRAY                   704  BND      REAL       ARRAY
   70  CORD         REAL       ARRAY    / /            410  DELF     REAL
  411  DELF1        REAL                               413  DELF2    REAL
  412  DELG         REAL                               711  EGA      REAL       ARRAY    / /
  521  EGI          REAL       ARRAY    / /           7460  F        REAL       ARRAY    / /
   20  FINC         REAL       ARRAY    / /          11064  FORCE    REAL       ARRAY    / /
10307  H            REAL       ARRAY    / /            401  I        INTEGER
 7140  ICOMM        INTEGER             / /            403  ICQ      INTEGER
  402  IC2          INTEGER                           1101  JCODE    INTEGER    ARRAY    / /
 1117  JGAP         INTEGER    ARRAY    / /           7142  KCODE    INTEGER             / /
 7141  NL           INTEGER             / /           7775  NUMEL    INTEGER             / /
  401  RK           REAL       ARRAY    / /            141  RN       REAL       ARRAY    / /
```

APPENDIX E

CURVE FIT EQUATION CONSTANTS FOR LOAD-SLIP CURVES

Appendix E Curve Fit Equation Constants For Load-Slip Curves

General Equation: $y = k_0 + k_1x + k_2x^2 + k_3x^3 + \ldots\ldots + k_9x^9$

Polynomial terms	Coefficient Constants (k): Nailed Connections: Douglas-fir sheathing + Douglas-fir joist	Nailed Connections: Douglas-fir sheathing + Engelmann spruce joist or Engelmann spruce sheathing + Douglas-fir joist	Nailed Connections: Engelmann spruce sheathing + Engelmann spruce joist	Nailed Connections: Particleboard + Plywood sheathing	Glued Connection: All combinations of joist and sheathing
k_0	0.41306856	-0.1924158	0.77542537	-0.29532266	1.2294028
k_1	55.078858	51.093127	41.444234	4.3900938	44.521205
k_2	-5.1638787	-12.223799	-7.6121221	-0.083501913	-7.2659378
k_3	-1.4495226	2.0295547	0.93648912	0.0057424903	0.70805607
k_4	0.55435434	-0.21368794	-0.070110229	$-0.2409156 \times 10^{-3}$	-0.042044914
k_5	-0.081201572	0.014506446	0.0032661775	$0.52880041 \times 10^{-5}$	0.0015616336
k_6	0.0065050283	$-0.63060451 \times 10^{-3}$	$-0.95097321 \times 10^{-4}$	$-0.65567654 \times 10^{-7}$	$-0.36410455 \times 10^{-4}$
k_7	$-0.29941299 \times 10^{-3}$	$0.16887354 \times 10^{-4}$	$0.16789401 \times 10^{-5}$	$0.46573539 \times 10^{-9}$	$0.51715645 \times 10^{-6}$
k_8	$0.74470527 \times 10^{-5}$	$-0.25297115 \times 10^{-6}$	$-0.16411157 \times 10^{-7}$	$-0.17727098 \times 10^{-11}$	$-0.40862412 \times 10^{-8}$
k_9	$-0.77699113 \times 10^{-7}$	0.1618386×10^{-8}	$0.68065454 \times 10^{-10}$	$0.28080726 \times 10^{-14}$	$0.13761924 \times 10^{-10}$
Number of points used	31	41	61	66	61
$\sum(Y_i-y_i)^2$	6.6402	5.3926	7.9310	3.8132	16.2454

Note:

Y_i = curve-fitted point

y_i = actual point

Y_i-y_i = residual